Synthesis and Characterization of Carbohydrate Mimics

By

Lucas K. Beagle

Submitted in Partial Fulfillment of the Requirements

for the Degree of

Master of Science

in the

Chemistry

Program

YOUNGSTOWN STATE UNIVERSITY

July, 2008

Synthesis and Characterization of Carbohydrate Mimics

Lucas K. Beagle

I hereby release this thesis to the public. I understand that this thesis will be made available from the OhioLINK ETD Center and the Maag Library Circulation Desk for public access. I also authorize the University or other individuals to make copies of this thesis as needed for scholarly research.

Signature: _____

Lucas K. Beagle Date

Approvals:

_____

Dr. Peter Norris Date
Thesis Advisor

_____

Dr. Allen Hunter Date
Thesis Advisor

_____

Dr. John Jackson Date
Committee Member

_____

Dr. Peter J. Kasvinsky Date
Dean of Graduate Studies

Thesis Abstract

The synthesis of *N*-acetyl-D-fucosamine and *N*-((2R,3R,4R)-2,4-dihydroxy-6-methylene-5-oxo-tetrahydro-2H-pyran-3-yl)acetamide will be pursued from the inexpensive starting material *N*-acetyl-D-glucosamine. These carbohydrates are mimics of intermediates used by *Staphylococcus aureus* in the construction of its protective capsular polysaccharide, which allows the bacteria to evade both the host immune system and antibiotics in current use. Synthesis of these molecules allows for carbohydrate mimics to be developed which can be used as targeted antibiotics needed for use against antibiotic-resistant *Staphylococcus aureus* strains.

Characterization by nuclear magnetic resonance spectroscopy will allow determination of structural conformation, of structures' dependence on solvent while in solution, and presence of the desired product. These studies will be carried out to be compared with other structural determination techniques in wide use today. Knowledge of the solution state structure of a molecule is necessary to understand the possible interactions in biological systems which must be understood in pharmaceutical development. Recent developments in NMR techniques allow for multi-dimensional spectra which can relate interconnected atoms in a molecule to provide information on the relative spatial orientation of atoms within a molecule.

Acknowledgements

I would like to thank the Youngstown State University Chemistry Department for the opportunity to obtain my MS degree and giving me a second chance to achieve my life long goals. I would also like to include special thanks to my advisors Dr. Norris and Dr. Hunter. Dr. Norris has allowed me to develop my talents as a chemist, not allowed me to quit, and helped me mature in my academic pursuits. Dr. Hunter along with Dr. Zeller have breathed new life into my academic career, allowed me to explore other areas of chemistry I may not get to experience again, and helped me to become independent in my endeavors. I would like to specially acknowledge Dr. Jackson, you are my rock and have helped me through the thick and thin of things over the past two years, you have helped to make me a better chemist and person.

I would also like to thank all my colleagues in my research groups, you have made the past two years interesting to say the least. I wish all you the best of luck and good fortune in your travels. Brian Dobosh, what could possibly be said about you other than you are truly a great friend. Daniel Kibler, your encouragement and support has been needed and appreciated. To my family your support has been a great help throughout the years. Most importantly I would like to thank my wife Kristen, without her support and encouragement I would not have been able to do anything. Kristen your sacrifice has been difficult, not appreciated or rewarded entirely enough; I do all this for you and hope you are proud. May the next journey we take be as fruitful, challenging and rewarding as this one.

Table of Contents

Title Page …….. i

Signature Page …….. ii

Thesis Abstract …….. iii

Acknowledgements …….. iv

Table of Contents …….. v

List of Tables …….. vi

List of Schemes …….. vi

List of Equations …….. vi

List of Figures …….. vii

Introduction …….. 1

Experimental …….. 23

Statement of Problem …….. 52

Results and Discussion …….. 53

Conclusions …….. 73

References …….. 75

Appendix A …….. 79

Appendix B …….. 164

Appendix C …….. 175

List of Tables

Table 1. Improvements shown for the first four steps of the Horton synthesis……... 53

Table 2. Information that can be obtained from selected individual NMR experiments. …….. 64

Table 3. t1 and t2 relaxation times for **14, 15, 16, 17** …….. 176

Table 4. Relative experiment times for **14, 15, 16, 17** ...…….. 178

List of Schemes

Scheme 1. The Horton Synthesis of *N*-acetyl-D-fucosamine from *N*-acetyl-D-glucosamine…….. 4

Scheme 2. Modified Horton synthesis to form protected *N*-((2*R*,3*R*,4*R*)-2,4-dihydroxy-6-methylene-5-oxotetrahydro-2*H*-pyran-3-yl)acetamide……..... 6

List of Equations

Equation 1. Formation of 4,6-*O*-isopropylidene-protected **3α/β** from **2α/β**..... 54

Equation 2. Formation of 1,3-*O*-benzyl-protected **5α/β** from **3α/β**……. 55

Equation 3. Formation of 4,6-Hydroxy-deprotected **6α/β** from **5α/β**…….. 56

Equation 4. Formation of 4,6-di-*O*-methylsulfonyl-protected **7α/β** from **6α/β**…….…….... 56

Equation 5. Formation of 1,3-*O*-acetyl-protected **4α/β** from **3α/β**……...…… 57

Equation 6. Formation of 4,6-Hydroxy-deprotected **10α/β** from **4α/β**……..... 58

Equation 7. Formation of methyl-*N*-glycosides **8α/β** from **2α/β**……. 58

Equation 8. Formation of 4,6-*O*-isopropylidene-protected **9α/β** from **8α/β**…….. 59

Equation 9. Formation of 4,6-di-*O*-methylsulfonyl-protected **11α/β** from **10α/β**……..… 60

Equation 10. Attempted formation of 6-methylene **12α/β** from **7α/β**…… 61

Equation 11. Formation of 6-mehtylene **12α/β** from **7α/β**……. 61

Equation 12. Attempted formation of 6-methylene **13α/β** from **11α/β**…….. 62

List of Figures

Figure 1. Structures of the repeating subunits which make up the capsular polysaccharides of serotype 5 and serotype 8 *Staphylococcus aureus*…….. 2

Figure 2. The three carbohydrate residues which constitute Serotype 5 and Serotype 8……. 3

Figure 3. *N*-((2*R*,3*R*,4*R*)-2,4-dihydroxy-6-methylene-5-oxotetrahydro-2*H*-pyran-3-yl)acetamide, an intermediate in the biological formation of *S. aureus* capsular polysaccharide……..… 6

Figure 4. An example of a pulse sequence, in particular the HMQCBI pulse sequence……..…. 8

Figure 5. Example of a nucleus aligned with the magnetic field and then after a pulse.……..... 9

Figure 6. 2,3,4,6-Tetra-*O*-Acetyl-1-azidodeoxy-β-D-glucopyranose used as an example for selected NMR experiments……. 11

Figure 7. 400 MHz ^{1}H spectrum of **1**……... 12

Figure 8. 100 MHz ^{13}C Spectrum of **1**……..... 12

Figure 9. 100 MHz ^{13}C DEPT-135 spectrum of 1…… 14

Figure 10. 400 MHz ^{1}H-^{1}H COSY Spectrum of **1**……. 16

Figure 11. 400 MHz ^{1}H-^{1}H NOESY Spectrum of **1**……..……... 17

Figure 12. 400 MHz ^{1}H-^{13}C HSQC Spectrum of **1**……..……. 18

Figure 13. 400 MHz ^{1}H-^{13}C HMQC Spectrum of **1**…….……. 19

Figure 14. 400 MHz ^{1}H-^{13}C HMBC Spectrum of **1**…….……. 20

Figure 15. Example of long distance coupling network, without NOE interactions……...…. 64

Figure 16. Representation of the triazole proton exhibiting nuclear Overhauser interactions with H-1, H-3 and H-5 of **14**…….……. 66

Figure 17. 400 MHz COSY-NOSEY spectrum overlay of **14**……... 66

Figure 18. 400 MHz COSY-NOSEY overlay of **15**…….. 68

Figure 19. 400 MHz COSY-NOSEY overlay of **16**……... 69

Figure 20. Orientation of **16** in solution state……. 69

Figure 21. 400 MHz COSY-NOSEY overlay of **17**……... 70

Figure 22. 400 MHz ^{1}H spectrum of **2α/β**.……..……... 80

Figure 23. 100 MHz ^{13}C Spectrum of **2α/β**……... 81

Figure 24. 400 MHz ^{1}H-^{1}H COSY Spectrum of **2α/β**…….…… 82

Figure 25. 400 MHz ^{1}H-^{13}C HSQC Spectrum of **2α/β**…….……. 83

Figure 26. 400 MHz ^{1}H spectrum of **3α/β**..…….... 84

Figure 27. 100 MHz ^{13}C Spectrum of **3α/β**..……... 85

Figure 28. 400 MHz ^{1}H-^{1}H COSY Spectrum of **3α/β**…….……... 86

Figure 29. 400 MHz ^{1}H-^{13}C HSQC Spectrum of **3α/β**…….…. 87

Figure 30. 400 MHz ^{1}H-^{13}C HMQC Spectrum of **3α/β**……. 88

Figure 31. 400 MHz ^{1}H spectrum of **4α/β**..…… 89

Figure 32. 100 MHz ^{13}C Spectrum of **4α/β**..……... 90

Figure 33. 400 MHz ^{1}H-^{1}H COSY Spectrum of **4α/β**…….…….. 91

Figure 34. 400 MHz ^{1}H-^{13}C HSQC Spectrum of **4α/β**…….. 92

Figure 35. 400 MHz ^{1}H-^{13}C HMQC Spectrum of **4α/β**……. 93

Figure 36. 400 MHz ^{1}H spectrum of **5α/β**..…….....94

Figure 37. 100 MHz ^{13}C Spectrum of **5α/β**..……... 95

Figure 38. 400 MHz ^{1}H-^{1}H COSY Spectrum of **5α/β**…….…….. 96

Figure 39. 400 MHz ^{1}H-^{13}C HSQC Spectrum of **5α/β**…….…. 97

Figure 40. 400 MHz ^{1}H-^{13}C HMQC Spectrum of **5α/β**……. 98

Figure 41. 400 MHz ^{1}H-^{13}C HMBC Spectrum of **5α/β**……. 99

Figure 42. 400 MHz ^{1}H-^{1}H NOESY Spectrum of **5α/β**…….……. 100

Figure 43. 400 MHz ^{1}H-^{1}H NOESY-COSY Spectrum Overlay of **5α/β**…. 101

Figure 44. 400 MHz ^{1}H spectrum of **6α/β**..……..… 102

Figure 45. 100 MHz ^{13}C Spectrum of **6α/β**..……...….. 103

Figure 46. 400 MHz ^{1}H-^{1}H COSY Spectrum of **6α/β**…….…. 104

Figure 47. 400 MHz ^{1}H-^{13}C HSQC Spectrum of **6α/β**…… 105

Figure 48. 400 MHz ^{1}H-^{13}C HMQC Spectrum of **6α/β**……..……. 106

Figure 49. 400 MHz ^{1}H spectrum of **7α/β**..…… 107

Figure 50. 100 MHz ^{13}C Spectrum of **7α/β**……..... 108

Figure 51. 400 MHz ^{1}H-^{1}H COSY Spectrum of **7α/β**……. 109

Figure 52. 400 MHz ^{1}H-^{13}C HSQC Spectrum of **7α/β**…… 110

Figure 53. 400 MHz ^{1}H-^{13}C HMQC Spectrum of **7α/β**……... 111

Figure 54. 400 MHz ^{1}H spectrum of **8α/β**..…… 112

Figure 55. 100 MHz ^{13}C Spectrum of **8α/β**……..... 113

Figure 56. 400 MHz ^{1}H-^{1}H COSY Spectrum of **8α/β**……. 114

Figure 57. 400 MHz ^{1}H-^{13}C HSQC Spectrum of **8α/β**…… 115

Figure 58. 400 MHz ^{1}H-^{13}C HMQC Spectrum of **8α/β**……... 116

Figure 59. 400 MHz ^{1}H spectrum of **9α/β**..…….. 117

Figure 60. 100 MHz ^{13}C Spectrum of **9α/β**……. 118

Figure 61. 400 MHz ^{1}H-^{1}H COSY Spectrum of **9α/β**……. 119

Figure 62. 400 MHz ^{1}H-^{13}C HSQC Spectrum of **9α/β**…… 120

Figure 63. 400 MHz ^{1}H-^{13}C HMQC Spectrum of **9α/β**……... 121

Figure 64. 400 MHz ^{1}H spectrum of **10α/β**..…… 122

Figure 65. 100 MHz ^{13}C Spectrum of **10α/β**……..... 123

Figure 66. 400 MHz ^{1}H-^{1}H COSY Spectrum of **10α/β**……..... 124

Figure 67. 400 MHz ^{1}H-^{13}C HSQC Spectrum of **10α/β**…….. 125

Figure 68. 400 MHz ^{1}H-^{13}C HMQC Spectrum of **10α/β**……. 126

Figure 69. 400 MHz ^{1}H spectrum of **11α/β**..……..... 127

Figure 70. 400 MHz ^{1}H spectrum of **13α/β**..……..... 128

Figure 71. 100 MHz ^{13}C Spectrum of **13α/β**……..... 129

Figure 72. 400 MHz ^{1}H-^{1}H COSY Spectrum of **13α/β**…….. 130

Figure 73. 400 MHz ^{1}H-^{13}C HSQC Spectrum of **13α/β**…….. 131

Figure 74. 400 MHz ^{1}H spectrum of **14**....……... 132

Figure 75. 100 MHz ^{13}C Spectrum of **14**...…… 133

Figure 76. 400 MHz ^{1}H-^{1}H COSY Spectrum of **14**…….……... 134

Figure 77. 400 MHz ^{1}H-^{13}C HSQC Spectrum of **14**…….……... 135

Figure 78. 400 MHz ^{1}H-^{13}C HMQC Spectrum of **14**…..……..…… 136

Figure 79. 400 MHz ^{1}H-^{13}C HMBC Spectrum of **14**……..……..…… 137

Figure 80. 400 MHz ^{1}H-^{1}H NOESY Spectrum of **14**…..……..…….. 138

Figure 81. 400 MHz ^{13}C CEPT-135 of **14**……..…….. 139

Figure 82. 400 MHz ^{1}H spectrum of **14**....……... 140

Figure 83. 100 MHz ^{13}C Spectrum of **14**...…… 141

Figure 84. 400 MHz ^{1}H-^{1}H COSY Spectrum of **14**…….……... 142

Figure 85. 400 MHz ^{1}H-^{13}C HSQC Spectrum of **14**…….……... 143

Figure 86. 400 MHz ^{1}H-^{13}C HMQC Spectrum of **14**…..……..…… 144

Figure 87. 400 MHz ^{1}H-^{13}C HMBC Spectrum of **14**……..……..…… 145

Figure 88. 400 MHz ^{1}H-^{1}H NOESY Spectrum of **14**…..……..…….. 146

Figure 89. 400 MHz ^{13}C CEPT-135 of **14**……..…….. 147

Figure 90. 400 MHz ^{1}H spectrum of **14**....……... 148

Figure 91. 100 MHz ^{13}C Spectrum of **14**...…… 149

Figure 92. 400 MHz ^{1}H-^{1}H COSY Spectrum of **14**…….……... 150

Figure 93. 400 MHz ^{1}H-^{13}C HSQC Spectrum of **14**…….……... 151

Figure 94. 400 MHz ^{1}H-^{13}C HMQC Spectrum of **14**…..……..…… 152

Figure 95. 400 MHz ^{1}H-^{13}C HMBC Spectrum of **14**…….……..…… 153

Figure 96. 400 MHz ^{1}H-^{1}H NOESY Spectrum of **14**…..……..…….. 154

Figure 97. 400 MHz ^{13}C CEPT-135 of **14**……..…….. 155

Figure 98. 400 MHz ^{1}H spectrum of **14**....……... 156

Figure 99. 100 MHz ^{13}C Spectrum of **14**...…….…. 157

Figure 100. 400 MHz ^{1}H-^{1}H COSY Spectrum of **14**…….……..... 158

Figure 101. 400 MHz ^{1}H-^{13}C HSQC Spectrum of **14**…….……... 159

Figure 102. 400 MHz ^{1}H-^{13}C HMQC Spectrum of **14**…..…..…… 160

Figure 103. 400 MHz ^{1}H-^{13}C HMBC Spectrum of **14**……..…….…… 161

Figure 104. 400 MHz ^{1}H-^{1}H NOESY Spectrum of **14**…..……..…….. 162

Figure 105. 400 MHz ^{13}C CEPT-135 of **14**……..…….. 163

Figure 106. Mass Spectrum of **3α/β**……... 165

Figure 107. Mass Spectrum of **4α/β**……... 166

Figure 108. Mass Spectrum of **5α/β**……... 167

Figure 109. Mass Spectrum of **6α/β**……... 168

Figure 110. Mass Spectrum of **7α/β**……... 169

Figure 111. Mass Spectrum of **8α/β**……... 170

Figure 112. Mass Spectrum of **9α/β**……... 171

Figure 113. Mass Spectrum of **10α/β**……..... 172

Figure 114. Mass Spectrum of **11α/β**……..... 173

Figure 115. Mass Spectrum of **12α/β**……..... 174

Introduction

Carbohydrate Research

Systematic studies on carbohydrates originated with Emil Fischer during the 1890s[1] and they have been explored extensively ever since. Carbohydrate research has emerged to become an important area of investigation in the biomedical sciences community over the last four decades. Interest has been piqued because of the important role that carbohydrates play in cellular and molecular recognition (the emergent field of *glycobiology*). Along with investigations in glycobiology, synthesis and modification of carbohydrate precursors has become an intense area of research for the organic chemistry community. Researchers hope that the synthesis and modification of these carbohydrates will allow for new treatments against diseases such as bacterial infections and various cancers that are currently receiving a great deal of attention from the biomedical community.

Staphylococcus aureus (*S. aureus*) has become a major concern because of the recent rise in antibiotic-resistant strains.[2] *S. aureus*, a Gram-positive bacterium, produces a capsular polysaccharide which masks the bacteria's cellular identification markers and thereby allows the bacterium to effectively evade the host immune system. The initial treatment for infection was the use of Penicillin (introduced in 1941), but *S. aureus* was showing signs of resistance after only three years of Penicillin use. More powerful antibiotics, such as Vancomycin and Methicillin, which were used to treat these multiple-antibiotic resistant strains, are now becoming less effective. Both Methicillin and Vancomycin were introduced in the 1960's to combat strains of *S. aureus* resistant to other antibiotics. Against Methicillin, which is a derivative of Penicillin, *S. aureus*

showed signs of resistance within one year (MRSA, Methicillin-resistant *S. aureus*), whereas it took almost forty years before Vancomycin-resistant (VRSA, Vancomycin-resistant *S. aureus*) strains were observed.[3] With what the biomedical profession considers the last-line-of-defense drugs becoming ineffective against *S. aureus*, it is becoming a worldwide challenge to find treatments that can bring infections by *S. aureus* under control.[4]

S. aureus, when isolated, has been shown to have eleven distinct serotypes, which are distinguished from one another by their capsular polysachharides.[5] The two antibiotic-resistant serotypes (VRSA and MRSA) of *S. aureus* that most often infect humans (75% of isolated cases),[6] were identified to be serotypes 5 and 8 (Figure 1).

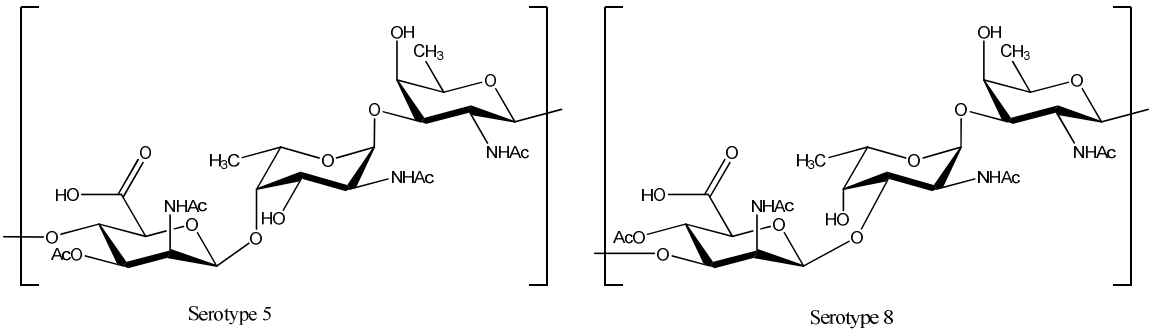

Figure 1: Structures of the repeating subunits which make up the capsular polysaccharides of serotype 5 and serotype 8 *Staphylococcus aureus*.

The same three carbohydrates are used as the building blocks of the serotype 5 and 8 biological polymers. These are: 2-acetamido-D-mannosamineuronic acid (*N*-acetyl-D-mannosamineuronic acid or D-ManAcA), 2-acetamido-2,6-dideoxy-L-galactose (*N*-acetyl-L-fucosamine or L-FucNAc), and 2-acetamido-2,6-dideoxy-D-galactose (*N*-acetyl-D-fucosamine or D-FucNAc) (Figure 2). Structurally, the serotypes differ in their linkages between the individual carbohydrates subunits to another. Serotype 5 has a

(→4)-3-*O*-Ac-β-D-ManNAcA-(1→4)-α-L-FucNAc-(1→3)-β-D-FucNAc-(1→) repeating polysaccharide, whereas serotype 8 has a (→3)-4-*O*-Ac-β-D-ManNAcA-(1→3)-α-L-FucNAc-(1→3)-α-D-FucNAc-(1→) repeating polysaccharide.[7] While the linkage between D-FucNAc and L-FucNAc remains constant, the linkages between L-FucNAc and D-ManAcA and between D-FucNAc of one monomer to D-ManAcA of the next monomer vary slightly between the two serotypes.

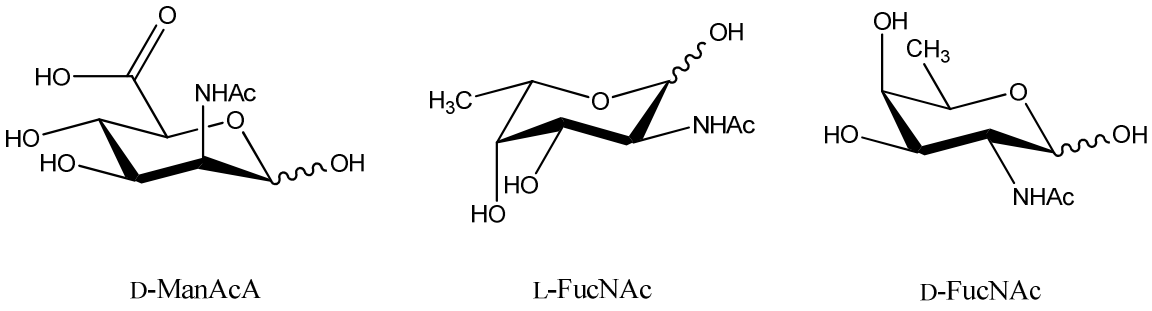

Figure 2: The three carbohydrate residues which constitute Serotype 5 and Serotype 8.

Aminodideoxy sugars, such as *N*-acetyl-D-fucosamine, are not readily available for purchase; they may be specially ordered but at a cost-prohibitive price, therefore they must be synthesized. If an aminodeoxy sugar, such as *N*-acetyl-D-fucosamine, is used as a precursor, *N*-acetyl-D-fucosamine can be synthesized. A solution to this problem was developed by Derek Horton and published in 1978.[8] He elaborated a synthesis from which *N*-acetyl-D-fucosamine can be taken through a series of protection and deprotection reactions and functional group interconversions that ultimately yield *N*-acetyl-D-fucosamine (Scheme 1). Because of this, the Horton Synthesis will serve as a model for synthesis of *N*-acetyl-D-fucosamine.

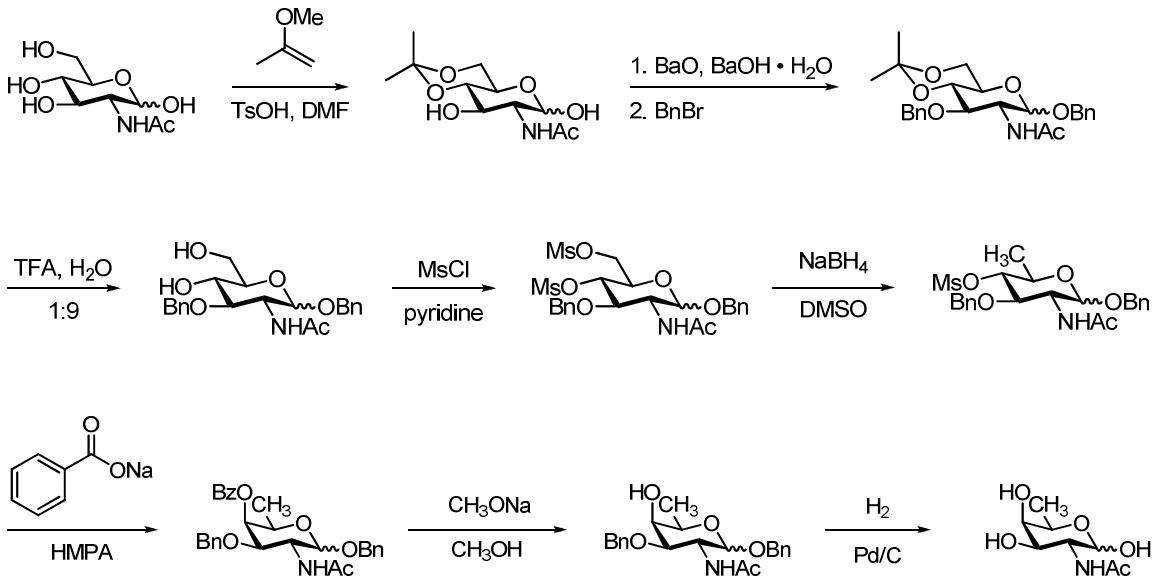

Scheme 1: The Horton Synthesis of *N*-acetyl-D-fucosamine from *N*-acetyl-D-glucosamine.

The Horton synthesis (Scheme 1) consists of 8 total steps that can be divided into the following reaction types: steps 1-4, 7, 8 are protection and deprotection reactions, step 5 is a functional group interconversion, and step 6 is an epimerization. First the hydroxyl groups on carbon's 4 and 6 are protected with an isopropylidene acetal, then the hydroxyl groups at carbon's1 and 3 are protected with benzyl groups, after which the acid-catalyzed hydrolysis of the isopropylidene acetal group is performed. Next, the hydroxyl groups which were just deprotected (4 and 6) are activated by deprotecting and converting to sulfonate esters. C-6 (the primary sulfonate ester) is then selectively reduced (over C-4, the secondary sulfonate ester) with sodium borohydride. C-4 (the secondary sulfonate ester) is then selectively epimerized using sodium benzoate in a bimolecular nucleophilic substitution reaction (S_N2 reaction mechanism). Sodium methoxide is added to deprotect carbon 4 after which a Parr hydrogenation is carried out

to remove the benzyl ether groups to deprotect carbon atoms 1 and 3 and reveal the D-FucNAc molecule.[8]

An alternative pathway for the synthesis of dideoxyamino sugars (i.e. D-FucNAc) from glycals has been carried out by a radical mechanism and introduction of an azide ion. These pathways however require extra steps and the same protection and deprotection reactions as are required in the Horton synthesis. A complication that can result is a mixture of diastereomers from the addition of the azide onto C-2 of the glycal.[9,10,11,12]

The *O*-glycosidic linkages between the sugar subunits are an area of intense research and concern and many methods for the synthetic formation of this functionality have been developed. Demchenko and associates published a method for using glycosyl thioimidates to allow for stereoselective glycosylation, a method which involves "arming and disarming" of the residues.[12,13] Another method, which also allows for radioactive labeling of the linkage, is a process developed by Illarionov and coworkers published in 2001. This method utilizes a uridine 5'-diphosphate unit linked to C-1 of the sugar and uses the complex to act as a chain inhibitor of the synthesis of the polymer.[14]

An intermediate in the *in vivo* formation of these biological polymers is *N*-((2R,3R,4R)-2,4-dihydroxy-6-methylene-5-oxo-tetrahydro-2H-pyran-3-yl)acetamide (Figure 3). This is further manipulated by the bacterium and used to build the capsular polysaccharide. A proposed synthesis (Scheme 2), borrowed partially from the Horton Synthesis, allows for the formation of *N*-((2R,3R,4R)-2,4-dihydroxy-6-methylene-5-oxo-tetrahydro-2H-pyran-3-yl)acetamide.

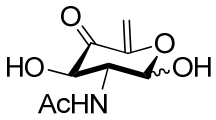

Figure 3: *N*-((2R,3R,4R)-2,4-dihydroxy-6-methylene-5-oxo-tetrahydro-2H-pyran-3-yl)acetamide, an intermediate in the biological formation of *S. aureus* capsular polysaccharide.

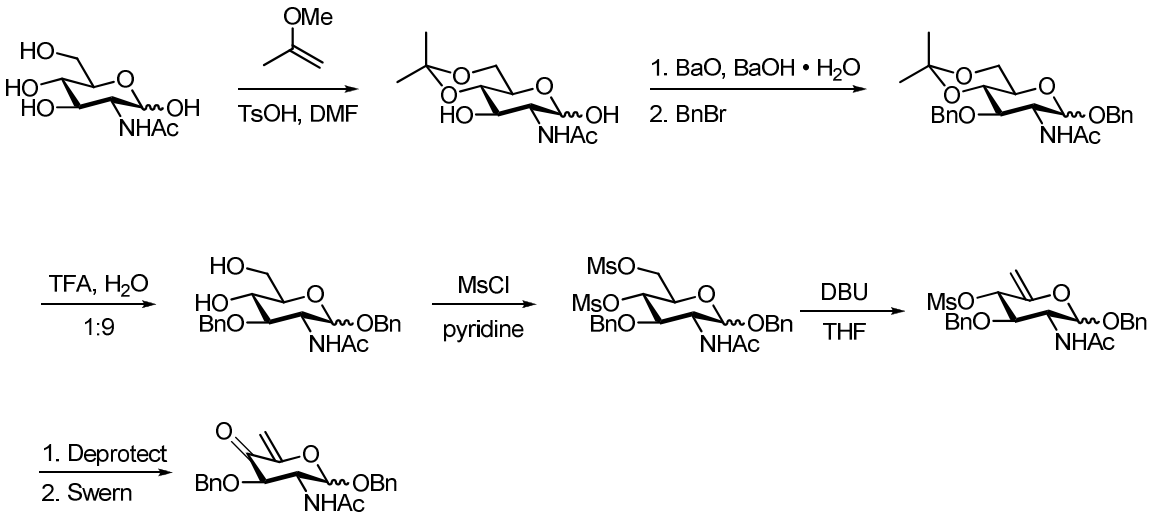

Scheme 2: Modified Horton synthesis to form protected *N*-((2R,3R,4R)-2,4-dihydroxy-6-methylene-5-oxo-tetrahydro-2H-pyran-3-yl)acetamide.

A problem is found in the synthesis of this intermediate; the benzyl protecting groups require that they are removed, e.g. via a Parr hydrogenation. If that is done, however, the double bond would also be reduced, therefore different protecting groups must be utilized.[15] Alternative pathways are also to be considered in the reduction at C- 6 (elimination reaction leading to the double bond formation), including the introduction of better leaving groups to facilitate the elimination reaction.[16,17]

Nuclear Magnetic Resonance Characterization

Unambiguous identification and full characterization is an important and challenging part of research associated with the synthesis of carbohydrates. The single most powerful method available today to do so for organic compounds in solution is without a doubt nuclear magnetic resonance, NMR, spectroscopy. It was first described by Isidor Rabi in molecular beams in 1938[18] and Purcell and Bloch (independently) first applied it to liquids and solids in 1946 for which they won the 1952 Nobel Prize.[19] NMR allows for observation of the resonance frequencies of magnetically active nuclei, of the associated coupling constants, and other properties of a chemical compounds to allow determination of structural information.[20] For example, a user can determine: the relative distances between atoms in a molecule, structural conformations, and the dependence of these properties on solvents. This information can then be used to verify the structure of synthesized molecules and provide information about that molecule's properties. A variety of experiments including one- and two-dimensional NMR and solvent suppression techniques can be used to obtain the information.[21,22]

Radio frequency pulses are the driving force of nuclear magnetic resonance spectroscopy; they are what we use to initiate signal generation in this technique. Pulse sequences (Figure 4) are the specific chronological order in which one or many radio frequency pulses are used to generate the signal for the individual experiment. The pulses in the sequence are what differentiates the outcome of signals between the experiments and permit acquisition of distinctly different information (i.e. correlation verses coherence spectra).[23] While the nuclei are in the probe of the instrument, the nuclei's spins are either aligned with or against the magnetic field, B_0, (Z-axis).

Depending on the strength of the magnetic field, a small excess of the nuclei's spins are aligned with the magnetic field, and this excess will stay in this alignment unless perturbed with a radio frequency pulse (Figure 4). When a pulse at the resonant frequency hits a nucleus, the spin is perturbed into the X-Y plane and continues to precess about the Z-axis (Figure 5). This precession around the Z-axis in the X-Y plane is what is recorded as a signal, this is because the probe was designed to have detection coils that are aligned to collect signal in this plane.[24,25] The time it takes for a spin to relax back to its original state is called relaxation time, and varies depending on the nucleus, the type of pulse that excited it, and its local magnetic environment (i.e. especially the molecule it is part of).[24] Common pulses within a sequence are 45°, 90°, and 180° pulses which refer to how far through space the nuclei are to be flipped. Field gradients can be used to force all the nuclei back into their initial starting alignments respective to the magnetic field.[26]

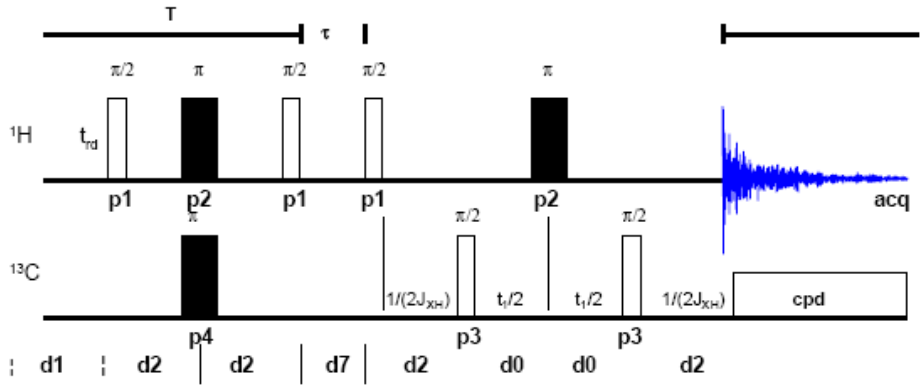

Figure 4: An example of a pulse sequence, in particular the HMQCBI pulse sequence.[20]

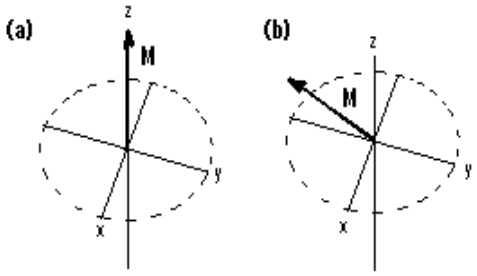

Figure 5: Example of a nucleus aligned with the magnetic field and then after a pulse.[20]

Nuclear Magnetic Resonance spectroscopy began as a direct observation of a nucleus upon perturbation via a radio frequency pulse in a magnetic field. This change in the magnetic environment at the nuclei's resonance frequency is recorded as a shift from the nucleus's resonant frequency with influence due to the local magnetic environment.[22,23] These are the familiar one dimensional spectra which we see, i.e., ^{1}H and ^{13}C NMR spectra. Later developments led to experiments involving indirect detection of a nucleus, where one nucleus is perturbed and the signal of a different nucleus is observed.[26] This technique is useful in observing nuclei which have a low magnetogyric ratio (a measure of how well a nucleus is susceptible to magnetic fields and observation in nuclear magnetic resonance spectroscopy) or for nuclei with a low natural abundance.[24,28] Other one-dimensional experiments have evolved from the direct and indirect observation experiments. These experiments deal with perturbing one type of nuclei and observing how it affects the other nuclei in the molecule. Examples of these would be the one-dimensional NOE (Nuclear Overhauser Effect) difference experiments, one dimensional TOCSY (Total Correlation Spectroscopy) experiments, decoupling experiments, and ^{13}C DEPT (Distortion Enhanced Proton Transfer) measurements.[26,29]

The next natural evolution of nuclear magnetic resonance was to go multi-dimensional. This deals with putting another nucleus on the Y-axis to give us a two-dimensional spectrum. Jeener, in a 1971 proposal, was the first to hypothesize that spectroscopy could be taken from linear analysis to multi-dimensional analysis while at the Ampere International Summer Session.[30] Aue, in 1975, was one of the first to publish work on these new ideas. He used a two-dimensional "tickling" experiment on the compound 1,1,2-trichloroethane as one of his first ventures into these new experiments. He broke the experiment into three distinct time periods: $t < 0$ the preparation period where the system is allowed to go to a suitable initial state and ends with a preparatory pulse, $0 < t < t_1$ the evolution period (also known as t_1 relaxation delay) where the system evolves under the preparatory pulse and that ends with the mixing pulse, and $t_1 < t$ the detection period where the system is observed and the spectrum recorded.[31]

Many two- (and more-) dimensional experiments have been developed over the years leading to advances in nuclear magnetic spectroscopy. These modern experiments involve more complex pulse sequences that allow for observation of the nucleus of interest to be observed in a variety of states of coupling and resonance. While these experiments follow Aue's ideas on periods they are by far more complex and are very intricate in design containing elements of indirect detection, hetero- and homonuclear correlation and coupling, and the Nuclear Overhauser Effects. Examples of these experiments are the COSY (Correlation Spectroscopy), NOESY (Nuclear Overhauser Effect Spectroscopy), HSQC (Heteronuclear Singular Quantum Coherence) and the HMBC (Heteronuclear Multiple Bond Coherence) experiments.[32]

One Dimensional NMR spectroscopy

^{1}H and ^{13}C NMR spectra (e.g. Figures 7 and 8 respectively) give a great deal of information into the composition of a molecule. These experiments elucidate the local magnetic environment around each hydrogen or carbon nucleus respectively and allow conjecture into the likely neighbors of each atom. It allows for discovery of coupling constants and the beginning of insight into the structure of a molecule.[33] 2,3,4,6-Tetra-*O*-Acetyl-1-azidodeoxy-β-D-glucopyranose (Figure 6) will be the molecule that is the model for the explanation of the following experiments, which are collected as described in detail in the following experimental section.

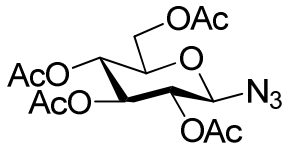

1

Figure 6: 2,3,4,6-Tetra-*O*-Acetyl-1-azidodeoxy-β-D-glucopyranose used as an example for selected NMR experiments.

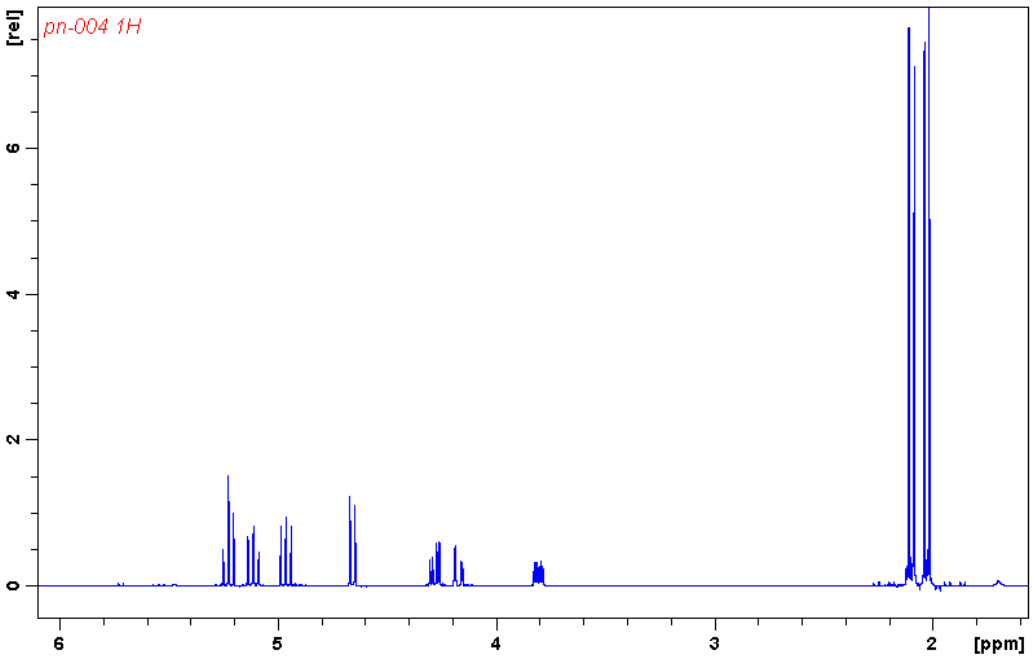

Figure 7: 400 MHz ^{1}H NMR spectrum of **1**.

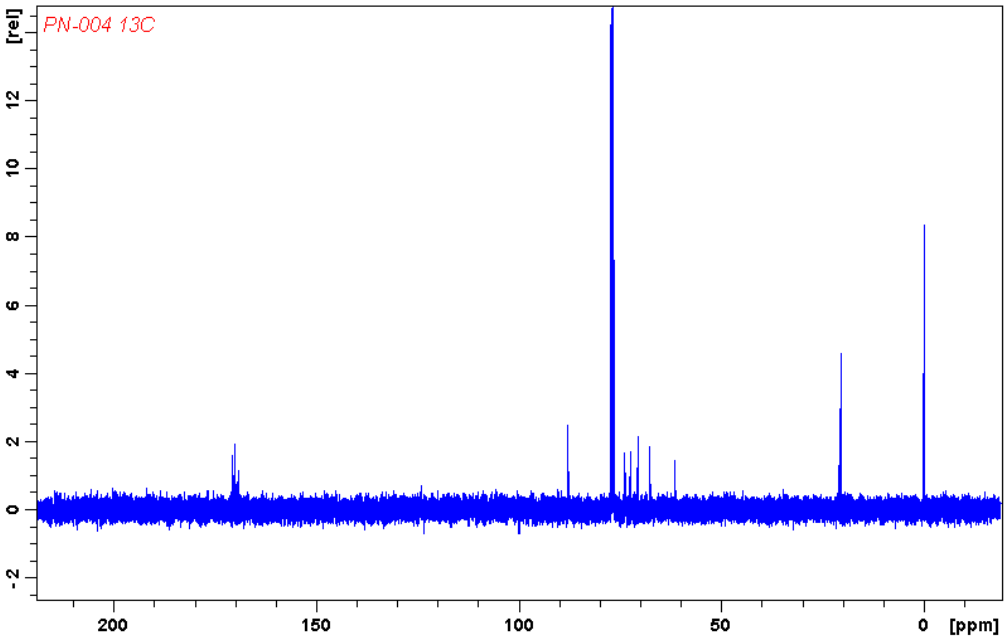

Figure 8: 100 MHz ^{13}C NMR Spectrum of **1**.

Decoupling experiments are performed to prevent the coupling of two nuclei when they are spinning in the plane of detection. These experiments involve a saturation signal at the resonant frequency of the coupling nucleus. This causes the coupled nuclei to be overwhelmed and therefore become scrambled where it will not influence the observed nucleus and therefore not couple. Decoupling experiments are useful especially in larger molecule's spectra where multiple overlap could occur and are an integral part of some of the two-dimensional experiments.[34] When this decoupling is applied to the same nucleus as the observed then it is called *homonuclear* decoupling; when it is applied to a different nucleus it is called *heteronuclear* decoupling.[24]

^{13}C DEPT-135 spectra (Figure 9) are very useful in determination of the count of protons bonded to a particular carbon. This usefulness is derived from the output showing $-CH_2$ (methylene) peaks below the baseline and -CH (methine) and $-CH_3$ (methyl) peaks appear above the baseline. The DEPT-135 is a combination of the DEPT-90 pulse which shows only methine as a positive (above the baseline) peak and the DEPT-45 pulse techniques which show all groups as positive peaks. This experiment will not work for quaternary carbons because they have no directly attached hydrogen atoms. This technique is based on a special multi-pulse sequence, which flip the nuclei and take advantage of certain well known quantum mechanical prinicples.[35,36] The pulse sequence is set up such that it involves inducing heteronuclear multiple quantum coherence where the carbon and hydrogen magnetization evolve coherently and then a 180° pulse is applied and separates the magnetization of the two nuclei and the carbon signal is then observed. The anti-phase flip that occurs so that the nuclei that can be observed are dependent on the multiplicity of the observed carbon nuclei, thereby giving

different magnitude peaks for the different multiplicities. The experiment is often run decoupled so that the multiplicity ratios of individual carbon nuclei are not seen.[32]

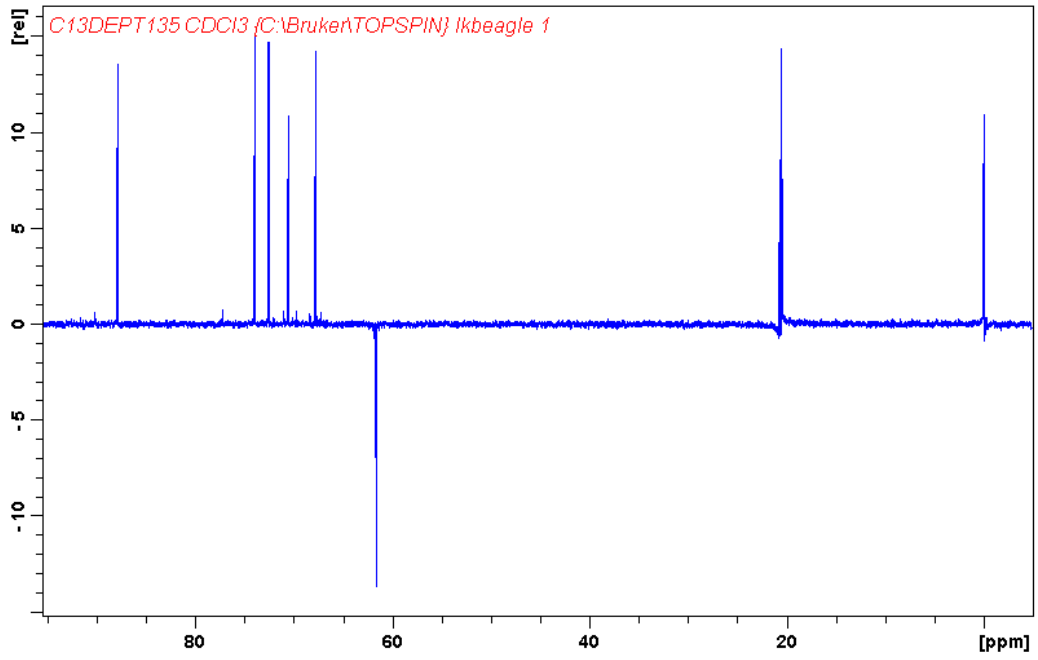

Figure 9: 100 MHz ^{13}C DEPT-135 spectrum of 1.

Experiments to find t_1 relaxation times are performed to measure the time it takes all the nuclei in a molecule to return to the initial equilibrium alignment with the magnetic field. Knowing the t_1 relaxation time allows for the setup of experiments with much reduced noise in the two-dimensional spectra; these experiments are necessary to reduce noise on spectrometers which do not have gradient pulses to realign the spins.[34] If the delay times in the pulse sequences are not set to longer than the longest nucleus' relaxation time (typically the delay is set to 3-5 times the longest relaxation time to ensure complete relaxation), then there is residual coupling from the last experiment pulses which bleed through and cause false signals to be recorded in the spectra.[21]

Nuclear Overhauser Effects (NOE) are caused by quantum mechanical effects whereby one nucleus' magnetic field will influence another nucleus' magnetic environment. These effects are seen over distance and not through bonds, therefore they are inversely proportional to the radius between the nuclei to the sixth power.[37,38] Therefore, the effect drops significantly over distance, and typically it is seen only over a maximum of about 6 Å. Although bond lengths within organic molecules are not very long, these effects can serve to intensify or reduce the signal for a given nucleus' signal because of the effect it has on a nucleus' magnetic environment.[39]

Two-Dimensional NMR Spectroscopy

J-Resolved spectra are used to allow overlapping multiplets that cannot be resolved using one-dimensional spectroscopy to be assigned and the scalar J-coupling to be determined.[40,41] The experiment relies on the spin-echo pulse sequence, which is a 90° pulse followed by a delay, then a 180° pulse followed by a delay and then acquisition. The peaks in the multiplicity will modulate at different rates and then can be resolved when one will become positive and the other negative. This is displayed on a two-dimensional grid where the Y-axis represents the J values doubled in Hertz and the X-axis the recorded spectrum.[24]

Correlation Spectroscopy (COSY) (Figure 10) relies on homonuclear coupling over two to four bonds. COSY experiments rely on a pulse sequence of a delay followed by a 90° pulse and then a relaxation delay and another 90° pulse.[23] This delay is important and must be set proportionally to the t_1 relaxation times of the molecule to prevent noise and Bloch-Siegert shifts in the spectra.[24] COSY spectra are used to identify

neighbors in a molecule and give structural informational in the area of arrangement of atoms within the molecules atoms.[31]

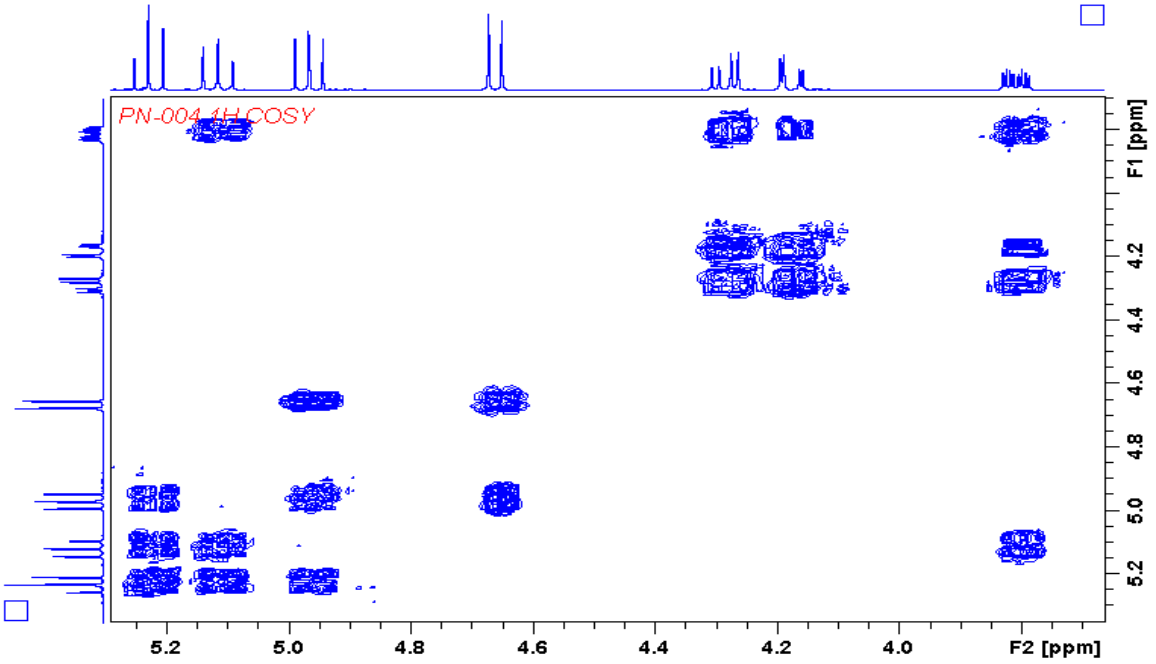

Figure 10: 400 MHz ^{1}H-^{1}H COSY Spectrum of **1**.

Nuclear Overhauser Effect Spectroscopy (NOESY) (Figure 11) relies on the Nuclear Overhauser Effect within a molecule and whether or not two nuclei are close in space to one another. NOESY experiments are performed with a pulse sequence of a 90° pulse, then a relaxation delay, another 90° pulse, then a mixing delay, another 90°pulse, and then detection.[32] This allows a buildup of the NOE and subsequent stimulation and transfer of magnetic effects between the nuclei. NOESY spectra look very similar to COSY spectra having the same peaks as the COSY spectra because of the close distances of neighboring closely bonded nuclei.[42] The distinct difference is that the COSY will not see interactions though space as it relies on coupling through bonds.[31] The NOESY

experiment will therefore lend much information about the three-dimensional structure of the molecule from the interactions through space.[39]

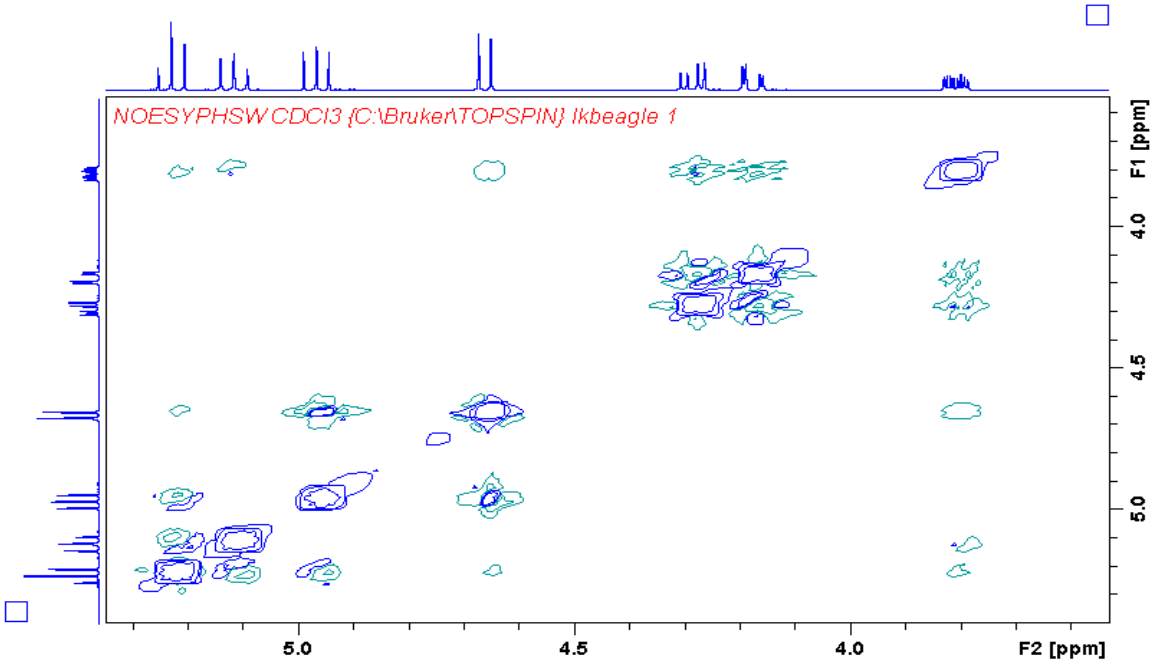

Figure 11: 400 MHz ^{1}H-^{1}H NOESY Spectrum of **1**.

Heteronuclear Multiple Quantum Coherence (HMQC) spectroscopy (Figure 12) relies on the quantum coherence property of sensitive (high magnetogyric) nuclei with less sensitive nuclei.[43] The experiment relies on multiple quantum coherence, which pools and transfers transverse magnetism across a single bond, giving directly connected nuclei. This technique is especially useful in identifying and assigning diastereotopic geminal pairs, which is an important facet in carbohydrate characterization, usually on carbon 6 of a hexose in its pyranose form. The pulse sequence involves a 90° pulse applied to the proton nuclei, which develops the transverse proton magnetization and creates antiphase magnetism, and then a 90° pulse to the carbon nuclei transforms the antiphase magnetization into double quantum magnetization where the transfer occurs. A

180° pulse then applied to the proton nuclei will eliminate the proton chemical shifts and a 90° pulse is applied to the carbon nuclei which converts the quantum magnetization back into antiphase magnetization which then transfers back to the proton. During acquisition carbon-proton coupling re-evolves and allows observation of the proton spectrum.[24,29]

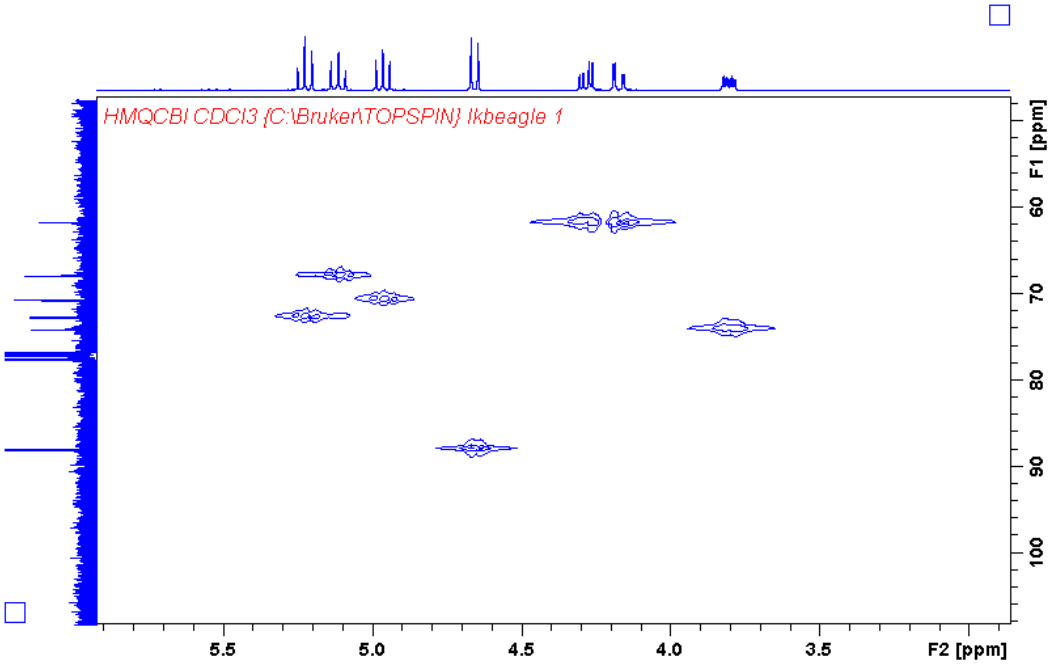

Figure 12: 400 MHz ^{1}H-^{13}C HMQC Spectrum of **1**.

Heteronuclear Single Quantum Coherence (HSQC) spectroscopy (Figure 13) relies on the quantum coherence property of sensitive (high magnetogyric ratios) nuclei with less sensitive nuclei. The experiment relies on single quantum coherence, which transfers transverse magnetism across a single bond, thus identifying directly connected nuclei.[29,44] HSQC relies on an Insensitive Nuclei Enhanced Polarization Transfer (INEPT), a pulse sequence often embedded within indirect detection pulse sequences which allows for transfer of magnetization between sensitive and non-sensitive nuclei

which will increase the observed signal for the non-sensitive nuclei (carbon in this case). The pulse sequence consists of an excitation of the proton, then an INEPT transfer (during the t_1 delay) of magnetism to the carbon nucleus, which involves an antiphase magnetization to the proton. Then a 90° pulse applied to the carbon and proton transfers the antiphase magnetization back to the proton from the carbon nucleus in a reverse INEPT transfer.[29] The HSQC experiment is more sensitive to experimental error than HMQC because it involves a ten-step pulse sequence, where the HMQC only involves a four-step pulse sequence.[24]

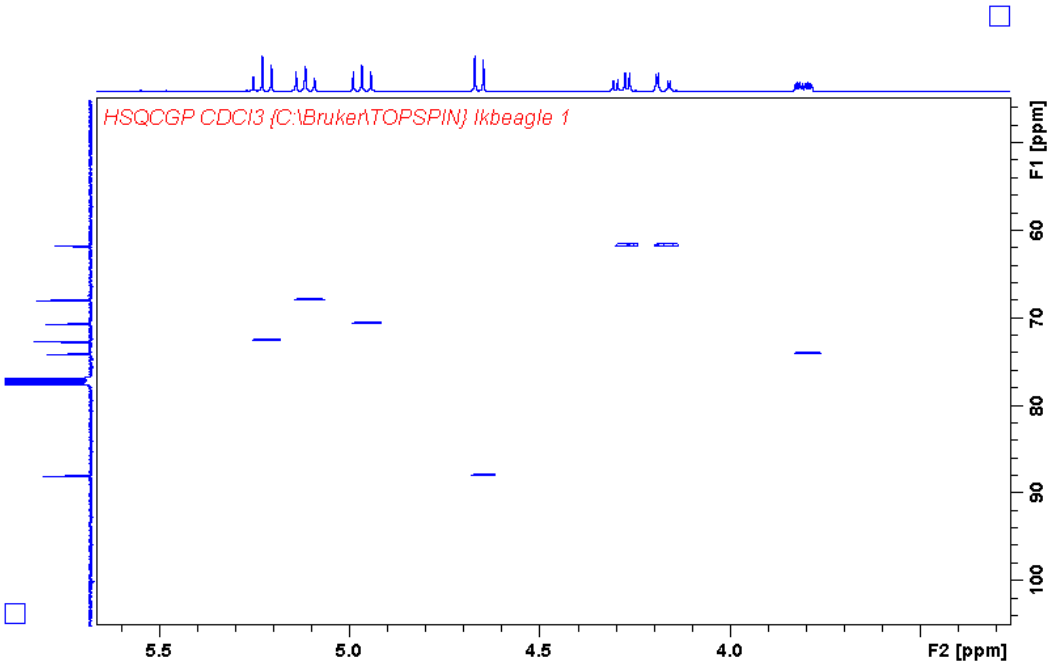

Figure 13: 400 MHz ^{1}H-^{13}C HSQC Spectrum of **1**.

Heteronuclear Multiple Bond Correlation (HMBC) spectroscopy (Figure 14) relies on the coupling between atoms through bonds. HMBC is often referred to as *long distance correlation*, because it allows for detection of interactions at distances of up to 5 bonds away. As with most hetero-correlation spectroscopy this relies on the indirect

detection of the carbon nuclei, which have a much lower magnetogyric ratio than the proton. Correctly setting the delays, which are often very long due to the long t_1 relaxation times of carbon, is imperative to getting spectra which are able to be interpreted. Otherwise the noise will overwhelm the spectra due to the intense parent resonance.[46] This can be avoided by using pulse field gradients to force relaxation of the nuclei and thereby decrease the acquisition time for the experiment. The pulse sequence utilized is very similar to the HMQC sequence just with longer delay times because of the desire to observe the ^{1}H-^{13}C couplings which tend to be rather large compared to ^{1}H-^{1}H couplings.[24,29]

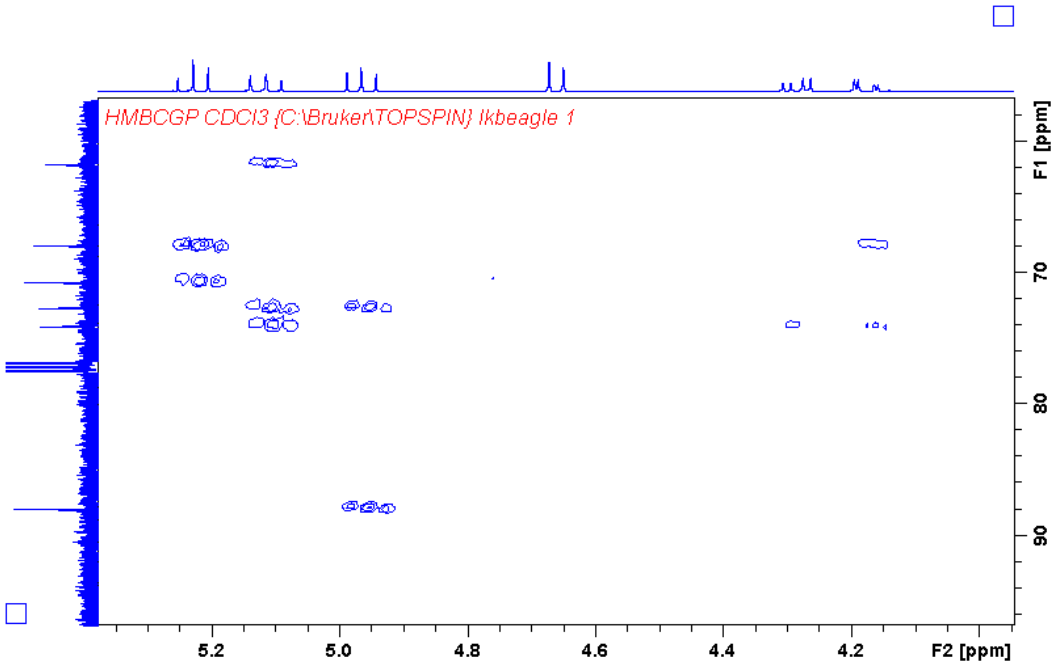

Figure 14: 400 MHz ^{1}H-^{13}C HMBC Spectrum of **1**.

All these techniques used in concert can allow for a full structural elucidation and characterization of carbohydrate compounds, and of organic compounds in general. This is done by determination of the chemical shifts of the carbon and hydrogen nuclei from

their respective one-dimensional spectra and assignment of coupling constants. Correlation spectroscopy (COSY) then shows neighboring proton nuclei within the molecule and we can begin to see spatial relations. Quantum coherence spectra (HSQC and HMQC) allow assignment of directly bonded carbon and hydrogen atoms and more spatial relation is gained. Correlation spectra (HMBC and COSY) will allow for a sequential ordering of the nuclei in the molecule by allowing elucidation of neighboring atoms. Ultimately the three-dimensional structure can be determined by utilization of the Nuclear Overhauser Effects and the information from the COSY spectra by knowing that the COSY is most strongly detectable for the *geminal* and *trans* coupling configurations and NOESY having the strongest interactions through space over short distances. From the combination of these experiments the three-dimensional structure can then be determined. The heteronuclear correlation and quantum coherence spectroscopy methods can also be extended from carbon to the other heteroelements and can, for example, be used to show nitrogen and hydrogen correlations in carbohydrates.

This research will attempt to apply these techniques to a variety of *N*-glycosides to elucidate their structure in solution as opposed to their structure in the solid state that can be obtained by X-ray and neutron diffraction techniques. In pharmaceutical and medicinal chemistry, this knowledge can be used in the targeted design of compounds with these kind of linkages as carbohydrate mimics. Stereochemistry and conformation are especially important to the design and synthesis of pharmaceuticals and these techniques will allow these to be quantified. Four compounds will be studied in depth in order to provide structural information on carbohydrates by using nuclear magnetic resonance techniques. These compounds are members of a family of substances that

often tend to not form single crystals suitable for X-ray diffraction and especially its larger and more complicated members tend to elude structural characterization in the solid state. Where solid state structural data are available the NMR methods used will provide information that differs greatly from that obtained from X-ray diffraction with pharmacologically important data on conformation and stereochemistry in solution not disturbed by packing and other solid state effects. X-ray crystallography also shows only a snapshot of one of many possible conformations, and interactions with the solvent via e.g. hydrogen bonding in solution are also lost in the solid state structure determinations. Nuclear magnetic resonance, on the other hand, provides data measured directly in solution and can thus answer structural questions due to solvent effects and give an accurate picture of the actual conformations in solution.

Experimental

General experimental procedure for synthesis

Unless otherwise noted, all reactions were conducted at ambient room temperature and did not require any special procedures to keep out atmosphere. Some reagents were checked for purity using nuclear magnetic resonance spectroscopy.

The ^{1}H NMR and ^{13}C NMR were recorded on a Varian Gemini-2000 400 MHz NMR spectrometer with broadband probe, Bruker Avance III 400 MHz NMR spectrometer with broadband probe, or Bruker Avance II 400 MHz NMR spectrometer with indirect detection probe with reference to the deuterium signal of the solvent. All nuclei were excited at their respective resonance frequencies for signal detection. Chemical Shifts were reported in parts per million (ppm) from a standard of tetramethylsilane in $CDCl_3$ (0.1% w/v TMS) or D6-DMSO (d_6, 99.9 atom % D). NMR spectra multiplicities are defined as follows: s (singlet), d (doublet), t (triplet), m (multiplet), dd (doublet of doublets), dt (doublet of triplets), ddd (doublet of doublet of doublets), and all coupling constants (J) are labeled in Hertz. The mass spectra were obtained on a Bruker Esquire-HP LC/MS spectrometer. Thin layer chromatography was performed on Whatman aluminum-backed plates with varying eluent systems. Flash column chromatography was performed using 32-60 mesh 60-Å silica gel with varying eluent systems. All spectra are included for reference in Appendix A.

Synthesis of *N*-Acetal-D-Fucosamine

Formation of 2-acetamido-2-deoxy-4,6-*O*-isopropylidene-α,β-D-glucopyranose (3α/β) from 2-acetamido-2-deoxy-α-D-glucopyranose (2α/β).

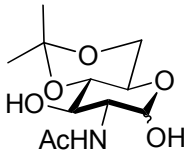

3α/β

At 80-85 °C a solution of **1** (3.000 g, 13.56 mmol), dimethyl formamide (40 mL), and *p*-toluene sulfonic acid monohydrate (0.032 g, cat.) was stirred for 15 minutes, then 2,2-dimethoxy propane (6.5 mL, 65.79 mmol) was added via syringe. Stirring was continued at 80-85 °C until the reaction showed completion by TLC (3 : 1 ethyl acetate : methanol). The mixture was then neutralized with sodium carbonate and filtered. The resulting solution was washed with methylene chloride (50 mL), and the remaining solvents were removed *en vacuo* to afford a pale yellow powder in a 92% Yield. The removal of solvents was facilitated by azeotroping the dimethyl formamide with toluene.

^{1}H NMR (d_6-DMSO): δ 1.31 (s, 3H, CH_3), 1.44 (s, 3H, CH_3), 1.83 (s, 3H, NHAc) 3.31 (s, 1H, OH), 3.40-3.46 (m, 1H, H-3), 3.53 (ddd, 1H, H-5, *J* = 4.74, 4.74, 14.28 Hz), 3.63-3.78 (m, 3H, OH, H-2, H-4), 4.80 (dd, 1H, H-6, *J* = 0.26, 6.02 Hz), 4.93 (dd, 1H, H-6, *J* = 4.04, 4.04 Hz), 6.61 (d, 1H, H-1, *J* = 3.84 Hz), 7.68 (d, 1H, NHAc, *J* = 8.44 Hz).

^{13}C NMR (d_6-DMSO): δ 19.63, 23.08, 29.66, 55.29, 63.37, 68.01, 75.54, 91.92, 99.33, 169.82.

m/z calculated: 261.12

m/z recorded: 284.1 (with sodium)

Formation of 2-acetamido-1,3-di-*O*-acetyl-2-deoxy-4,6-*O*-isopropylidene-α,β-D-glucopyranoside (4α/β) from 2-acetamido-2-deoxy-4,6-*O*-isopropylidene-α,β-D-glucopyranose (3α/β).

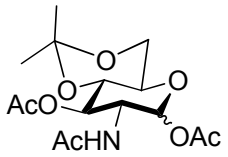

4α/β

Acetic anhydride (2.36 mL, 25.00 mmol) was added dropwise via syringe to **3α/β** (0.30g, 1.15 mmol) in anhydrous pyridine (10 mL) under nitrogen atmosphere. The reaction continued to stir for 18 hours, and then was poured over an ice (2.0 g) and deionized water (150 mL) mixture. The mixture was extracted three times with methylene chloride (20 mL) and washed with a 5% sulfuric acid solution (20 mL) then deionized water (20 mL). The organics were dried over magnesium sulfate and filtered. The methylene chloride was removed *en vacuo* to give a yellowish colored oil in a 63% yield.

^{1}H NMR ($CDCl_3$): δ 1.40 (s, 3H, CH_3), 1.50 (s, 3H, CH_3), 1.94 (s, 3H, NHAc), 2.11 (s, 3H, CH_3), 2.19 (s, 3H, CH_3), 3.73 -3.91 (m, 4H, H-4, H-5, H-6), 4.43 (ddd, 1H, H-2, *J* = 2.62, 7.98, 11.78 Hz), 5.17 (dd, 1H, H-3, *J* = 9.30, 10.6635 Hz), 5.78 (d, 1H, NHAc, *J* = 9.20 Hz), 6.10 (d, 1H, H-1, *J* = 3.79 Hz).

^{13}C NMR ($CDCl_3$): 18.98, 20.94, 21.00, 23.03, 28.94, 51.67, 62.06, 65.88, 70.21, 71.30, 91.30, 100.00, 169.04, 170.12, 171.95.

m/z calculated: 345.14

m/z recorded: 368.2 (with sodium)

Formation of benzyl 2-acetamido-3-*O*-benzyl-2-deoxy-4,6-*O*-isopropylidene-α,β-D-glucopyranoside (5α/β) from 2-acetamido-2-deoxy-4,6-*O*-isopropylidene-α,β-D-glucopyranose (3α/β).

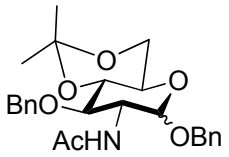

5α/β

To an ice-cold solution of **3α/β** (2.34 g, 8.96 mmol) in dimethyl formamide (100 mL), barium oxide (13.74 g, 89.60 mmol) and barium hydroxide octahydrate (5.653 g, 17.92 mmol), benzyl bromide (6.38 mL) was added dropwise via syringe. Stirring was continued for 2 hours at 0 °C, then the reaction was checked for completeness by TLC (3 : 1 ethyl acetate : methanol). The reaction mixture was then diluted with methylene chloride (100 mL), filtered, and the inorganic layer was washed twice with methylene chloride (50 mL). The combined organic solutions were washed three times with deionized water (50 mL), then dried over magnesium sulfate and filtered. The solution was then evaporated at 80 °C to an oil; the oil was then stirred with deionized water (30 mL) and hexanes (30 mL) to afford a white solid in 58% yield. The solid was filtered off and recrystallized from ethanol to afford a white powder of the β anomer. The mother

liquor was evaporated to a solid and column chromatography (1 : 1 hexane : ethyl acetate) to give the α anomer.

^{1}H NMR ($CDCl_3$): δ 1.43 (s, 3H, CH_3), 1.50 (s, 3H, CH_3), 1.84 (s, 3H, NHAc), 3.30-3.41 (m, 2H, H-2, H-5), 3.73 (dd, 1H, H-3, *J* = 8.84, 9.52 Hz), 3.82 (dd, 1H, H-4, *J* = 10.22, 10.74 Hz), 3.95 (dd, 1H, H-6, *J* = 4.66, 10.02 Hz), 3.99 (dd, 1H, H-6, *J* = 8.08, 9.32 Hz), 4.57 (dd, 2H, PhCH$_2$, *J* = 12.09, 18.17 Hz), 4.84 (dd, 2H, PhCH$_2$, *J* = 12.49, 12.65 Hz), 4.91 (d, 1H, H-1, *J* = 12.09 Hz), 5.41 (d, 1H, NHAc, *J* = 7.84 Hz), 7.27-7.37 (m, 10H, PhCH$_2$).

^{13}C NMR ($CDCl_3$): δ 19.07, 23.52, 66.08, 71.13, 76.85, 99.26, 127.66, 127.92, 127.99, 128.09, 128.30, 128.40, 137.18, 138.65.

m/z calculated: 441.22

m/z recorded: 464.1 (with sodium)

Formation of 2-acetamido-3-*O*-benzyl-2-deoxy-α,β-D-glucopyranoside (6α/β) from benzyl 2-acetamido-3-*O*-benzyl-2-deoxy-4,6-*O*-isopropylidene-α,β-D-glucopyranoside (5α/β).

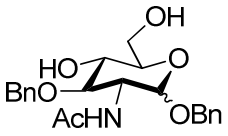

6α/β

5α/β (0.42 g, 0.95 mmol) was dissolved in 1,4-dioxane (10 mL), then 1 : 9 trifloroacetic acid (3 mL) : deionized water (27 mL) was added. The reaction mixture was checked for completeness by TLC (3 : 1 ethyl acetate : methanol). The mixture was then neutralized with saturated sodium bicarbonate (30 mL) and diluted with methylene

chloride (150 mL) and filtered. The organics were washed three times with deionized water (50 mL) and dried over magnesium sulfate and filtered. The solvent was then removed *en vacuo* and then re-dissolved into methylene chloride (50 mL). The solution was placed in the freezer overnight and the precipitate was collected. The process was repeated three times for precipitate collection. The precipitate collected was a white powder in 92% yield.

^{1}H NMR (d_6-DMSO): δ 1.79 (s, 1H, NHAc), 3.17 (ddd, 1H, H-5, *J* = 2.13, 5.92, 9.56 Hz), 3.27-3.77 (m, 3H, H-2, H-6), 4.42-4.48 (m, 1H, H-3), 4.56 (dd, 2H, PhCH_2, *J* = 8.68, 11.32 Hz), 4.67 (dd, 1H, H-4, *J* = 10.38, 23.87 Hz), 4.79 (dd, 2H, PhCH_2, *J* = 8.34, 12.02 Hz), 5.24 (d, 1H, H-1, *J* = 6.44 Hz), 7.23-7.43 (m, 10H, PhCH_2), 7.87 (d, 1H, NHAc, *J* = 9.12 Hz).

^{13}C NMR (d_6-DMSO): δ 22.96, 23.39, 61.36, 69.89, 70.60, 73.81, 74.05, 77.51, 83.19, 100.93, 127.56, 127.69, 127.78, 127.81, 127.82, 127.98, 128.19, 128.41, 128.61, 128.67, 138.52, 138.51, 139.73, 169.36, 169.73.

m/z calculated: 401.18

m/z recorded: 424.1 (with sodium)

Formation of benzyl 2--acetamido-3-*O*-benzyl-2-deoxy-4,6-di-*O*-methylsulfonyl -α,β-D-glucopyranoside (7α/β) from 2-acetamido-3-*O*-benzyl-2-deoxy-α,β-D-glucopyranoside (6α/β).

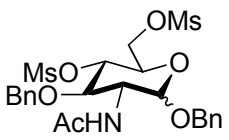

7α/β

To an ice-cold mixture of **6α/β** (0.100 g, 0.249 mmol) and pyridine (5 mL) under nitrogen atmosphere, mesyl chloride (0.06 mL) was added via syringe. The mixture was stirred for ninety minutes at 0 °C, then for one hour at room temperature. Two to three pieces of ice (~ 2.0 g) were added and the mixture was diluted in half with deionized water (5 mL). Stirring then continued for three hours and followed by filtering of the suspension. The solid was washed with deionized water (20 mL) and then recrystallized from methanol. The solid collected was white upon drying and was collected in 70% yield.

^{1}H NMR (d_6-DMSO): δ 1.82 (s, 3H, NHAc), 3.15 (s, 3H, CH_3), 3.21 (s, 3H, CH_3), 3.87-3.91 (m, 1H, H-2), 3.96 (ddd, 1H, H-5, *J* = 2.22, 5.72, 9.72 Hz), 4.34 (dd, 1H, H-3, *J* = 5.82, 11.54 Hz), 4.46-4.81 (m, 8H, PhCH$_2$,PhCH$_2$, H-1, H-3, H-6), 8.13 (d, 1H, NHAc, *J* = 8.68 Hz).

^{13}C NMR (d_6-DMSO): δ 22.77, 22.83, 36.82, 36.99, 38.30, 54.46, 68.04, 70.04, 70.67, 73.42, 76.81, 78.88, 99.98, 127.25, 127.33, 127.49, 127.57, 127.85, 127.91, 128.11, 128.18, 137.52, 137.66, 168.93, 169.23.

m/z calculated: 557.14

m/z recorded: 580.1 (with sodium)

Formation of methyl 2-acetamido-2-deoxy-α-D-glucopyranose (8α/β) from 2-acetamido-2-deoxy-α-D-glucopyranose (2α/β).

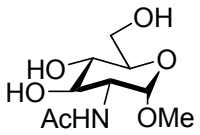

8α/β

Gaseous hydrochloric acid was bubble through methanol (25 mL) for 15 minutes and then added to a solution of **2α/β** (3.00 g, 13.56 mmol) and methanol (25 mL). The reaction was checked by TLC (3 : 1 ethyl acetate : methanol) and showed no change in Rf value. The reaction was neutralized with saturated sodium bicarbonate (30 mL) and filtered. The solvent was removed *en vacuo* and a pale yellow powder resulted in 96% yield.

^{1}H NMR (d_6-DMSO): δ 1.83 (s, 3H, NHAc), 3.04-3.15 (m, 1H, H-5), 3.24 (s, 3H, CH_3) 3.26-3.35 (m, 1H, H-3), 3.37-3.52 (m, 2H, H-6), 3.70-3.60 (m, 2H, H-2, H-4), 4.53 (d, 1H, H-1, J = 3.48 Hz), 4.63-4.89 (m, 3H, OH), 7.71 (d, 1H, NHAc, J = 8.08 Hz),

^{13}C NMR (d_6-DMSO): δ 23.07, 23.55, 54.26, 54.71, 61.32, 70.90, 71.17, 71.30, 73.15, 98.38, 127.66, 169.52, 169.86.

m/z calculated: 235.11

m/z recorded: 258.2 (with sodium)

Formation of methyl 2-acetamido-2-deoxy-4,6-*O*-isopropylidene–α,β-D-glucopyranose (9α/β) from methyl 2-acetamido-2-deoxy-α-D-glucopyranose (8α/β).

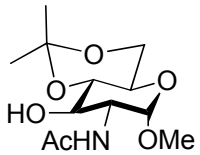

9α/β

At 80-85 °C a solution of **8α/β**, dimethyl formamide, and *p*-toluene sulfonic acid monohydrate were stirred for 15 minutes, then 2,2-dimethoxypropane was added via syringe. Stirring was continued at 80-85 °C for until the reaction showed completion by TLC (3 : 1 ethyl acetate : methanol). The mixture was then neutralized with sodium carbonate and filtered. The resulting solution was washed with methylene chloride, and the remaining solvents were removed *en vacuo* to afford a pale yellow powder. The removal of solvents was facilitated by azeotroping the dimethyl formamide with toluene.

^{1}H NMR (d_6-DMSO): δ 1.44 (s, 3H, CH_3), 1.53 (s, 3H, CH_3), 1.73 (s, 1H, OH), 2.07 (s, 3H, NHAc), 3.37 (s, 3H, CH_3), 3.58-3.64 (m, 2H, H-3, H-4), 3.72-3.96 (m, 3H, H-5, H-6), 4.17 (ddd, 1H, H-2, J = 2.50, 7.46, 11.36 Hz), 4.67 (d, 1H, H-1, J = 3.84 Hz), 5.92 (d, 1H, NHAc, J = 8.60 Hz).

^{13}C NMR (d_6-DMSO): δ 19.04, 23.35, 29.08, 31.42, 36.49, 54.18, 55.14, 63.17, 71.26, 98.71, 99.86, 162.54.

m/z calculated: 275.14

m/z recorded: 300.00 (with sodium)

Formation of 2-acetamido-1,3-di-*O*-acetyl-2-deoxy-α,β-D-glucopyranoside (10α/β) from 2-acetamido-1,3-di-*O*-acetyl-2-deoxy-4,6-*O*-isopropylidene-α,β-D-glucopyranoside (4α/β).

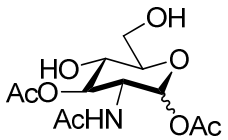

10α/β

4α/β was dissolved in 1,4-dioxane (30 mL), then 1 : 9 trifloroacetic acid (3 mL) : deionized water (27 mL) was added. The reaction mixture was stirred for thirty minutes, and checked for completeness by TLC (3 : 1 ethyl acetate : methanol). The mixture was then neutralized with saturated sodium bicarbonate (50 mL), diluted with methylene chloride (150 mL) and filtered. The organics were washed three times with deionized water (50 mL) and dried over magnesium sulfate and filtered. The solvent was then removed *en vacuo* and dissolved in methylene chloride (50 mL). The solution was placed in the freezer overnight and the precipitate was collected. The process was repeated three times for precipitate collection. The precipitate collected was a white powder in a 68% yield.

^{1}H NMR (d_6-DMSO): δ 1.80 (s, 3H, NHAc), 2.01 (s, 3H, OAc), 2.18 (s, 3H, OAc), 3.36 (s, 2H, OH), 3.99 (dd, 1H, H-4, *J* = 2.12, 12.28 Hz), 4.12 (ddd, 1H, H-5, *J* = 3.29, 6.25, 12.61 Hz), 4.17 (dd, 1H, H-3, *J* = 3.88, 12.61 Hz), 4.24 (ddd, 1H, H-2, *J* = 0.01, 2.87, 11.71 Hz), 4.99 (dd, 1H, H-6, *J* = 9.73, 9.87 Hz), 5.17 (dd, 1H, H-6, *J* = 9.53, 11.05 Hz), 5.93 (d, 1H, H-1, *J* = 3.51 Hz), 8.06 (d, 1H, NHAc, *J* = 8.78 Hz)

^{13}C NMR (d_6-DMSO): δ 20.94, 21.30, 22.67, 50.29, 61.78, 68.48, 69.54, 70.33, 90.12, 169.59, 169.65, 170.08, 170.20, 170.30, 170.42, 170.50, 170.58.

m/z calculated: 305.11

m/z recorded: 308.2

Formation of 2-acetamido-1,3-di-*O*-acetyl-2-deoxy-4,6-di-*O*-methylsulfonyl-α,β-D-glucopyranoside (11α/β) from 2-acetamido-1,3-di-*O*-acetyl-2-deoxy-α,β-D-glucopyranoside (10α/β).

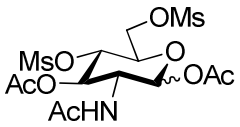

11α/β

To an ice-cold mixture of **10α/β** (0.073 g, 0.240 mmol) and pyridine (5 mL) under nitrogen atmosphere, mesyl chloride (0.06 mL,) was added via syringe. The mixture was stirred for ninety minutes at 0 °C, then for one hour at room temperature. Two to three pieces of ice (~ 2.0 g) were added and the mixture was diluted in half with deionized water (5 mL). Stirring then continued for three hours and followed by filtering of the suspension. The solid was washed with deionized water (20 mL) and then recrystallized from methanol. The precipitate collected was a white powder in a 21% overall yield.

^{1}H NMR (d_6-DMSO): δ 1.67 (s, 3H, NHAc), 2.20 (s, 3H, OAc), 2.33 (s, 3H, OAc), 2.91 (s, 3H, CH_3), 3.04 (s, 3H, CH_3), 3.89-3.97 (m, 2H, H-2,H-5), 4.52-4.68 (m, 2H, H-6), 4.74-4.91 (m, 2H, H-3,H-4), 5.36 (d, 1H, H-1, *J* = 3.51 Hz), 7.82 (d, 1H, NHAc, *J* = 8.51 Hz).

m/z calculated: 461.07

m/z recorded: 481.3 (with sodium)

Synthesis of 2-acetamido-2,6-deoxy-α,β-D-glucopyranose

Attempted formation of benzyl 2-acetamido-3-*O*-benzyl-2,6-deoxy-4-*O*-methylsulfonyl-α,β-D-glucopyranoside (11α/β) from benzyl 2--acetamido-3-*O*-benzyl-2-deoxy-4,6-di-*O*-methylsulfonyl -α,β-D-glucopyranoside (7α/β).

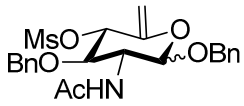

12α/β

To mixture of **7α/β** (0.100 g, 0.180 mmol) and THF (2 mL) under nitrogen, DBU (0.036 mL) was added via syringe. The mixture was stirred for 3 hours and checked by TLC (3 : 1 ethyl acetate: methanol), which showed no indication of product formation. The reaction then was allowed to stir overnight, again giving no indication of product formation by TLC. Another equivalence of DBU (0.036 mL) was added, and the reaction was allowed to stir. for twenty-four hours. After the twenty-four hours, no indication that product formation had occurred.

Formation of benzyl 2-acetamido-3-*O*-benzyl-2,6-deoxy-4-*O*-methylsulfonyl-α,β-D-glucopyranoside (11α/β) from benzyl 2--acetamido-3-*O*-benzyl-2-deoxy-4,6-di-*O*-methylsulfonyl -α,β-D-glucopyranoside (7α/β).

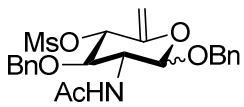

12α/β

To mixture of **7α/β** (0.078 g, 0.140 mmol) and acetonitrile (2 mL) under nitrogen, DBU (0.031 mL) was added via syringe. The mixture was stirred for 3 hours and checked via TLC (3 : 1 ethyl acetate : methanol), which gave an indication of product formation (appearance of a second more polar spot). Column chromatography was performed using an eluent of 3 : 1 ethyl acetate : methanol.

^{1}H NMR (d_6-DMSO): δ 1.82 (s, 3H, NHAc), 3.21 (m, 3H, CH_3), 3.47-3.55 (m, 1H, H-2), 3.67 (dd, 1H, H-3, J = 4.14, 12.92 Hz), 3.89 (d, 1H, H-4, J = 3.26 Hz), 4.49-4.57 (m, 4H,

PhCH$_2$,PhCH$_2$), 4.69 (d, 1H, H-6, *J* = 11.79 Hz), 4.85 (d, 1H, H-4, *J* = 11.79 Hz), 5.27 (d, 1H, NHAc, *J* = 8.28 Hz), 5.83 (d, 1H, H-1, *J* = 6.27 Hz).

^{13}C NMR (d$_6$-DMSO): δ 29.93, 29.96, 37.29, 44.95, 49.59, 64.82, 64.41, 71.65, 72.24, 73.51, 127.91, 127.99, 128.00, 128.39, 128.43, 137.72, 170.26, 170.97, 175.94, 177.06.

m/z calculated: 461.15

m/z recorded: 472.5 (loss of methyl, with sodium)

Attempted formation of 2-acetamido-1,3-di-*O*-acetyl-2,6-deoxy-4-*O*-methylsulfonyl-α,β-D-glucopyranoside (13α/β) from 2-acetamido-1,3-di-*O*-acetyl-2-deoxy-4,6-di-*O*-methylsulfonyl-α,β-D-glucopyranoside (11α/β).

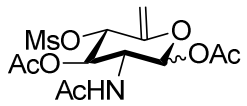

13α/β

To mixture of **11α/β** (0.078 g, 0.140 mmol) and acetonitrile (2 mL) under nitrogen, DBU (0.031 mL) was added by syringe. The mixture was stirred for 3 hours and checked using TLC (3 : 1 ethyl acetate : methanol), which gave no indication of product formation.

NMR Characterization of Carbohydrates

General experimental procedure for characterization

All NMR spectra, used in the NMR characterize ation, were recorded on a Bruker Avance III 400 MHz NMR spectrometer with broadband probe, or Bruker Avance II 400

MHz NMR spectrometer with indirect detection probe with reference to the deuterium signal of the solvent. All nuclei were excited at their respective resonance frequencies. Chemical Shifts were reported in parts per million (ppm) from a standard of tetramethylsilane in $CDCl_3$ (0.1% w/v TMS). All spectra are included for reference in Appendix A.

Characterization of *N*-glycosides

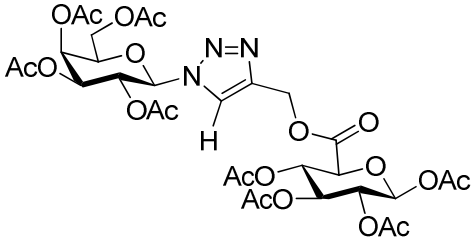

14

^{1}H for **14**

The parameters included use of: the zg30 pulse program, DQD acquisition mode, 512 scans collected, sw = 20.6885 ppm, o1 = 2470.97 Hz, delay (D1) = 1.0 s, 90° = 7.83 μs, and rg = 143.7 for receiver gain.

^{1}H ($CDCl_3$) δ 1.89 (s, 3H, O<u>Ac</u>), 2.00 (s, 3H, O<u>Ac</u>), 2.01 (s, 3H, O<u>Ac</u>), 2.02 (s, 3H, O<u>Ac</u>), 2.03 (s, 3H, O<u>Ac</u>), 2.06 (s, 3H, O<u>Ac</u>), 2.12 (s, 3H, O<u>Ac</u>), 2.24 (s, 3H, O<u>Ac</u>), 4.13-

4.23 (m, 3H, H-5, H-6), 5.12-5.33 (m, 6H, C-H, H-2, H-3, H-4,), 5.54-5.64 (m, 2H, H-2, H-4), 5.76 (d, 1H, H-1, *J* = 7.72 Hz), 5.84 (d, 1H, H-1, *J* = 9.35 Hz), 7.95 (s, 1H, triazole ring).

^{13}C-CPD for **14**

This experiment is a proton decoupled carbon. The parameters included use of: nucleus one as carbon while nucleus two as proton, the zgpg30 pulse program, qsim acquisition mode, 15,360 scans collected, sw = 238.3238 ppm, ^{13}C o1 = 10060.80 Hz, ^{1}H o2 = 1600.52 Hz, delay (D1) = 2.0 s, 90° = 14.90 μs, and rg = 101.6 for receiver gain.

^{13}C ($CDCl_3$) δ 20.26, 20.46, 20.51, 20.53, 20.56, 20.66, 20.70, 20.79, 58.80, 61.21, 66.80, 67.73, 68.65, 70.09, 70.76, 71.81, 72.64, 74.06, 86.25, 91.22, 99.99, 123.22, 142.08, 166.45, 168.83, 169.05, 169.22, 169.46, 169.83, 170.04, 170.35.

^{13}C DEPT-135 for **14**

The parameters included use of: nucleus one as carbon while nucleus two was proton, dept135 pulse program, DQD acquisition mode, 1024 scans collected, sw = 238.3238 ppm, ^{13}C o1 = 10060.80 Hz, ^{1}H o2 = 1600.52 Hz, delay (D1) = 2.0 s, 90° = 14.90 μs, and rg = 2050 for receiver gain.

t_1 relaxation experiment for **14**

The parameters included use of: nucleus one and two as proton, the t1ir pulse program, F1 = undefined and F2 = DQD acquisition modes, 8 scans per experiment collected, F2

axis = 16384 experiments, F2 sw = 20.6885 ppm, F2 o1 = 2470.97 Hz, F1 axis = 10 experiments, F1 sw = 1.9995 ppm, F1 o1 = 2470.97 Hz, delay (D1) = 10 s, ^{1}H 90° = 7.83 μs, and rg = 71.8 for receiver gain.

t_2 relaxation experiment for **14**

The parameters included use of: nucleus one and two as proton, the t1ir pulse program, F1 = undefined and F2 = DQD acquisition modes, 8 scans per experiment collected, F2 axis = 16384 experiments, F2 sw = 20.6885 ppm, F2 o1 = 2470.97 Hz, F1 axis = 10 experiments, F1 sw = 1.9995 ppm, F1 o1 = 2470.97 Hz, delay (D1) = 10 s, ^{1}H 90° = 7.83 μs, and rg = 71.8 for receiver gain.

^{1}H-^{1}H COSY for **14**

The parameters included use of: nucleus one and two as proton, the cosygpqf pulse program, F1 = QF and F2 = DQD acquisition modes, 1 scan per experiment collected, F2 axis = 2048 experiments, nucleus 2 sw = 9.2425 ppm, nucleus 2 o1 = 1523.83 Hz, F1 axis = 128 experiments, nucleus 1 sw = 9.2425 ppm, nucleus 1 o1 = 1523.83 Hz, delay (D1) = 5.09215879 s, ^{1}H 90° = 7.83 μs, and rg = 64 for receiver gain.

^{1}H-^{13}C HSQC for **14**

The parameters included use of: nucleus one as carbon and two as proton, the hsqcetgpsi2 pulse program, F1 = Echo-antiecho and F2 = qsim acquisition modes, 2 scans per experiment collected, F2 axis = 2048 experiments, nucleus 2 sw = 165.6500 ppm, nucleus 2 o1 = 7543.36 Hz, F1 axis = 2048 experiments, nucleus 1 sw = 9.2558 ppm,

nucleus o1 = 1560.93 Hz, delay (D1) = 1.41562200 s, ^{1}H 90° = 7.83 μs, ^{13}C 90° = 14.90 μs, and rg = 2050 for receiver gain.

^{1}H-^{13}C HMQC for **14**

The parameters included use of: nucleus one as carbon and two as proton, the hmqcgpqf pulse program, F1 = QF and F2 = DQD acquisition modes, 16 scans per experiment collected, F2 axis = 1024 experiments, nucleus 2 sw = 165.6392 ppm, nucleus 2 o1 = 7545.01 Hz, F1 axis = 128 experiments, nucleus 1 sw = 6.9887 ppm, nucleus 1 o1 = 1891.89 Hz, delay (D1) = 1.44368005 s, ^{1}H 90° = 7.83 μs, ^{13}C 90° = 14.90 μs, and rg = 20642.5 for receiver gain.

^{1}H-^{13}C HMBC for **14**

The parameters included use of: nucleus one as carbon and two as proton, the hmbcgplpndqf pulse program, F1 = QF and F2 = DQD acquisition modes, 8 scans per experiment collected, F2 axis = 2048 experiments, nucleus 2 sw = 165.0000 ppm, nucleus 2 o1 = 10044.78 Hz, F1 axis = 2048 experiments, nucleus 1 sw = 6.9887 ppm, nucleus 1 o1 = 1891.89 Hz, delay (D1) = 1.16003203 s, ^{1}H 90° = 7.83 μs, ^{13}C 90° = 14.90 μs, and rg = 16384 for receiver gain.

^{1}H-^{1}H NOESY for **14**

The parameters included use of: nucleus one and two as proton, the noesyph pulse program, F1 = States-TPPI and F2 = DQD acquisition modes, 16 scans per experiment collected, F2 axis = 6144 experiments, nucleus 2 sw = 9.0288 ppm, nucleus 2 o1 =

1550.23 Hz, F1 axis = 256 experiments, nucleus 1 sw = 9.0288 ppm, nucleus 1 o1 = 1550.23 Hz, delay (D1) = 2.50000000 s, ^{1}H 90° = 7.83 μs, and rg = 256 for receiver gain.

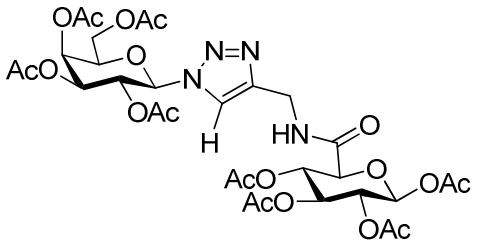

15

^{1}H for **15**

The parameters included use of: the zg30 pulse program, DQD acquisition mode, 512 scans collected, sw = 20.6885 ppm, o1 = 2470.97 Hz, delay (D1) = 1.0 s, 90° = 7.83 μs, and rg = 143.7 for receiver gain.

^{1}H ($CDCl_3$) δ 1.88 (s, 3H, O<u>Ac</u>), 2.00 (s, 3H, O<u>Ac</u>), 2.01 (s, 3H, O<u>Ac</u>), 2.04 (s, 3H, O<u>Ac</u>), 2.05 (s, 3H, O<u>Ac</u>), 2.09 (s, 3H, O<u>Ac</u>), 2.12 (s, 3H, O<u>Ac</u>), 2.22 (s, 3H, O<u>Ac</u>), 4.10-4.25 (m, 4H, H-5, H-6), 4.52 (quasi-ddd, 2H, CH_2, *J* = 5.88, 15.27, 39.96 Hz), 5.10 (dd, 1H, H-2, *J* = 8.12, 9.01 Hz), 5.19 (dd, 1H, H-4, *J* = 9.49, 9.61 Hz), 5.24 (dd, 1H, H-4, *J* = 3.43, 10.26 Hz), 5.29 (dd, 1H, H-3, *J* = 9.10, 18.27 Hz), 5.54-5.59 (m, 2H, H-2, H-3),

5.75 (d, 1H, H-1, *J* = 8.04 Hz), 5.81 (d, 1H, H-1, *J* = 9.28 Hz), 6.89 (t, 1H, N-H, *J* = 5.86 Hz), 7.84 (s, 1H, triazole ring).

^{13}C-CPD for **15**

This experiment is a proton decoupled carbon. The parameters included use of: nucleus one as carbon with nucleus two as proton, the zgpg30 pulse program, qsim acquisition mode, 15,360 scans collected, sw = 238.3238 ppm, ^{13}C o1 = 10060.80 Hz, ^{1}H o2 = 1600.52 Hz, delay (D1) = 2.0 s, 90° = 14.90 μs, and rg = 101.6 for receiver gain.

^{13}C ($CDCl_3$) δ 20.26, 20.46, 20.51, 20.54, 20.56, 20.66, 20.70, 20.79, 58.80, 61.21, 66.80, 67.73, 68.65, 70.09, 70.78, 71.81, 72.64, 74.06, 86.25, 91.22, 99.99, 123.22, 142.08, 166.45, 168.83, 169.05, 169.22, 169.46, 169.83, 170.04, 170.35.

^{13}C DEPT-135 for **15**

The parameters included use of: nucleus one as carbon and nucleus two as proton, dept135 pulse program, DQD acquisition mode, 2096 scans collected, sw = 238.3238 ppm, ^{13}C o1 = 10060.80 Hz, ^{1}H o2 = 1600.52 Hz, delay (D1) = 2.0 sec., 90° = 14.90 μs, and rg = 26008 for receiver gain.

t_1 relaxation experiment for **15**

The parameters included use of: nucleus one and two as proton, the t1ir pulse program, F1 = undefined and F2 = DQD acquisition modes, 8 scans per experiment collected, F2

axis = 16384 experiments, F2 sw = 20.6885 ppm, F2 o1 = 2470.97 Hz, F1 axis = 10 experiments, F1 sw = 1.9995 ppm, F1 o1 = 2470.97 Hz, delay (D1) = 15 s, ^{1}H 90° = 7.83 μs, and rg = 71.8 for receiver gain.

t_2 relaxation experiment for **15**

The parameters included use of: nucleus one and two as proton, the t1ir pulse program, F1 = undefined and F2 = DQD acquisition modes, 8 scans per experiment collected, F2 axis = 16384 experiments, F2 sw = 20.6885 ppm, F2 o1 = 2470.97 Hz, F1 axis = 10 experiments, F1 sw = 1.9995 ppm, F1 o1 = 2470.97 Hz, delay (D1) = 15 s, ^{1}H 90° = 7.83 μs, and rg = 71.8 for receiver gain.

^{1}H-^{1}H COSY for **15**

The parameters included use of: nucleus one and two as proton, the cosygpqf pulse program, F1 = QF and F2 = DQD acquisition modes, 1 scan per experiment collected, F2 axis = 2048 experiments, nucleus 2 sw = 7.8888 ppm, nucleus 2 o1 = 1800.03 Hz, F1 axis = 2048 experiments, nucleus 1 sw = 7.8888 ppm, nucleus 1 o1 = 1800.03 Hz, delay (D1) = 4.86810923 s, ^{1}H 90° = 7.83 μs, and rg = 25.4 for receiver gain.

^{1}H-^{13}C HSQC for **15**

The parameters included use of: nucleus one as carbon and two as proton, the hsqcetgpsi2 pulse program, F1 = Echo-antiecho and F2 = qsim acquisition modes, 2 scans per experiment collected, F2 axis = 1024 experiments, nucleus 2 sw = 165.6500 ppm, nucleus 2 o1 = 7543.36 Hz, F1 axis = 256 experiments, nucleus 1 sw = 9.4096 ppm,

nucleus 1 o1 = 1588.63 Hz, delay (D1) = 1.54935706 s, ^{1}H 90° = 7.83 μs, ^{13}C 90° = 14.90 μs, and rg = 18390.4 for receiver gain.

^{1}H-^{13}C HMQC for **15**

The parameters included use of: nucleus one as carbon and two as proton, the hmqcbiqf pulse program, F1 = QF and F2 = DQD acquisition modes, 16 scans per experiment collected, F2 axis = 1024 experiments, nucleus 2 sw = 154.3231 ppm, nucleus 2 o1 = 6980.49 Hz, F1 axis = 512 experiments, nucleus 1 sw = 7.8888 ppm, nucleus 1 o1 = 1800.33 Hz, delay (D1) = 1.46354496 s, ^{1}H 90° = 7.83 μs, ^{13}C 90° = 14.90 μs, and rg = 256 for receiver gain.

^{1}H-^{13}C HMBC for **15**

The parameters included use of: nucleus one as carbon and two as proton, the hmbclpndqf pulse program, F1 = QF and F2 = DQD acquisition modes, 32 scan per experiment collected, F2 axis = 4096 experiments, nucleus 2 sw = 222.0951 ppm, nucleus 2 o1 = 10044.29 Hz, F1 axis = 512 experiments, nucleus 1 sw = 7.8888 ppm, nucleus 1 o1 = 1800.33 Hz, delay (D1) = 1.34762800 s, ^{1}H 90° = 7.83 μs, ^{13}C 90° = 14.90 μs, and rg = 50.8 for receiver gain.

^{1}H-^{1}H NOESY for **15**

The parameters included use of: nucleus one and two as proton, the noesyph pulse program, F1 = States-TPPI and F2 = DQD acquisition modes, 16 scan per experiment collected, F2 axis = 2048 experiments, nucleus 2 sw = 9.4096 ppm, nucleus 2 o1 =

1588.63 Hz, F1 axis = 256 experiments, nucleus 1 sw = 9.4096 ppm, nucleus 1 o1 = 1588.63 Hz, delay (D1) = 5.09871292 s, ^{1}H 90° = 7.83 μs, and rg = 64 for receiver gain.

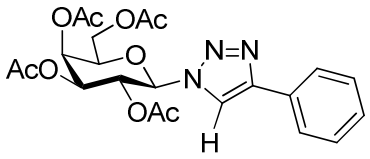

16

^{1}H for **16**

The parameters included use of: the zg30 pulse program, DQD acquisition mode, 256 scans collected, sw = 20.5514 ppm, o1 = 2471.09 Hz, delay (D1) = 1.0 s, 90° = 7.83 μs, and rg = 203 for receiver gain.

^{1}H ($CDCl_3$) δ 1.90 (s, 3H, O<u>Ac</u>), 2.02 (s, 3H, O<u>Ac</u>), 2.05 (s, 3H, O<u>Ac</u>), 2.25 (s, 3H, O<u>Ac</u>), 4.15-4.27 (m, 3H, H-5, H-6), 5.27 (dd, 1H, H-4, *J* = 3.31, 10.31 Hz), 5.58 (dd, 1H, H-3, *J* = 0.64, 3.28 Hz), 5.64 (dd, 1H, H-2, *J* = 9.80, 9.80 Hz), 5.90 (d, 1H, H-1, *J* = 9.36 Hz), 7.35 (t, 1H, Ar-H , *J* = 7.28 Hz), 7.44 (t, 2H, Ar-H , *J* = 7.48 Hz), 7.86 (d, 2H, Ar-H , *J* = 7.03 Hz), 8.05 (s, 1H, NH).

^{13}C-CPD for **16**

This experiment is a proton decoupled carbon. The parameters included use of: nucleus one as carbon while nucleus two as proton, the zgpg30 pulse program, qsim acquisition

mode, 15,360 scans collected, sw = 238.8848 ppm, ^{13}C o1 = 10061.31 Hz, ^{1}H o2 = 1600.60 Hz, delay (D1) = 2.0 s, 90° = 14.90 μs, and rg = 2050 for receiver gain.

^{13}C ($CDCl_3$) δ 20.28, 20.50, 20.65, 20.69, 61.23, 66.95, 67.79, 70.90, 74.14, 86.38, 117.82, 125.95, 128.54, 128.86, 130.01, 148.49, 169.17, 169.81, 169.97, 170.34.

^{13}C DEPT-135 for **16**

The parameters included use of: nucleus one as carbon with nucleus two as proton, dept135 pulse program, DQD acquisition mode, 1024 scans collected, sw = 238.8848 ppm, ^{13}C o1 = 10061.31 Hz, ^{1}H o2 = 1600.60 Hz, delay (D1) = 2.0 s, 90° = 14.90 μs, and rg = 2050 for receiver gain.

t_1 relaxation experiment for **16**

The parameters included use of: nucleus one and two as proton, the t1ir pulse program, F1 = undefined and F2 = DQD acquisition modes, 8 scans per experiment collected, F2 axis = 16384 experiments, F2 sw = 20.6885 ppm, F2 o1 = 2470.97 Hz, F1 axis = 10 experiments, F1 sw = 1.9995 ppm, F1 o1 = 2470.97 Hz, delay (D1) = 10 s, ^{1}H 90° = 7.83 μs, and rg = 71.8 for receiver gain.

t_2 relaxation experiment for **16**

The parameters included use of: nucleus one and two as proton, the t1ir pulse program, F1 = undefined and F2 = DQD acquisition modes, 8 scans per experiment collected, F2 axis = 16384 experiments, F2 sw = 20.6885 ppm, F2 o1 = 2470.97 Hz, F1 axis = 10

experiments, F1 sw = 1.9995 ppm, F1 o1 = 2470.97 Hz, delay (D1) = 10 s, ^{1}H 90° = 7.83 μs, and rg = 71.8 for receiver gain.

^{1}H-^{1}H COSY for **16**

The parameters included use of: nucleus one and two as proton, the cosygpqf pulse program, F1 = QF and F2 = DQD acquisition modes, 1 scan per experiment collected, F2 axis = 2048 experiments, nucleus 2 sw = 10.3443 ppm, nucleus 2 o1 = 1553.64 Hz, F1 axis = 2048 experiments, nucleus 1 sw = 10.3443 ppm, nucleus 1 o1 = 1553.64 Hz, delay (D1) = 1.43077695 s, ^{1}H 90° = 7.83 μs, and rg = 64 for receiver gain.

^{1}H-^{13}C HSQC for **16**

The parameters included use of: nucleus one as carbon and two as proton, the hsqcetgpsi2 pulse program, F1 = Echo-antiecho and F2 = qsim acquisition modes, 2 scans per experiment collected, F2 axis = 1024 experiments, nucleus 2 sw = 165.6500 ppm, nucleus 2 o1 = 7543.36 Hz, F1 axis = 1024 experiments, nucleus 1 sw = 10.3443 ppm, nucleus 1 o1 = 1553.64 Hz, delay (D1) = 1.47194195 s, ^{1}H 90° = 7.83 μs, ^{13}C 90° = 14.90 μs, and rg = 18390.4 for receiver gain.

^{1}H-^{13}C HMQC for **16**

The parameters included use of: nucleus one as carbon and two as proton, the hmqcbiqf pulse program, F1 = QF and F2 = DQD acquisition modes, 16 scans per experiment collected, F2 axis = 1024 experiments, nucleus 2 sw = 154.3231 ppm, nucleus 2 o1 = 6980.49 Hz, F1 axis = 256 experiments, nucleus 1 sw = 10.3443 ppm, nucleus 1 o1 =

1553.64 Hz, delay (D1) = 1.50143301 s, ^{1}H 90° = 7.83 μs, ^{13}C 90° = 14.90 μs, and rg = 256 for receiver gain.

^{1}H-^{13}C HMBC for **16**

The parameters included use of: nucleus one as carbon and two as proton, the hmbclpndqf pulse program, F1 = QF and F2 = DQD acquisition modes, 32 scans per experiment collected, F2 axis = 4096 experiments, nucleus 2 sw = 222.0951 ppm, nucleus 2 o1 = 10044.29 Hz, F1 axis = 512 experiments, nucleus 1 sw = 10.3443 ppm, nucleus 1 o1 = 1553.64 Hz, delay (D1) = 1.38777006 s, ^{1}H 90° = 7.83 μs, ^{13}C 90° = 14.90 μs, and rg = 16384 for receiver gain.

^{1}H-^{1}H NOESY for **16**

The parameters included use of: nucleus one and two as proton, the noesyph pulse program, F1 = States-TPPI and F2 = DQD acquisition modes, 16 scans per experiment collected, F2 axis = 2048 experiments, nucleus 2 sw = 10.3443 ppm, nucleus 2 o1 = 1553.64 Hz, F1 axis = 1024 experiments, nucleus 1 sw = 10.3443 ppm, nucleus 1 o1 = 1553.64 Hz, delay (D1) = 2.00286698 s, ^{1}H 90° = 7.83 μs, and rg = 161.3 for receiver gain.

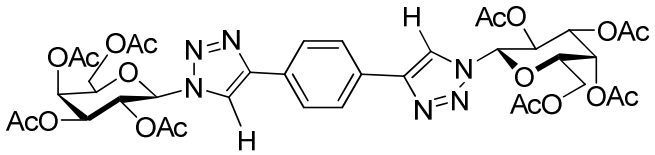

17

^{1}H for **17**

The parameters included use of: the zg30 pulse program, DQD acquisition mode, 256 scans collected, sw = 20.6885 ppm, o1 = 2470.97 Hz, delay (D1) = 1.0 s, 90° = 7.83 μs, and rg = 143.7 for receiver gain.

^{1}H ($CDCl_3$) δ 1.92 (s, 6H, O<u>Ac</u>), 2.03 (s, 6H, O<u>Ac</u>), 2.06 (s, 6H, O<u>Ac</u>), 2.26 (s, 6H, O<u>Ac</u>), 4.17-4.27 (m, 6H, H-5, H-5, H-6, H-6), 5.29 (dd, 2H, H-3, J = 3.32, 10.32 Hz), 5.58 (dd, 2H, H-4, H-4, J = 0.60, 3.84 Hz), 5.65 (dd, 2H, H-2, H-2, J = 9.80, 9.80 Hz), 5.91 (d, 2H, H-1, H-1, J = 9.43 Hz), 7.95 (s, 4H, Ar-H), 8.10 (s, 1H, triazole ring).

^{13}C-CPD for **17**

This experiment is a proton decoupled carbon. The parameters included use of: nucleus one as carbon while nucleus two as proton, the zgpg30 pulse program, qsim acquisition mode, 10,240 scans collected, sw = 238.8848 ppm, ^{13}C o1 = 10061.31 Hz, ^{1}H o2 = 1600.60 Hz, delay (D1) = 2.0 s, 90° = 14.90 μs, and rg = 2050 for receiver gain.

^{13}C ($CDCl_3$) δ 20.27, 20.47, 20.61, 20.65, 61.23, 66.95, 67.84, 70.84, 74.11, 86.33, 118.02, 126.31, 130.07, 169.18, 169.79, 169.96, 170.32.

^{13}C DEPT-135 for **17**

The parameters included use of: nucleus one as carbon with nucleus two as proton, dept135 pulse program, DQD acquisition mode, 2096 scans collected, sw = 238.8848 ppm, ^{13}C o1 = 10060.31 Hz, ^{1}H o2 = 1600.60 Hz, delay (D1) = 2.0 s, 90° = 14.90 μs, and rg = 2050 for receiver gain.

t_1 relaxation experiment for **17**

The parameters included use of: nucleus one and two as proton, the t1ir pulse program, F1 = undefined and F2 = DQD acquisition modes, 8 scans per experiment collected, F2 axis = 16384 experiments, F2 sw = 20.6885 ppm, F2 o1 = 2470.97 Hz, F1 axis = 10 experiments, F1 sw = 1.9995 ppm, F1 o1 = 2470.97 Hz, delay (D1) = 25 s, ^{1}H 90° = 7.83 μs, and rg = 71.8 for receiver gain.

t_2 relaxation experiment for **17**

The parameters included use of: nucleus one and two as proton, the t1ir pulse program, F1 = undefined and F2 = DQD acquisition modes, 8 scans per experiment collected, F2 axis = 16384 experiments, F2 sw = 20.6885 ppm, F2 o1 = 2470.97 Hz, F1 axis = 10 experiments, F1 sw = 1.9995 ppm, F1 o1 = 2470.97 Hz, delay (D1) = 25 s, ^{1}H 90° = 7.83 μs, and rg = 71.8 for receiver gain.

^{1}H-^{1}H COSY for **17**

The parameters included use of: nucleus one and two as proton, the cosygpqf pulse program, F1 = QF and F2 = DQD acquisition modes, 1 scan per experiment collected, F2 axis = 2048 experiments, nucleus 2 sw = 10.1587 ppm, nucleus 2 o1 = 1661.44 Hz, F1 axis = 2048 experiments, nucleus 1 sw = 10.1587 ppm, nucleus 1 o1 = 1661.44 Hz, delay (D1) = 1.42668104 s, ^{1}H 90° = 7.83 μs, and rg = 57 for receiver gain.

^{1}H-^{13}C HSQC for **17**

The parameters included use of: nucleus one as carbon and two as proton, the hsqcetgpsi2 pulse program, F1 = Echo-antiecho and F2 = qsim acquisition modes, 2 scans per experiment collected, F2 axis = 2048 experiments, nucleus 2 sw = 165.6500 ppm, nucleus 2 o1 = 7543.36 Hz, F1 axis = 512 experiments, nucleus 1 sw = 10.0127 ppm, nucleus 1 o1 = 1521.18 Hz, delay (D1) = 1.58560598 s, ^{1}H 90° = 7.83 μs, ^{13}C 90° = 14.90 μs, and rg = 18390.4 for receiver gain.

^{1}H-^{13}C HMQC for **17**

The parameters included use of: nucleus one as carbon and two as proton, the hmqcbiqf pulse program, F1 = QF and F2 = DQD acquisition modes, 16 scans per experiment collected, F2 axis = 1024 experiments, nucleus 2 sw = 154.3231 ppm, nucleus 2 o1 = 6980.49 Hz, F1 axis = 256 experiments, nucleus 1 sw = 10.1587 ppm, nucleus 1 o1 = 1661.44 Hz, delay (D1) = 2.99938512 s, ^{1}H 90° = 7.83 μs, ^{13}C 90° = 14.90 μs, and rg = 287 for receiver gain.

^{1}H-^{13}C HMBC for **17**

The parameters included use of: nucleus one as carbon and two as proton, the hmbclpndqf pulse program, F1 = QF and F2 = DQD acquisition modes, 32 scans per experiment collected, F2 axis = 4096 experiments, nucleus 2 sw = 222.0951 ppm, nucleus 2 o1 = 10044.29 Hz, F1 axis = 256 experiments, nucleus 1 sw = 10.0127 ppm, nucleus 1 o1 = 1521.18 Hz, delay (D1) = 1.67121196 s, ^{1}H 90° = 7.83 μs, ^{13}C 90° = 14.90 μs, and rg = 16384 for receiver gain.

^{1}H-^{1}H NOESY for **17**

The parameters included use of: nucleus one and two as proton, the noesyph pulse program, F1 = States-TPPI and F2 = DQD acquisition modes, 16 scans per experiment collected, F2 axis = 4096 experiments, nucleus 2 sw = 10.0127 ppm, nucleus 2 o1 = 1521.18 Hz, F1 axis = 512 experiments, nucleus 1 sw = 10.0127 ppm, nucleus 1 o1 = 1521.18 Hz, delay (D1) = 2.17121196 s, ^{1}H 90° = 7.83 μs, and rg = 64 for receiver gain.

Statement of Problem

Staphylococcus aureus bacteria synthesize a capsular polysaccharide to evade detection and destruction by the host immune system. This capsular polysaccharide therefore is a logical target for carbohydrate-based antibiotics. If the polysaccharide can be disrupted by using mimics of the natural building blocks, it can be detected and eliminated by the immune system alone or in conjunction with traditional antibiotics. Both *N*-acetyl-D-fucosamine and *N*-((2R,3R,4R)-2,4-dihydroxy-6-methylene-5-oxo-tetrahydro-2H-pyran-3-yl)acetamide can be synthesized by using variants of the Horton synthesis. Nuclear magnetic resonance spectroscopy can provide confirmation of products present, structural conformations of the product, and the structures' dependence on solvent while in solution through a variety of one- and two-dimensional nuclear magnetic resonance techniques.

Results and Discussion

Synthesis of *N*-Acetyl-D-Fucosamine

The purpose of this project was to synthesize the naturally occurring product *N*-acetyl-D-fucosamine from the inexpensive precursor, *N*-acetyl-D-glucosamine. This synthesis was modeled after the Horton synthesis (Scheme 1), which was first published in 1978.[8] Upon review of the carbohydrates which occur in the type 5 and type 8 capsular polysaccharides of methicillin-resistant *Staphylococcus aureus*, one can see that *N*-acetyl-D-fucosamine is used in the construction of these polysaccharides. This naturally leads to modification of the synthesis to allow for mimics which can be used in enzymatic inhibition studies on bacteria which use these carbohydrates in synthesizing these capsular polysaccharides.

Improvements in the original synthesis (Scheme 1) allow for less product loss due to column chromatography and a more scalable synthesis if put into industrial use. These improvements (Table 1) show improved yields in all four of the first steps in either purification techniques or increased yields due to less loss due to column chromatography or improved reaction conditions.

Synthetic Step	Literature Yield	Literature Purification	Research Yield	Research Purification
4,6-*O*-Isopropylidene protected **3α/β** from **2α/β**	purchased protected	purchased protected	92 %	ethyl acetate and methylene chloride
1,3-*O*-Benzyl protected **5α/β** from **3α/β**	47 %	column chromatography	58 %	DI water, hexanes and 95 % ethanol
4,6-Hydroxy deprotected **6α/β** from **5α/β**	100 %	titration with petroleum ether	92 %	addition of methylene chloride and refrigeration
4,6-Di-*O*-methylsulfonyl protected **7α/β** from **6α/β**	78.6 %	trituration with water (multiple times)	70 %	trituration with water a single time

Table 1: Improvements shown for the first four steps of the Horton synthesis.

The Horton synthesis must also be modified when attempting the synthesis of *N*-((2R,3R,4R)-2,4-dihydroxy-6-methylene-5-oxo-tetrahydro-2H-pyran-3-yl)acetamide. The benzyl protected ethers must be removed via Parr hydrogenation, which would hydrogenate the double bond between C-5 and 6. To circumvent this problem an alternative protection scheme is proposed where the benzyl ethers are replaced by acetyl protecting groups. Mass spectrometry was performed using electro spray ionization, which often leads to detection of a molecule as a salt, this accounts for the sodium seen in the mass.

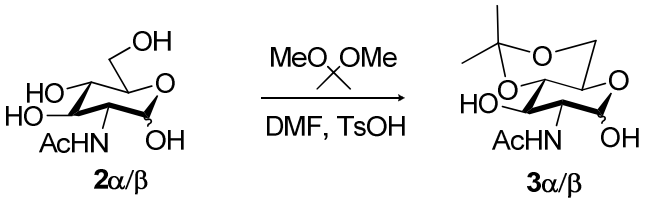

Equation 1: Formation of 4,6-*O*-isopropylidene-protected **3α/β** from **2α/β**.

The first step in synthesizing *N*-acetyl-D-fucosamine involves protection of O-4 and O-6 using an isopropylidene group yielding **3α/β** (Equation 1). This is seen in ^{1}H NMR by the appearance of two methyl signals at 1.31 and 1.44 ppm and in the ^{13}C NMR by resonance at 19.63 and 29.66 ppm. The two methyl peaks show differing shifts because they are locked into a ring in a chair conformation giving one an axial and one an equatorial disposition. Protons on the ring show sequential ordering by COSY, and correlation to their respective carbons by HSQC and HMQC. Additional confirmation of synthesis by mass spectrometry gave an *m/z* of 284.1 which accounts for the mass plus sodium. This reaction was purified in the literature by column chromatography; however

through the course of this research we have found a more practical and higher yielding procedure to purify by triturating. The reaction mixture is diluted with methylene chloride and ethyl acetate, and then triturated with 95% ethanol. The solid then would be forced out of solution and be vacuum filtered.

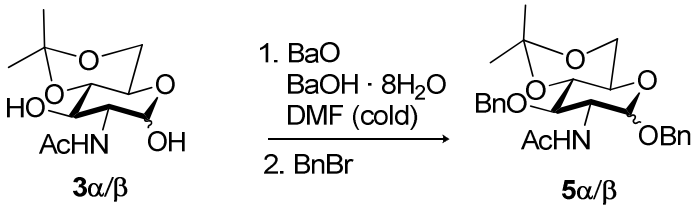

3α/β **5**α/β

Equation 2: Formation of 1,3-*O*-benzyl-protected **5α/β** from **3α/β**.

Following **3α/β**, protection of O-1 and O-3 through benzyl ethers was performed yielding **5α/β** (Equation 2). This is seen from ^{1}H NMR by the appearance of a multiplet between 7.27-7.37 ppm with integration of approximately 10 H and in the ^{13}C NMR by peaks between 127.66-138.65 ppm. ^{1}H NMR shows the anomeric proton with a chemical shift of 4.91 ppm, the other ring protons can then be assigned by following the cross-peak signals in the COSY spectrum, and correlation to carbons by HSQC and HMQC. Additional confirmation of synthesis by mass spectrometry gave an *m/z* of 464.2 which accounts for the mass plus sodium. Upon workup and subsequent stirring with deionized water and hexanes, it was found that upon addition of 95% ethanol a layer of solid product was forced out of solution between the hexanes and water layers. This increased the yield over performing column chromatography from literature standards. Several eluent systems were attempted to increase the lower yield reaction, but none showed the effectiveness of the trituration techniques.

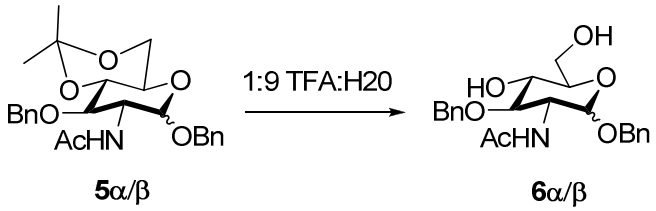

Equation 3: Formation of 4,6-Hydroxy-deprotected **6α/β** from **5α/β**.

Subsequent to forming **5α/β**, deprotection of O-4 and O-6 with 1 : 9 H_2O : trifloroacetic acid was performed yielding **6α/β** (Equation 3). This is seen in ^1H NMR by the disappearance of two methyl peaks at 1.31 and 1.44 ppm. COSY spectral cross peaks were used to sequentially order the ring protons, H-1 was found to have a 1H doublet signal at 5.24 ppm. Following the cross peaks the two H-6 were found to correspond to part of a 6H multiplet signal at 3.27-3.77 ppm. The HSQC and HMQC spectra allowed for assignment of the carbon peaks from the previously assigned proton spectra. Confirmation of successful synthesis by mass spectrometry, gave an *m/z* of 424.3 which accounts for the mass plus sodium. During the course of this research it was found that upon workup and solvent removal *en vacuo*, redissolving the solid in methylene chloride and refrigeration overnight yielded a solid product that was filtered off. This increased yields compared the literature precedent and previous group research.

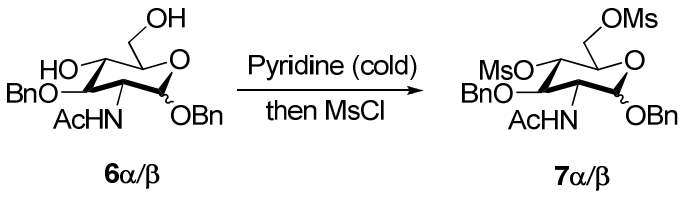

Equation 4: Formation of 4,6-di-*O*-methylsulfonyl-protected **7α/β** from **6α/β**.

Following formation of **6α/β**, reaction of O-4 and O-6 with methane sulfonyl chloride was performed yielding **7α/β** (Equation 4). This is seen in ^{1}H NMR by the appearance of two methyl signals at 3.15 and 3.21 ppm. COSY was used to assist in determining ring protons, while HMQC allowed determination of the ^{13}C signal of the mesyl groups at 36.99 and 38.31 ppm respectively. Confirmation of successful synthesis by mass spectrometry gave an *m/z* of 580.2 which accounts for the mass of **7α/β** plus sodium. Upon finishing the reaction procedure from literature, addition of water and subsequent refrigeration, allows for formation of a solid which is filtered out of the solution. The technique used to obtain the solid (**7α/β**), when recrystallized from 95% ethanol, allows for high yields without having to perform column chromatography and multiple triturations with water.

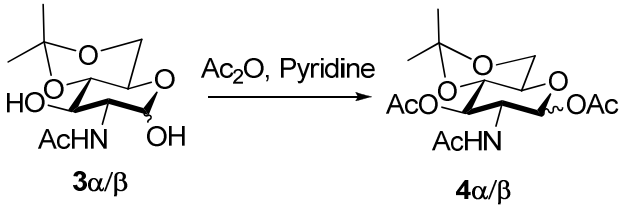

3α/β **4**α/β

Equation 5: Formation of 1,3-*O*-acetyl-protected **4α/β** from **3α/β**.

Alternatively following successful synthesis of **3α/β**, protection of O-1 and O-3 can also be obtained through acetylation, yielding **4α/β** (Equation 5). Evidence of acetylation is seen in ^{1}H NMR by the appearance of two methyl peaks at 2.11 and 2.19 ppm and in the ^{13}C NMR by peaks between 20.94 and 21.00 ppm. The same methods used in characterizing **5α/β** were used for characterizing **4α/β**, differing in the absence of aromatic protons. Verification of synthesis is seen through mass spectrometry, giving an

m/z of 368.2 which accounts for the mass plus sodium. This reaction showed the same novel ability for purification as **5α/β**.

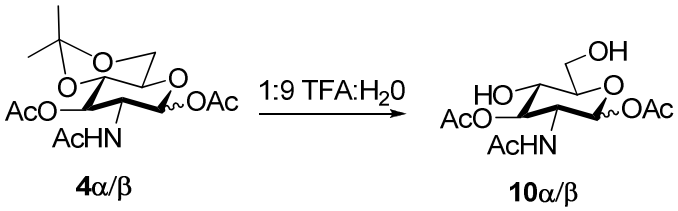

4α/β **10**α/β

Equation 6: Formation of 4,6-Hydroxy-deprotected **10α/β** from **4α/β**.

Showing successful formation of **4α/β**, deprotection of O-4 and O-6 with trifloroacetic acid was performed yielding **10α/β** (Equation 6). This is seen in ^{1}H NMR by the disappearance of two methyl peaks at 1.31 and 1.44 ppm which belonged to the isopropylidene group. Spectroscopy involving ^{13}C showed the disappearance of two methyl carbon peaks at 18.98 and 28.94 ppm and one quaternary carbon peak at 170.15 ppm. Additional confirmation of synthesis by mass spectrometry gave an *m/z* of 308.2 this accounts for the mass without the sodium. This reaction showed the same novel ability for purification as **6α/β**.

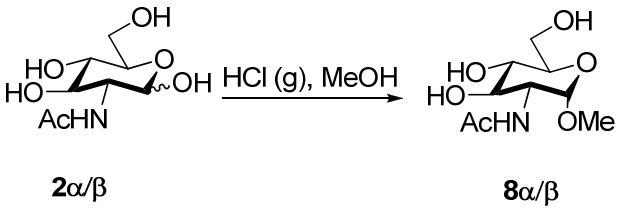

2α/β **8**α/β

Equation 7: Formation of methyl-*N*-glycosides **8α/β** from **2α/β**.

Alternatively following **2α/β**, protection of C-1 can also be performed through methoxylation yielding **8α/β** (Equation 7). This is seen in ^{1}H NMR by the appearance of one methyl peak at 3.37 ppm and in the ^{13}C NMR by peak at 54.70 ppm. Due to multiple hydroxyls remaining on the molecule, determination of individual ring protons was difficult without the use of COSY spectroscopy. The anomeric proton was determined to have a signal at 4.53 ppm, from this the protons could be determined by successive cross peak signals, finishing with assignment of the two H-6 protons to be a portion of a 3H multiplet from 3.37-3.52 ppm. Upon successful determination of the proton spectrum the carbon could be assigned from the HSQC and HMQC spectra. Confirmation of synthesis by mass spectrometry gave an *m/z* of 258.2 which accounts for the mass plus sodium. Purification of this reaction involved removal of solvent *en vacuo*.

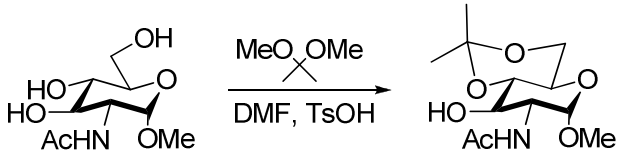

8α/β **9**α/β

Equation 8: Formation of 4,6-*O*-isopropylidene-protected **9α/β** from **8α/β**.

Following successful methoxylation and formation of **8α/β**, protection of O-4 and O-6 using an isopropylidene group yielding **9α/β** (Equation 8) was performed. This is shown in the ^{1}H NMR spectrum by the appearance of two methyl peaks at 1.44 and 1.53 ppm and in the ^{13}C NMR by peaks at 19.04 and 29.08 ppm. The two methyl peaks show differing shifts because they are locked into ring in a chair confirmation giving one an axial and one an equatorial position. The anomeric proton was determined to have a

signal at 4.67 ppm, from this the protons could be determined by successive cross peak signals, finishing with assignment of the two H-6 protons to be a portion of a 3H multiplet from 3.72-3.96 ppm. Upon successful determination of the proton spectrum the carbon could be assigned from the HSQC and HMQC spectra. Additional proof of synthesis by mass spectrometry gave an m/z of 300.0 which accounts for the mass plus sodium. The reaction mixture is diluted with methylene chloride and ethyl acetate, and then triturated with 95% ethanol. Upon trituration, the solid was collected by vacuum filtration and washed with methylene chloride, the remaining solvent was removed *en vacuo*.

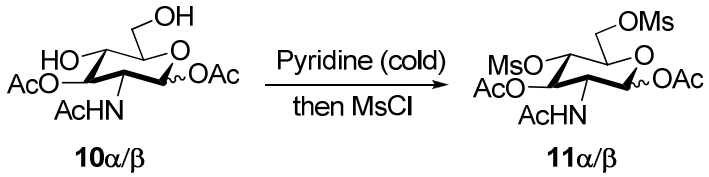

10α/β **11**α/β

Equation 9: Formation of 4,6-di-*O*-methylsulfonyl-protected **11α/β** from **10α/β**.

Following **10α/β**, protection of O-4 and O-6 with methane sulfonyl chloride was performed yielding **11α/β** (Equation 9). This is seen in ^{1}H NMR by the appearance of two methyl peaks at 2.91 and 3.04 ppm. Additional confirmation of successful synthesis by mass spectrometry gave an *m/z* of 481.3 which accounts for the mass plus sodium. The crude reaction mixture would not crystallize out as well as **7α/β**, so therefore column chromatography was performed. This reaction also did not perform well in column chromatography, it was attempted using 3 : 1 ethyl acetate : methanol as the eluent system. The reaction was not very clean via NMR spectroscopy, although certain key peaks were clearly discernable.

Attempted Synthesis of *N*-((2R,3R,4R)-2,4-dihydroxy-6-methylene-5-oxo-tetrahydro-2H-pyran-3-yl)acetamide

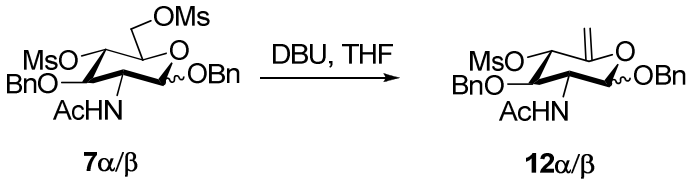

7α/β **12**α/β

Equation 10: Attempted formation of 6-methylene **12α/β** from **7α/β**.

Following **7α/β**, elimination at C-6 with DBU to form **12α/β** (Equation 12) was attempted. This reaction was unsuccessful; there was no evidence of a reaction taking place according to TLC. NMR of the crude extract showed no evidence of product formation (disappearance of 3H methyl singlet signal at 3.15 ppm and downfield shift of H-6 signal). No mass spectrometry was performed because no sign of reaction was seen. The starting material was recovered in a yield of 78% to be used in subsequent reactions.

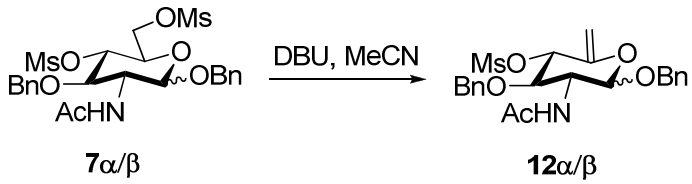

7α/β **12**α/β

Equation 11: Formation of 6-mehtylene **12α/β** from **7α/β**.

Following the successful isolation of **7α/β**, elimination at C-6 with DBU was performed yielding **11α/β** (Equation 11). This is seen in ^{1}H NMR by the disappearance of a methyl peak at 3.15 ppm and the downfield shift of the H-6 protons to around 7 ppm. Confirmation of successful synthesis by mass spectrometry gave an m/z of 480.1, which accounts for the mass plus sodium. TLC (3 : 1 ethyl acetate : methanol) showed

indication of successful reaction upon appearance of a second more polar spot. This reaction required purification via column chromatography using a 3 : 1 ethyl acetate : methanol eluent system.

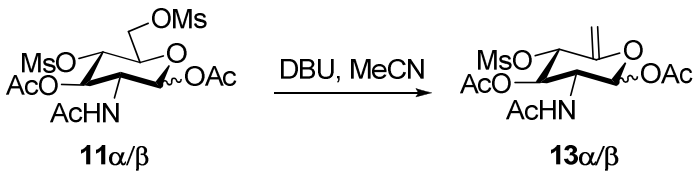

11α/β **13**α/β

Equation 12: Attempted formation of 6-methylene **13α/β** from **11α/β**.

Using the alternative synthesis product **11α/β**, elimination at C-6 with DBU to form **13α/β** (Equation 12) was attempted. This reaction was unsuccessful; there was no evidence of a reaction taking place according to TLC. NMR of the crude extract showed no evidence of product formation (disappearance of 3H methyl singlet signal at 3.15 ppm and downfield shift of H-6 signal). It would appear that the reaction needs to have a cleaner starting material (**11α/β**). No mass spectrometry was performed because no sign of reaction was seen.

NMR Characterization

Characterization by NMR allows for a piece-by-piece analysis of confirmation of synthesis and structural conformation of a molecule in the solution state. The individual experiments work in concert to determine the three-dimensional structure of these molecules. The one-dimensional spectra show the local magnetic environments, within which each individual nucleus is located. We also gain information about what kind of

neighbors a nucleus has as well as the amount of neighbors a given nucleus has. The two-dimensional spectra provide exact confirmation of the identity of the neighboring nuclei and in what spatial relation they are in respect to the other nuclei. The correlation spectra (HMBC and COSY), indicate neighbor which are 1-5 bonds away, and allow us to determine the secondary structure (the physical line-up of a molecule). The quantum coherence spectra (HMQC and HSQC), allow for directly connected nuclei to be identified, providing they are bonded to a high magnetogyric ratio nuclei. Upon complete assignment of all resonance signals, due to successful acquisition and interpretation of the previously mentioned experiments, analysis can then be completed on the secondary structure. These two-dimensional spectra also assist in determining the one-dimensional spectra in signal assignment and coupling constants, due to overlapping signals or a more crowded spectrum. Experiments which allow detection of nuclear Overhauser effects allow for interpretation into a molecules three-dimensional structure. This effect is seen over distance and not solely through bonds; therefore the resulting information will allow determination of the relative spatial orientation of the molecule while it is in solution. If two nuclei are exhibiting a signal they must be oriented closer than 6 Å from each other in space. In the COSY-NOESY spectrum overlay, we see the overlay of the two independent experiments, which display two different types of information (COSY-showing coupling networks, NOESY-showing spatial orientation effects). The cross peaks were overlap occurs, are due to both correlation through bonds and interactions through space, indicating the signals belonging to closely neighboring nuclei. Where only the COSY cross peaks show through, there is long distance correlation occurring through bonds, this is often seen through aromatic systems (Figure

15). Where only NOESY cross peaks are seen, there are no coupling network interactions, and the signal is due purely to orientation effects of the nuclei involved.

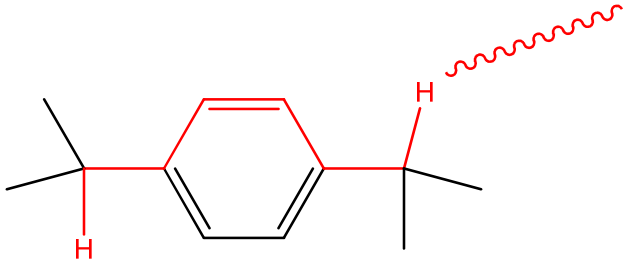

Figure 15: Example of long distance coupling network, without NOE interactions

Experiment	Resulting useful information
^{1}H	individual protons and their environment
^{13}C (proton decoupled)	individual carbons and their environment
^{13}C DEPT-135	multiplicity of carbons
HSQC	directly connected carbons-protons
HMQC	directly connected carbons-protons
COSY	neighboring protons
HMBC	neighboring carbons and protons
NOESY	proximity in space

Table 2: Information that can be obtained from selected individual NMR experiments.

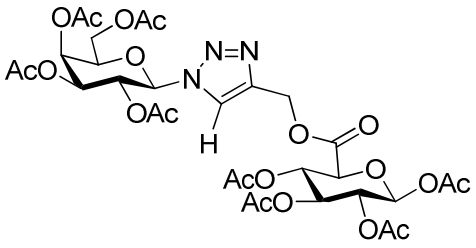

14

The ^{1}H spectrum of **14** shows specific information about the individual proton nuclei. The triazole ring proton show a signal a singlet at 7.95 ppm, this is due to the deshielding effects of the sp^2 hybridized carbon and the electronegativity of the nitrogen

it is attached to. All the acetyl peaks were observed in a range of 1.89 - 2.24 ppm. Due to the nature of the similar carbohydrates, many of the ring protons signals overlap; therefore to resolve the peaks, the COSY spectrum was used to determine the identity of the individual protons in an overlap based upon sequential ordering around the ring which is obtained from the spectrum. Information obtained by the proton spectrum allows for determination of the assignments of corresponding hydrogen-carbon pairs from the HSQC and HMQC experiment spectra. The ^{13}C DEPT-135, allows C-6 can be determined due to the below the baseline signal at 61.21 ppm, indicating a methylene-type carbon signal. The signals from the individual carbohydrates were determined by the lack of correlation to the C-6 protons for the protected glucose carbohydrate and the presence of the C-6 correlation for the protected galactose carbohydrate. In the NOESY spectra, 1-3, 1-5, and 3-5 diaxial interactions seen, these are expected due to the nature of the compounds containing ring structures and therefore being close together in space. The triazole ring proton also has some through space interaction with H-3 and H-5. This information leads us to the triazole ring proton and the H-3 and H-5 ring protons being oriented so they are near in space, as well as the expected triazole ring and H-1 proton, by virtue of them being close within the structure (Figure 16). There are also some through-space interactions with varying acetyl groups from both carbohydrates as well. Interpretation of the information gained from this experiment leads to the compound folding to house the triazole ring proton in a pocket-like area. An overlay spectrum (Figure 17) showing the through-space interactions and the through-bond interactions which give proof to the pocket-like area.

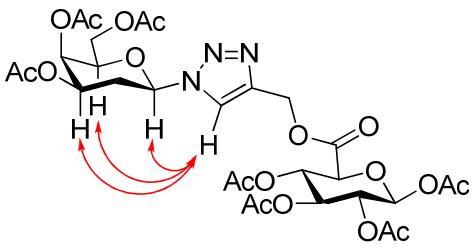

Figure 16: Representation of the triazole proton exhibiting nuclear Overhauser interactions with H-1, H-3 and H-5 of **14**.

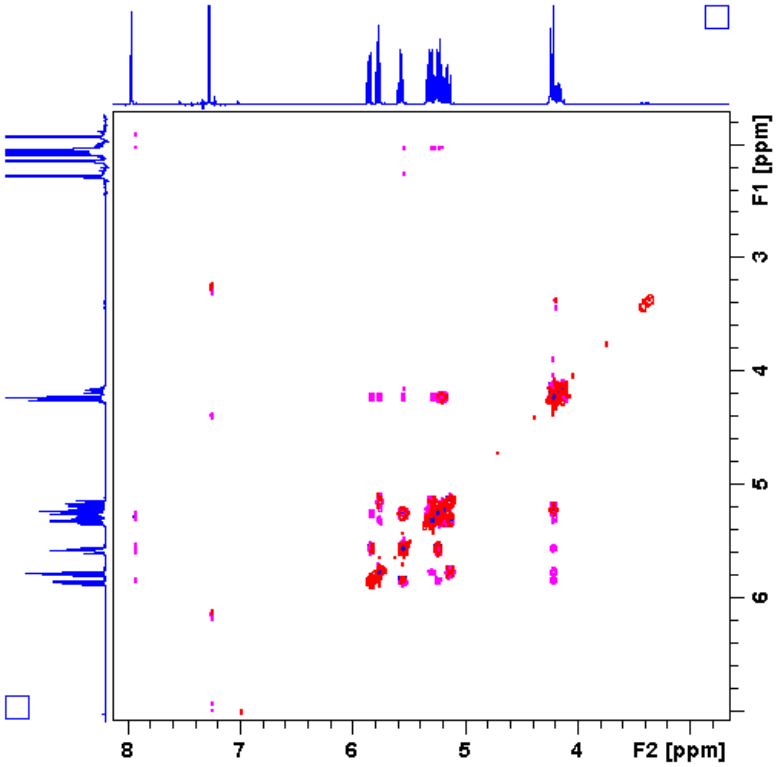

Figure 17: 400 MHz COSY-NOSEY spectrum overlay of **14**.

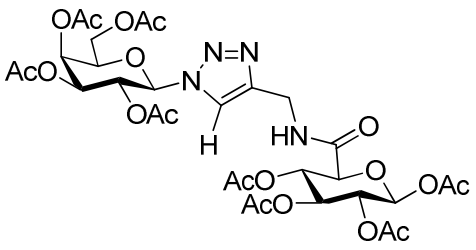

15

Compounds **14** and **15** are very similar with the exception being in the linkages, **14** has a carboxyl linkage between the protected glucose and the triazole ring, whereas **15** has an amide linkage. Due to the nature of the similarities between the compounds, many of the NMR signals are the same. There is however an emergence of a 1H triplet signal at 6.89 ppm, which corresponds to the proton at the amide linkage, and a downfield shift of the H-5 signal on the protected glucose ring. This is evidenced in the COSY spectrum by cross peaks which show the appearance of interactions between the N-H and H-5. Again, efficient determinations of the C-6 and H-6 signals on the protected galactose are made from observation of the ^{13}C DEPT-135 (61.22 ppm) spectrum and the HSQC spectrum (4.10-4.25 ppm). Complete assignment of the ring protons was determined by following the cross peak interaction on the COSY spectrum. Once the protons were determined, the HSQC and HMQC facilitated assignment of the other carbon signals in their respective spectrums. In the NOESY spectrum, the 1-3, 1-5, and 3-5 diaxial interactions are seen once again due to the nature of the compounds containing ring structures and therefore have a close orientation in space. The triazole ring proton also has some through space interaction with H-3 and H-5. This again leads us to the triazole ring proton and the H-1, H-3, and H-5 ring protons having a configuration near each other in space. This shows that the triazole ring proton is folded under protected

galactose carbohydrate as we saw in the analysis of **14**. However we do not see the interactions with the same acetyl groups observed in **14**, therefore the analysis leads to less of an encompassing pocket in **15**. The data suggests that the folding only occurs on the protected galactose molecule side of the ring. There were no observable interactions through space between the N-H proton and the triazole ring proton or the protected galactose, however, the data does show interaction with the H-5 on the glucose protected carbohydrate from data in both the COSY and NOESY spectra. The COSY-NOESY spectrum overlay (Figure 18) showing the interactions of both through-bond correlation and through-space interactions; the resulting cross peaks showing the previously stated interactions.

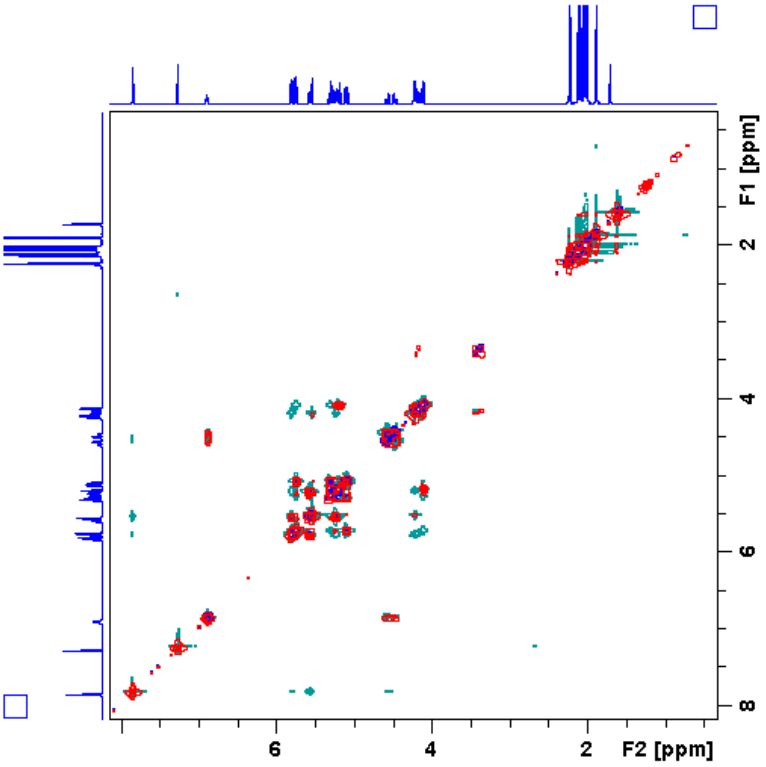

Figure 18: 400 MHz COSY-NOSEY overlay of **15**.

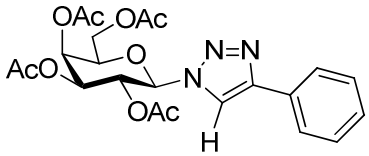

16

Containing only the protected galactose carbohydrate, **16** allows investigation into the magnitude of influence having a second carbohydrate has on the structural conformation. The ^{1}H spectra had great resolution in the aromatic region, allowing the individual aromatic protons to be resolved. Using a ^{13}C DEPT-135 experiment allowed for determination of C-6 (methylene peak, 61.22 ppm), and subsequent analysis of the HSQC spectrum afforded identification of the H-6 protons (4.15-4.27 ppm). Using the COSY spectrum and following the cross peak interactions the remaining ring protons could be identified and assigned. Compound **16** containing a ring structure, exhibits the 1-3, 1-5, and 3-5 as is expected, as well as interaction through space from the triazole ring proton to H-3. There was a notable absence of any interaction between the triazole ring proton and H-1 and H-5 (Figure 19). There is however COSY interactions between the triazole ring proton and H-1, this suggests the triazole ring is in an orientation such that its proton is close in space to H-3 but not with H-1. The nitrogen in the triazole would then be oriented towards the oxygen on the carbohydrate ring (Figure 20). This is contrary to the previous examples where the triazole proton was folded under towards the protected galactose ring (i.e. the pocket likes structure). There were no nuclear Overhauser effect interaction between the aromatic ring and anything else, giving it an orientation that was not close to the carbohydrate or the triazole ring protons. From this

information, we can see that having the second carbohydrate in the structure will affect the conformation of the structure in solution state.

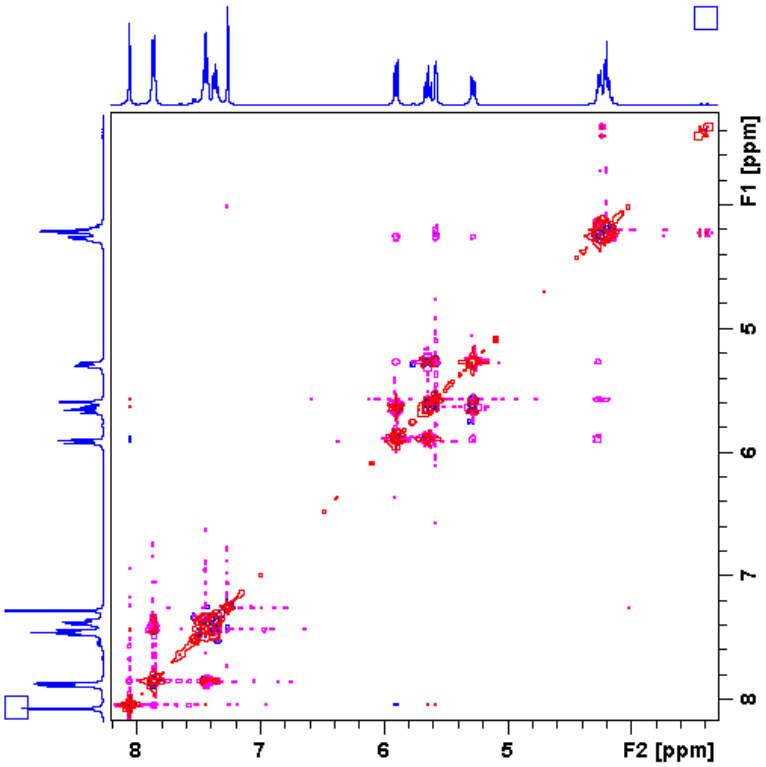

Figure 19: 400 MHz COSY-NOSEY overlay of **16**.

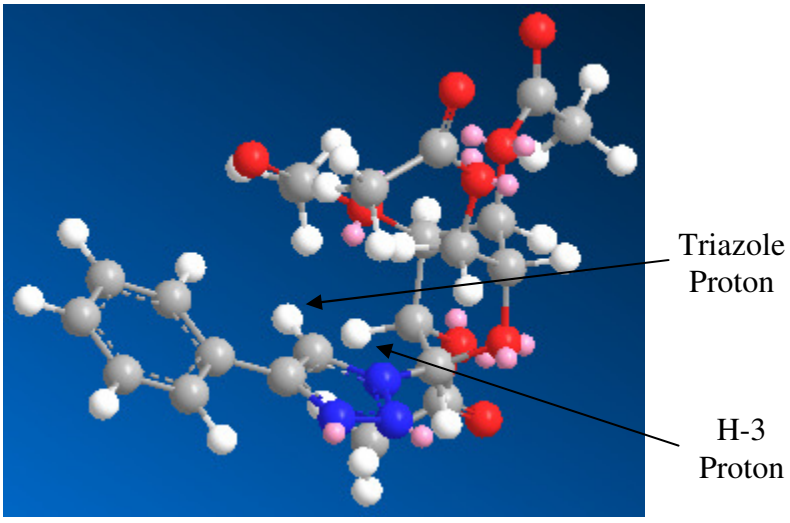

Figure 20: Orientation of **16** in solution state.

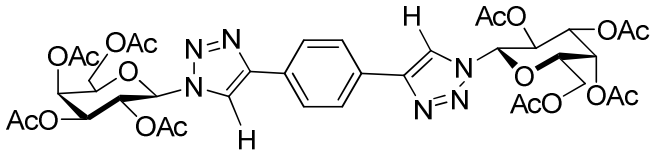

17

Compound **17** is symmetric about the center of the benzene ring, this allows for complete overlap of all signals about the molecular center. In this instance both carbohydrates are the acetyl protect galactose and are linked as *N*-glycosides. The ^{1}H spectrum of **17** shows the triazole ring proton at 8.10 ppm and all four benzene protons at 7.95 ppm. Assignment of the ring protons was aided by ^{13}C DEPT-135 and assignment of C-6 (methylene, 61.23 ppm) and using the HSQC spectrum to assign H-6 protons (dd, 4H, 4.17-4.27 ppm). Through NOSEY spectroscopy the typical 1-3, 1-5, and 3-5 diaxial interactions are seen, as well as interactions between the triazole proton and H-1 and H-3. There are no nuclear Overhauser effect interactions between the triazole ring proton and the H-5 proton unlike what is seen in the other two carbohydrate systems (Figure 21). This leads to the interpretation that the length of the linkage off the triazole ring to the protected glucose carbohydrate is an important factor in determining the conformation that the molecule will take in solution. Further studies involving the length of this linkage would need to be undertaken to accurately describe the exact amount necessary to allow a folding pocket-like interaction.

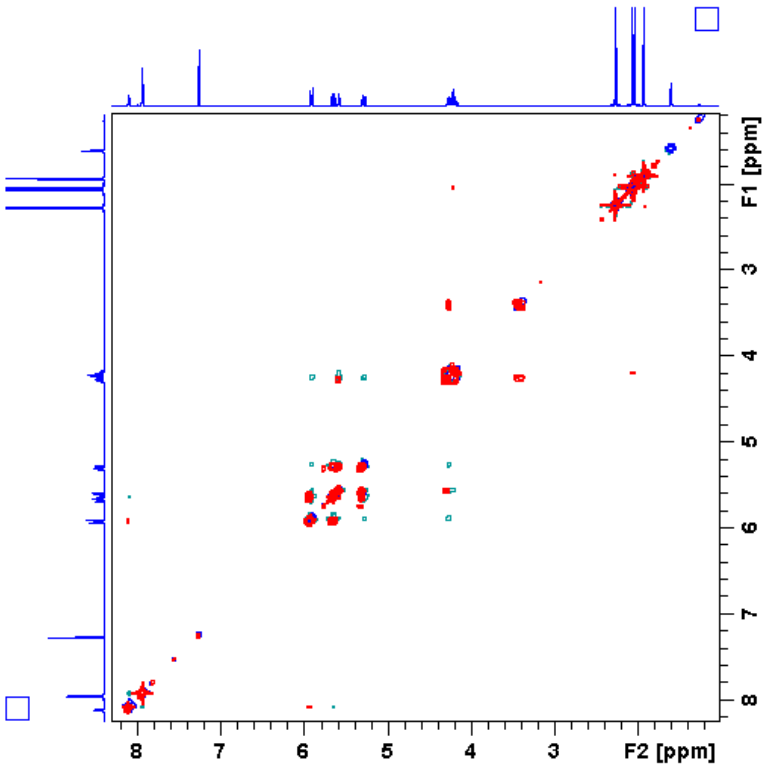

Figure 21: 400 MHz COSY-NOSEY overlay of **17**.

Many different interactions are seen from these experiments, some of the most useful information about two-dimensional structure really comes from the COSY spectra, whereas the most useful three-dimensional structure comes from the NOSEY spectra. These two spectra also allow the assignment of the one-dimensional spectra when there is intense overlap often found in carbohydrate chemistry (due to the ring protons often having similar shifts, especially when they have similar groups attached). Experiments that would have help to resolve the overlaps as well as define coupling constants, are the *J*-resolved spectra, which allow for the peaks to be separated by their individual coupling constants. This would allow for resolution of these higher order NMR peaks that do not currently allow for definition of the *J* values for the ring peaks which happen to overlap.

Conclusions

The complete synthesis of *N*-acetyl-D-fucosamine was not finished; this was due to a change in the nature of the performed research. The synthesis was halted after the completion of the 4,6-*O*-di-mesylate protection step. Multiple improvements were shown to increase yields and reaction times, which can also be useful for scaling of the synthesis.

The attempt at synthesizing *N*-((2R,3R,4R)-2,4-dihydroxy-6-methylene-5-oxo-tetrahydro-2H-pyran-3-yl)acetamide was unsuccessful. The initial elimination using 1,3-*O*-di-benzyl protected glucosamine, yielded less than satisfactory yields and needs to be investigated further. The alternative protection scheme using 1,3-*O*-di-acetyl, needs further development, as it is the only viable method explored that could result in completing the synthesis. With the large protecting groups around the proton at C-5, investigative methods should be performed to determine which base allows for the highest yields.

NMR characterization of carbohydrate mimics showed confirmation of known solid state structures and lead to elucidation of the solution state conformation among the studied *N*-glycoside molecules. These methods involved the setup and implementation of YSU's NMR facility. Further investigation should involve studies on how the length of the 1,2,3-triazole linkage between the two carbohydrates on the studied molecules affects the structural conformation of the molecules. It was seen through research that the type and length of linkage, along with differing carbohydrates allowed for alternative

conformation in solution. Further investigation should also involve implementation of *J*-resolved spectroscopy as well as three-dimensional NMR spectroscopy to aid in the analysis of these molecules.

References

1. Hornbeck, J.; Organic Chemistry 1998, Brooks/Cole 1, 113.
2. Howe, R. A.; Monk, A.; Wootton, M.; Walsh, T. R.; Enright, M. C. *Emerging Infect. Dis.* **2004**, *10*, 855-857.
3. Chambers, H. F. *Emerging Infect. Dis.* **2001**, *7*, 178-182.
4. Tenover, T. C.; Biddle, J. W.; Lancaster, M. V. *Emerging Infect. Dis.* **2001**, *7*, 327-332.
5. Honeyman, A., Friedman, H., Bendinelli, M., Eds.; *Staphylococcus aureus: Infection and Disease*; Plenum Publishers: New York, 2001.
6. O'Riordan, K.; Lee, J. C. *J. Clin. Microbiol. Rev.* **2004**, *17*, 218-234.
7. Jones, C. *Carbohydr. Res.* **2005**, *340*, 1097-1106.
8. Horton, D.; Saeki, H. *Carbohydr. Res.* **1978**, *63*, 270-276.
9. Lemieux, R.; Nagabush, T. L.; O'Neill, I. K. *Tetrahedron Lett.* **1964**, *5*, 1909-1916.
10. Lemieux, R.; Nagabush, T. L.; O'Neill, I. K. *Can. J. Chem.* **1968**, *46*, 413-418.
11. Trahanovsky, W. S.; Robbins, M. D. *J. Am. Chem. Soc.* **1971**, *93*, 5256-5258.
12. Bongat, A. F. G.; Demchenko, A. *Carbohydr. Res.* **2007**, *342*, 374-406.
13. Bongat, A. F. G.; Kamat, M. N.; Demchenko, A. *J. Org. Chem.* **2007**, *72*, 1480-1483.
14. Illarionov, P.; Torgov, V.; Hancock, I.; Shibaev, V. *Russ. Chem. Bull.* **2001**, *181*, 1303-1308.
15. Petursson, S. *J. Chem. E.* **1997**, *74*, 1297-1303.
16. Kulikova, N. Y.; Shpirt, A. M.; Kononov, L. O. *Synthesis* **2006**, *24*, 4113-4114.

17. Okamoto, K.; Kondo, T.; Goto, T. *Bull. Chem. Soc. Jpn.* **1987**, *60*, 631-636.

18. Rabi, I. I.; Zacharias, J. R.; Millman, S.; Kusch, P. *Phys. Rev.* **1938**, *53*, 318.

19. Purcell, E. M.; Torrey H. C.; Pound R. V. *Phys. Rev.* **1946**, *69***,** 37-38.

20. Butler, E. Bruker Topspin Manuals, Bruker, Rheinstetten, Germany 2003.

21. Freibolin, H. Basic One- and Two-Dimensional NMR Spectroscopy, Wiley-VCH, Germany 2005.

22. Akitt, J. W. NMR and Chemistry-An Introduction to modern NMR Spectroscopy, Chapman and Hall, London 1992.

23. Marion, D.; Desvaux, H. *J. Magn. Res.* **2008**, *193*, 153-157.

24. Claridge, T. High-Resolution NMR Techniques in Organic Chemistry, Elsevier, England, 2006.

25. Ernst, R. R.; Bodenhausen, G.; Wokaun, A. Principles of Nuclear Magnetic Resonance in One and Two Dimensions, Oxford University Press, England, 1987.

26. Levitt, M. Spin Dynamics Basics of Nuclear Magnetic Resonance, John Wiley and Sons Ltd., England, 2001.

27. Hore, P.; Jones, J; Wimperis, S. NMR: The Toolkit, Oxford University Press, Great Britain, 2000.

28. Iggo, J. NMR Spectroscopy in Inorganic Chemistry, Oxford University Press, Great Britain, 1999.

29. Berger, S.; Braun, S. 200 and More NMR Experiments, Wiley-VCH, Germany, 2004.

30. Jenner, J. Ampere International Summer School II, Basko Polje, Yugoslavia, 1971.

31. Aue, W. P.; Bartholdi, E.; Ernst, R. R. *J. Chem. Phys.* **1976**, *64*, 2229-2246.

32. Braun, S.; Kalinowski H.-O.; Berger, S. 150 and More Basic NMR Experiments, Wiley-VCH, Germany, 1998.

33. Roberts, J. ABC's of FT-NMR, University Science Books, Sausalito, California, 2000.

34. Derome, A. Modern NMR Techniques for Chemistry Research, Pergamon Press, England, 1987.

35. Schenker, K. V.; Philipsborn, W. V. *J. Magn. Res.* **1986**, *66*, 219-229.

36. Bendall, M. R.; Doddrell, D. M.; Pegg, D. T. *J. Am. Chem. Soc.* **1981**, *103*, 4603-4605.

37. States, D. J.; Meier, B. H.; Bachmann, P.; Ernst, R. R. *J. Magn. Res.* **1982**, *48*, 286-292.

38. Bodenhausen, G.; Kogler, H.; Ernst, R. R. *J. Magn. Res. B* **1984**, *58*, 370-388.

39. Neuhaus, D.; Williamson, M. P. The NOE in Structural and Confirmational Analysis 2nd Edition, Wiley-VCH, Germany, 2000.

40. Sanders, J.; Hunter, B. Modern NMR Spectroscopy - A Guide For Chemists 2nd Edition, Oxford University Press, Great Britain, 1993.

41. Macomber, R. A Complete Introduction to Modern NMR Spectroscopy, Wiley-Interscience, Germany, 1998.

42. Jenner, J.; Meier, B. H.; Bachmann, P.; Ernst, R. R. *J. Chem Phys.* **1979**, *71*, 4546-4563.

43. Muller, L. *J. Am. Chem. Soc.* **1979**, *101*, 4481-4484.

44. Sklenar, V.; Piotto, M.; Leppik, R.; Saudek, V. *J. Magn. Res.* **1993**, *102*, 241-245.

45. Bodenhausen, G.; Ruben, D. J. *Chem. Phys. Lett.* **1980**, *69*, 185-189.

46. Bax, A; Summers, M. F. *J. Am. Chem. Soc.* **1986**, *108*, 2093-2094.

Appendix A

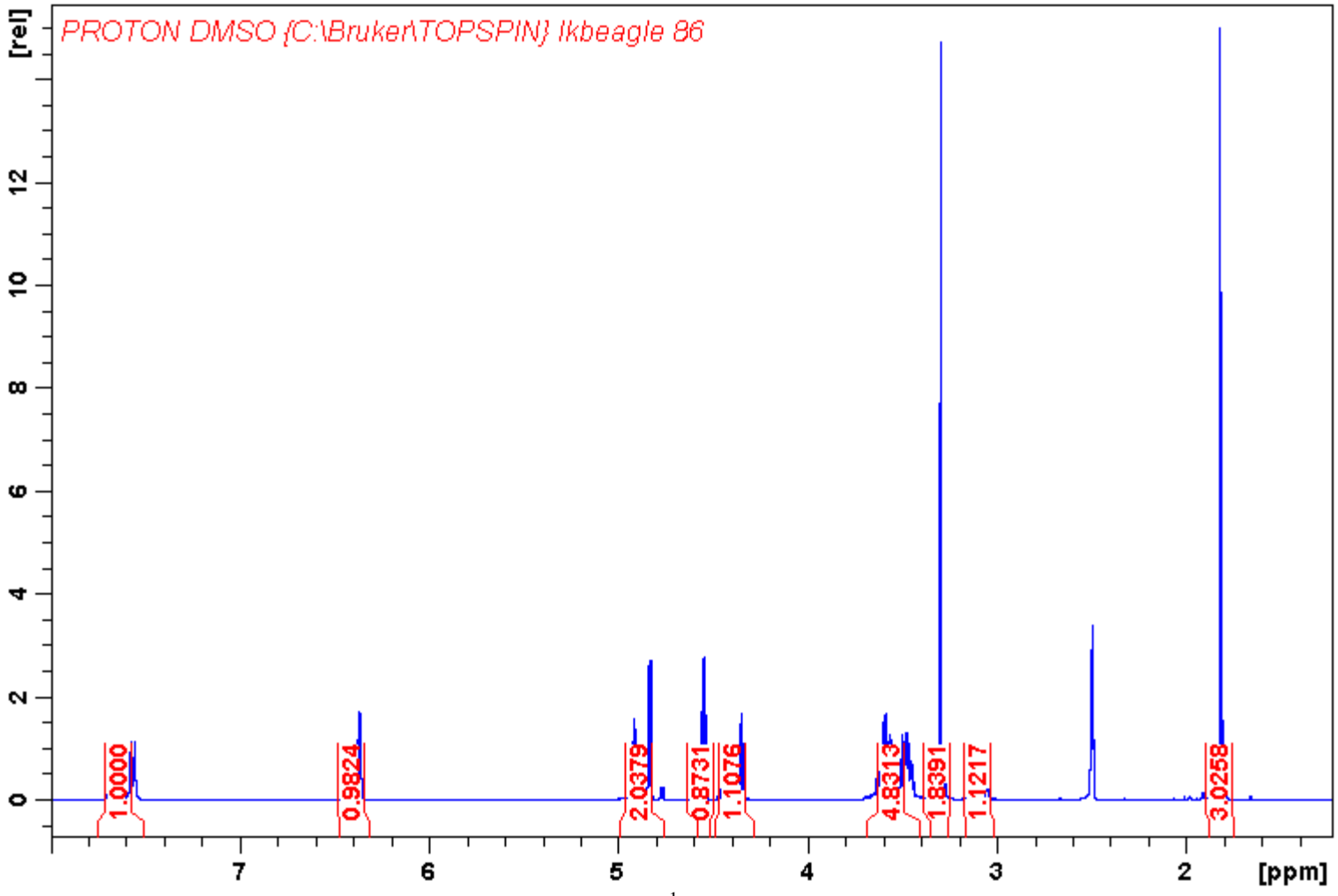

Figure 22: 400 MHz ^{1}H Spectrum of **2α/β**.

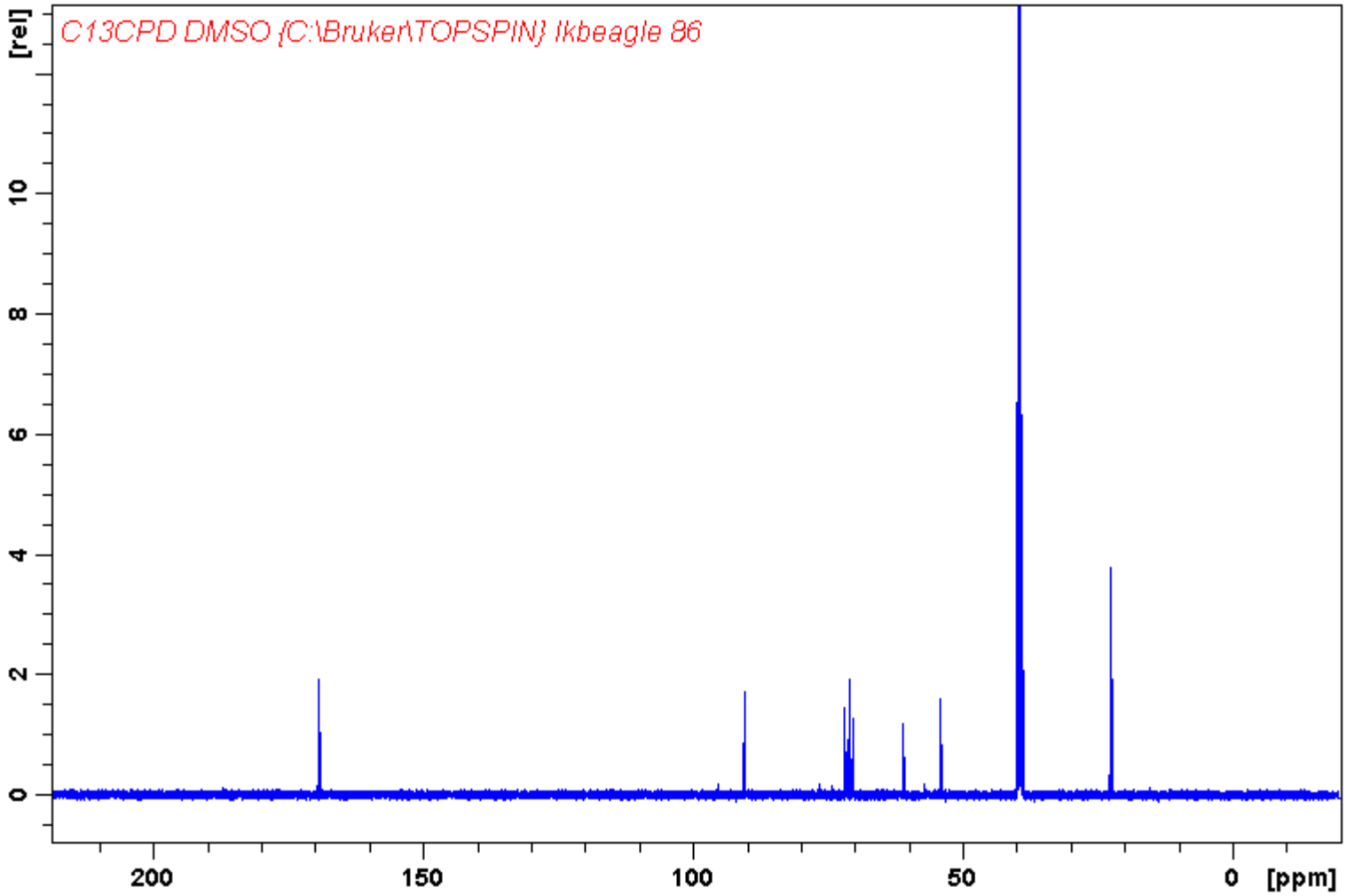

Figure 23: 100 MHz ^{13}C Spectrum of **2α/β**.

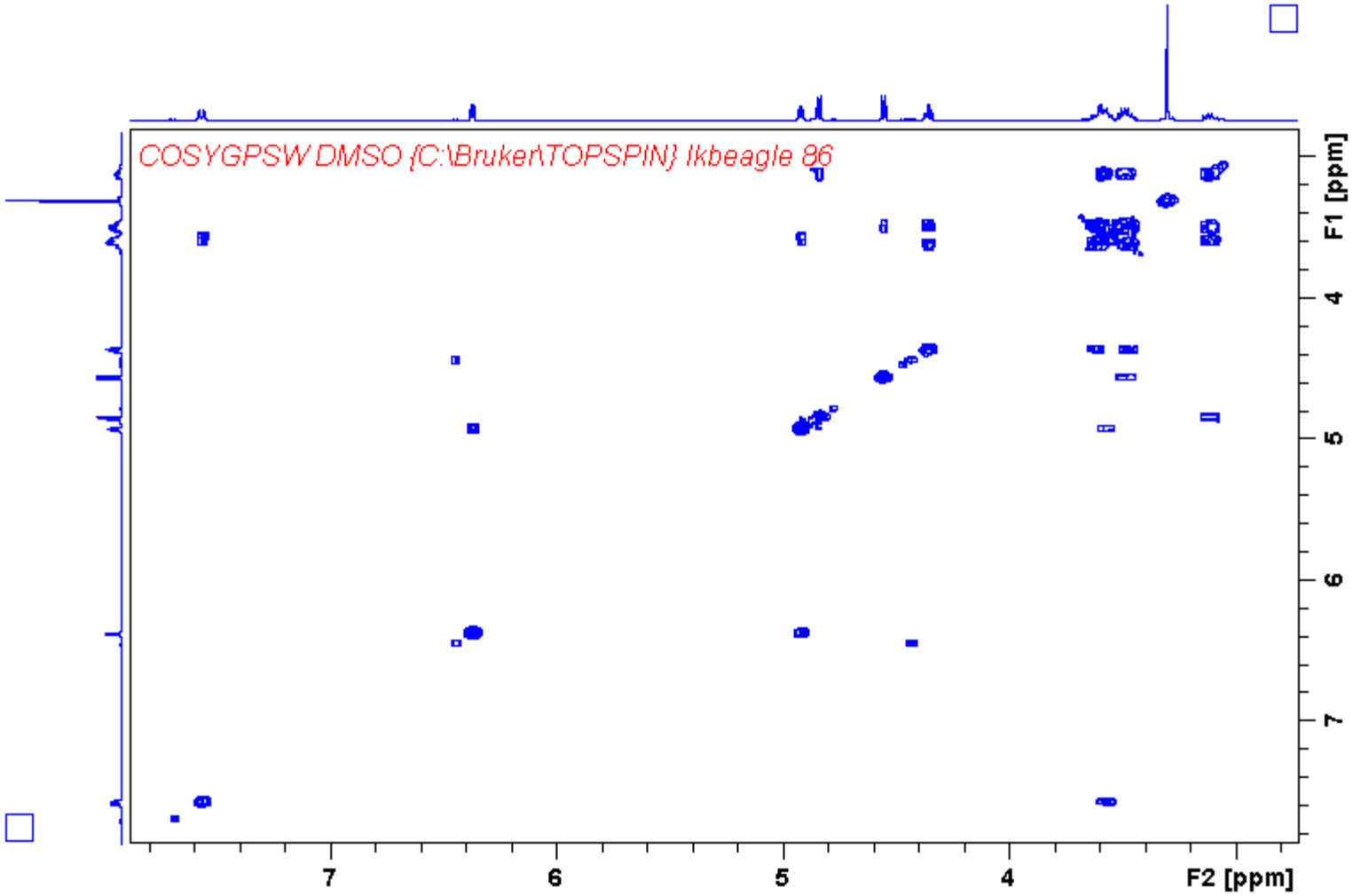

Figure 24: 400 MHz ^{1}H-^{1}H COSY Spectrum of **2α/β**.

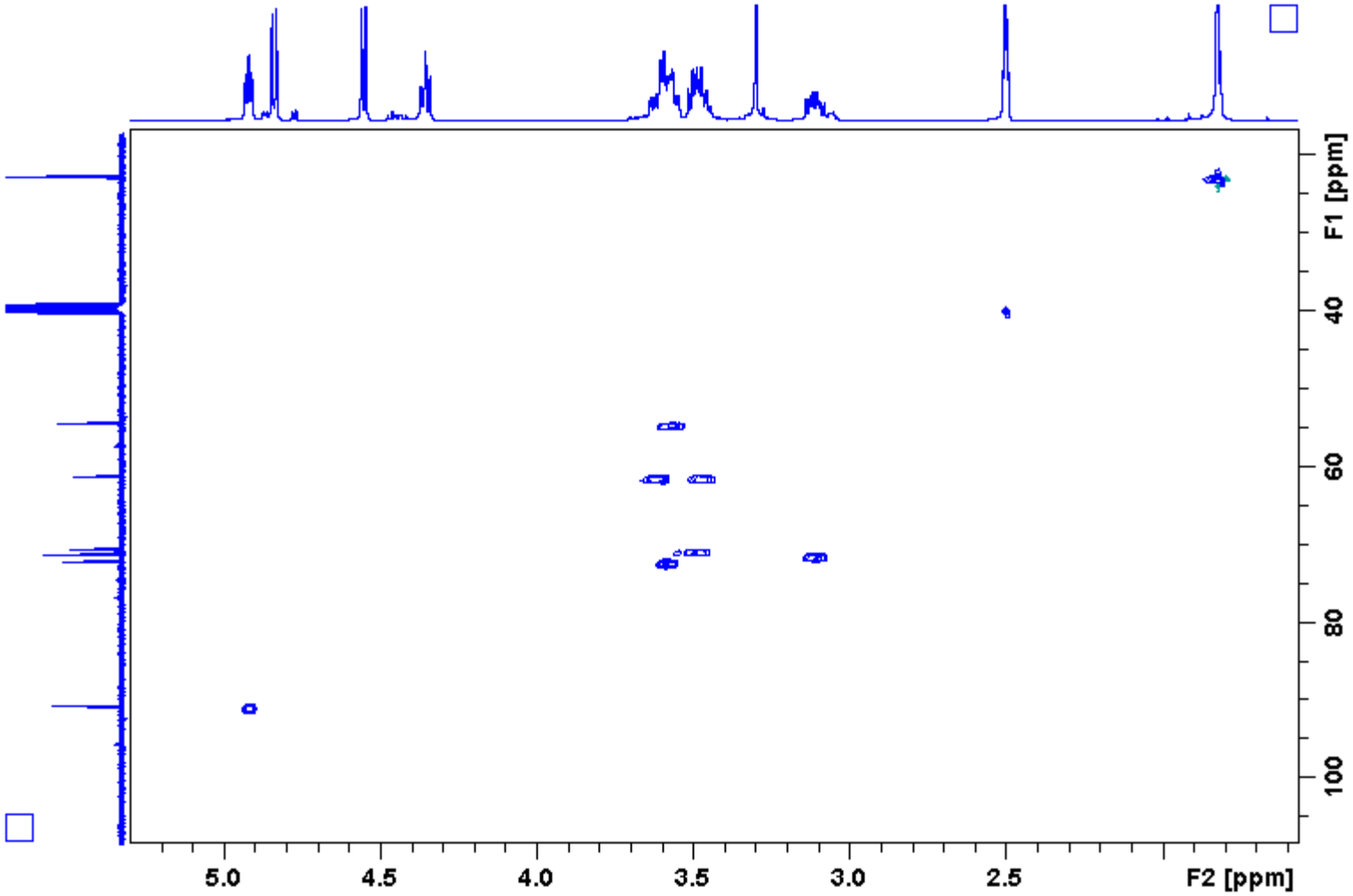

Figure 25: 400 MHz ^{1}H-^{13}C HSQC Spectrum of **2α/β**.

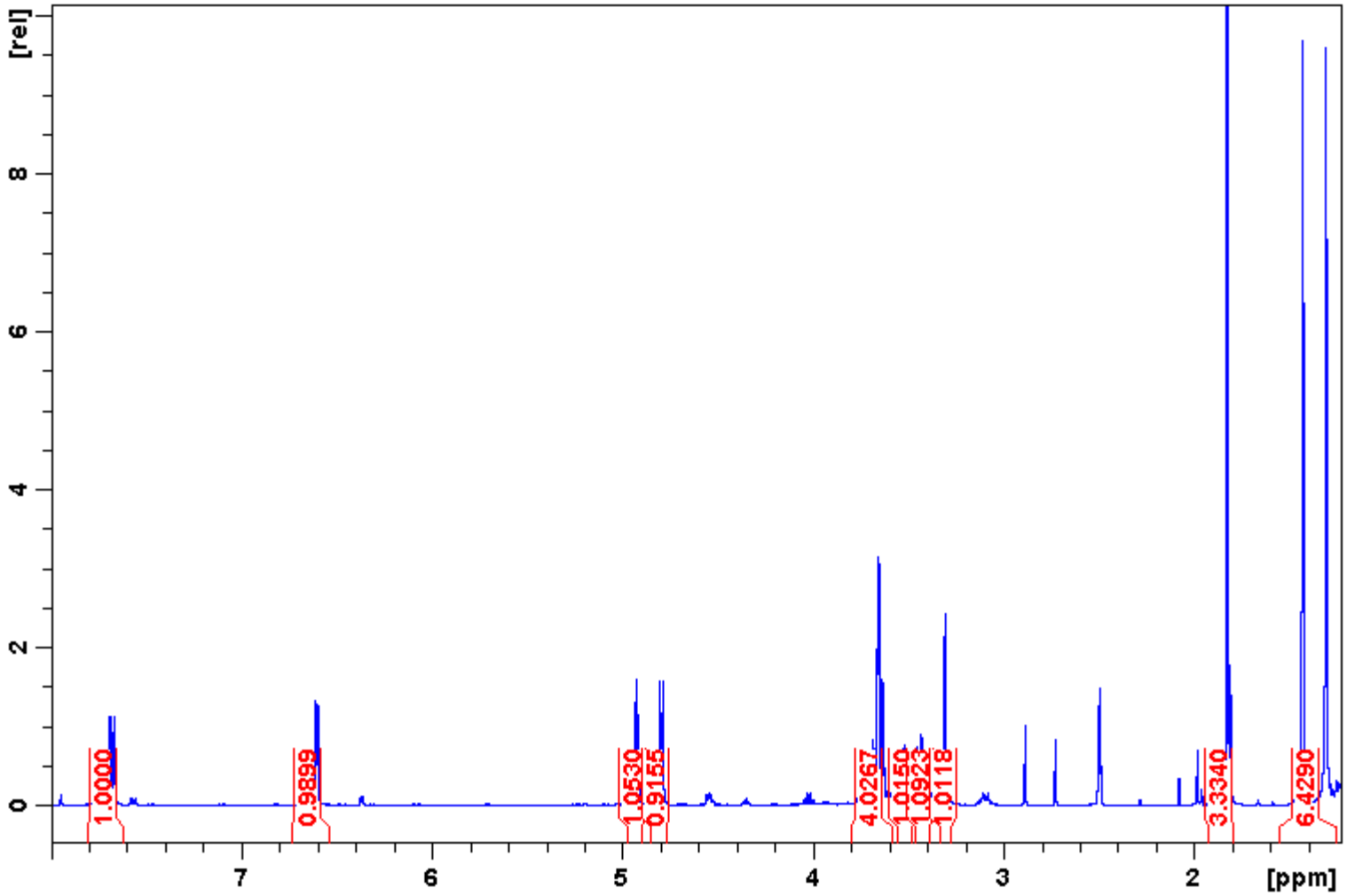

Figure 26: 400 MHz ^{1}H Spectrum of **3α/β**.

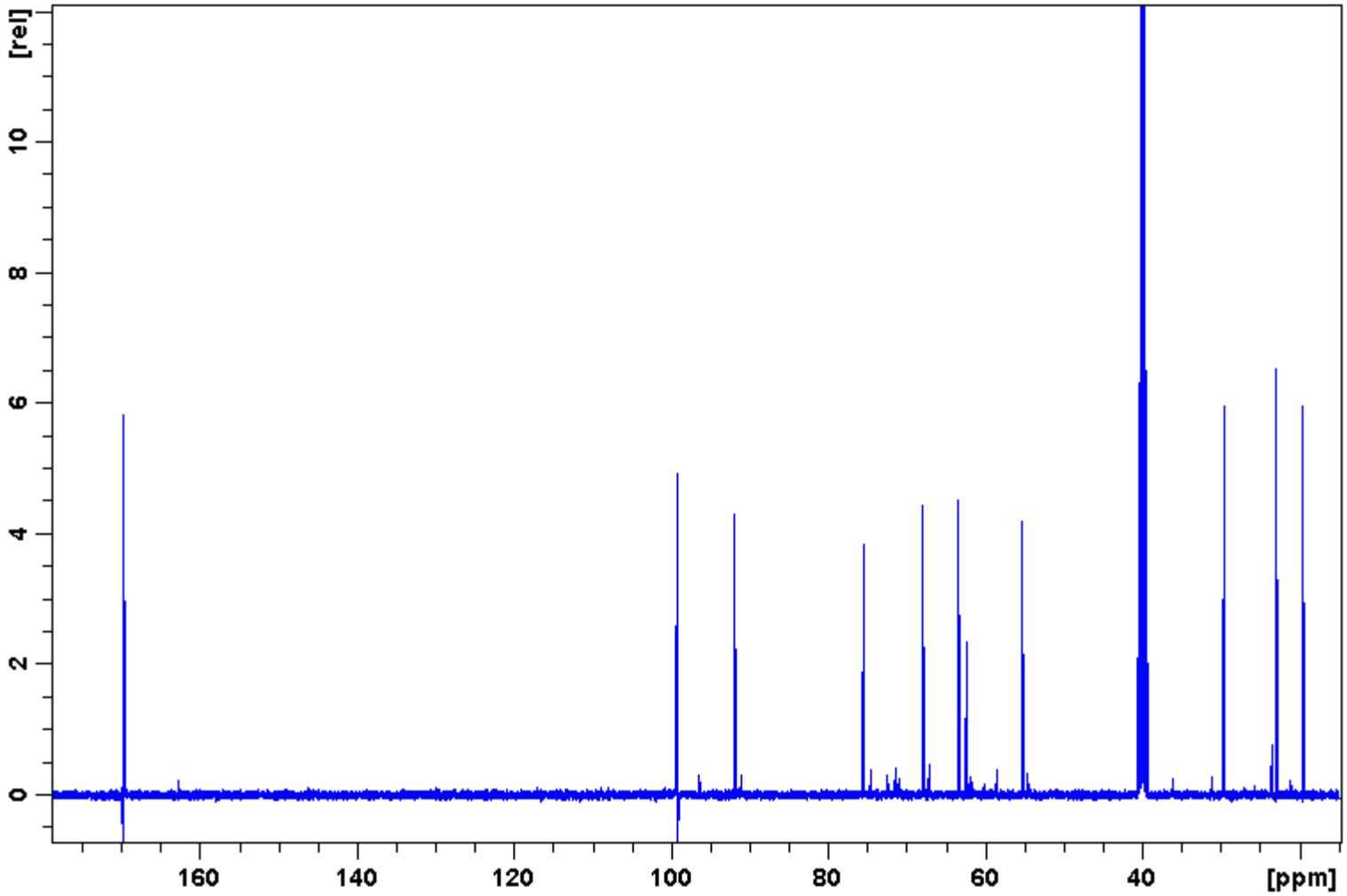

Figure 27: 100 MHz ^{13}C Spectrum of **3α/β**.

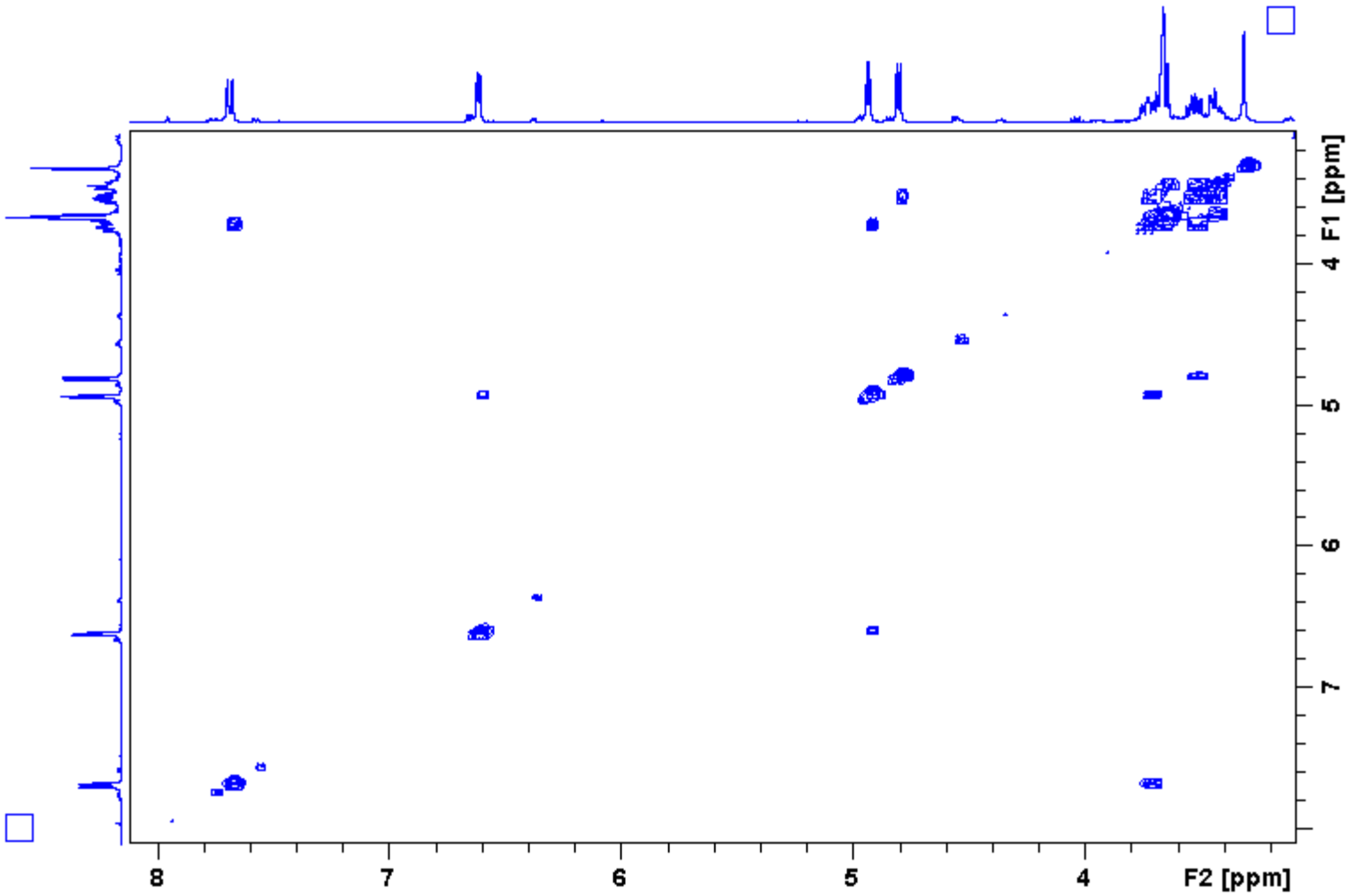

Figure 28: 400 MHz ^{1}H-^{1}H COSY Spectrum of **3α/β**.

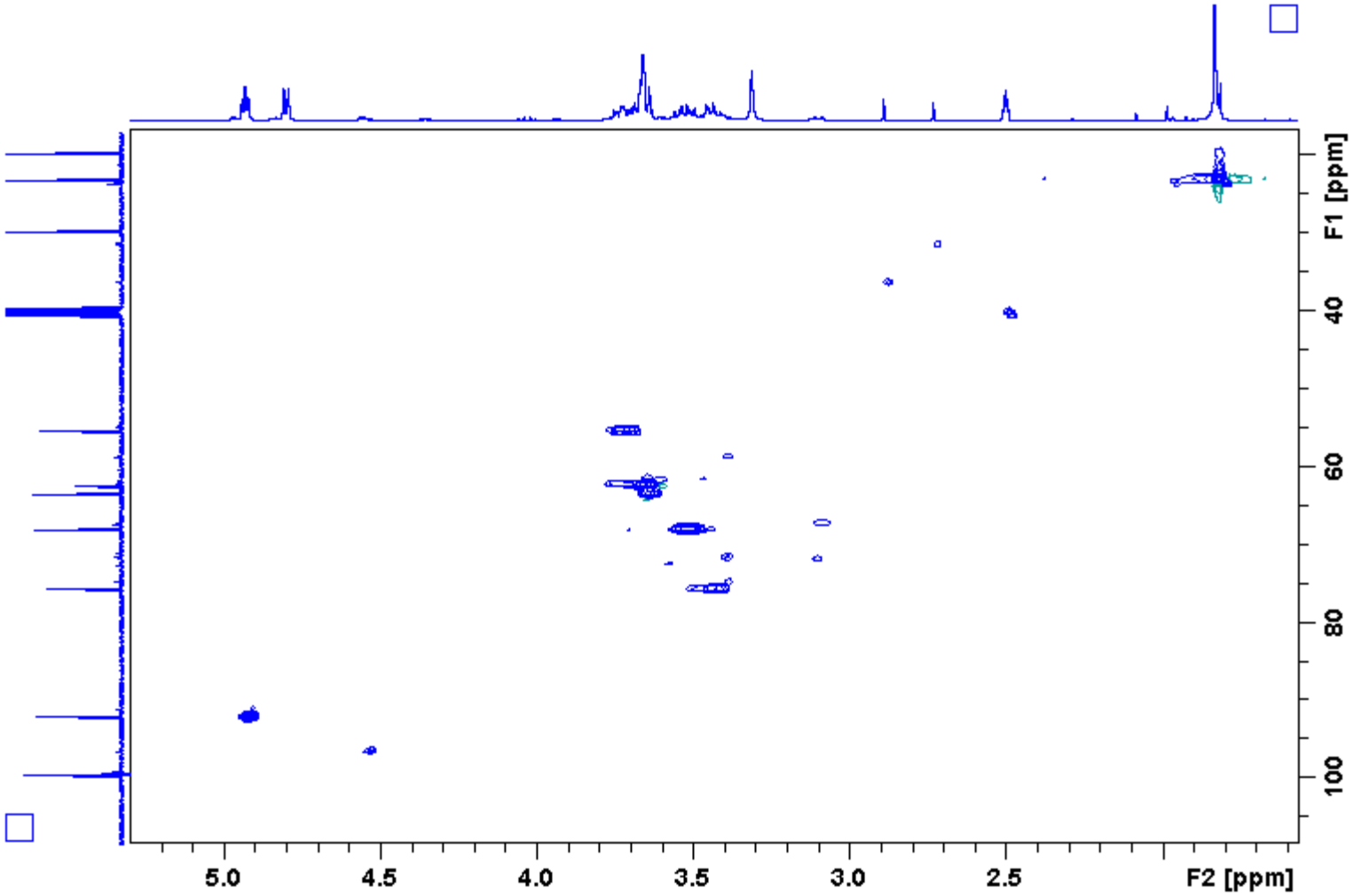

Figure 29: 400 MHz ^{1}H-^{13}C HSQC Spectrum of **3α/β**.

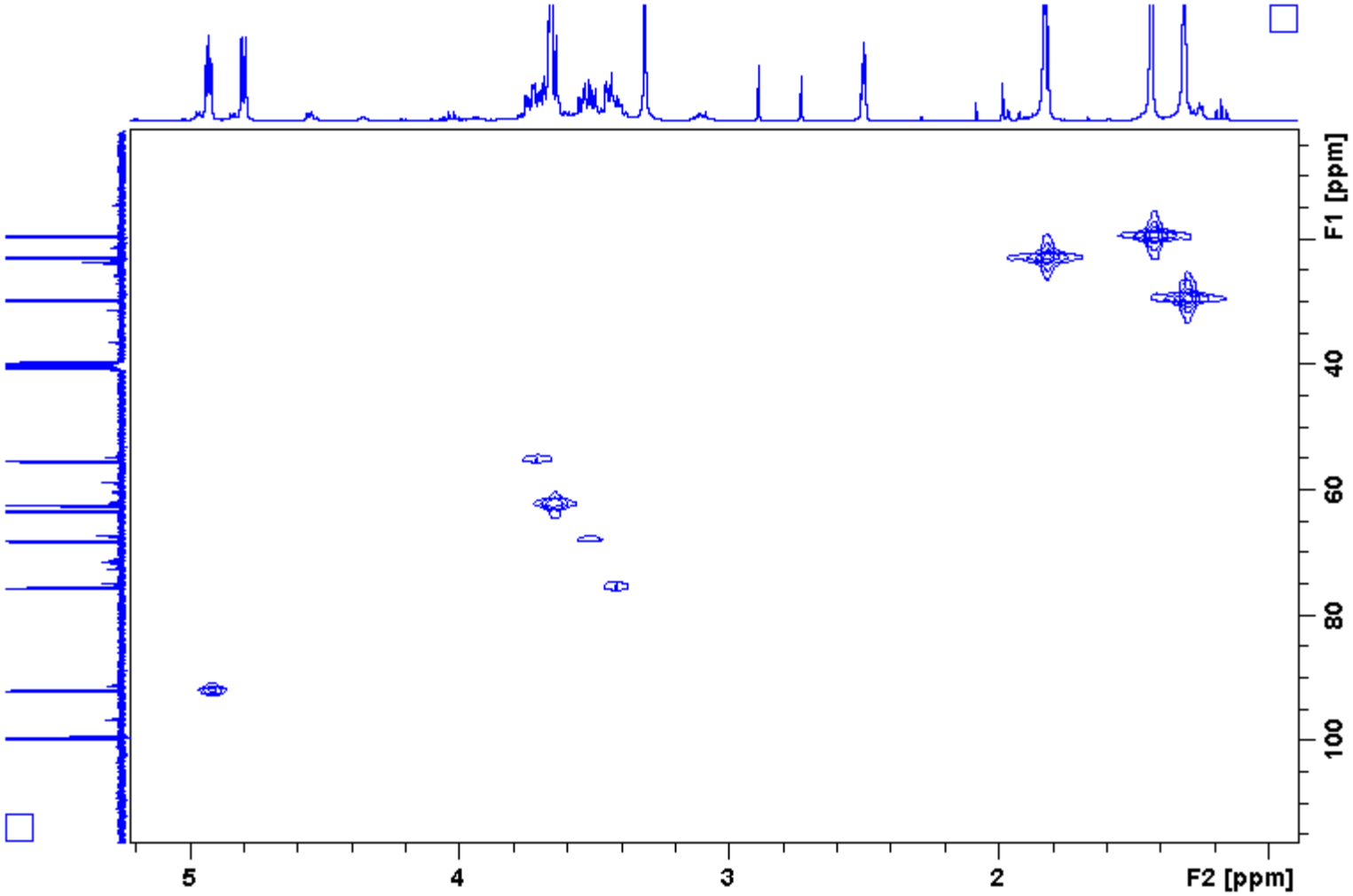

Figure 30: 400 MHz ^{1}H-^{13}C HMQC Spectrum of **3α/β**.

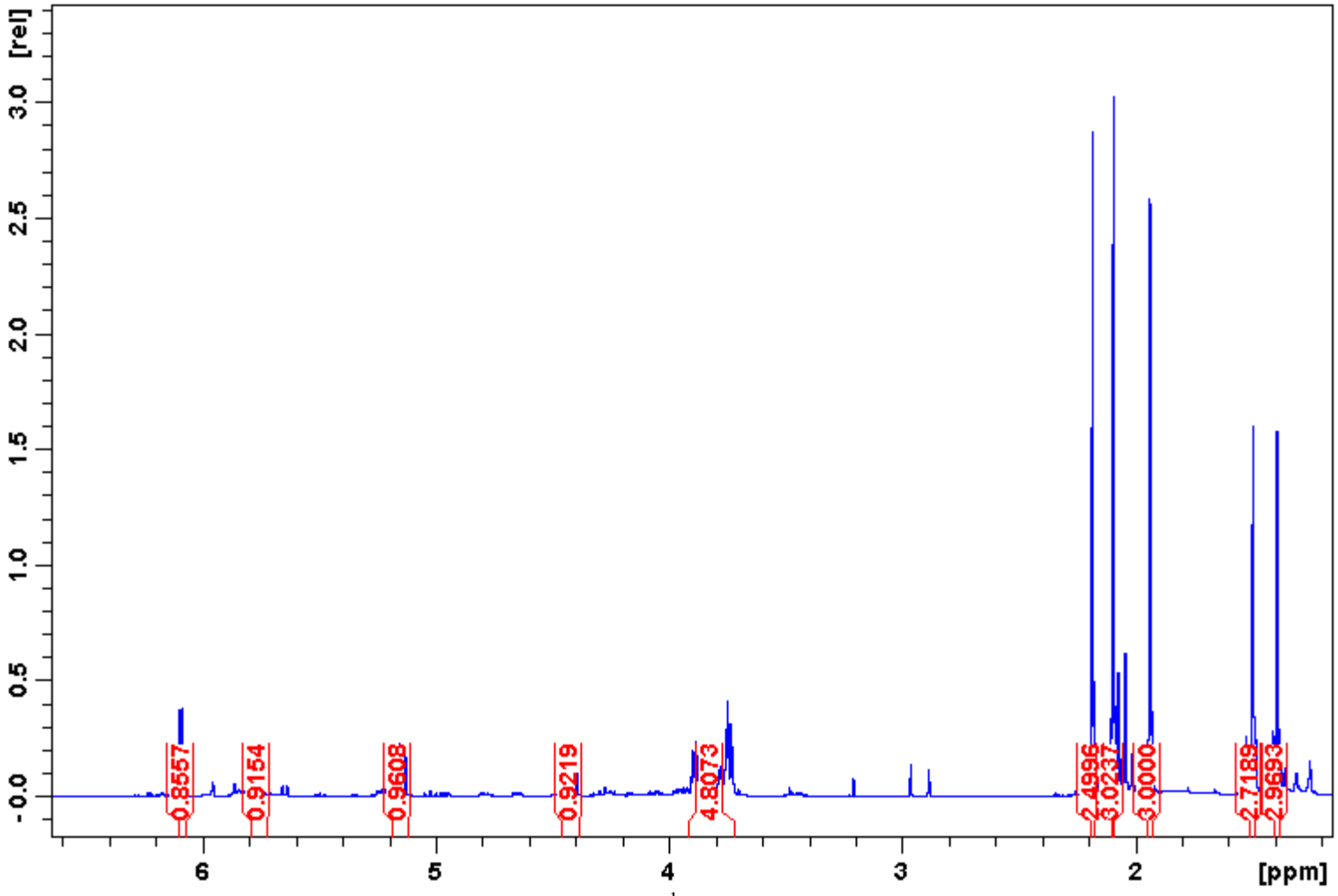

Figure 31: 400 MHz ^{1}H Spectrum of **4α/β**.

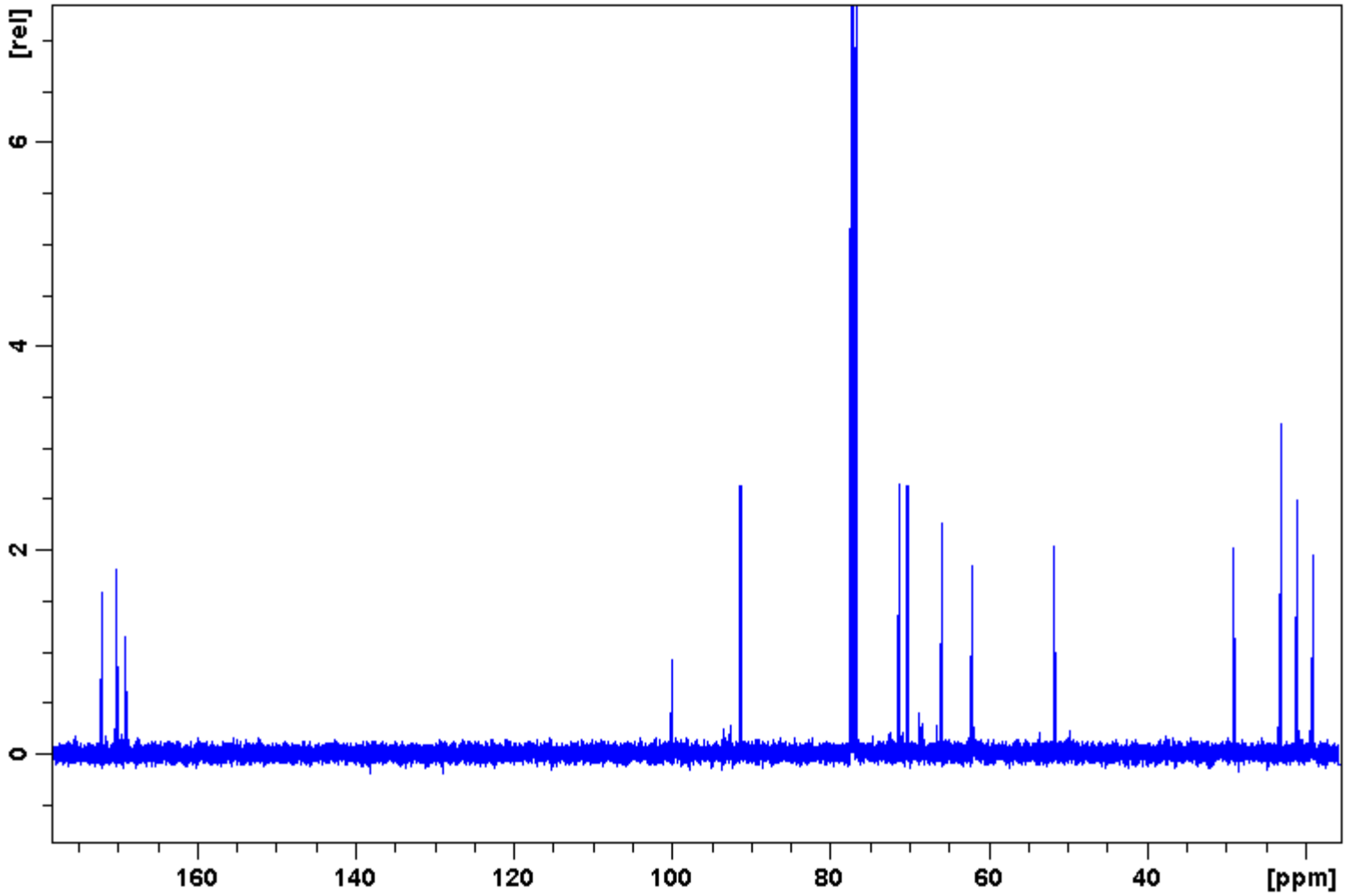

Figure 32: 100 MHz ^{13}C Spectrum of **4α/β**.

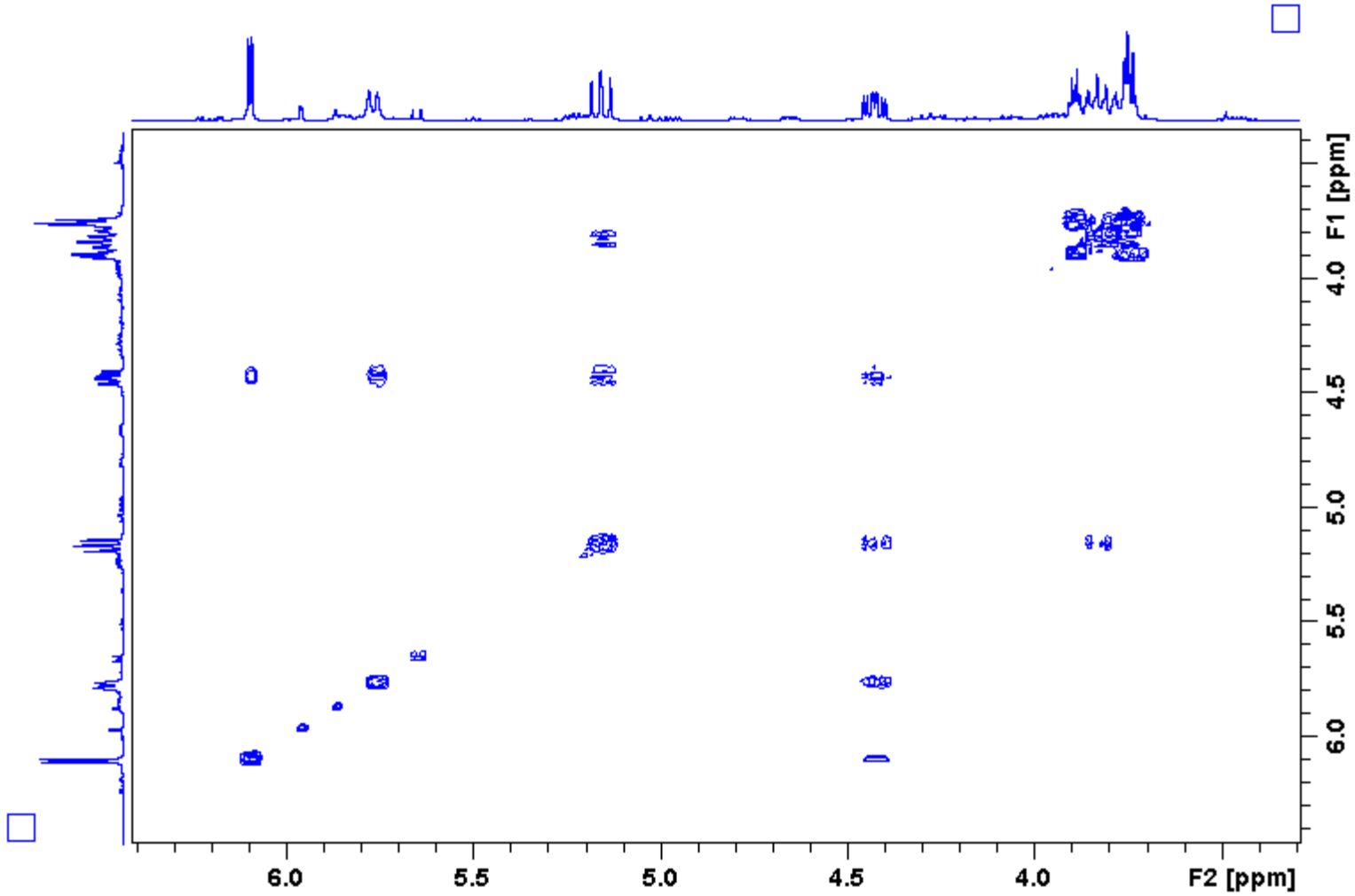

Figure 33: 400 MHz ^{1}H-^{1}H COSY Spectrum of **4α/β**.

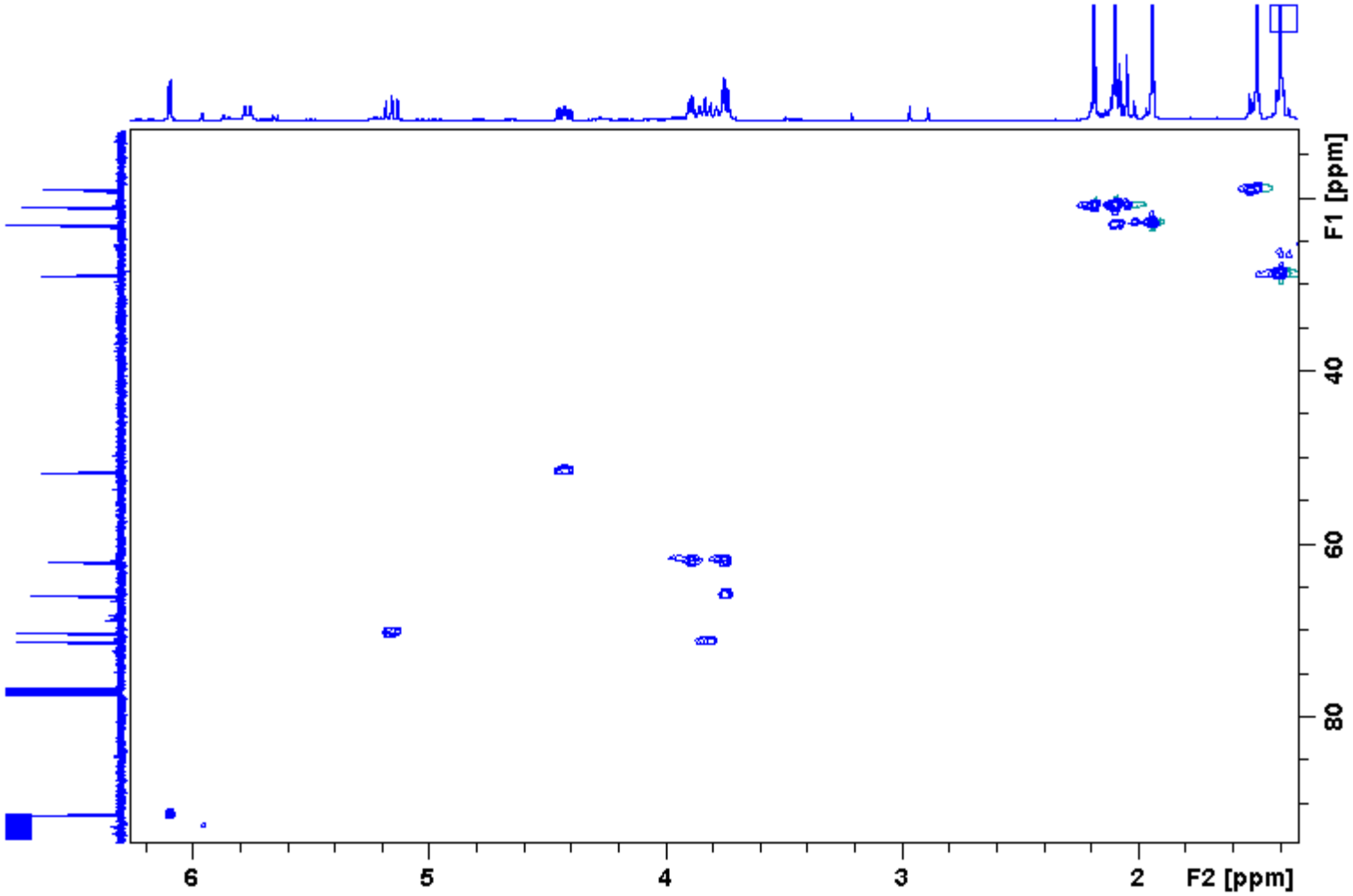

Figure 34: 400 MHz ^{1}H-^{13}C HSQC Spectrum of **4α/β**.

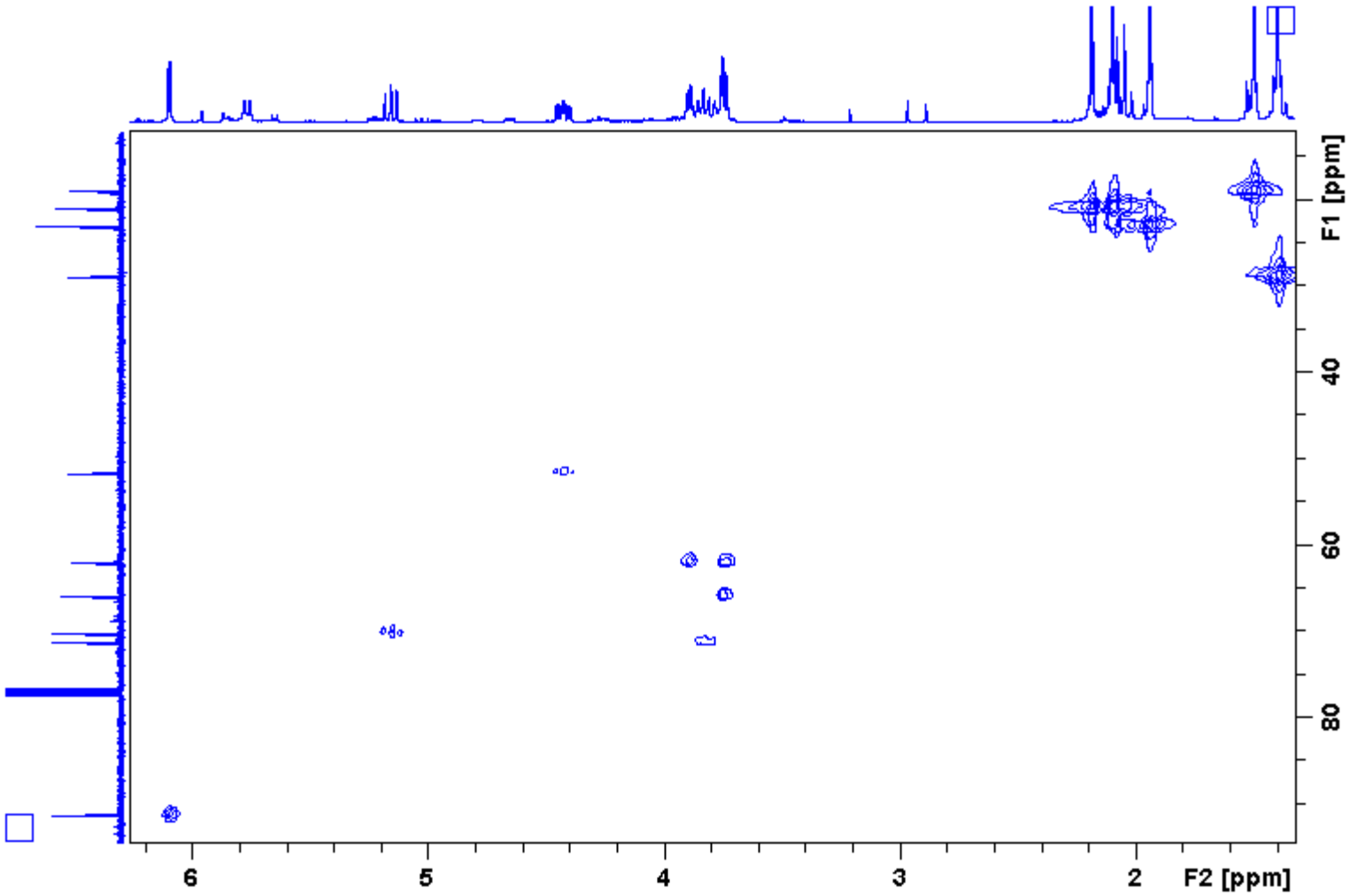

Figure 35: 400 MHz ^{1}H-^{13}C HMQC Spectrum of **4α/β**.

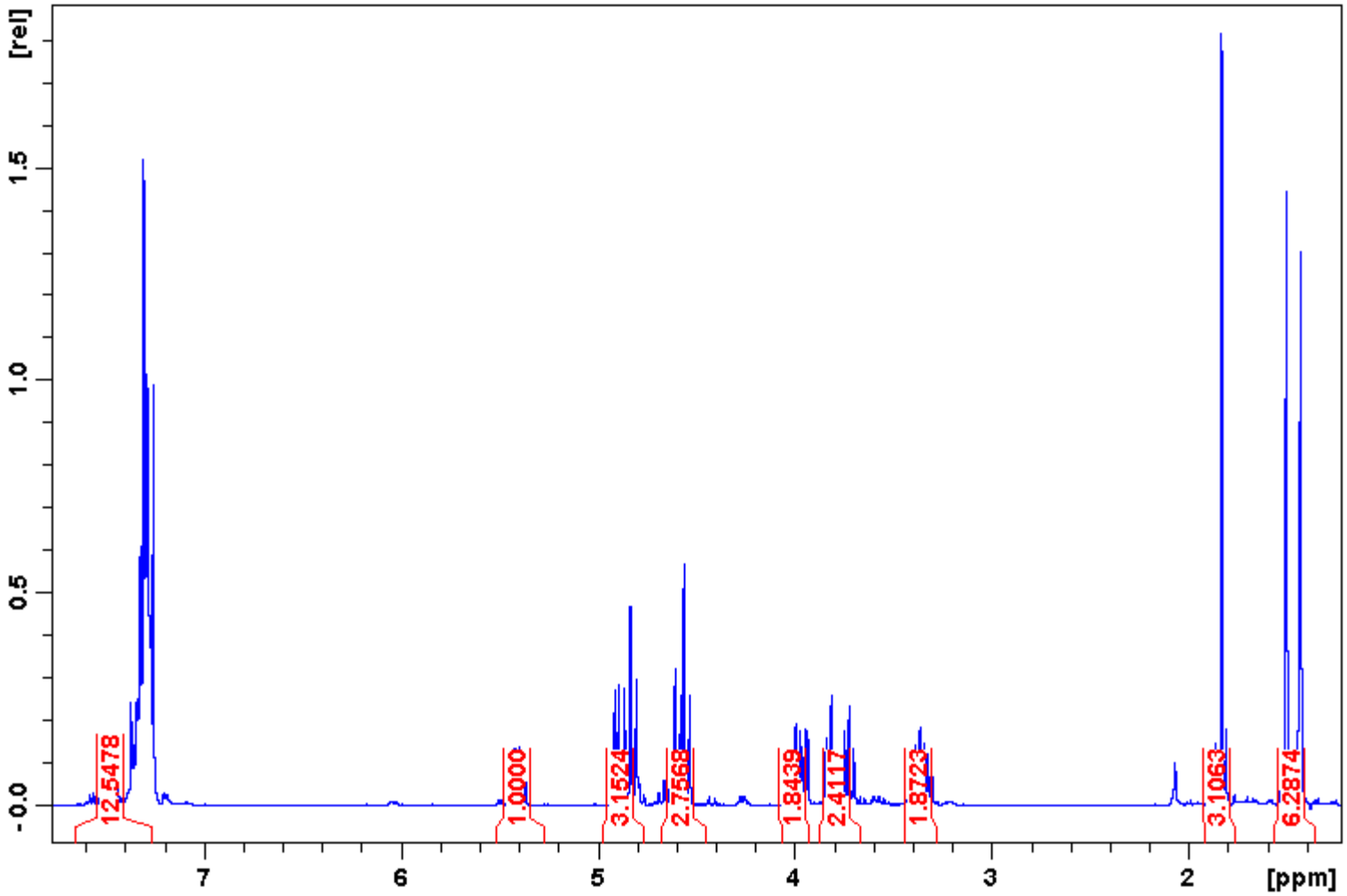

Figure 36: 400 MHz ^{1}H Spectrum of **5α/β**.

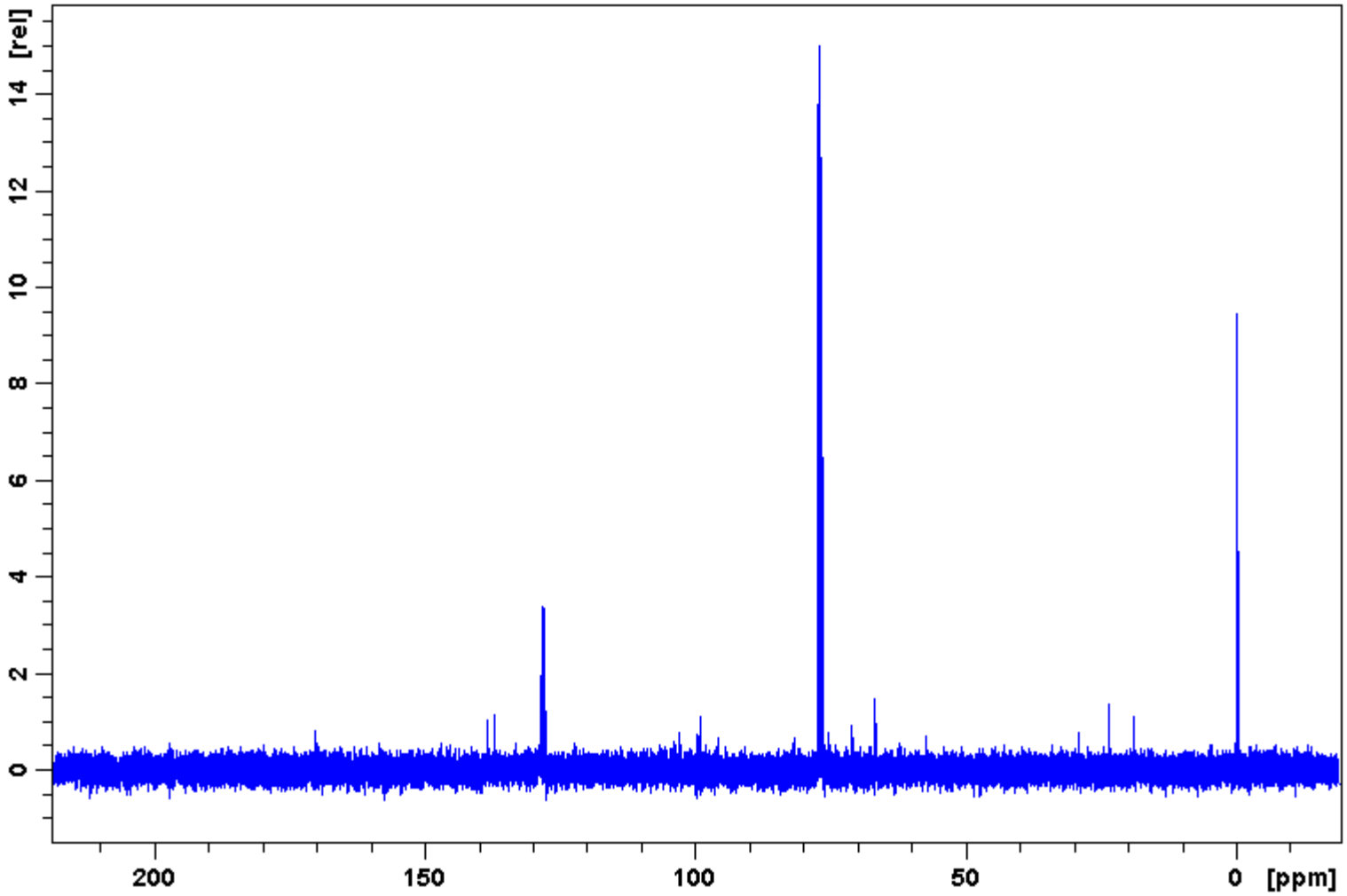

Figure 37: 100 MHz ^{13}C Spectrum of **5α/β**.

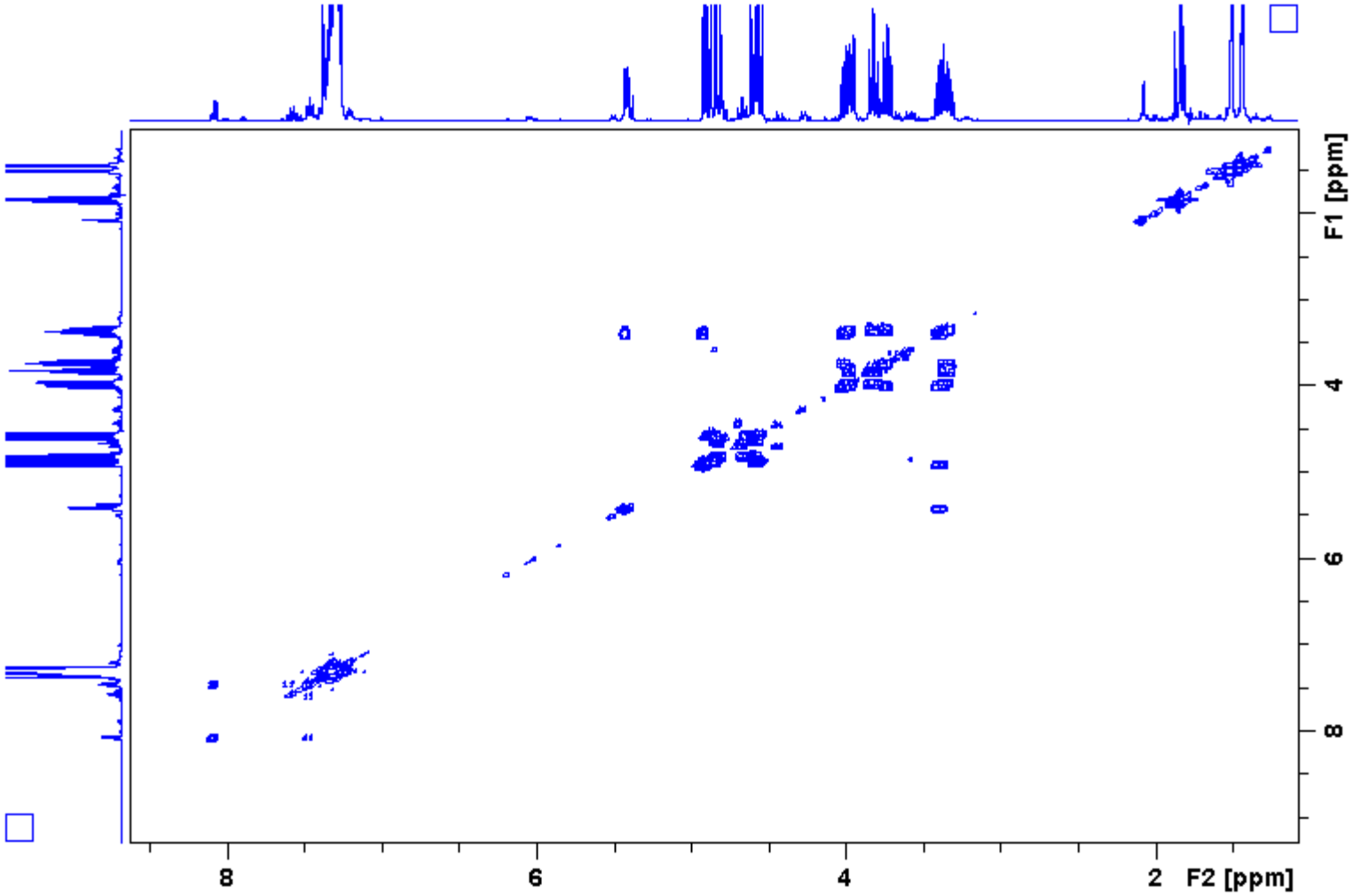

Figure 38: 400 MHz ^{1}H-^{1}H COSY Spectrum of **5α/β**.

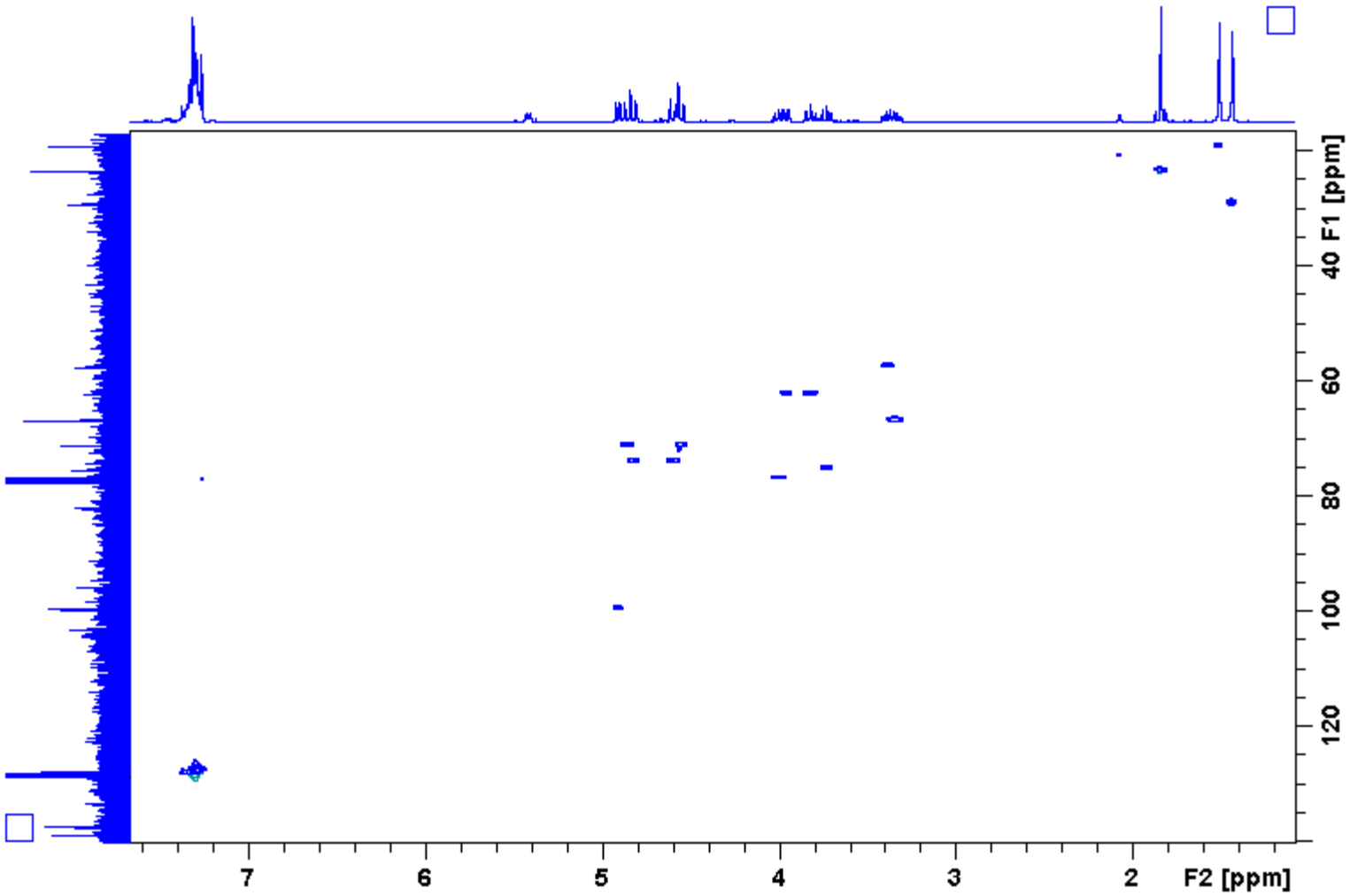

Figure 39: 400 MHz ^{1}H-^{13}C HSQC Spectrum of **5α/β**.

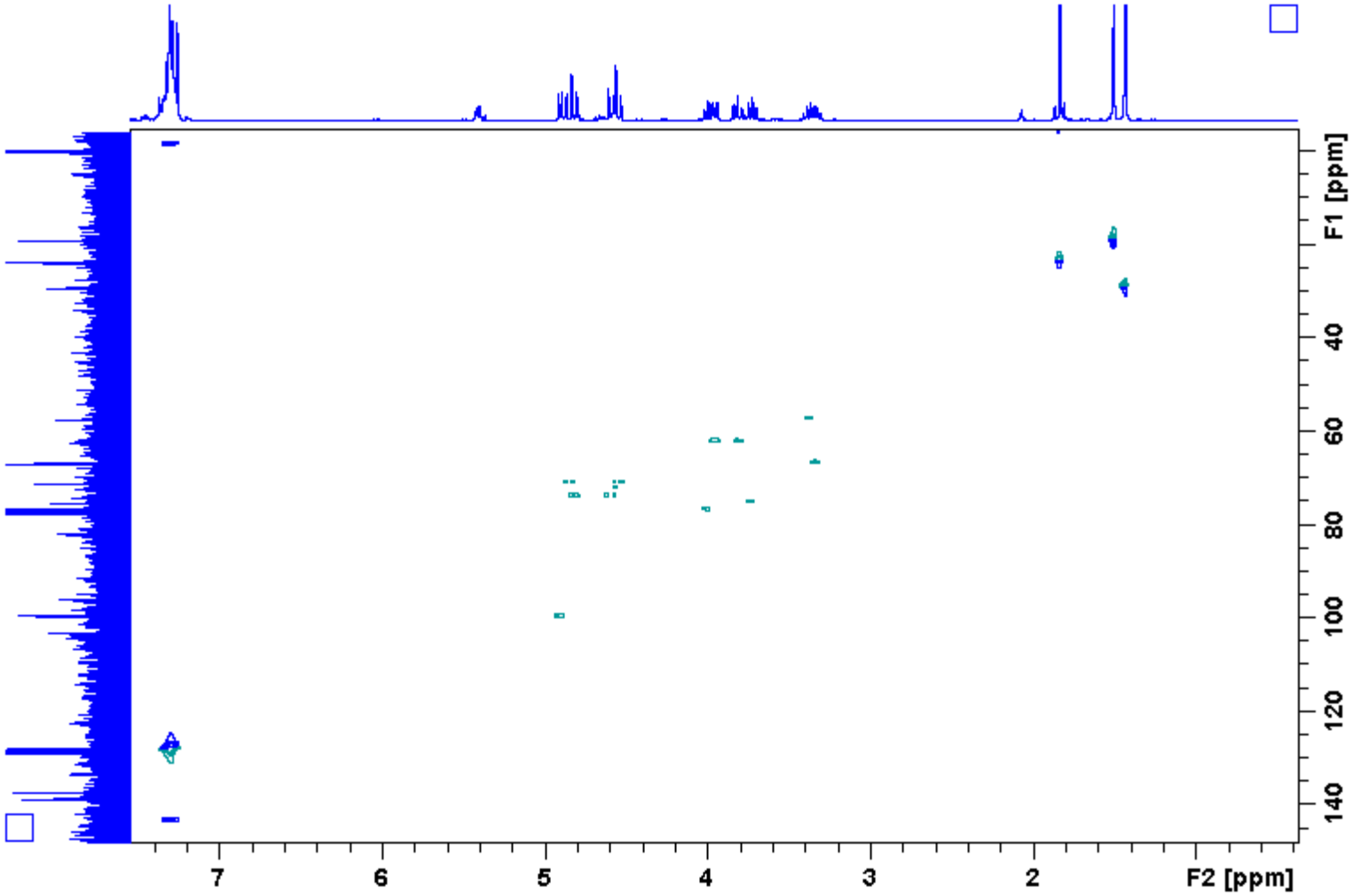

Figure 40: 400 MHz ^{1}H-^{13}C HMQC Spectrum of **5α/β**.

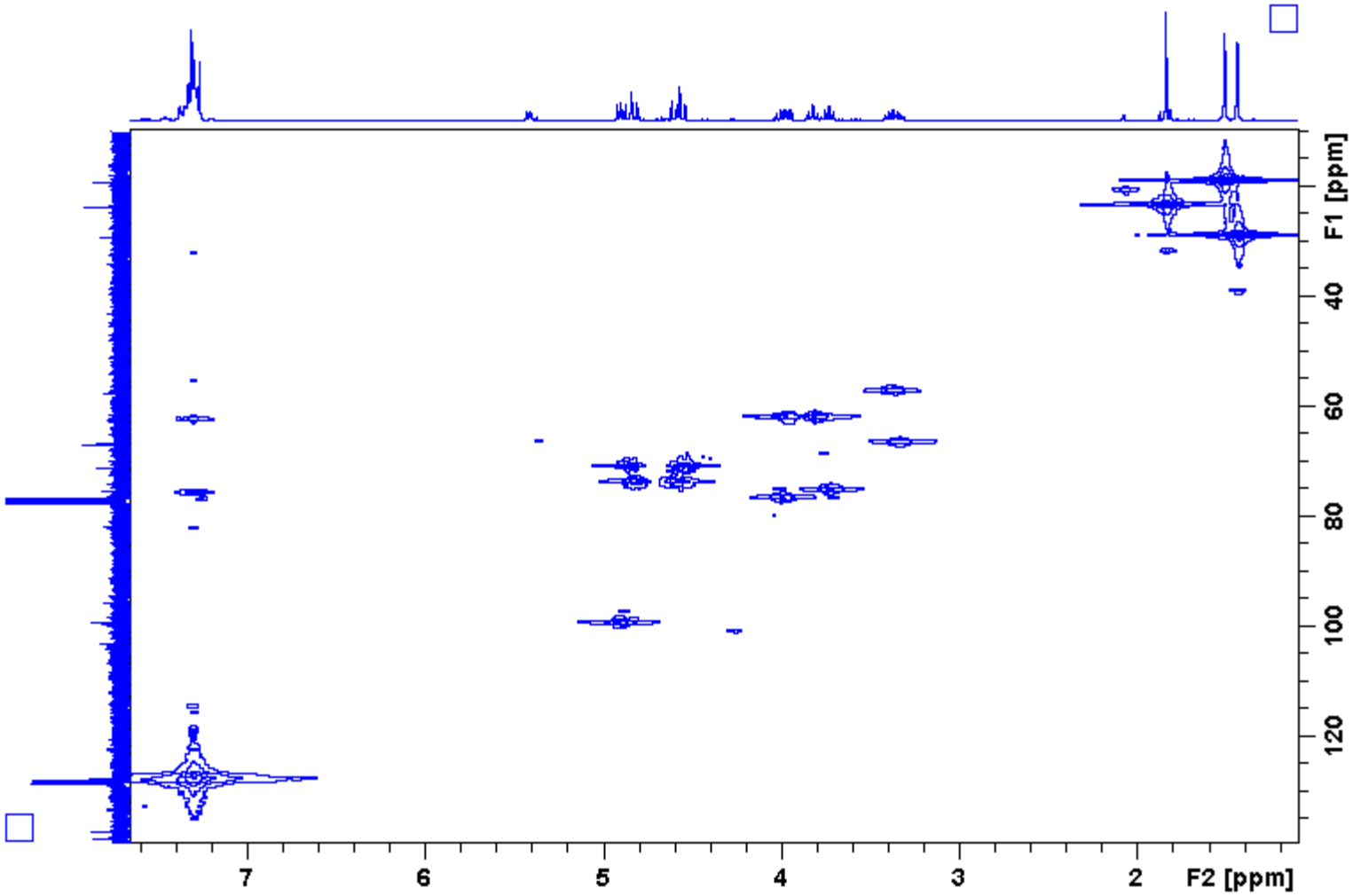

Figure 41: 400 MHz ^{1}H-^{13}C HMBC Spectrum of **5α/β**.

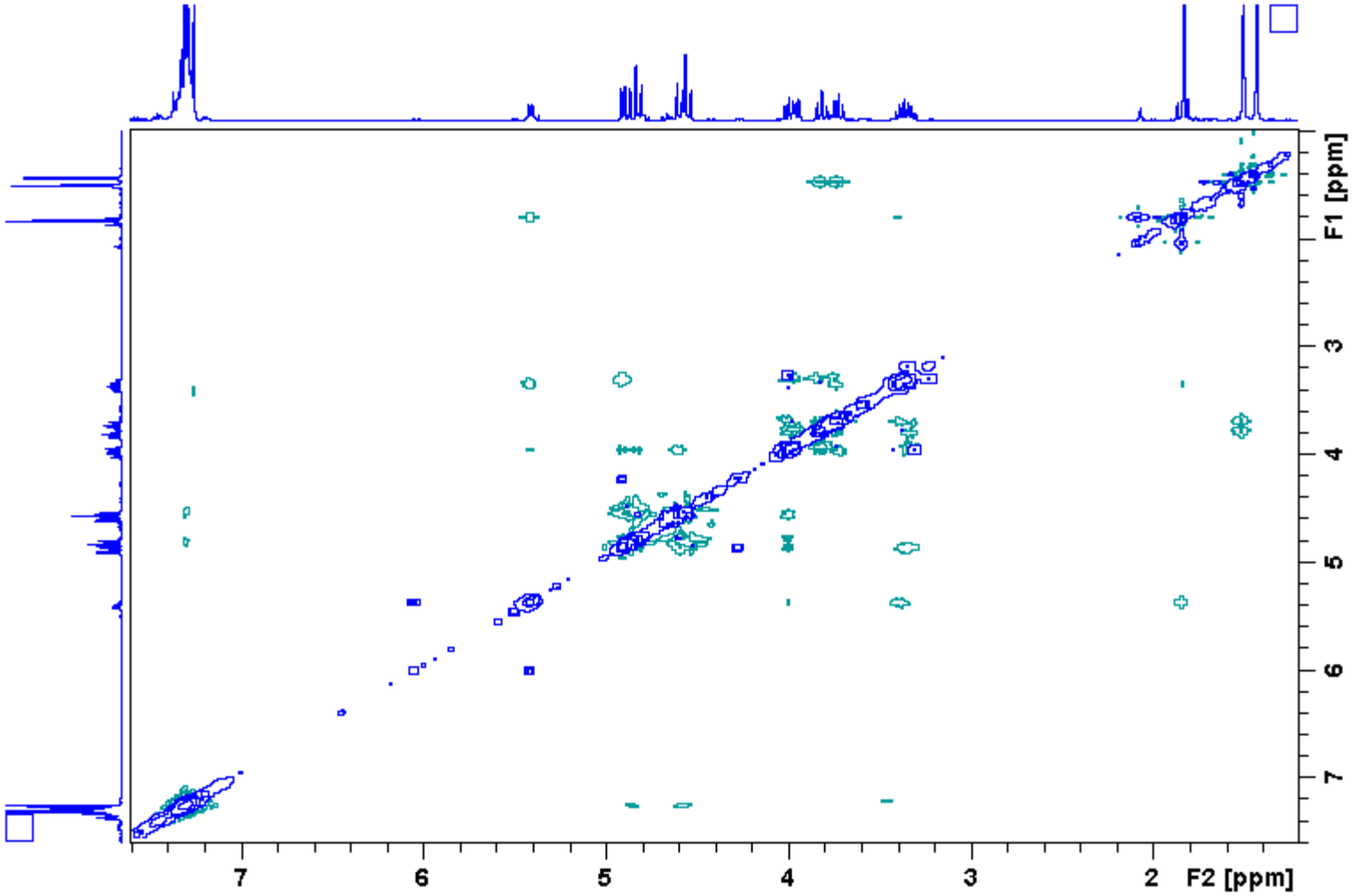

Figure 42: 400 MHz ^{1}H-^{1}H NOESY Spectrum of **5α/β**.

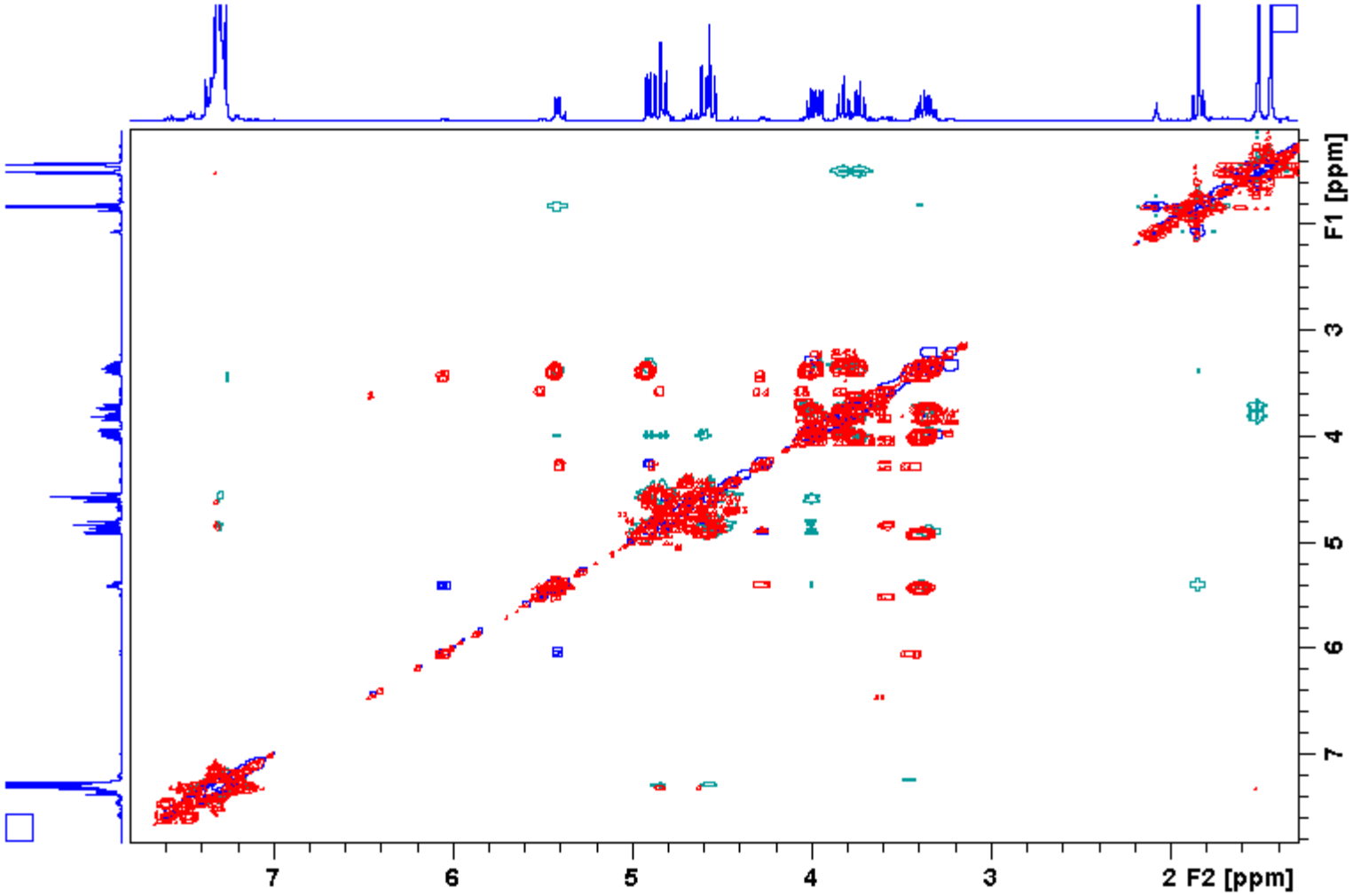

Figure 43: 400 MHz ^{1}H-^{1}H NOESY-COSY Spectrum Overlay of **5α/β**.

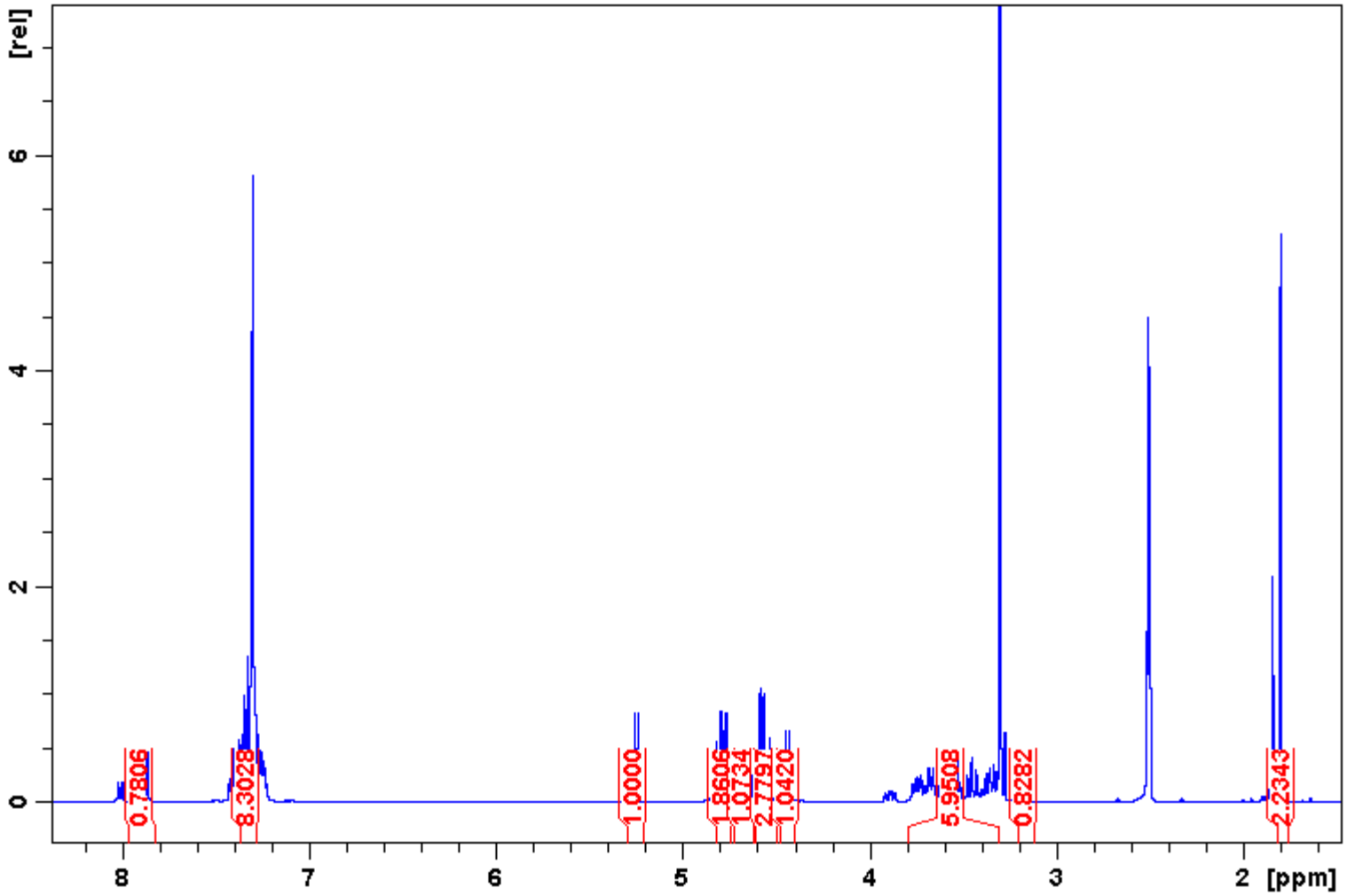

Figure 44: 400 MHz ^{1}H Spectrum of **6α/β**.

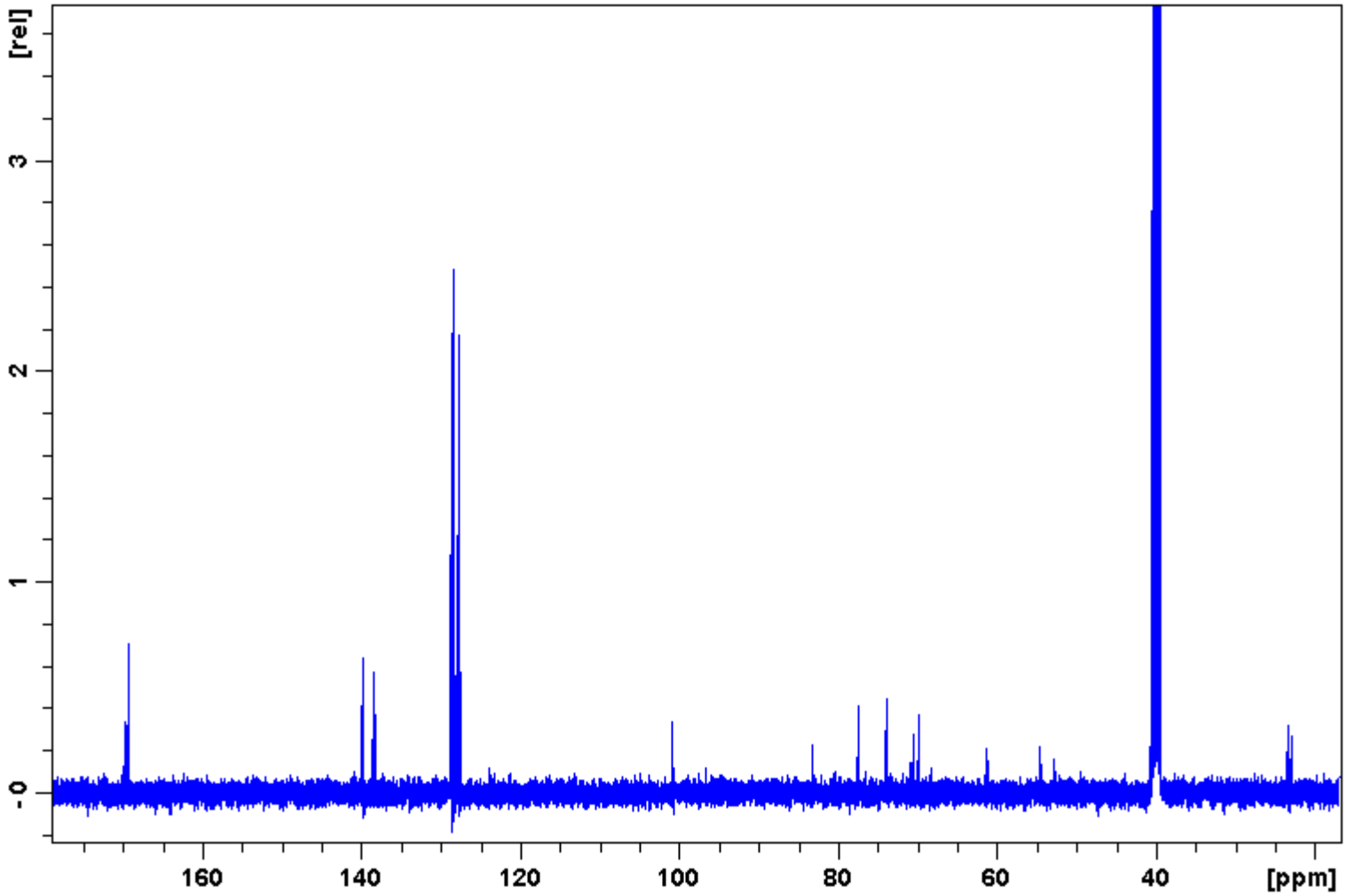

Figure 45: 100 MHz ^{13}C Spectrum of **6α/β**.

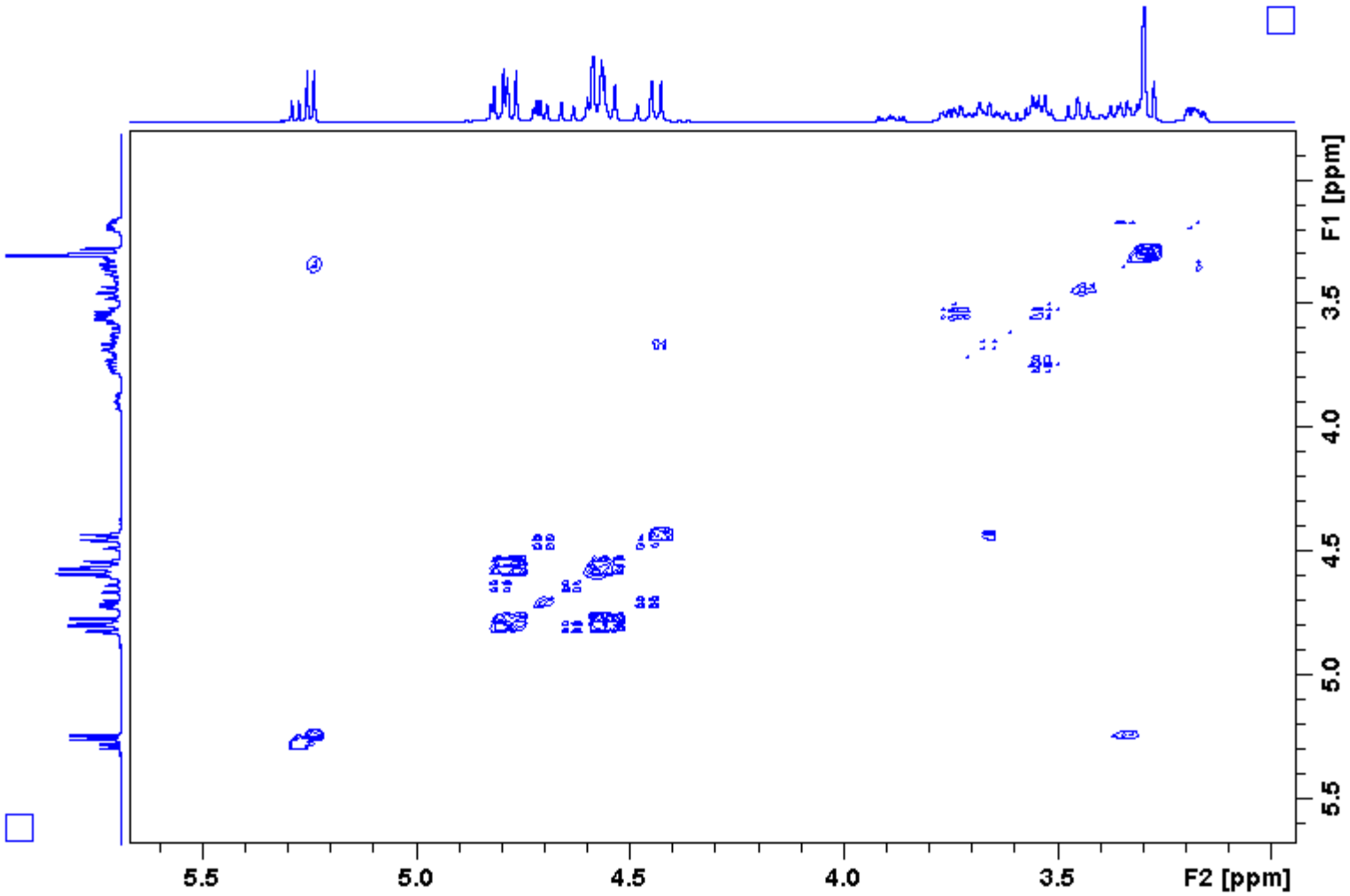

Figure 46: 400 MHz ^{1}H-^{1}H COSY Spectrum of **6α/β**.

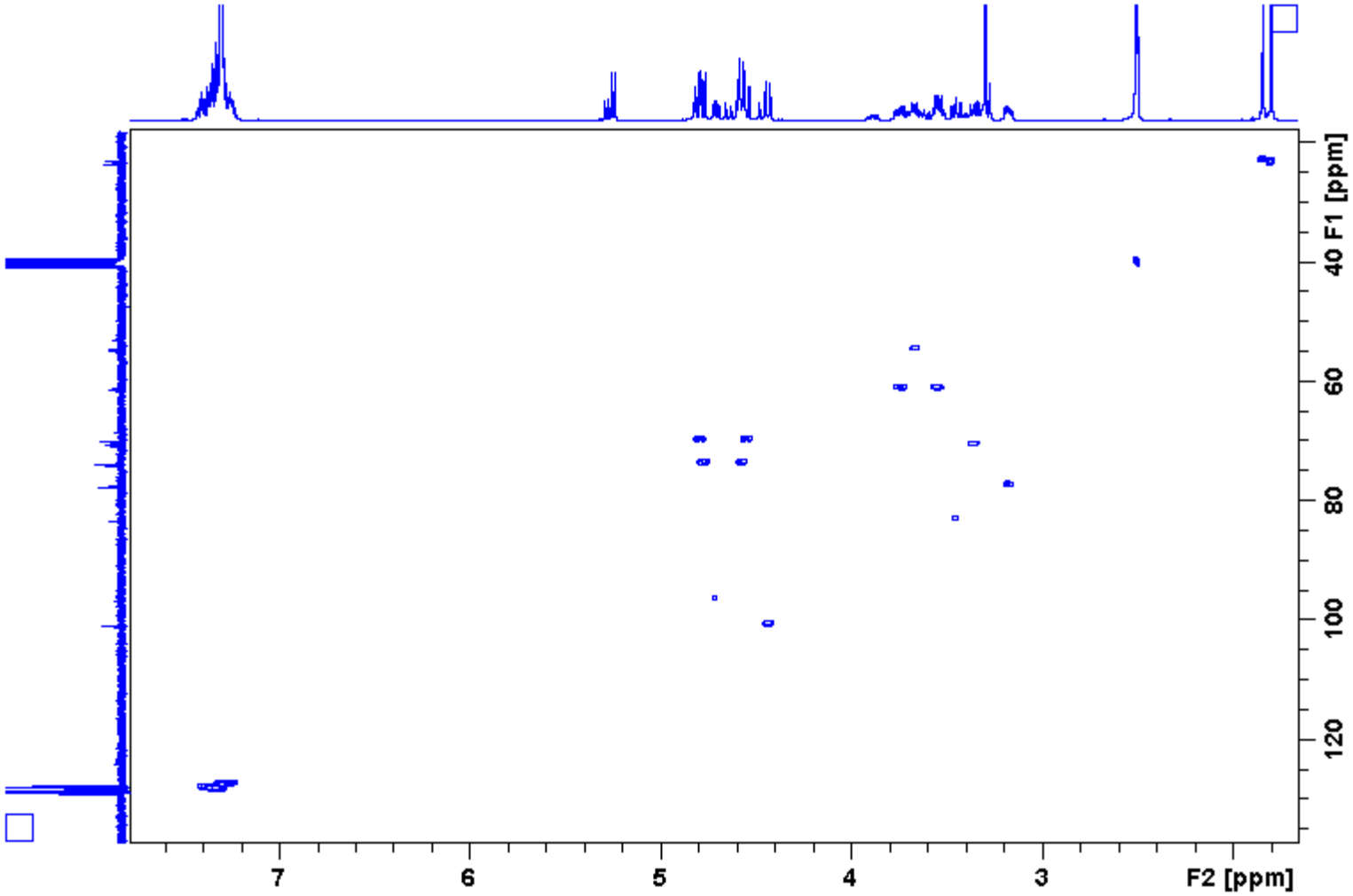

Figure 47: 400 MHz ^{1}H-^{13}C HSQC Spectrum of **6α/β**.

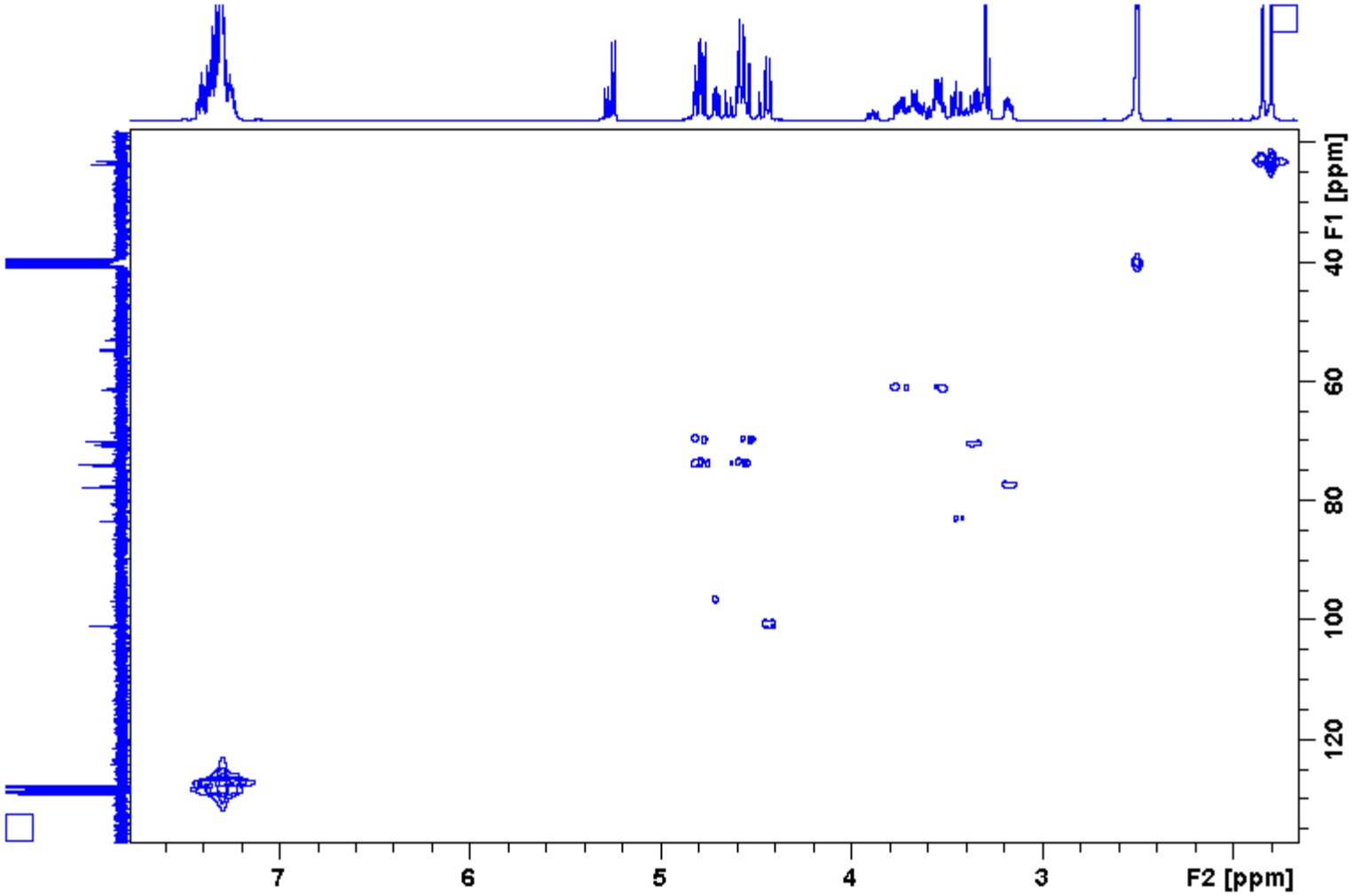

Figure 48: 400 MHz ^{1}H-^{13}C HMQC Spectrum of **6α/β**.

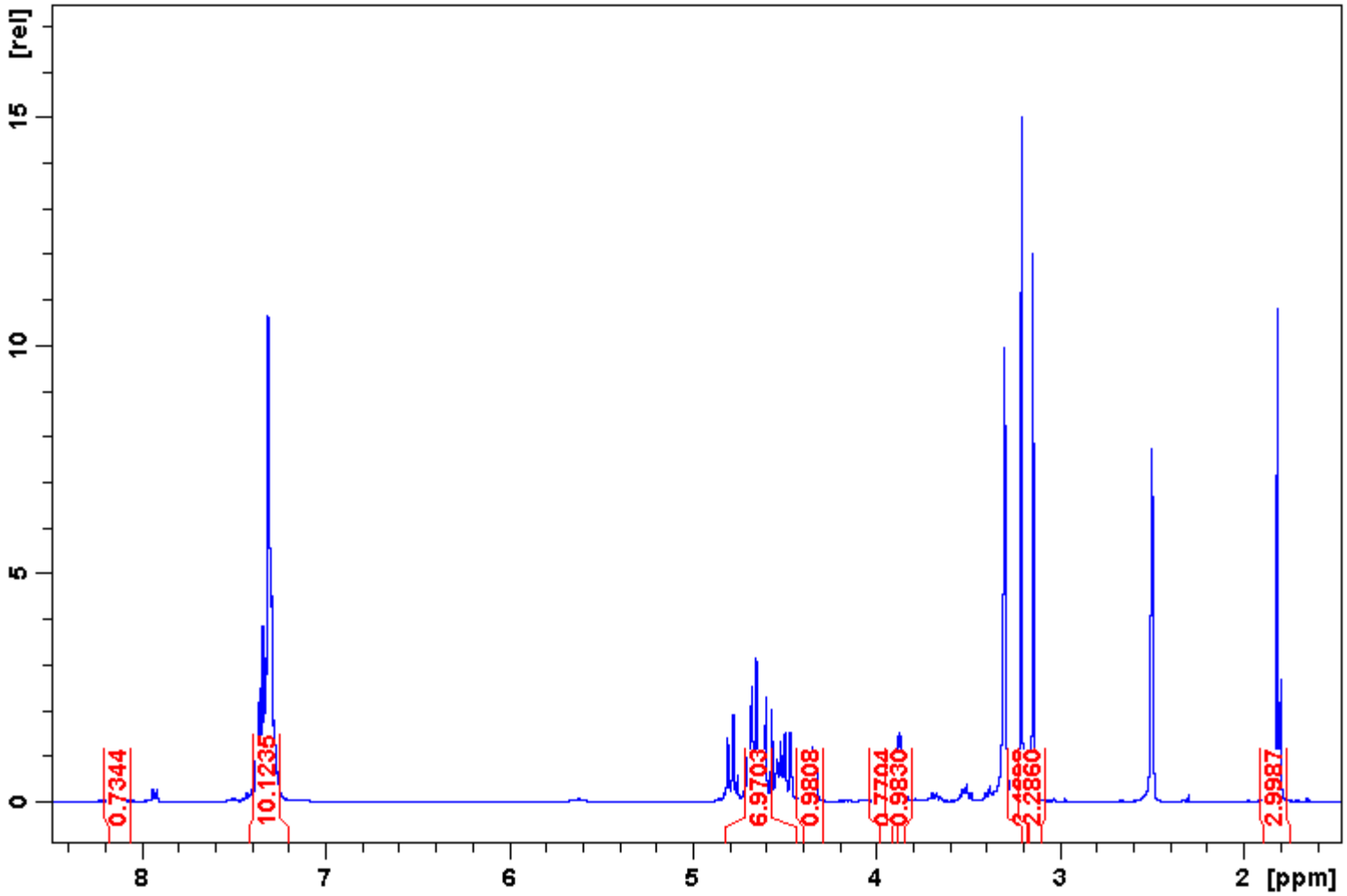

Figure 49: 400 MHz ^{1}H Spectrum of **7α/β**.

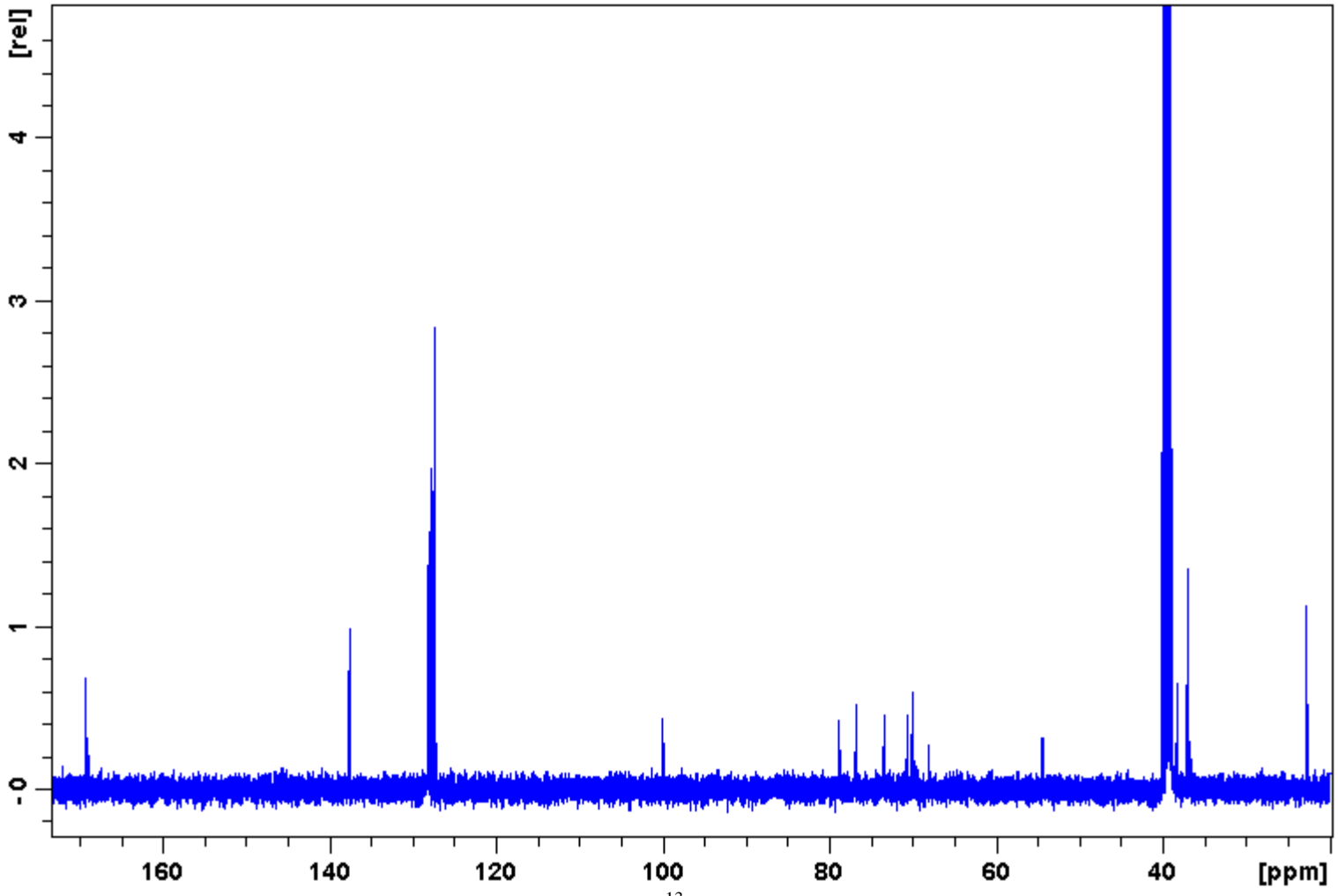

Figure 50: 100 MHz ^{13}C Spectrum of **7α/β**.

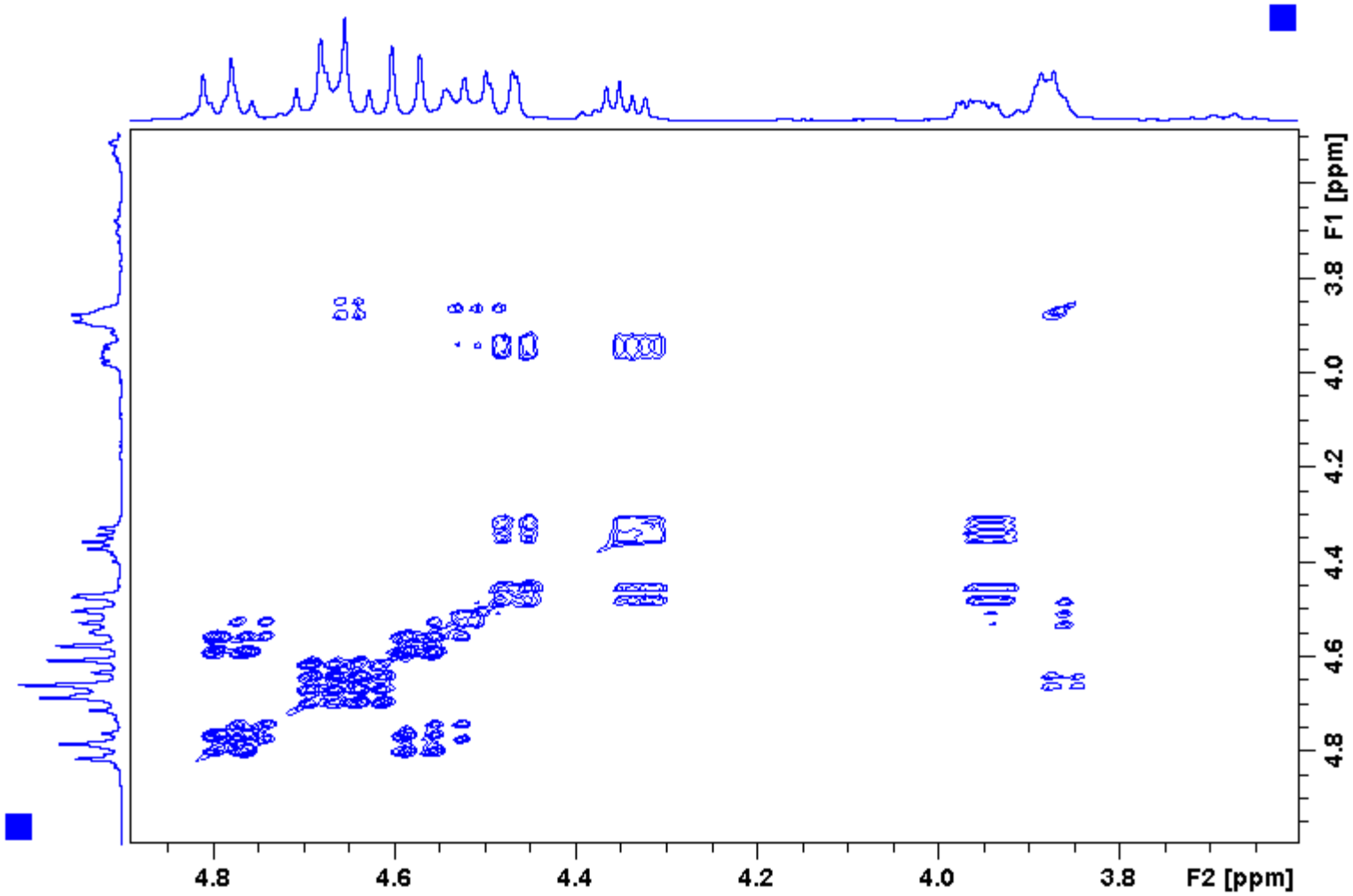

Figure 51: 400 MHz ^{1}H-^{1}H COSY Spectrum of **7α/β**.

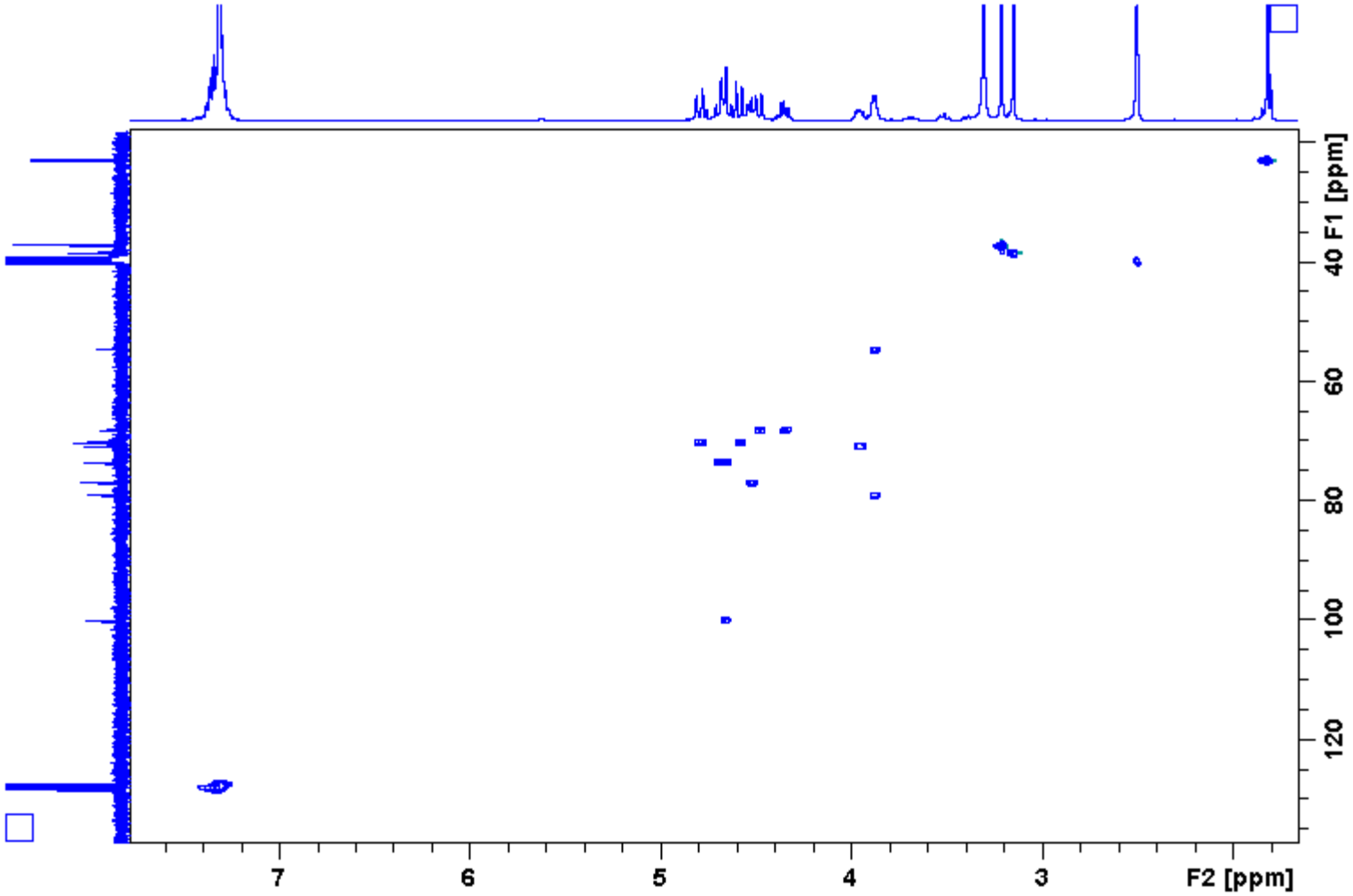

Figure 52: 400 MHz ^{1}H-^{13}C HSQC Spectrum of **7α/β**.

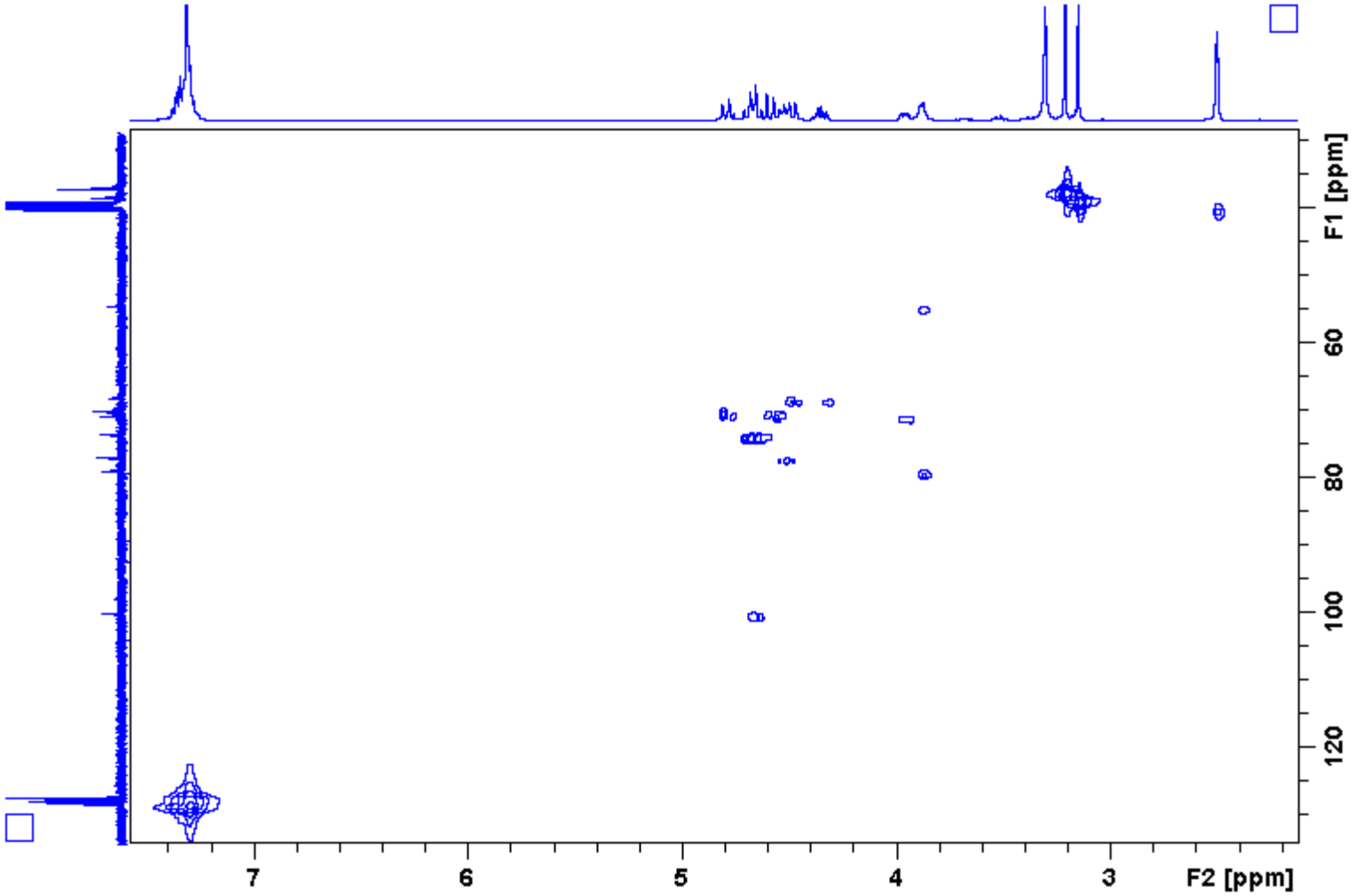

Figure 53: 400 MHz ^{1}H-^{13}C HMQC Spectrum of **7α/β**.

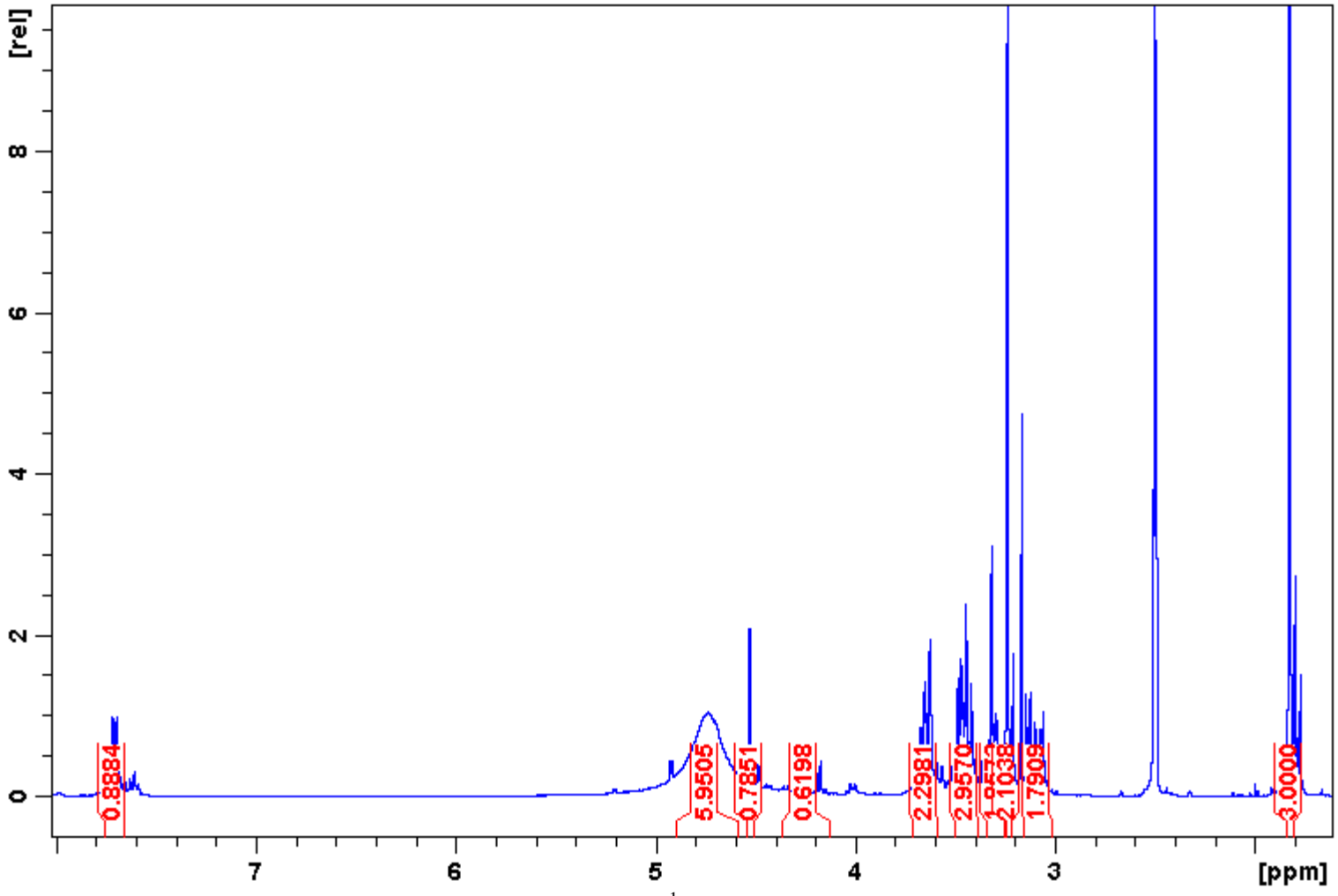

Figure 54: 400 MHz ^{1}H Spectrum of **8α/β**.

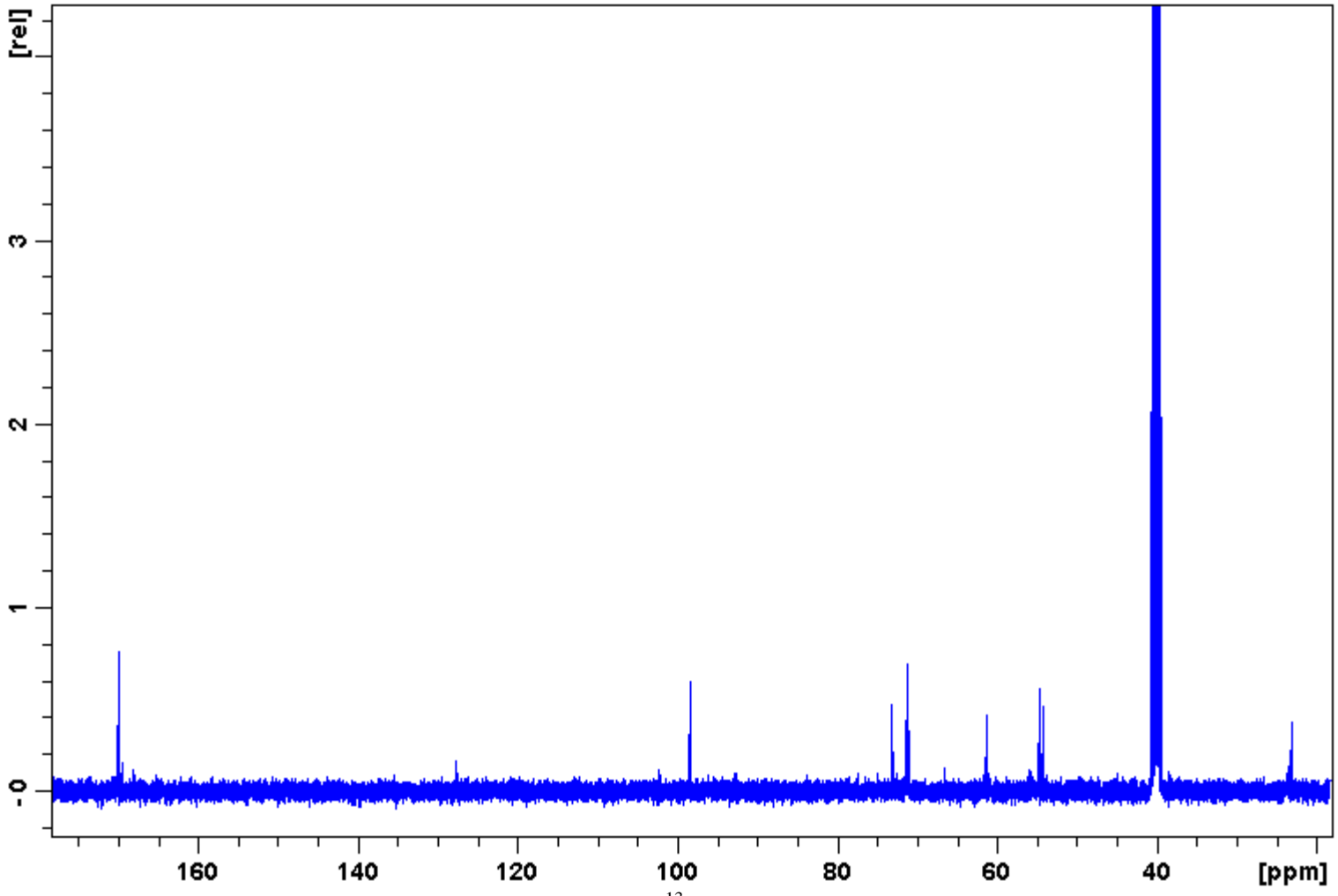

Figure 55: 100 MHz ^{13}C Spectrum of **8α/β**.

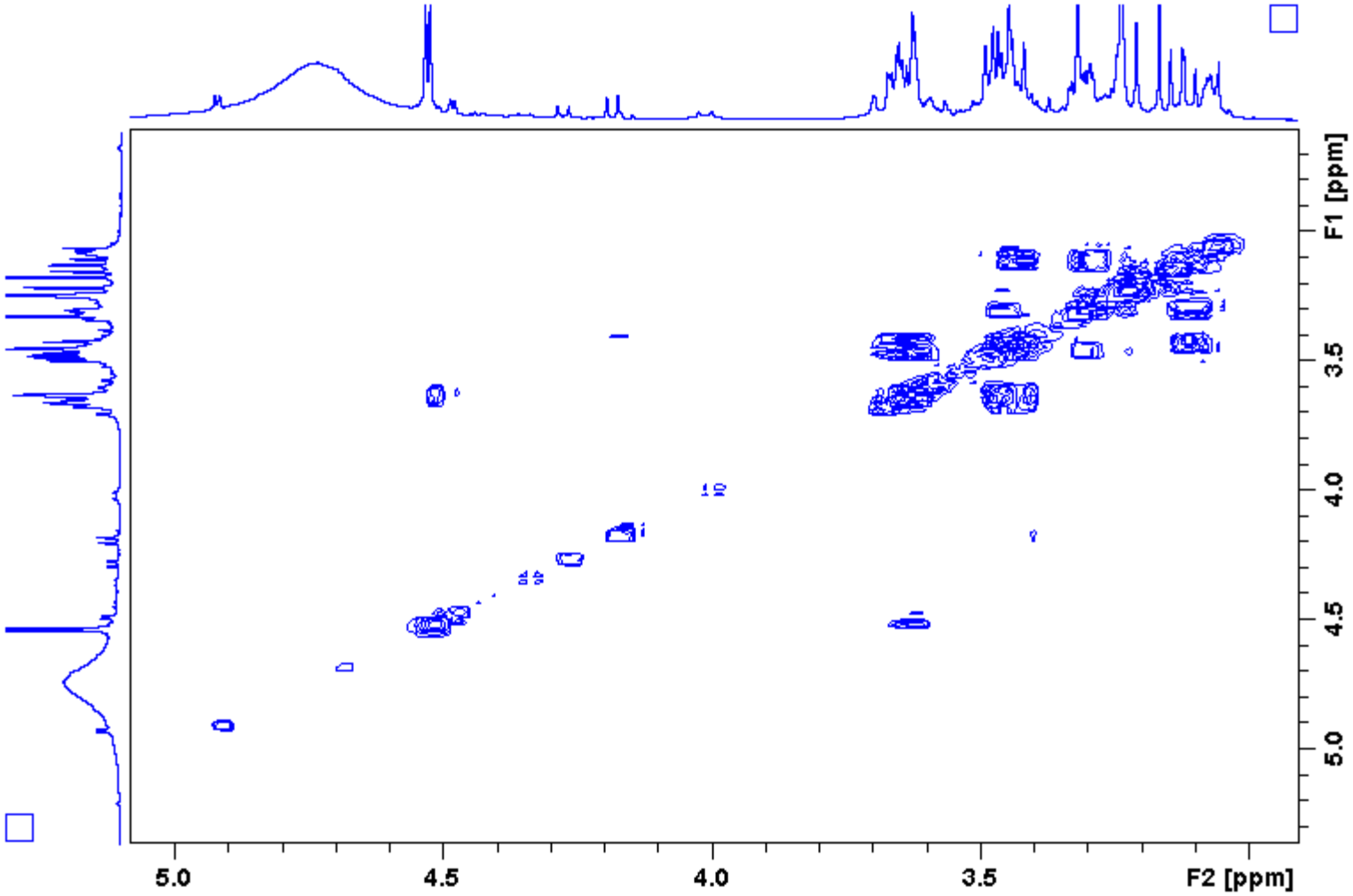

Figure 56: 400 MHz ^{1}H-^{1}H COSY Spectrum of **8α/β**.

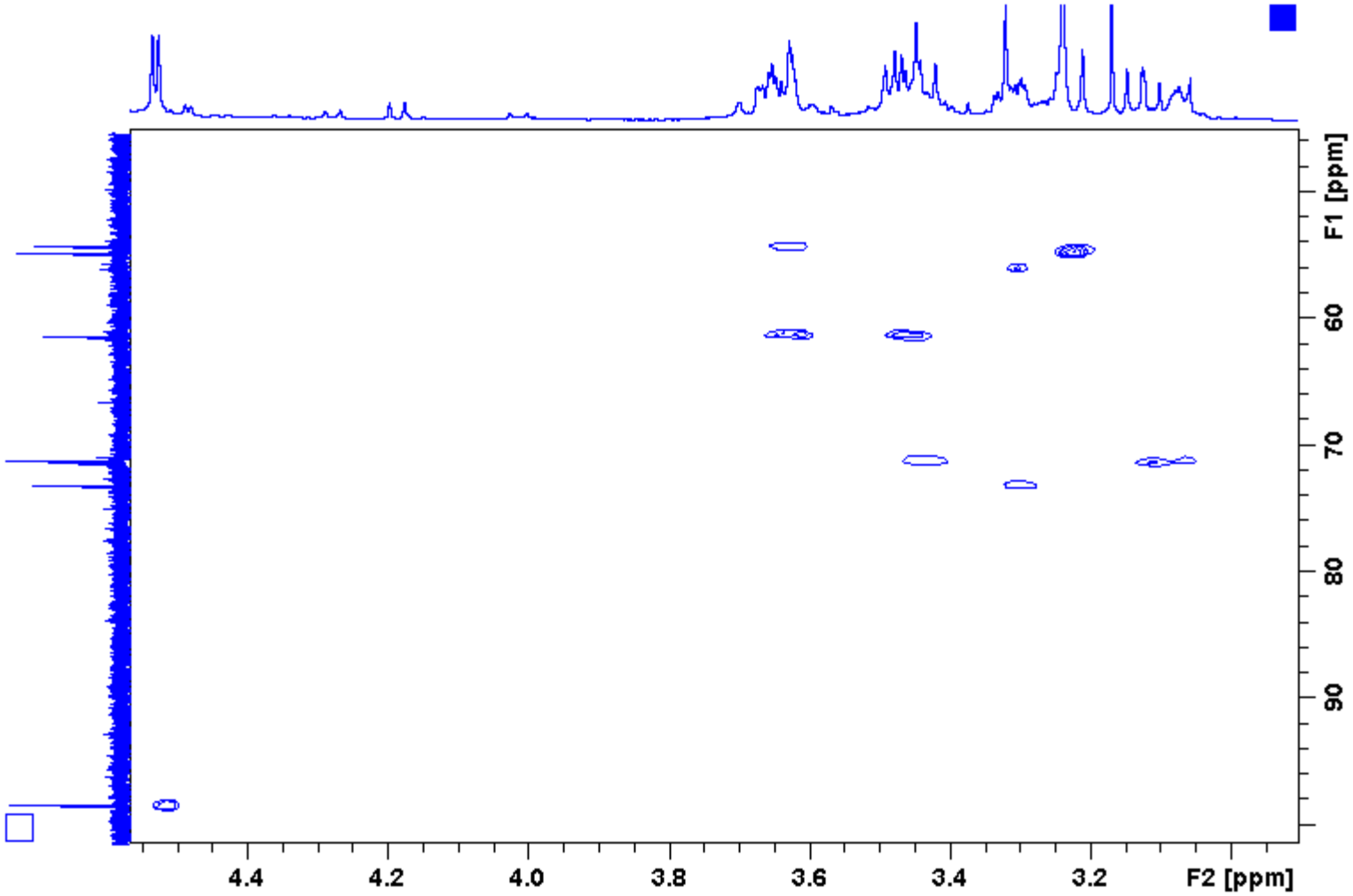

Figure 57: 400 MHz ^{1}H-^{13}C HSQC Spectrum of **8α/β**.

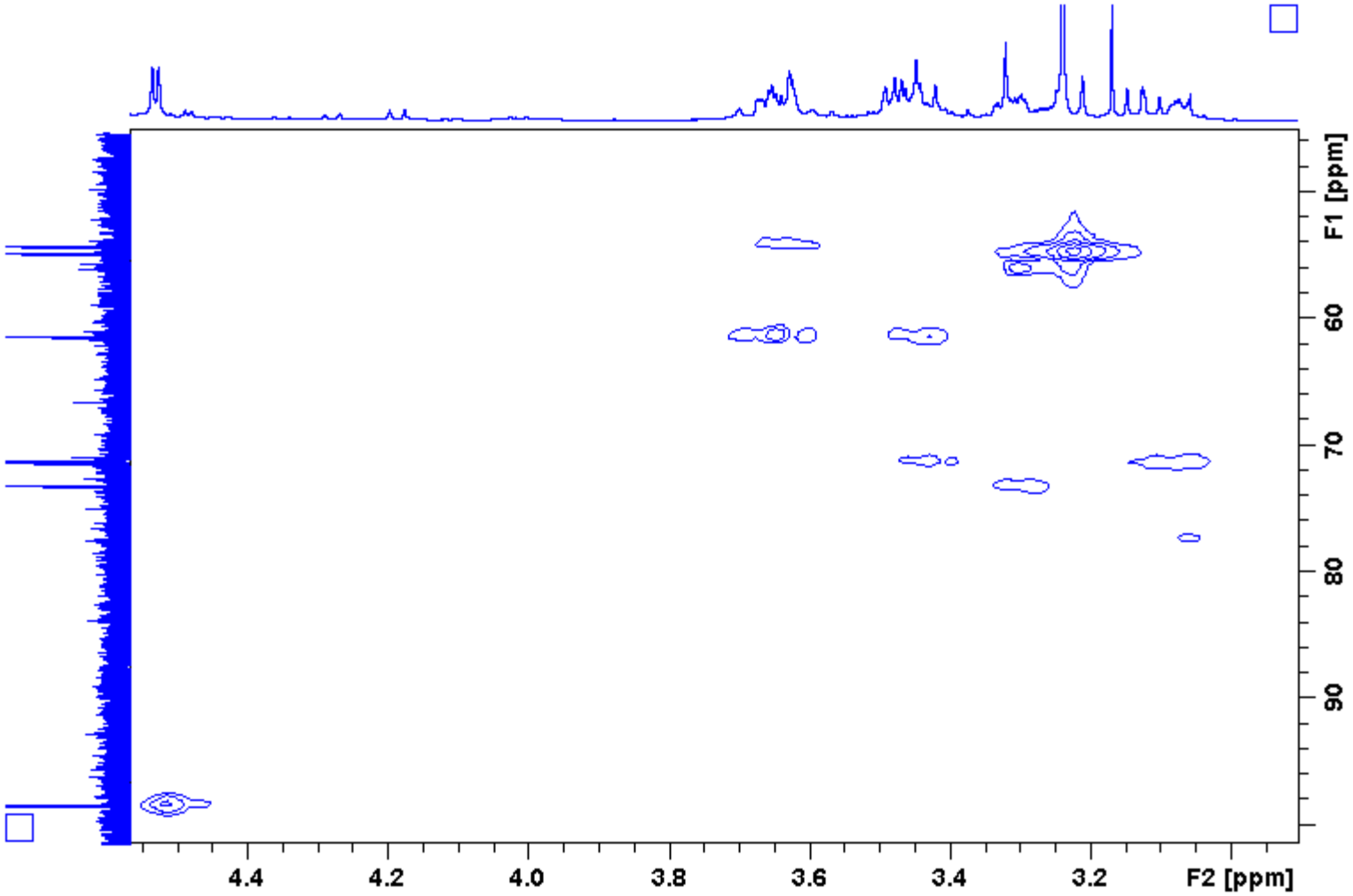

Figure 58: 400 MHz ^{1}H-^{13}C HMQC Spectrum of **8α/β**.

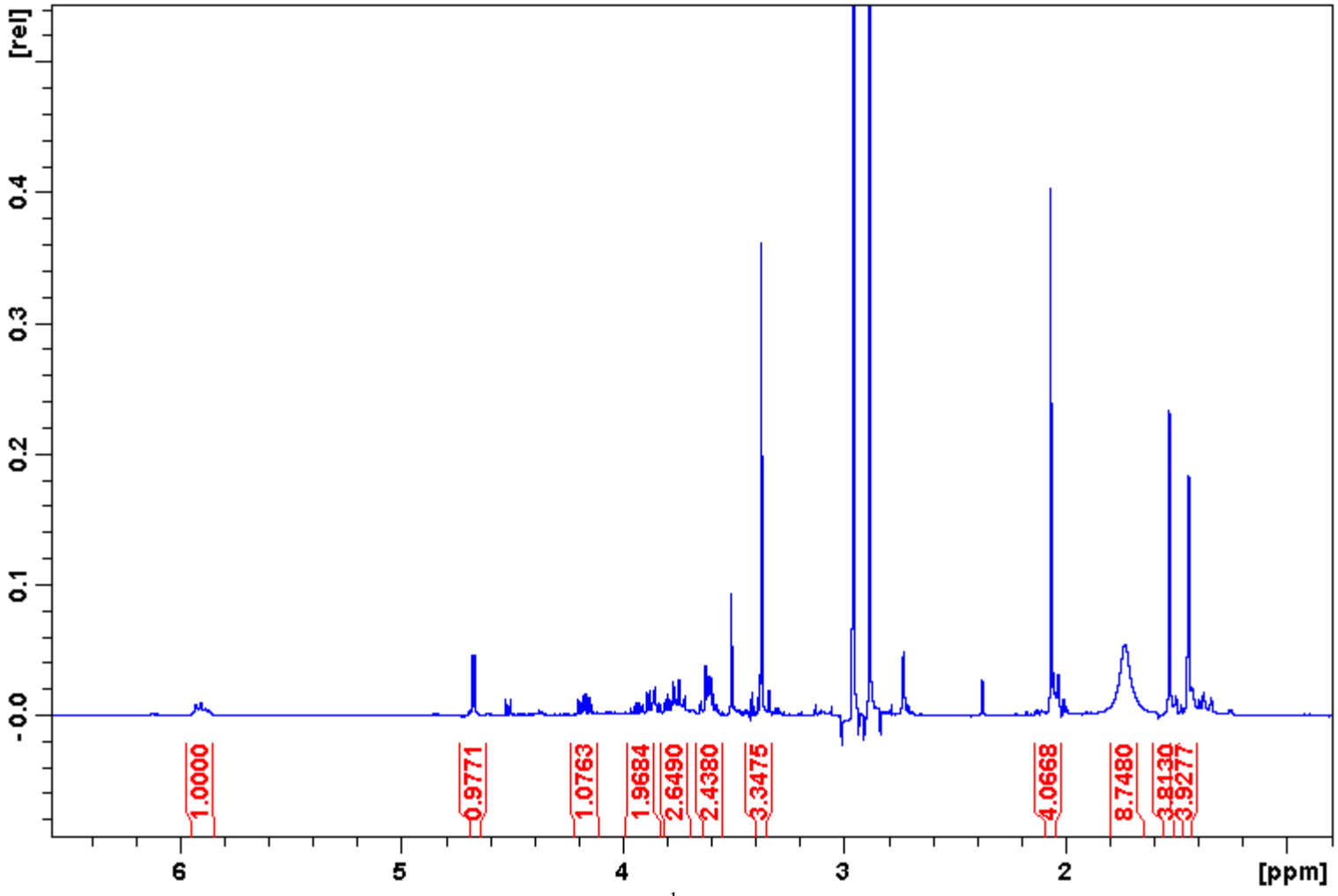

Figure 59: 400 MHz ^{1}H Spectrum of **9α/β**.

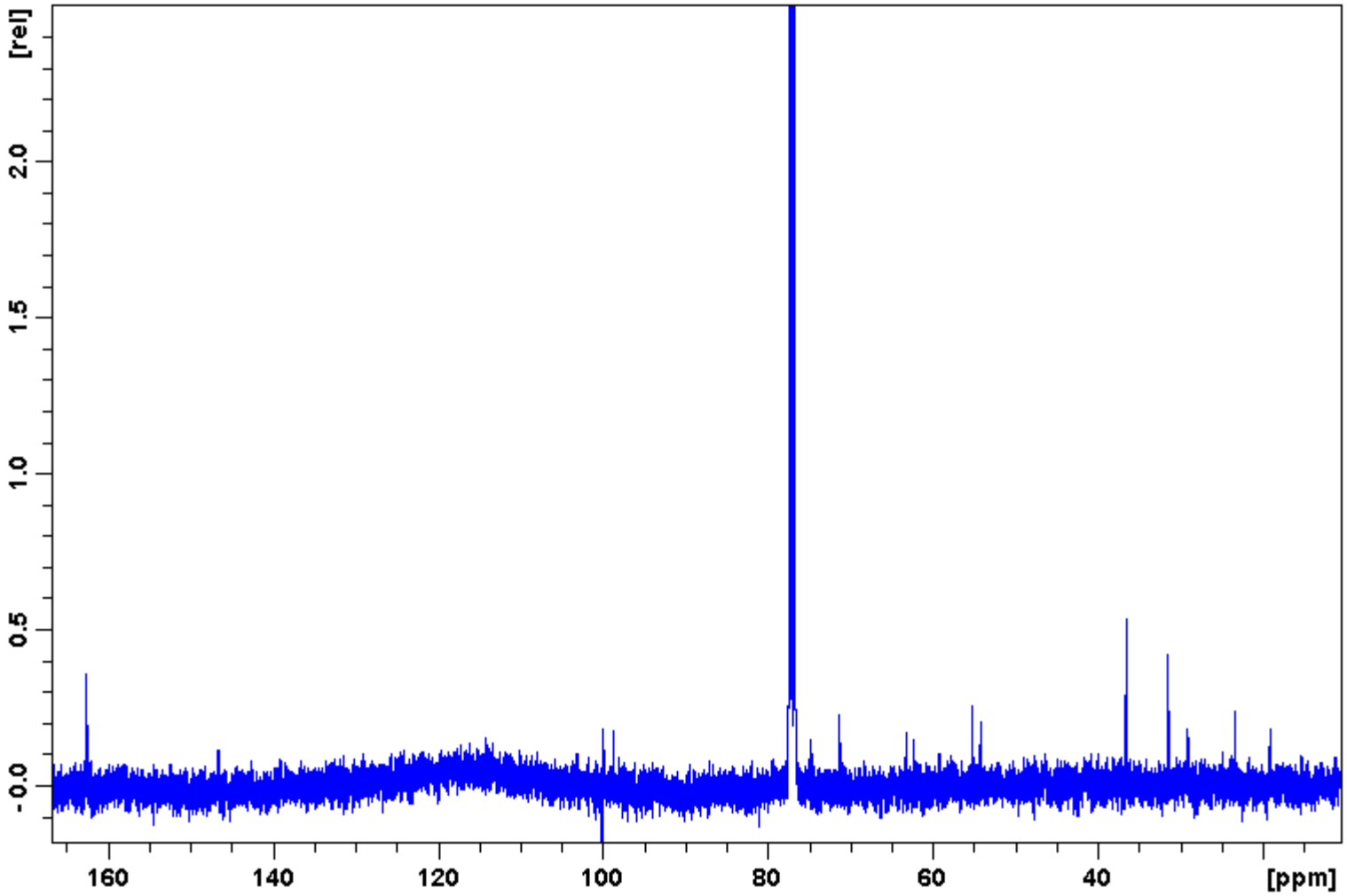

Figure 60: 100 MHz ^{13}C Spectrum of **9α/β**.

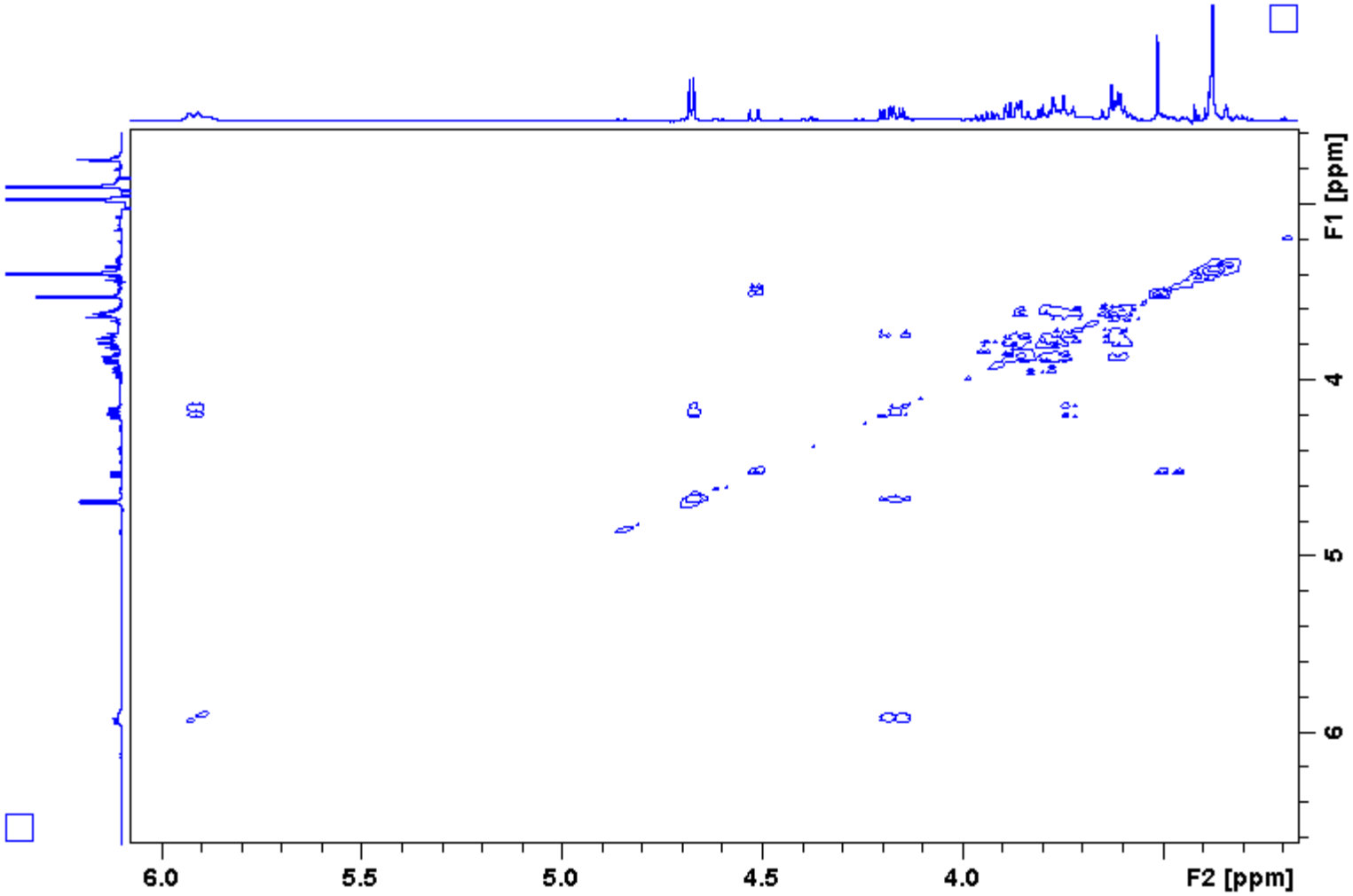

Figure 61: 400 MHz ^{1}H-^{1}H COSY Spectrum of **9α/β**.

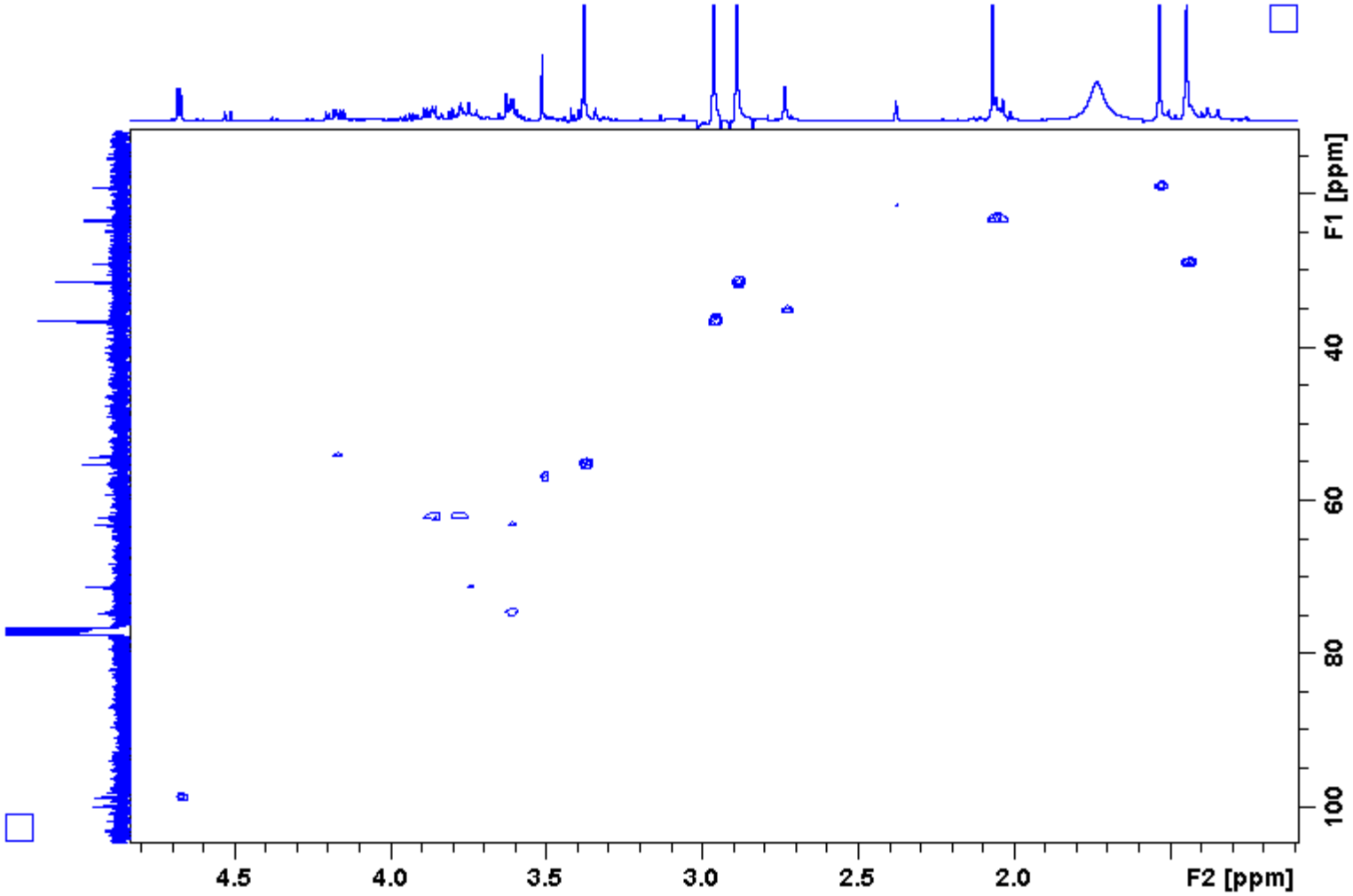

Figure 62: 400 MHz ^{1}H-^{13}C HSQC Spectrum of **9α/β**.

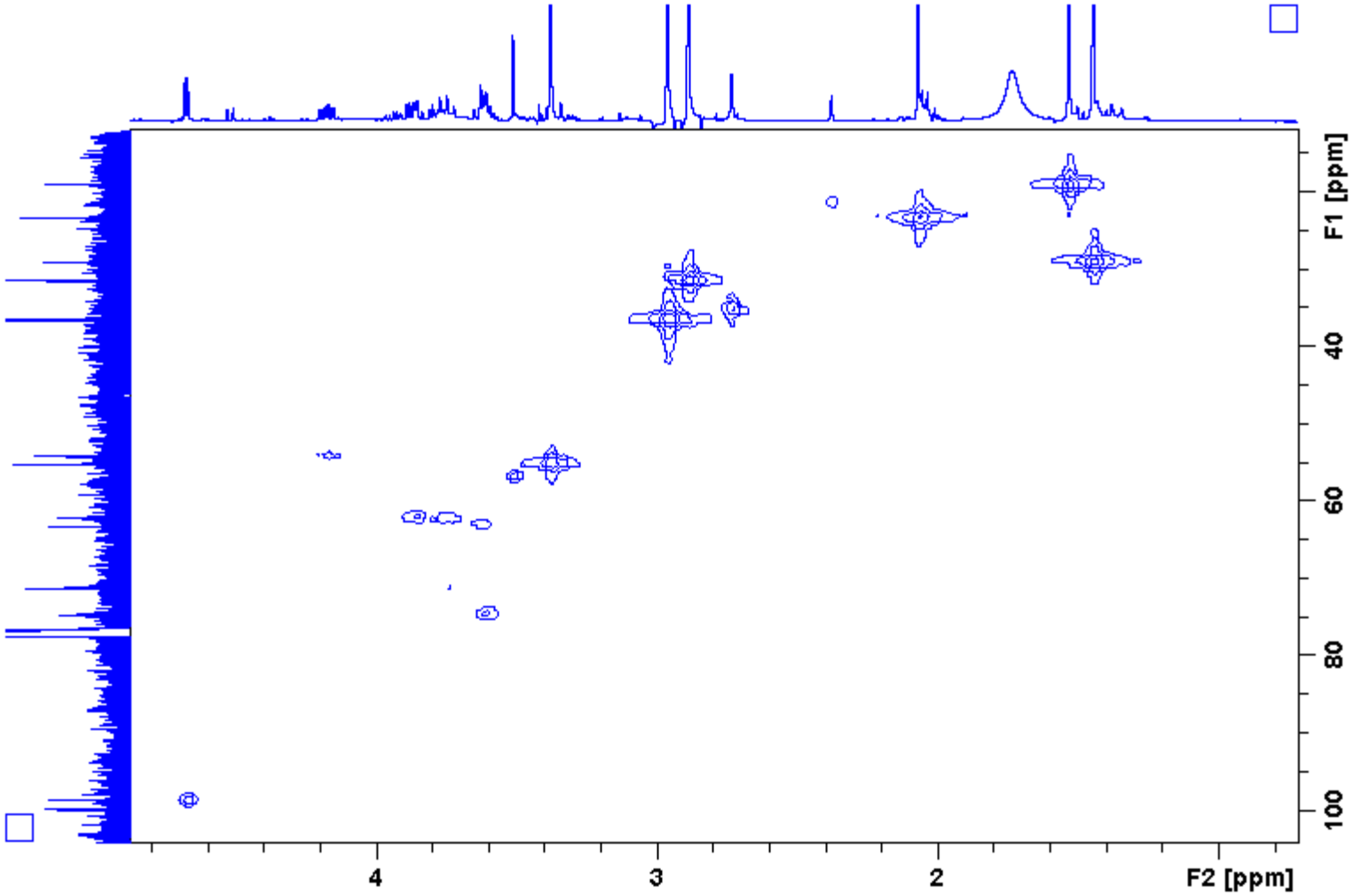

Figure 63: 400 MHz ^{1}H-^{13}C HMQC Spectrum of **9α/β**.

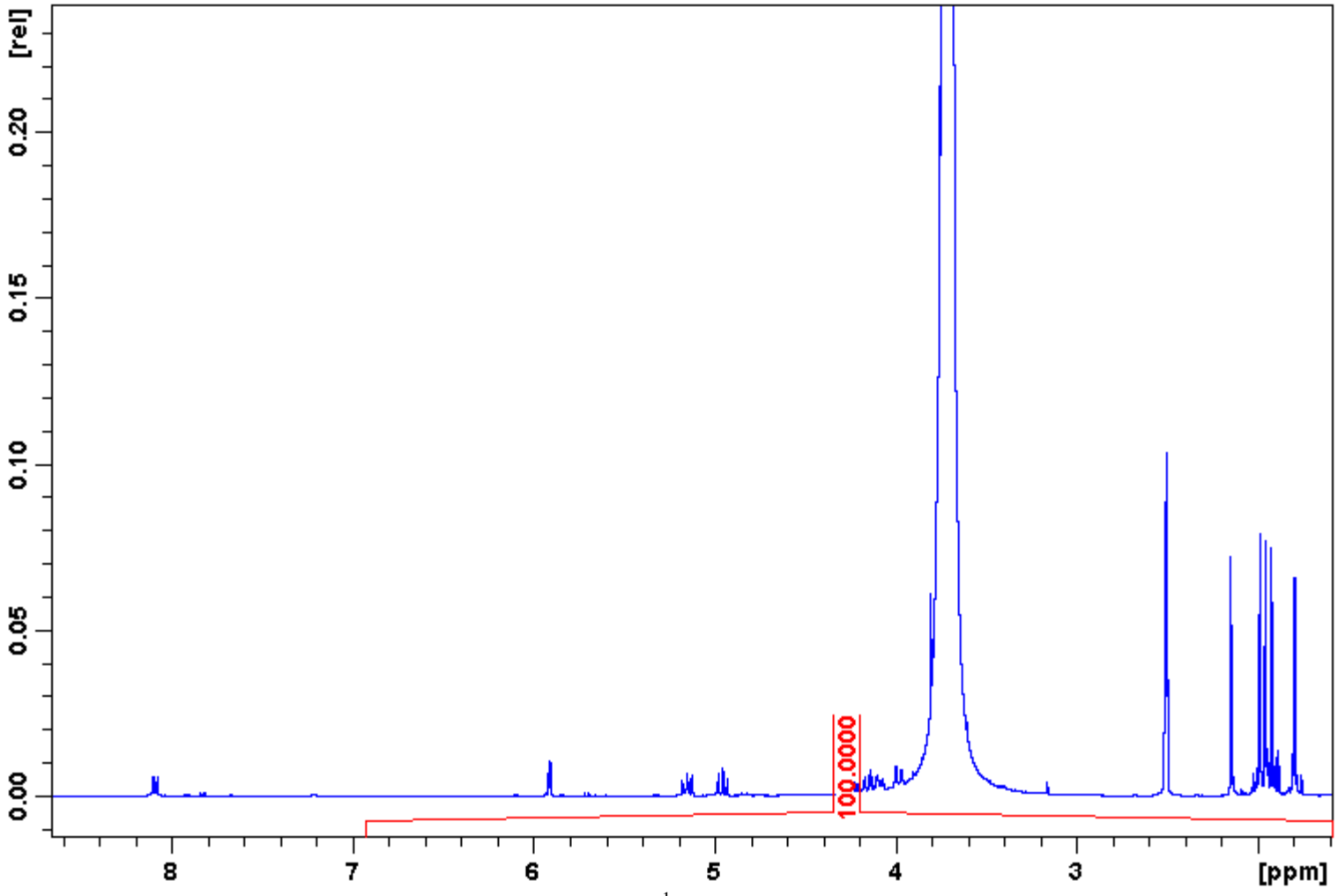

Figure 64: 400 MHz ^{1}H Spectrum of **10α/β**.

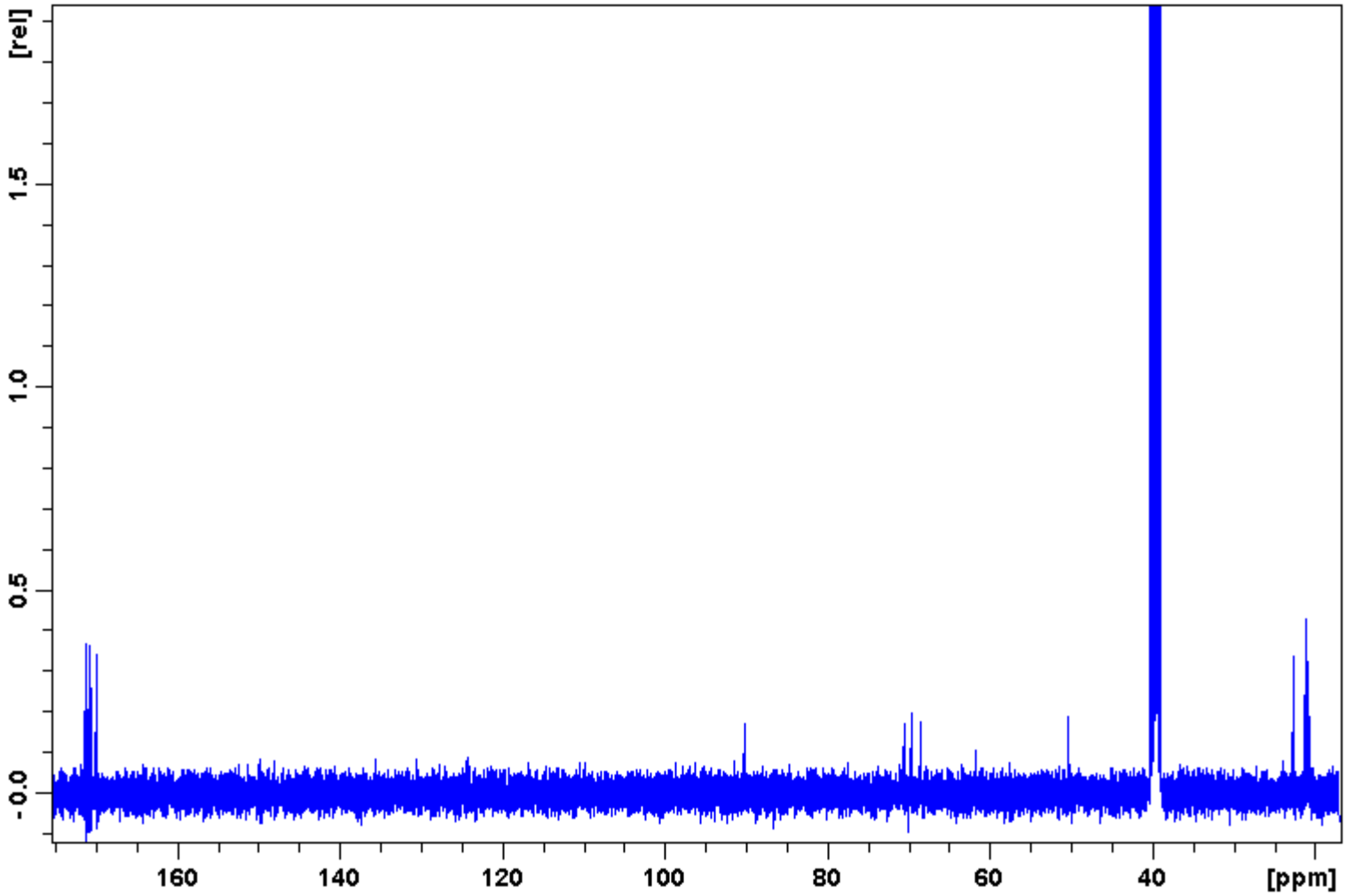

Figure 65: 100 MHz ^{13}C Spectrum of **10α/β**.

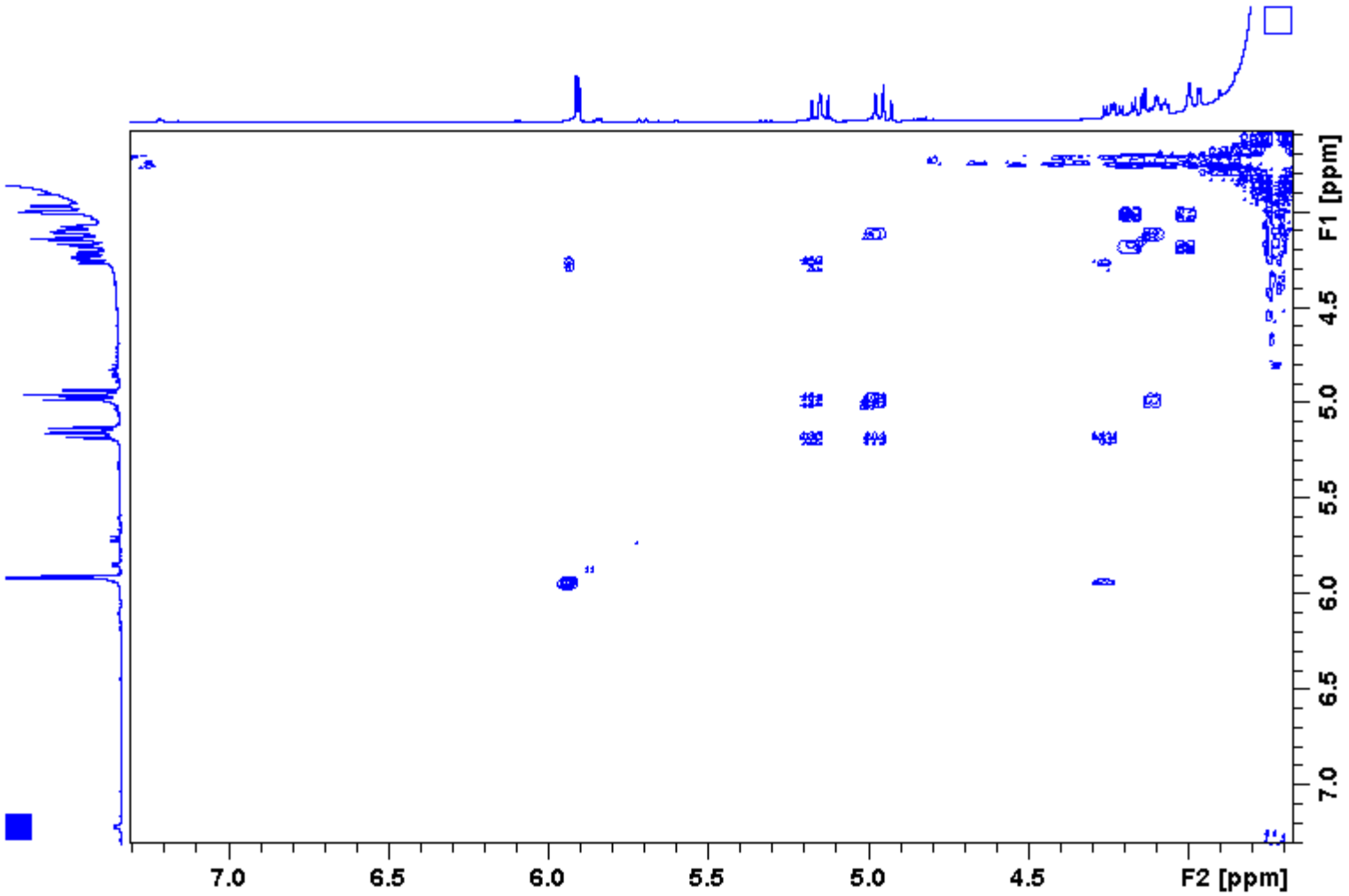

Figure 66: 400 MHz ^{1}H-^{1}H COSY Spectrum of **10α/β**.

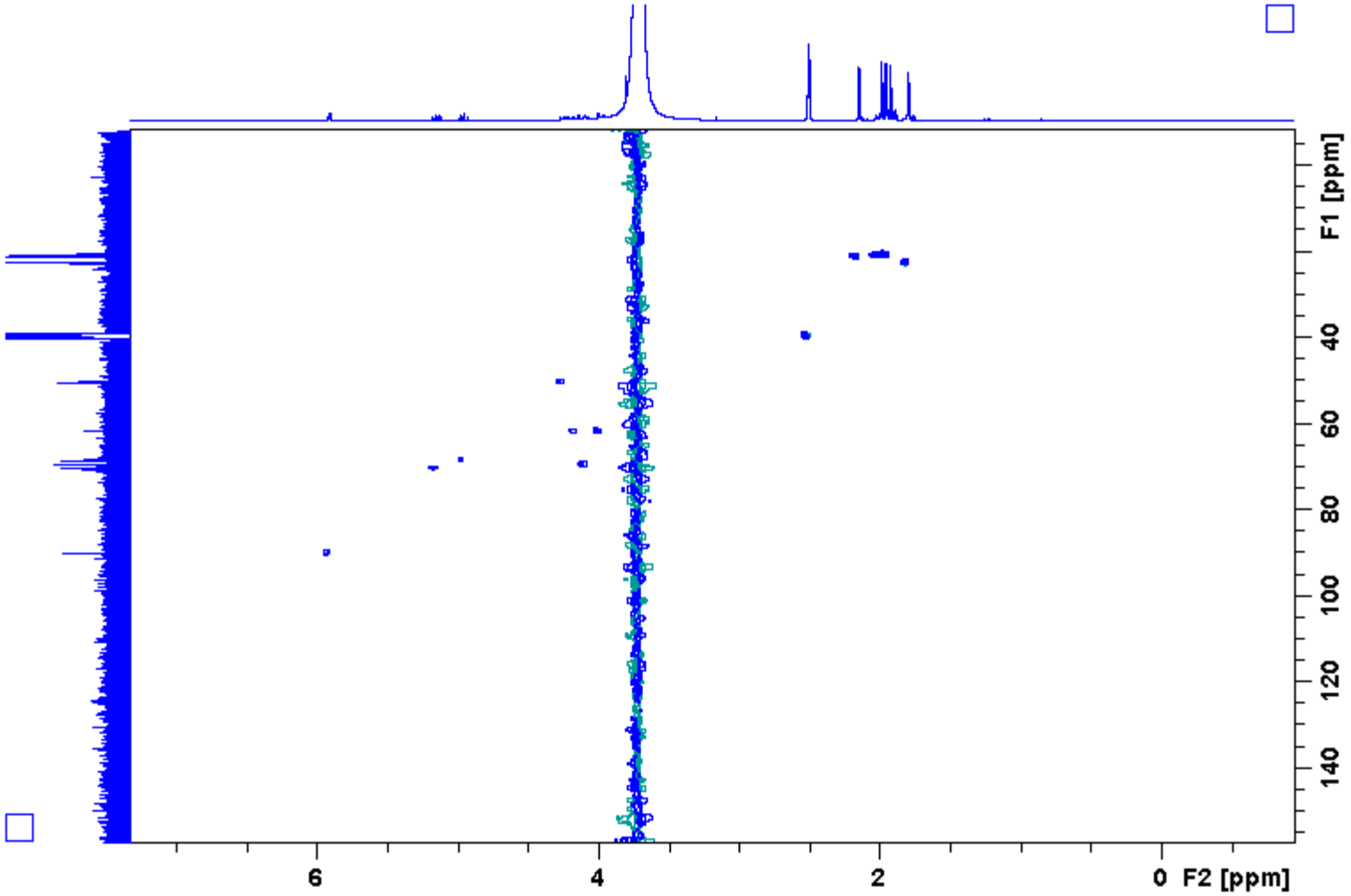

Figure 67: 400 MHz ^{1}H-^{13}C HSQC Spectrum of **10α/β**.

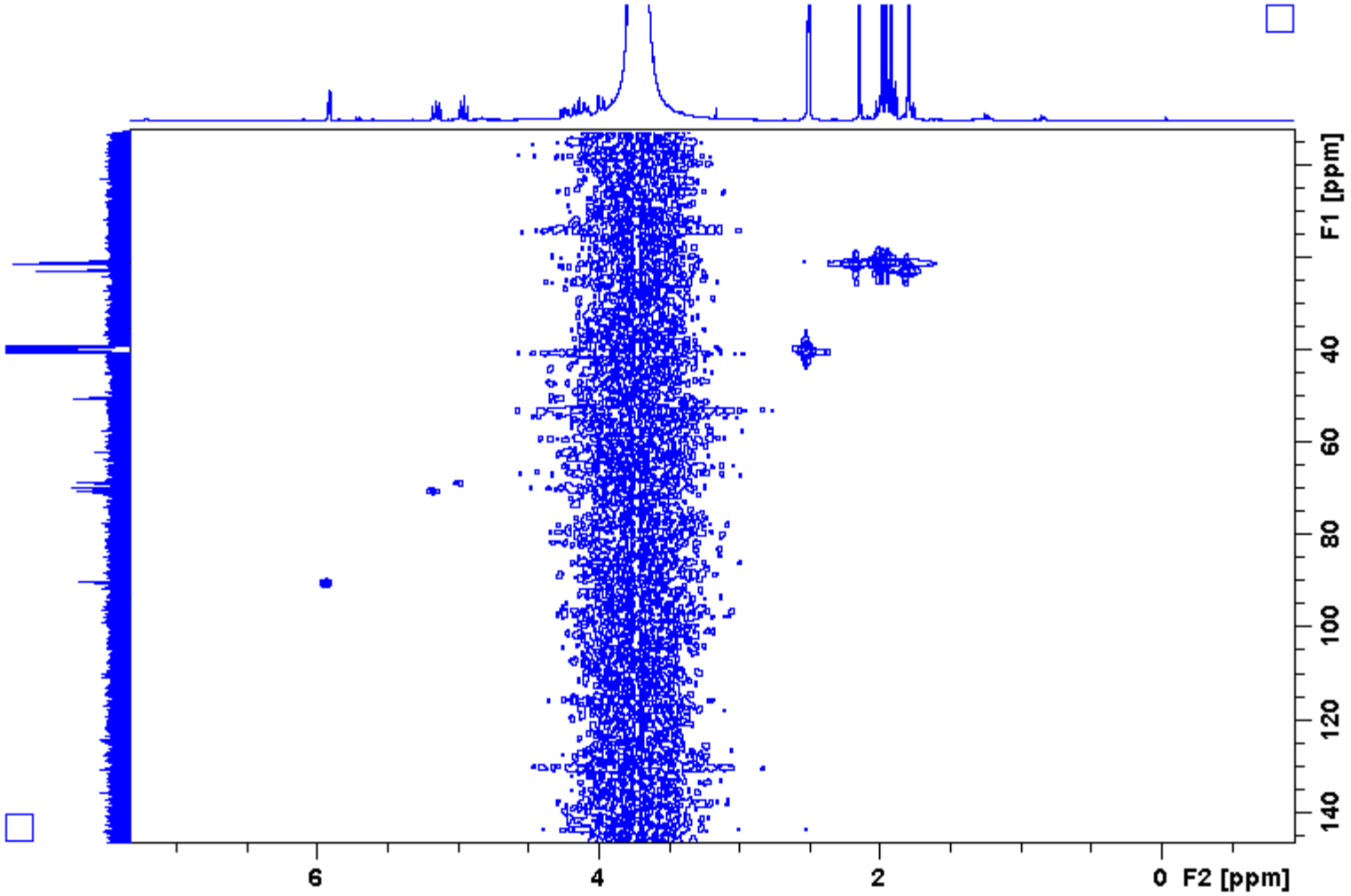

Figure 68: 400 MHz ^{1}H-^{13}C HMQC Spectrum of **10α/β**.

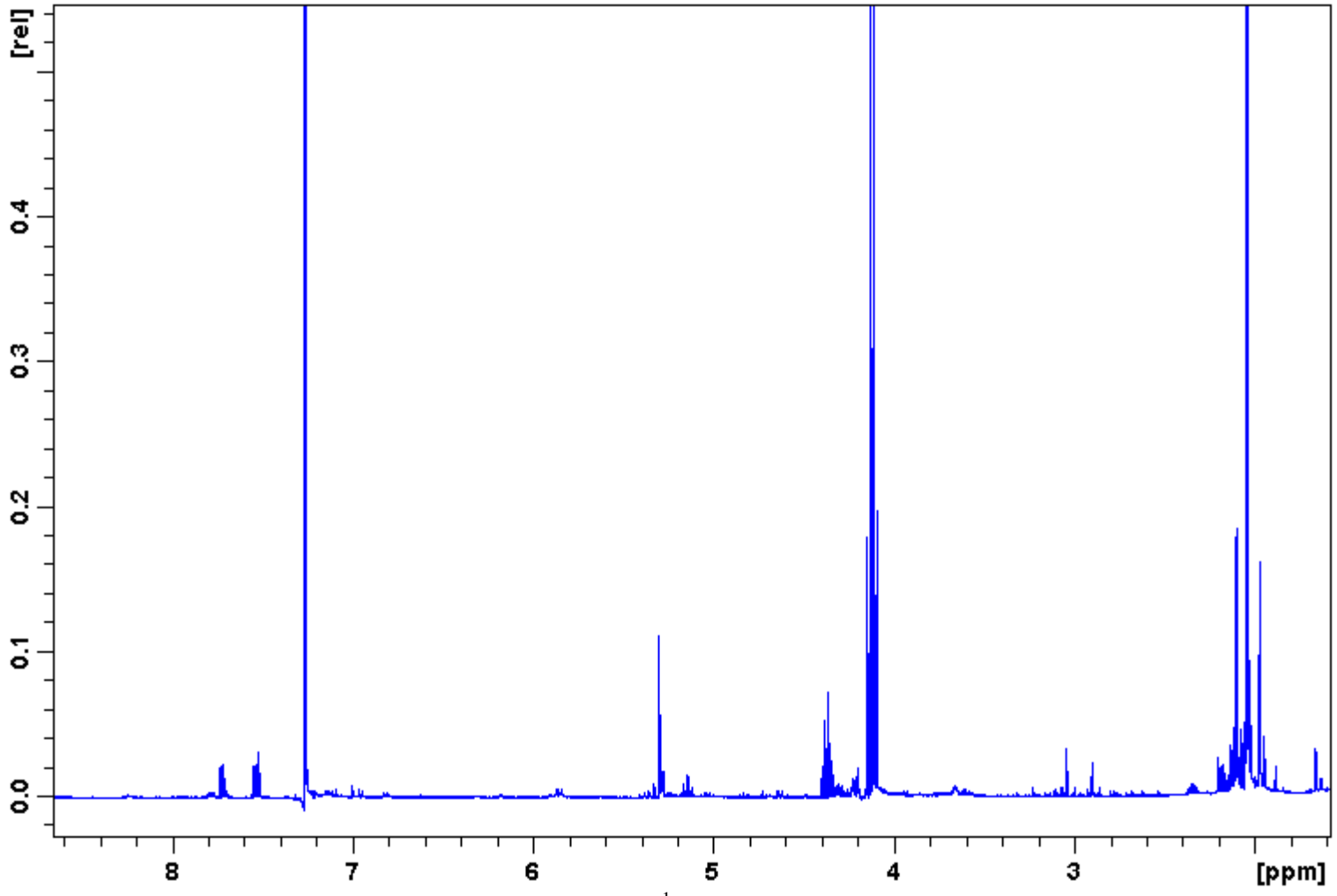

Figure 69: 400 MHz ^{1}H Spectrum of **11α/β**.

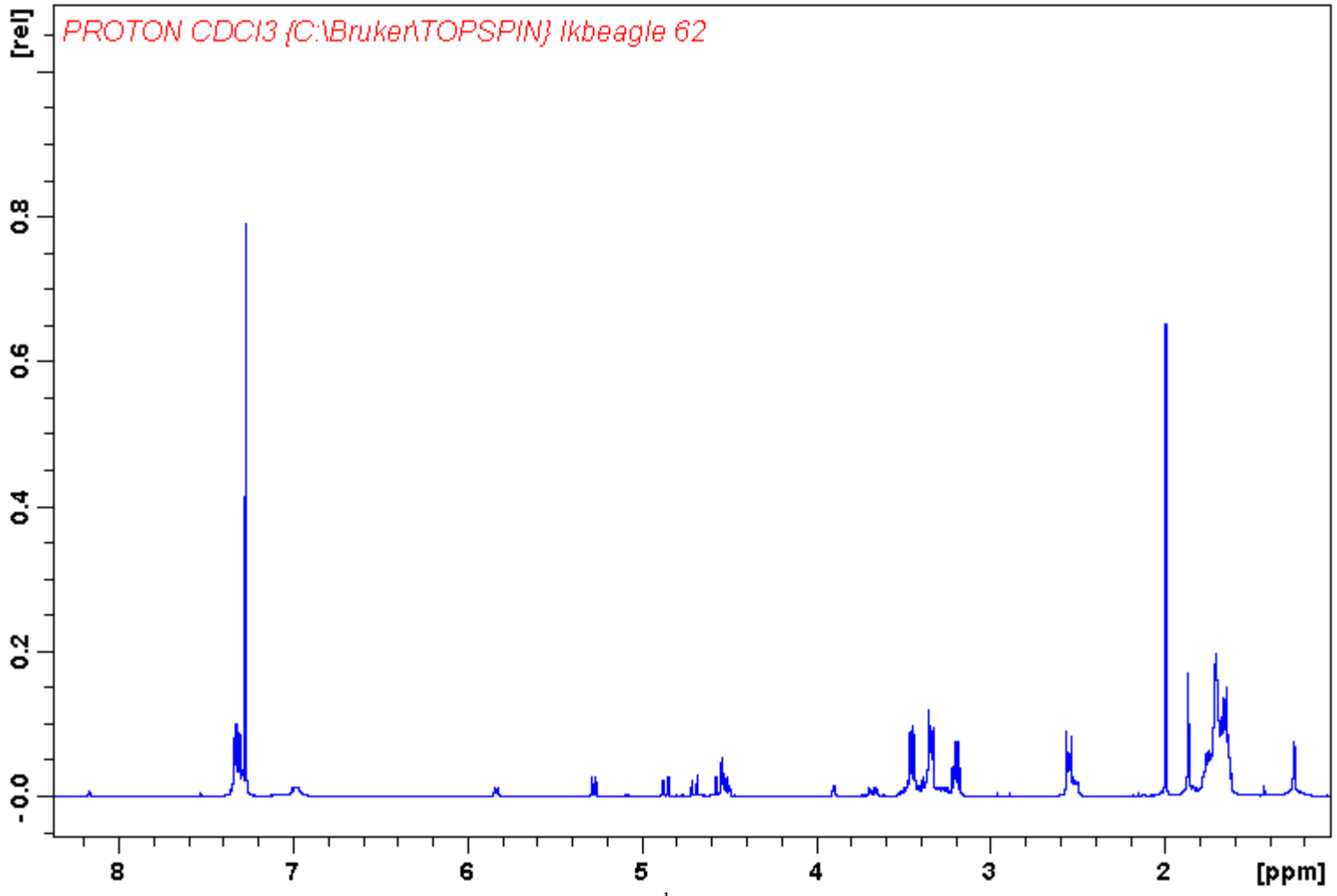

Figure 70: 400 MHz ^{1}H Spectrum of **12α/β**.

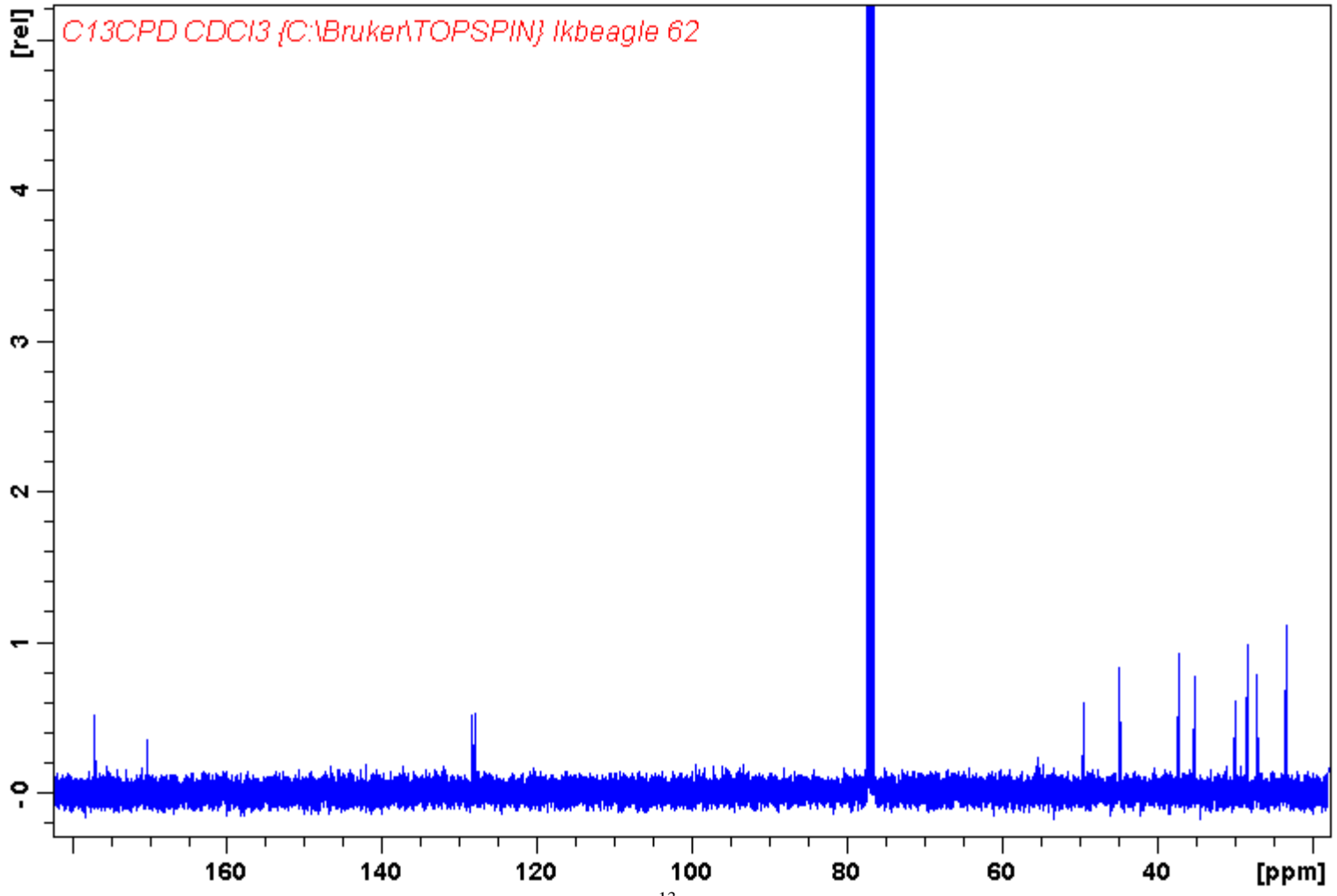

Figure 71: 100 MHz ^{13}C Spectrum of **12α/β**.

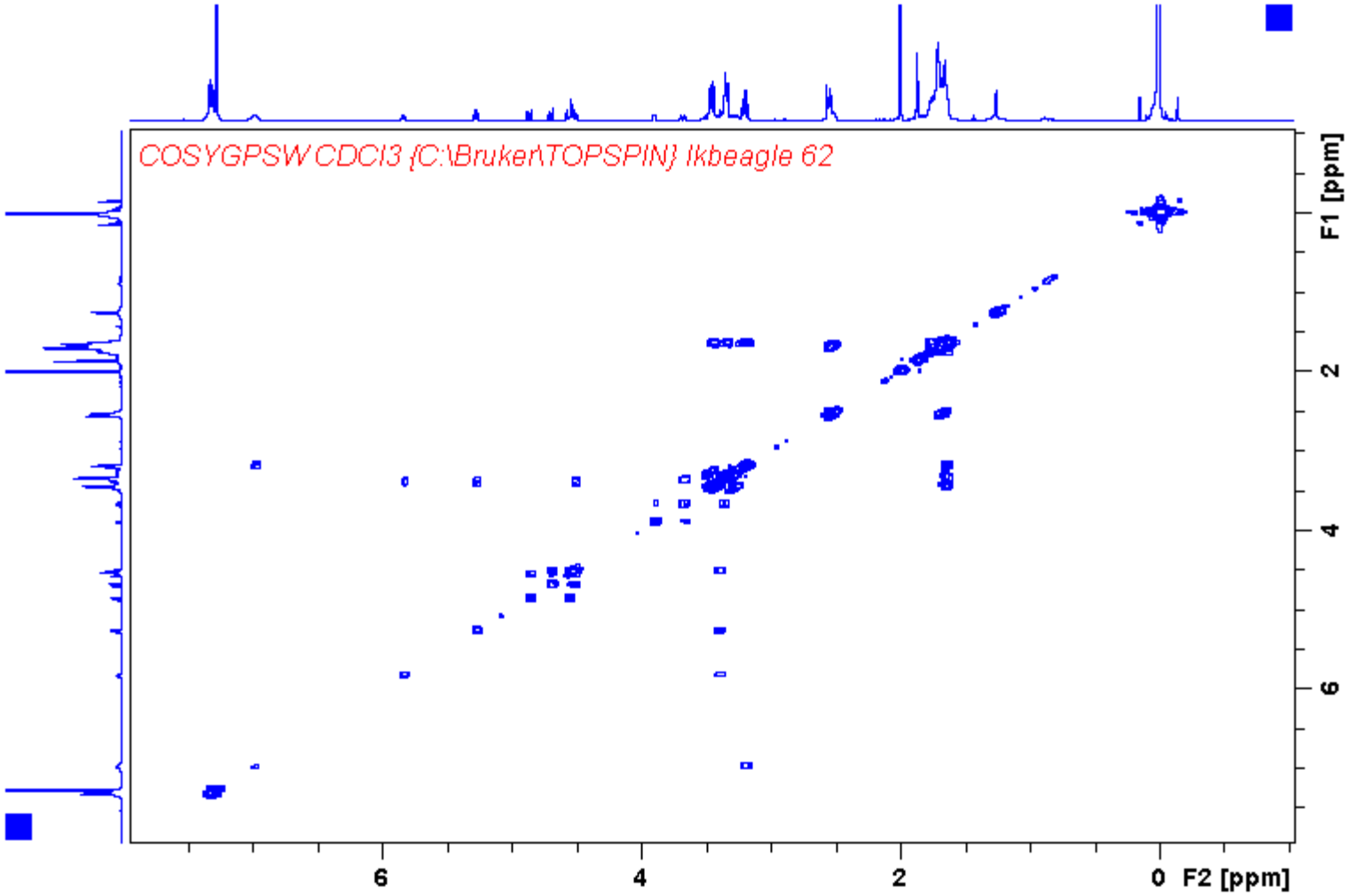

Figure 72: 400 MHz ^{1}H-^{1}H COSY Spectrum of **12α/β**.

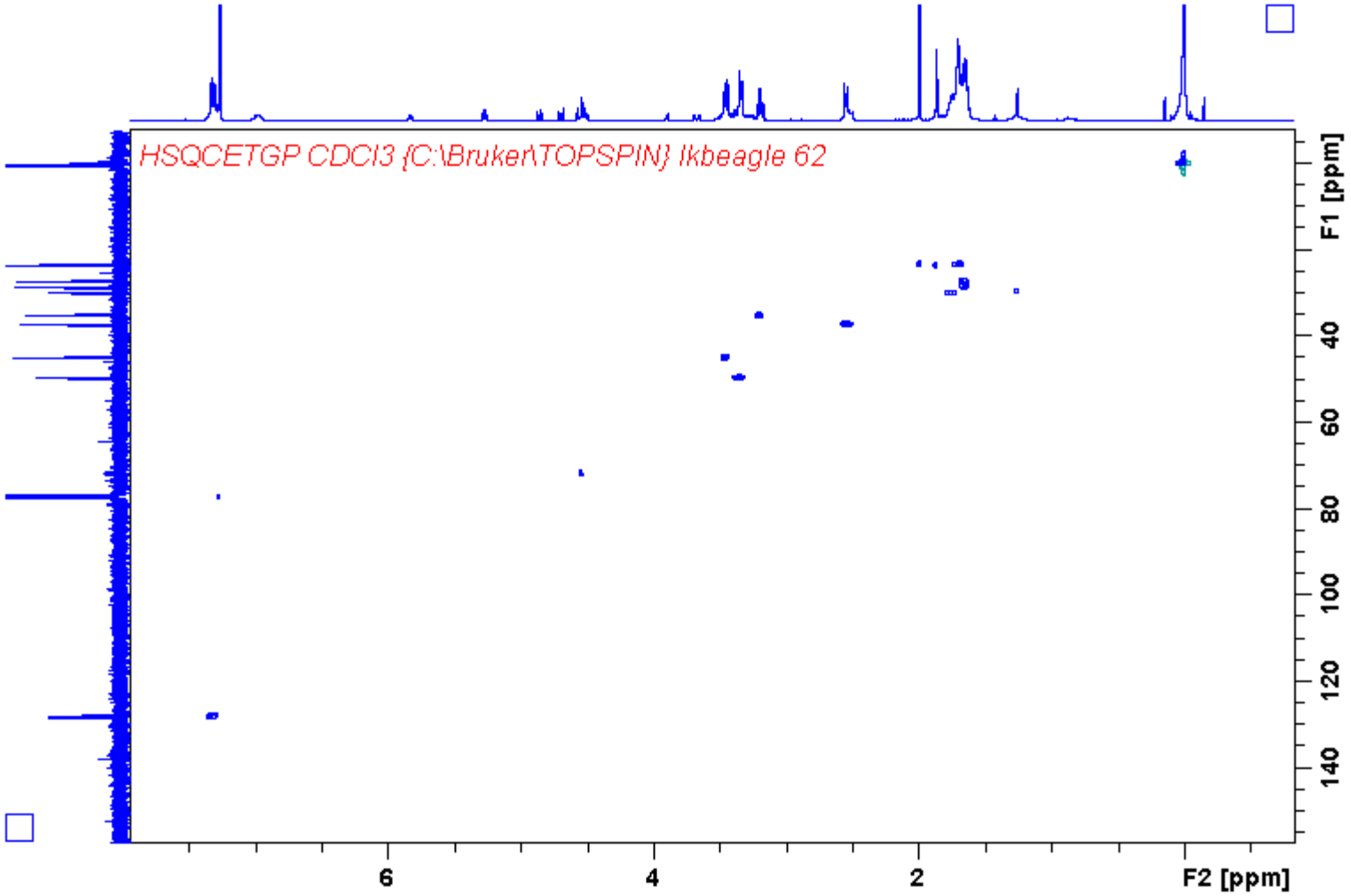

Figure 73: 400 MHz ^{1}H-^{13}C HSQC Spectrum of **12α/β**.

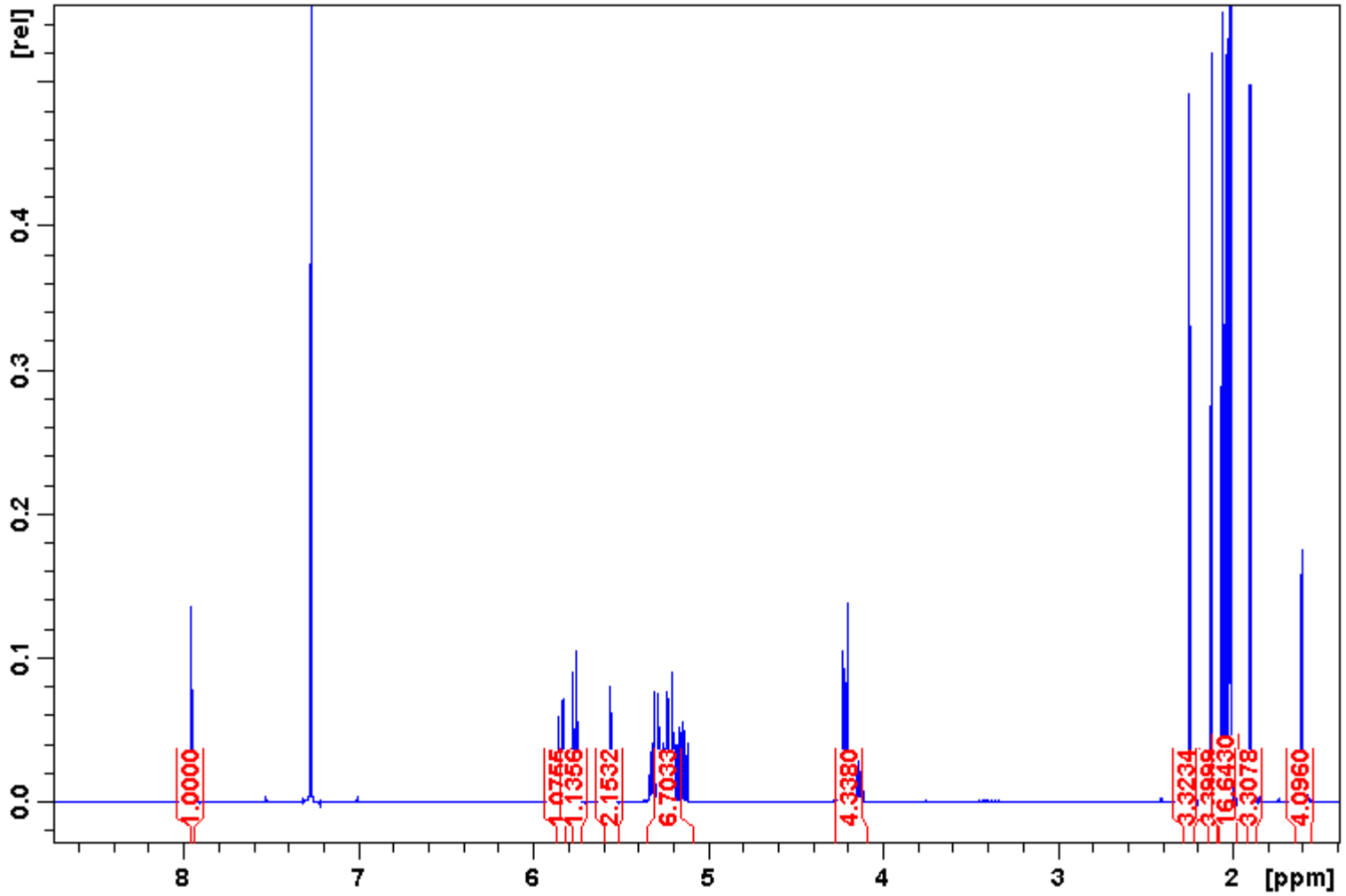

Figure 74: 400 MHz ^{1}H Spectrum of **14**.

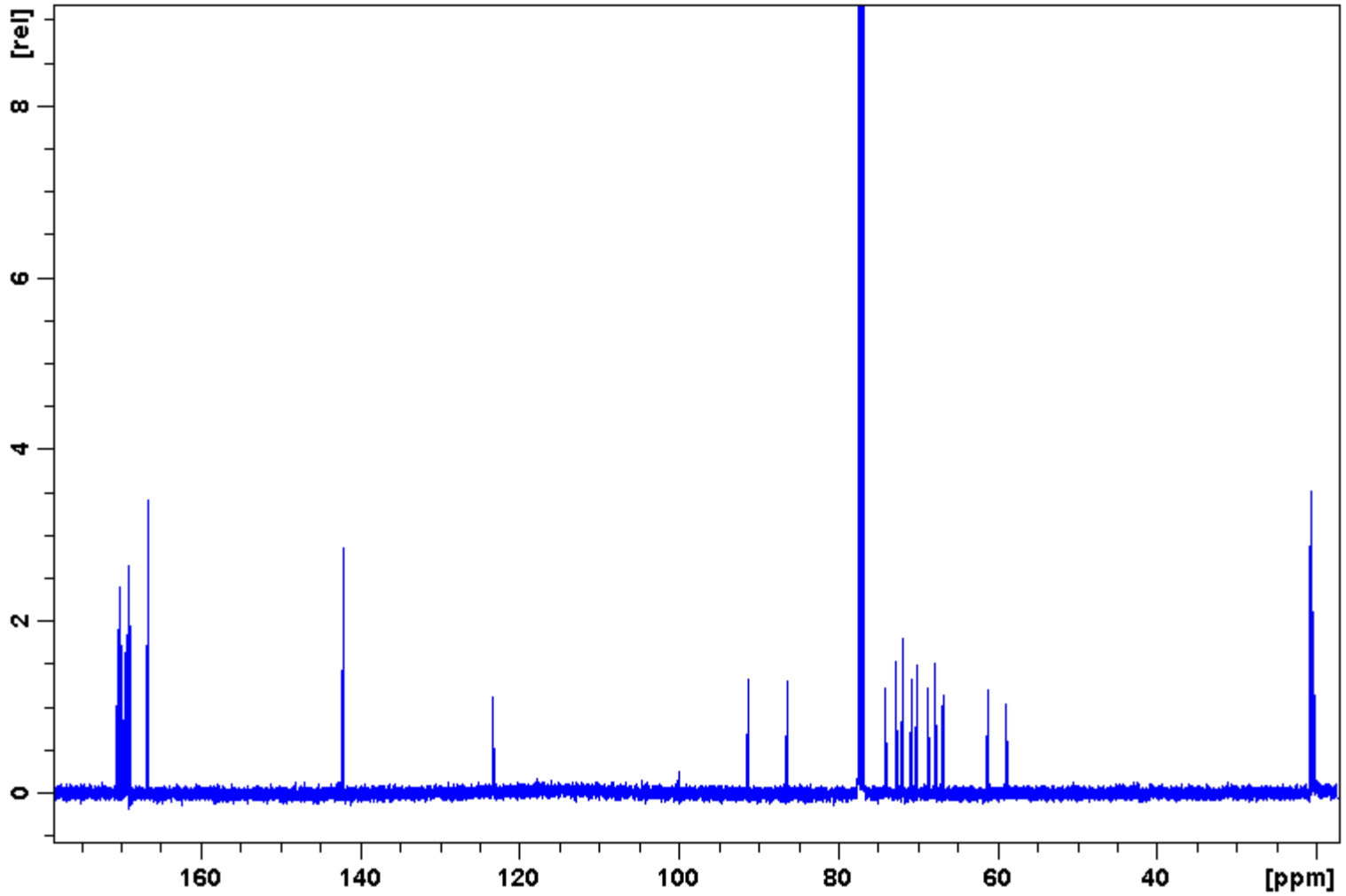

Figure 75: 100 MHz ^{13}C Spectrum of **14**.

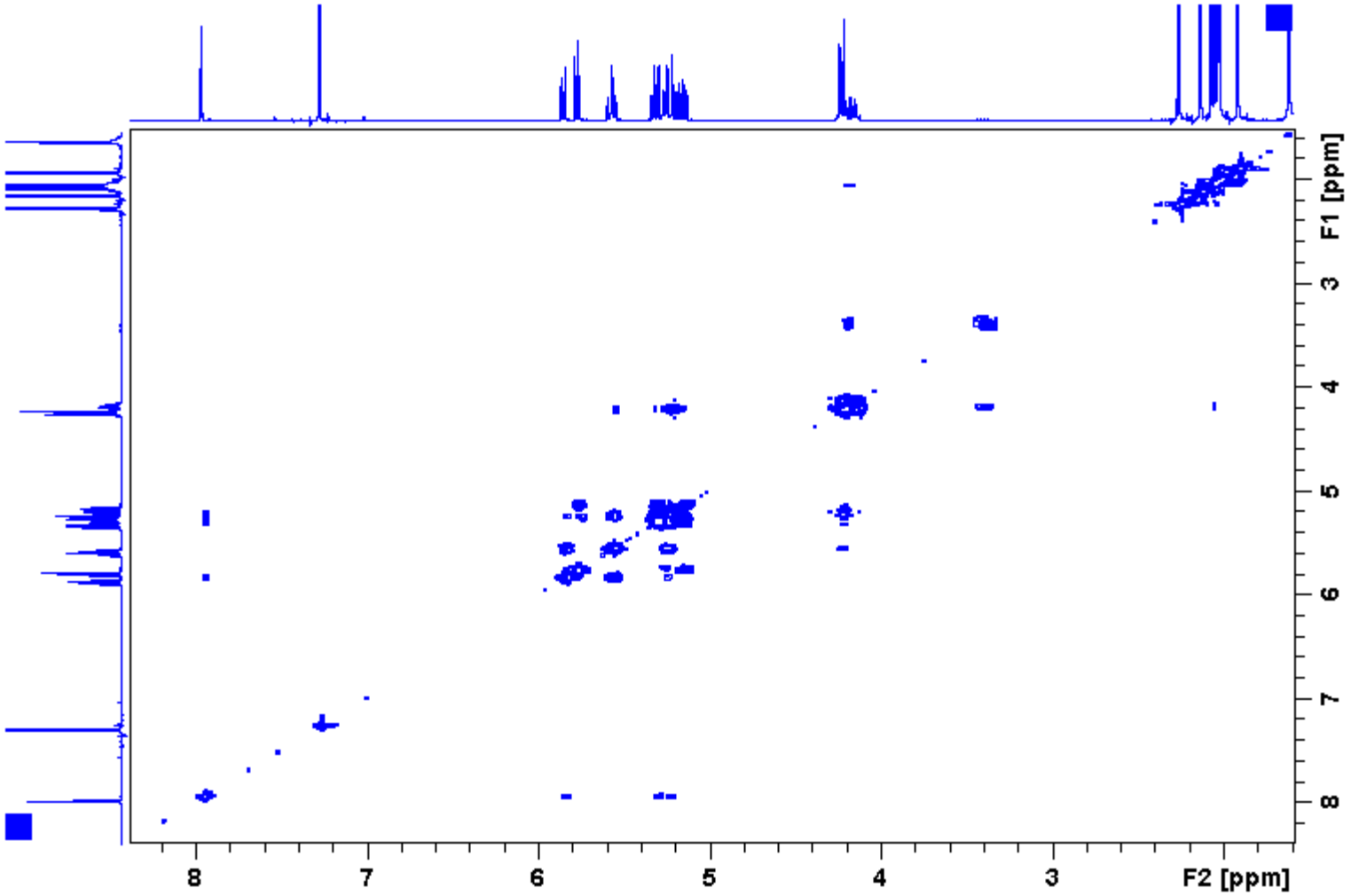

Figure 76: 400 MHz ^{1}H-^{1}H COSY Spectrum of **14**.

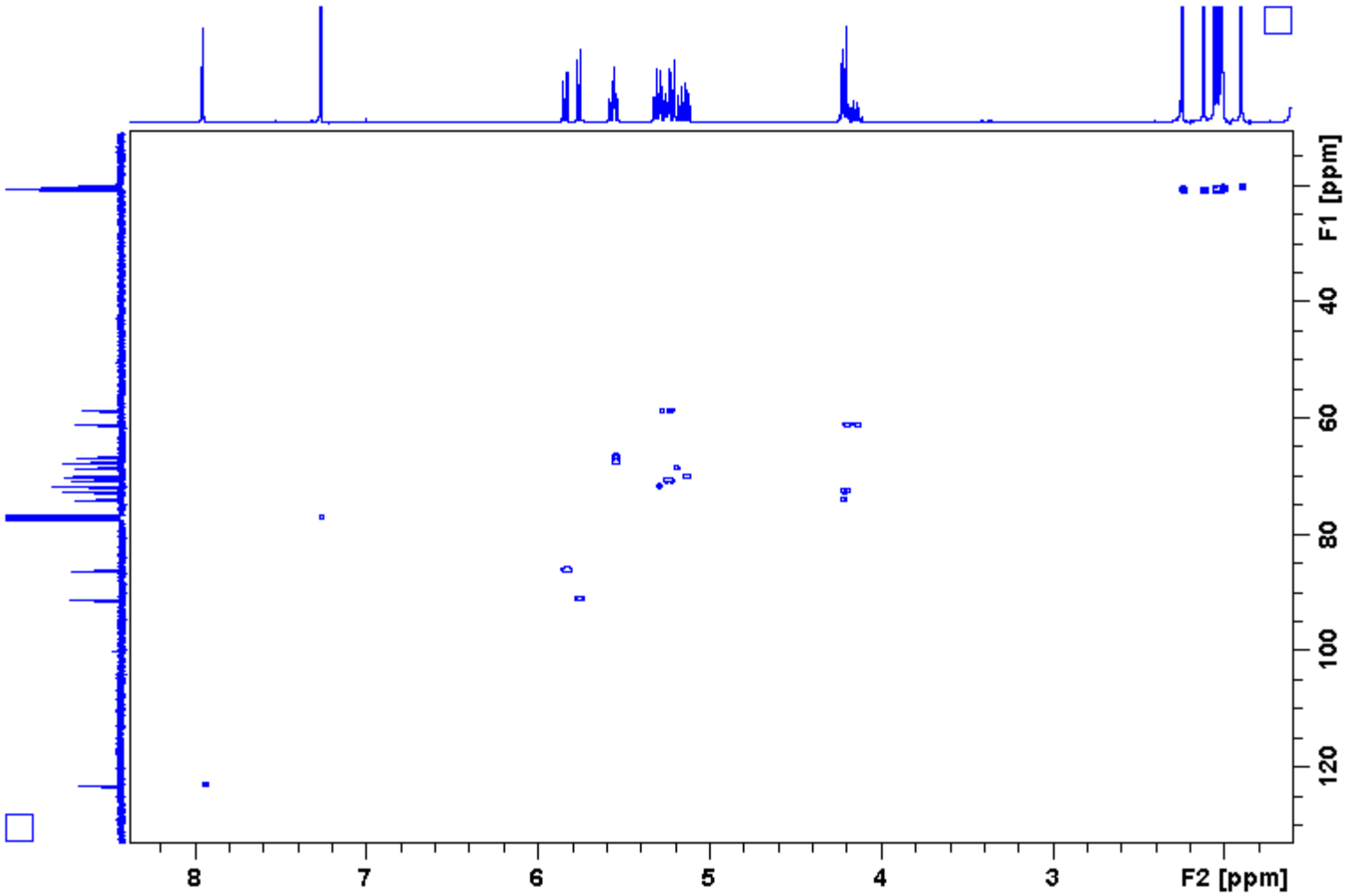

Figure 77: 400 MHz ^{1}H-^{13}C HSQC Spectrum of **14**.

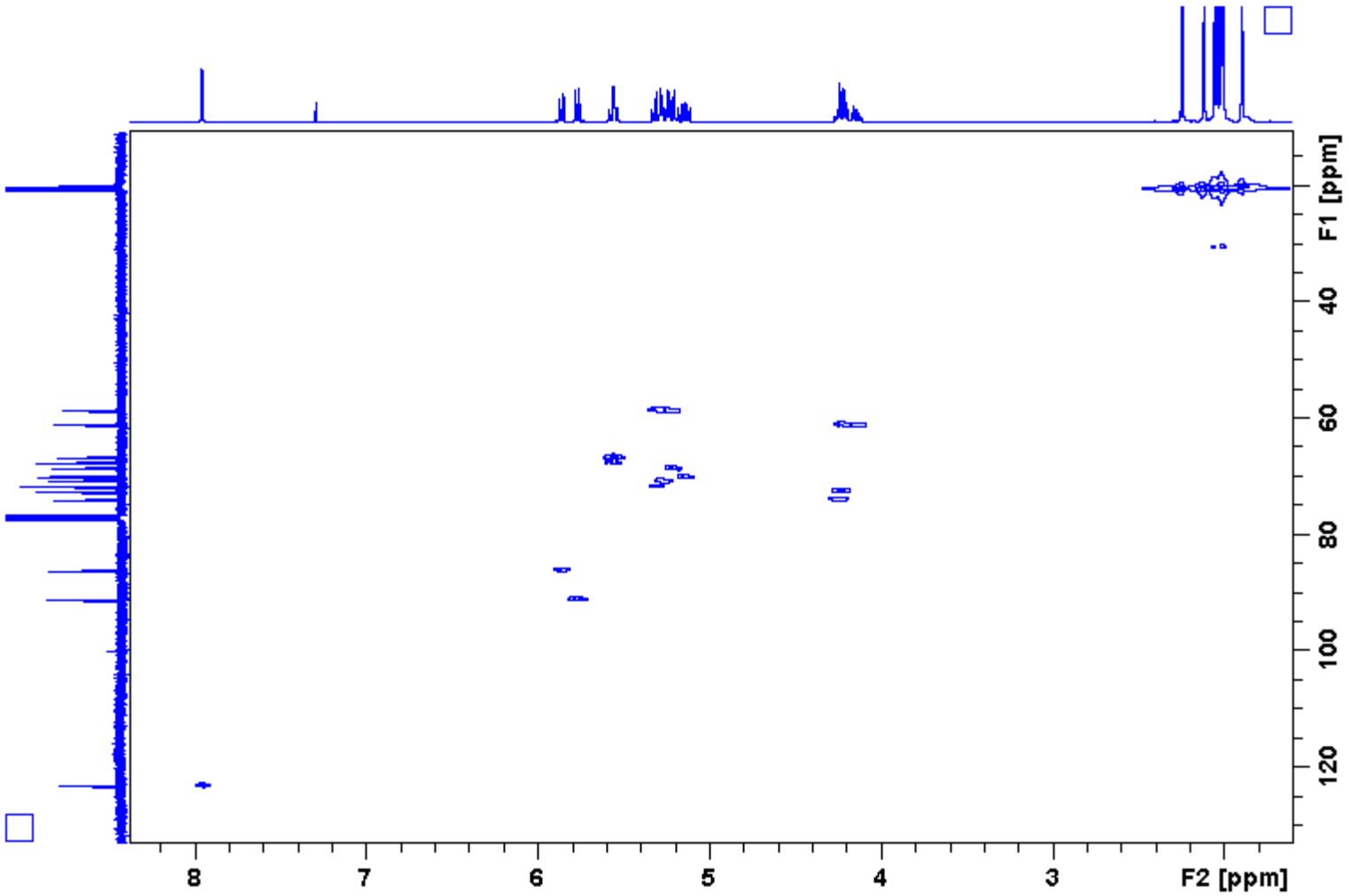

Figure 78: 400 MHz ^{1}H-^{13}C HMQC Spectrum of **14**.

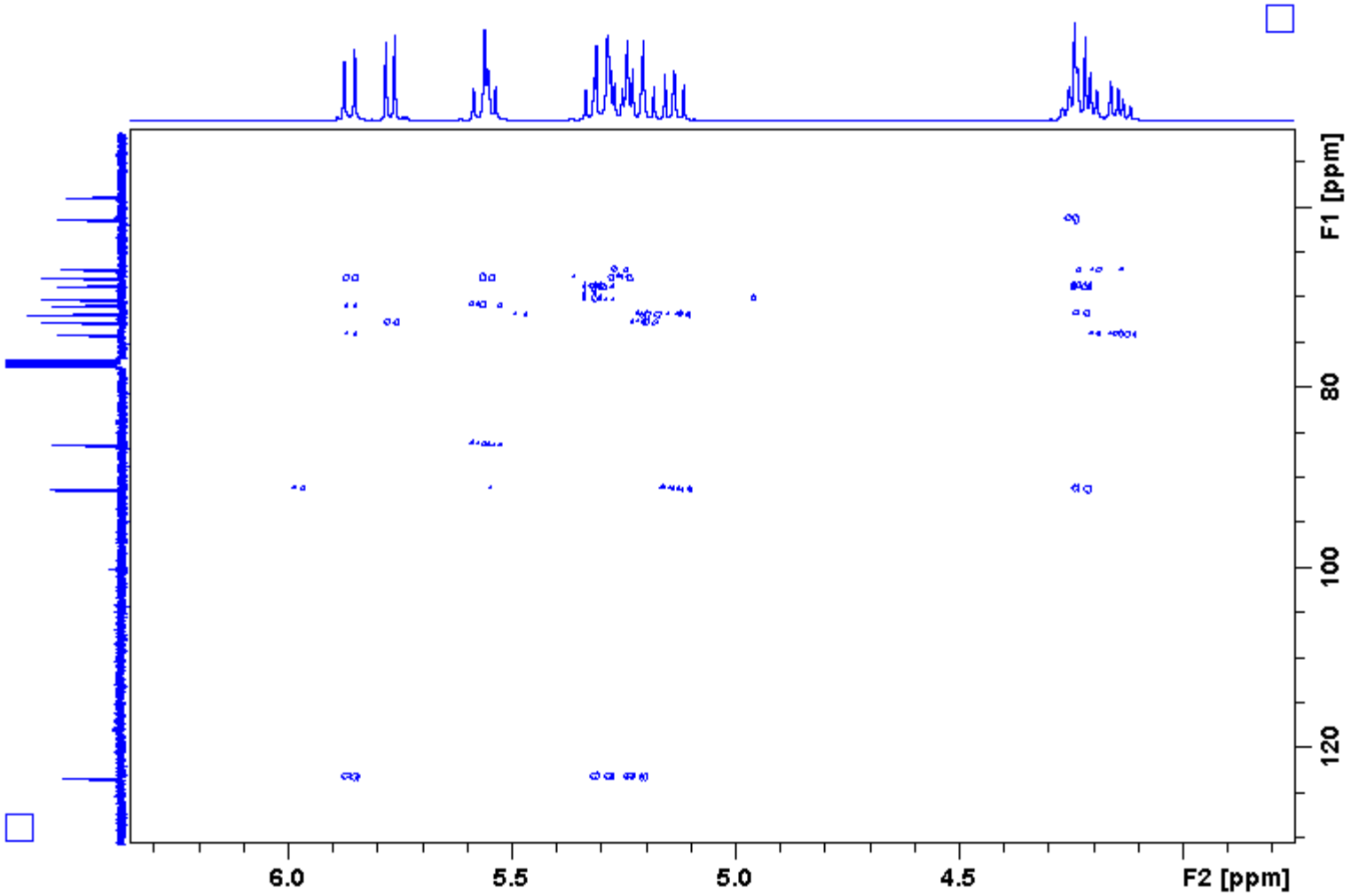

Figure 79: 400 MHz ^{1}H-^{13}C HMBC Spectrum of **14**.

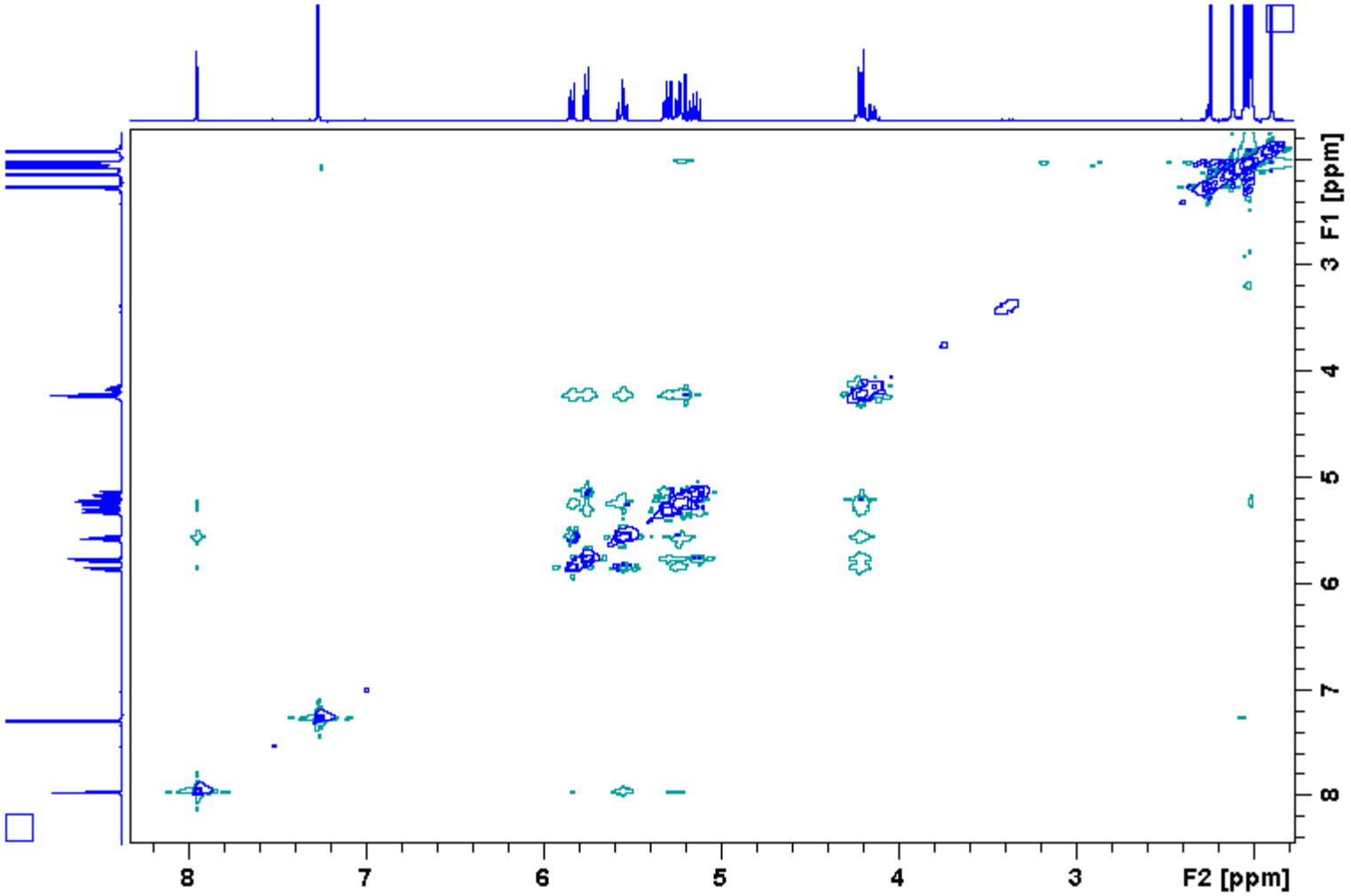

Figure 80: 400 MHz ^{1}H-^{1}H NOESY Spectrum of **14**.

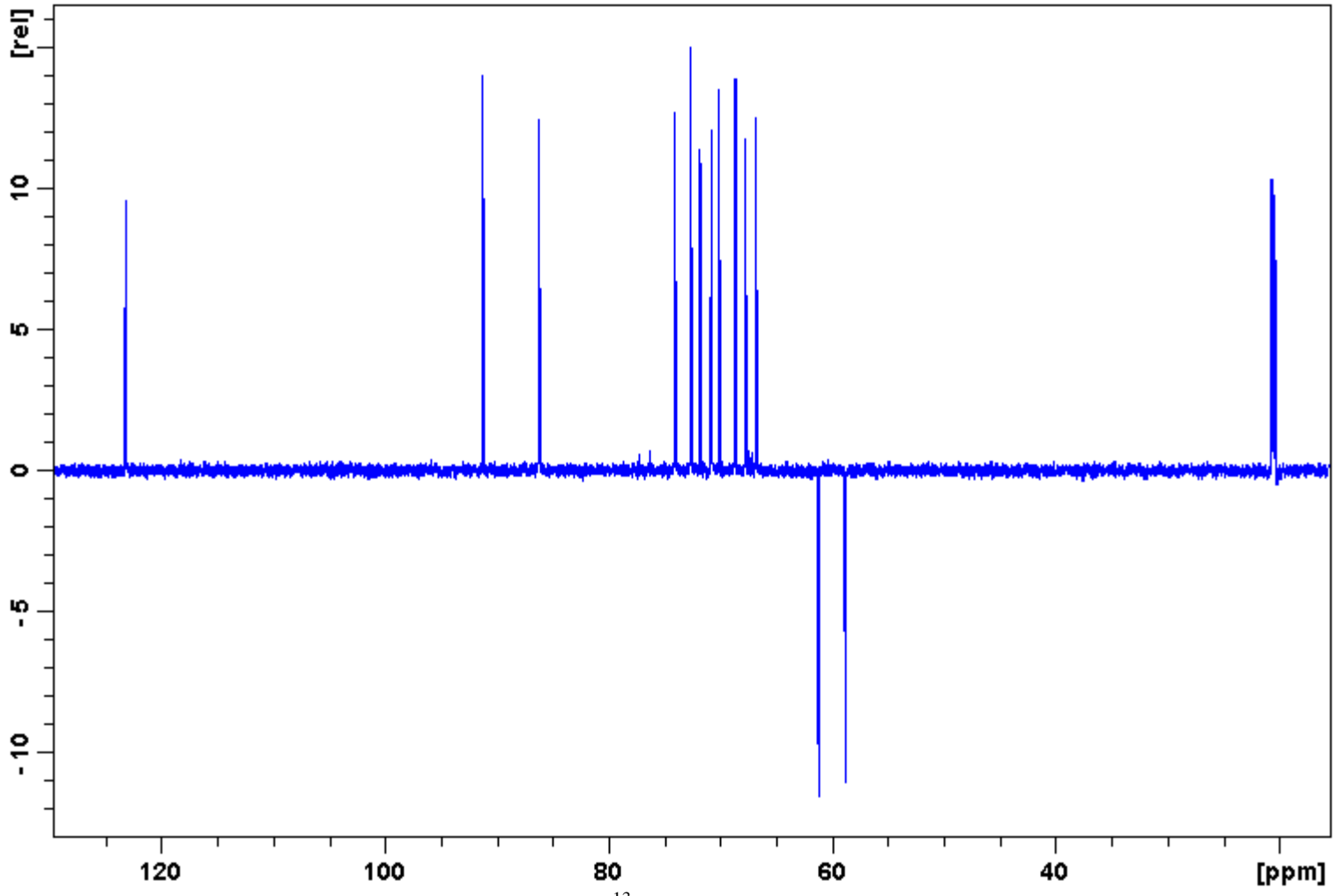

Figure 81: 100 MHz ^{13}C DEPT-135 Spectrum of **14**.

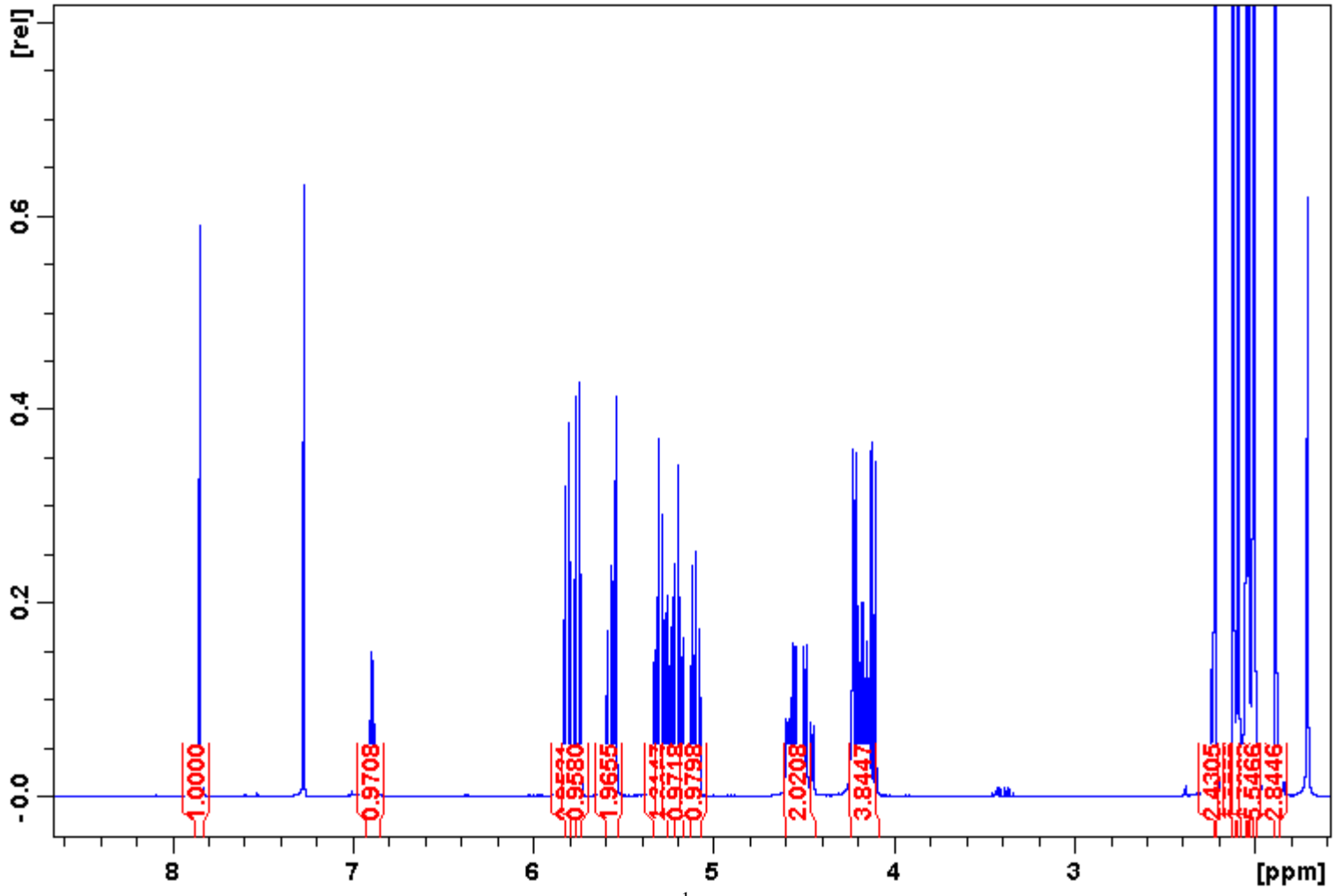

Figure 82: 400 MHz ^{1}H Spectrum of **15**.

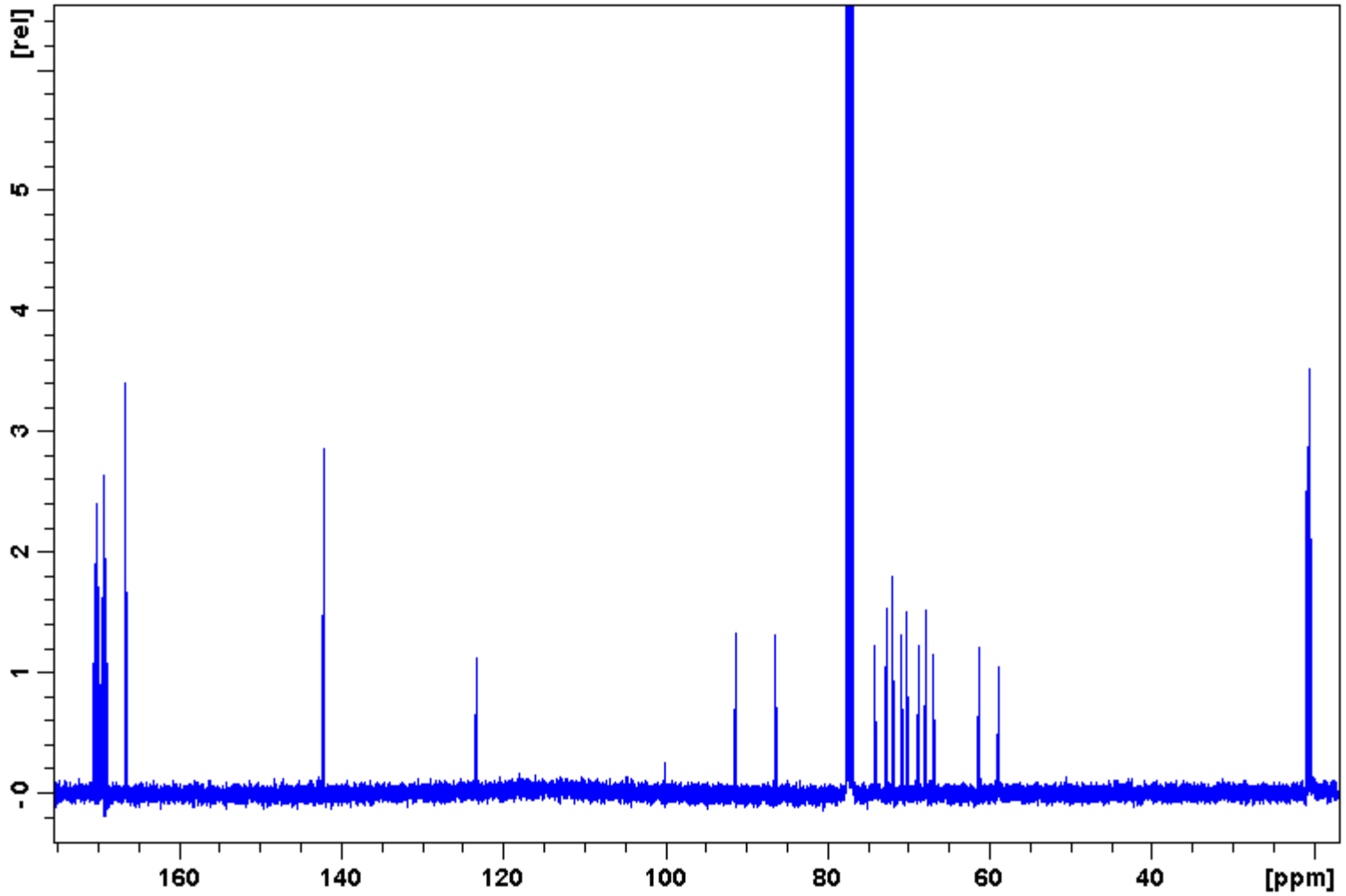

Figure 83: 100 MHz ^{13}C Spectrum of **15**.

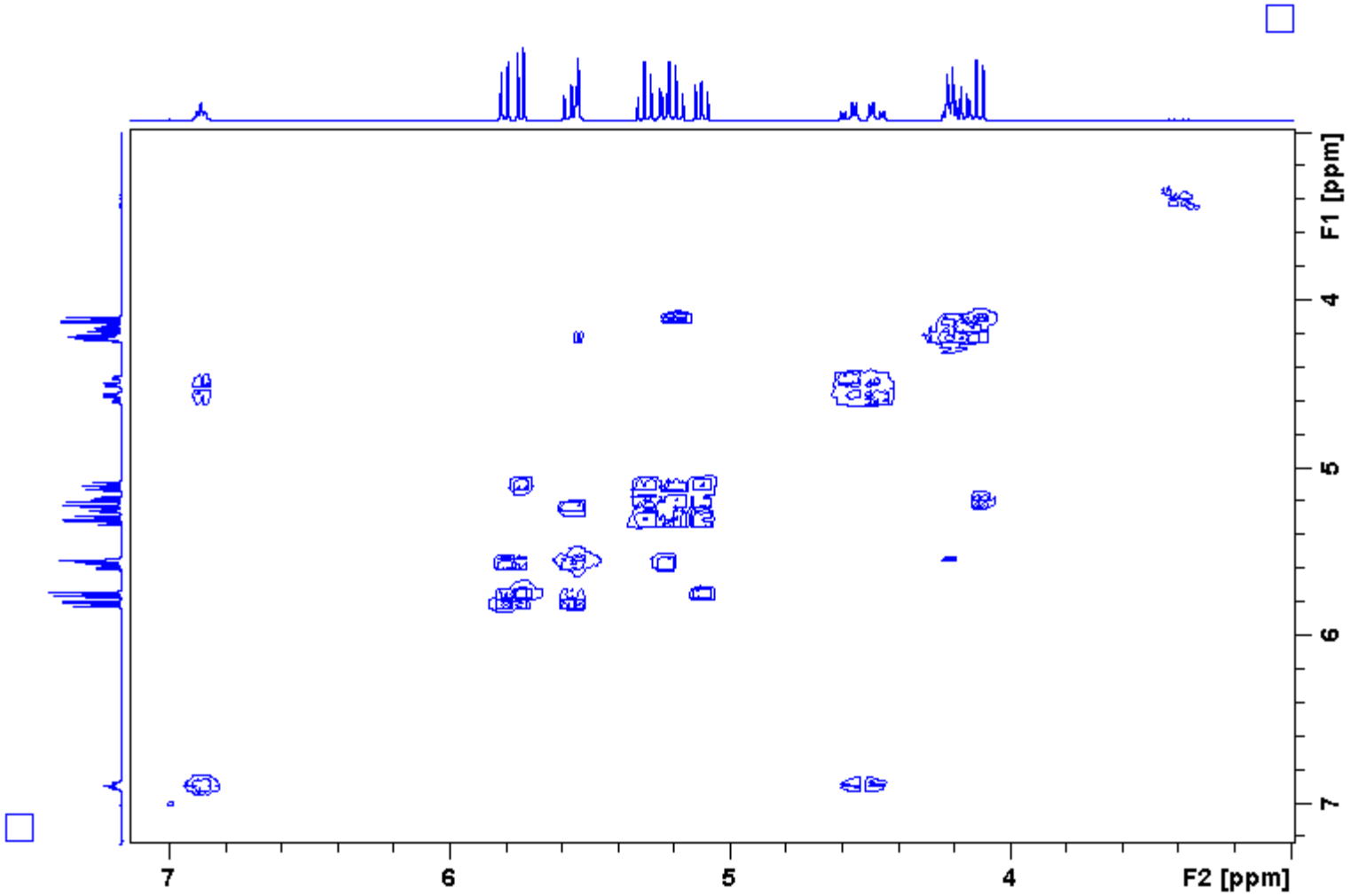

Figure 84: 400 MHz ^{1}H-^{1}H COSY Spectrum of **15**.

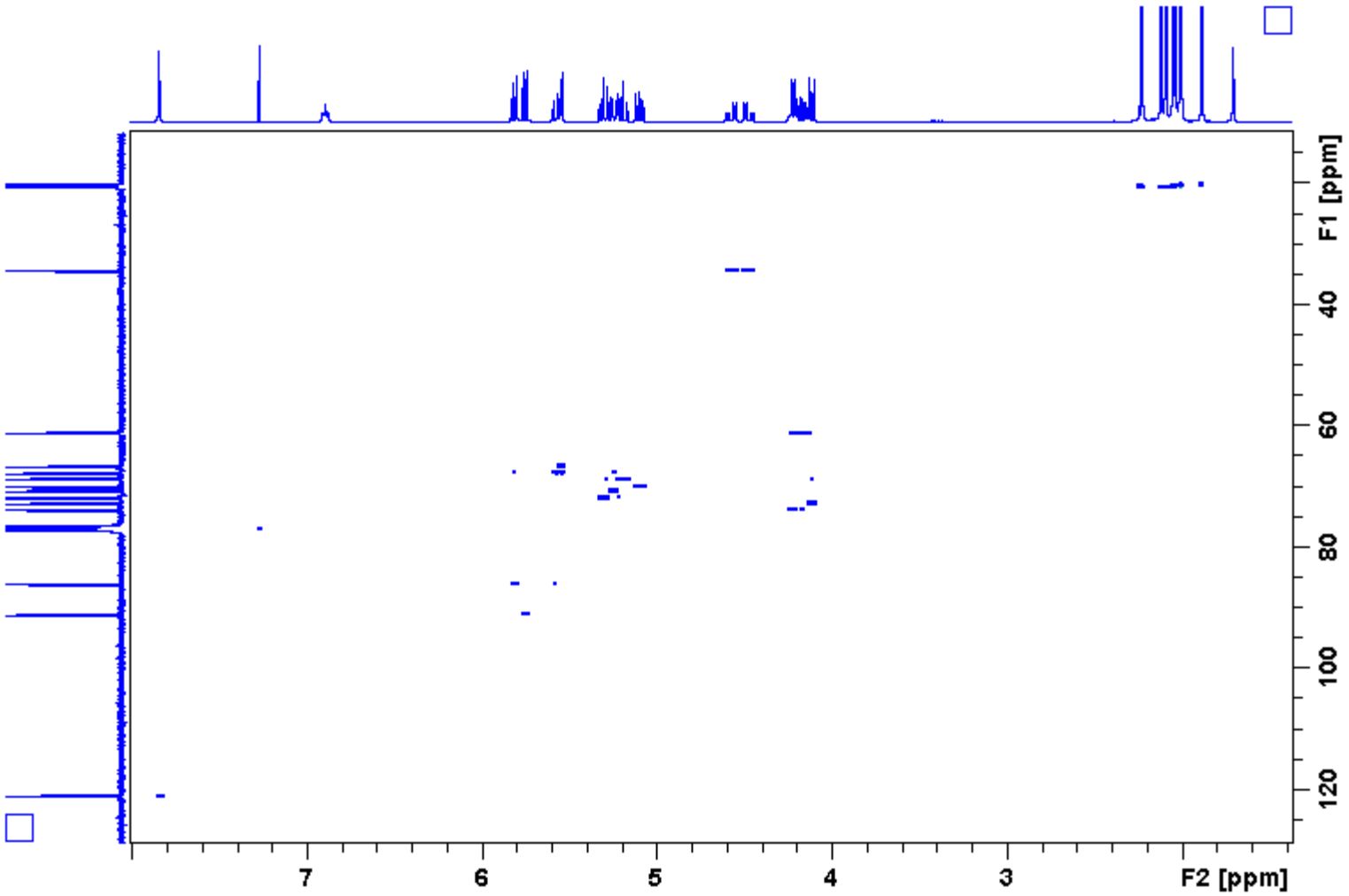

Figure 85: 400 MHz ^{1}H-^{13}C HSQC Spectrum of **15**.

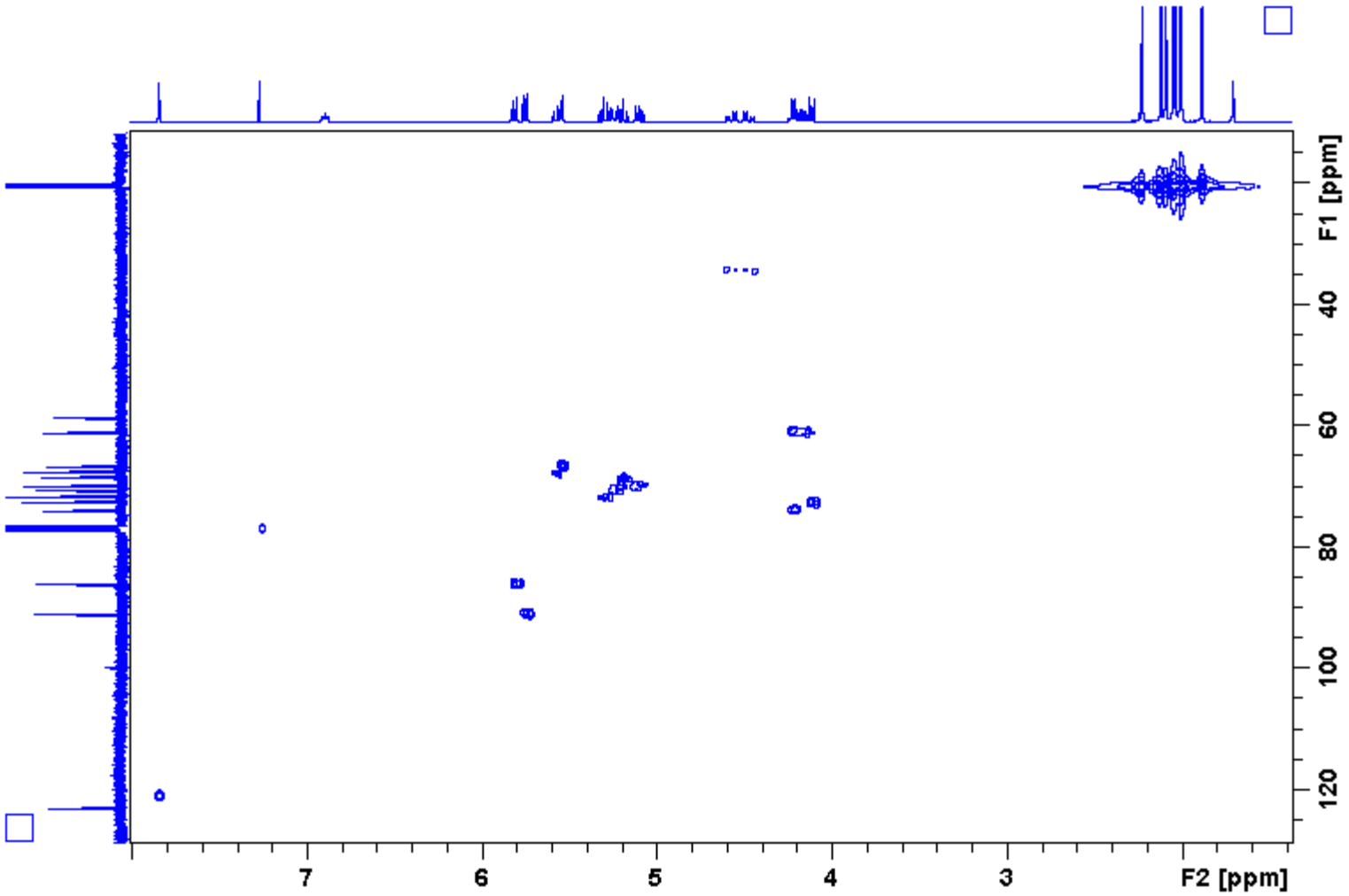

Figure 86: 400 MHz ^{1}H-^{13}C HMQC Spectrum of **15**.

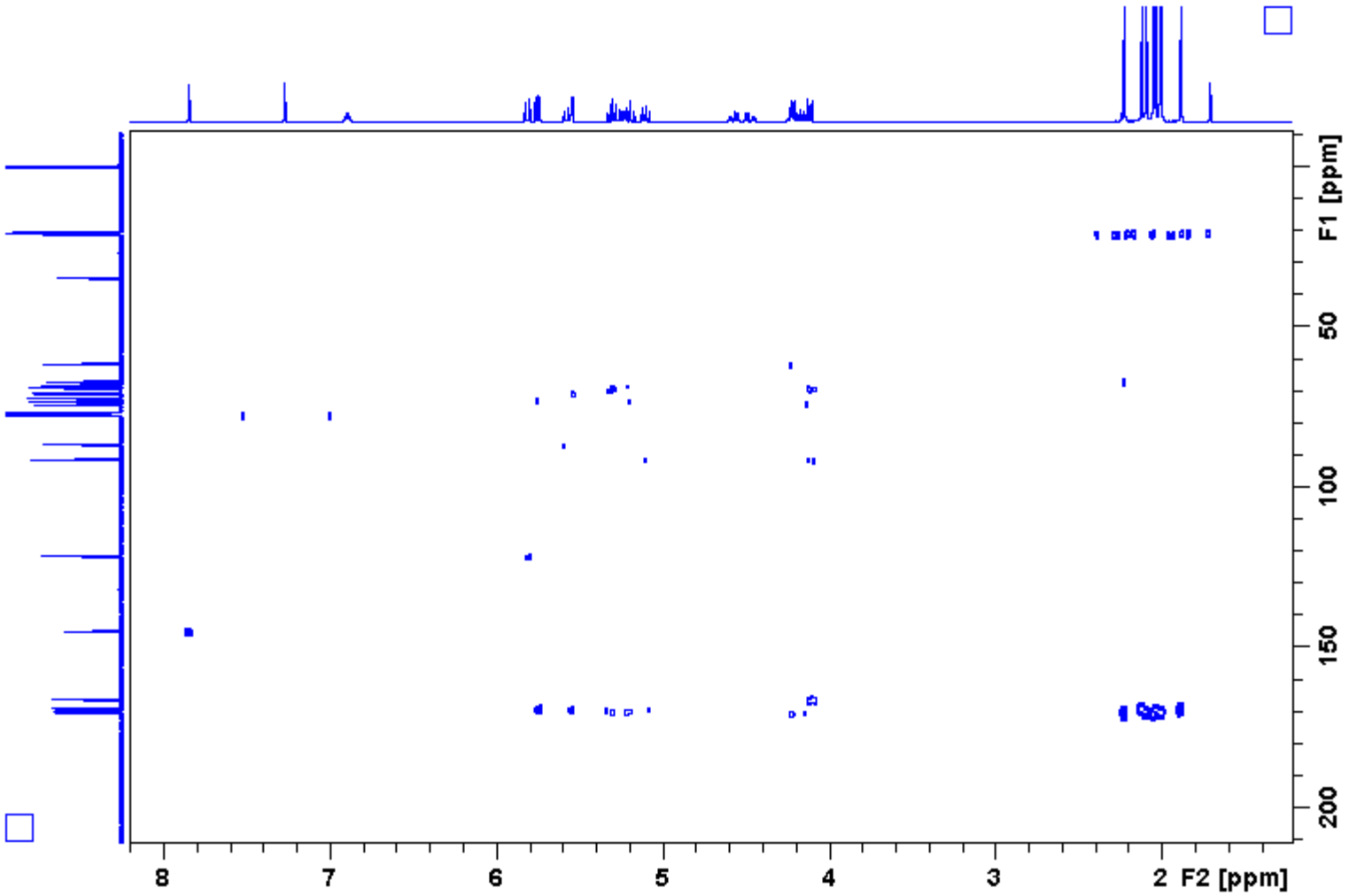

Figure 87: 400 MHz ^{1}H-^{13}C HMBC Spectrum of **15**.

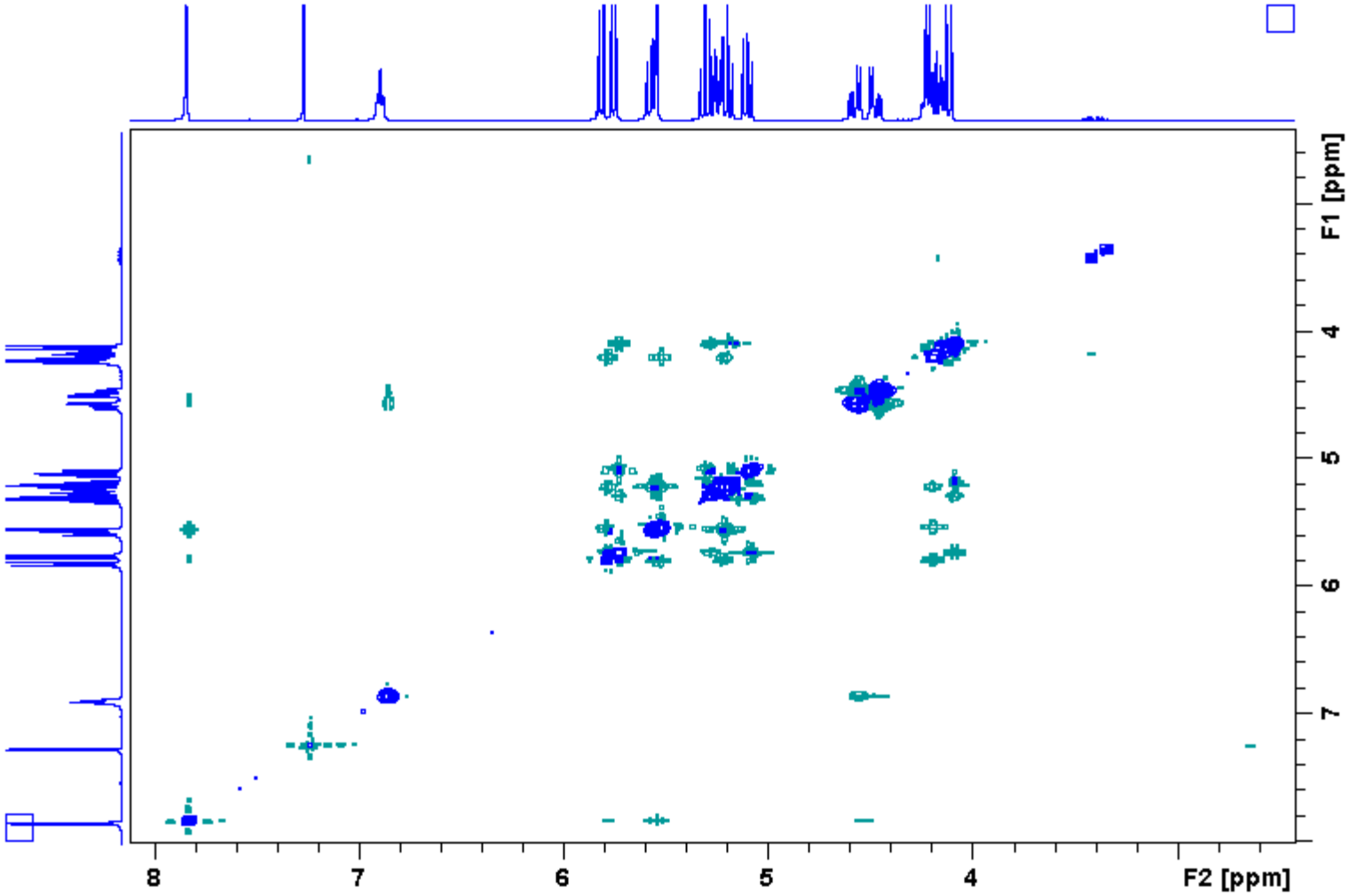

Figure 88: 400 MHz ^{1}H-^{1}H NOESY Spectrum of **15**.

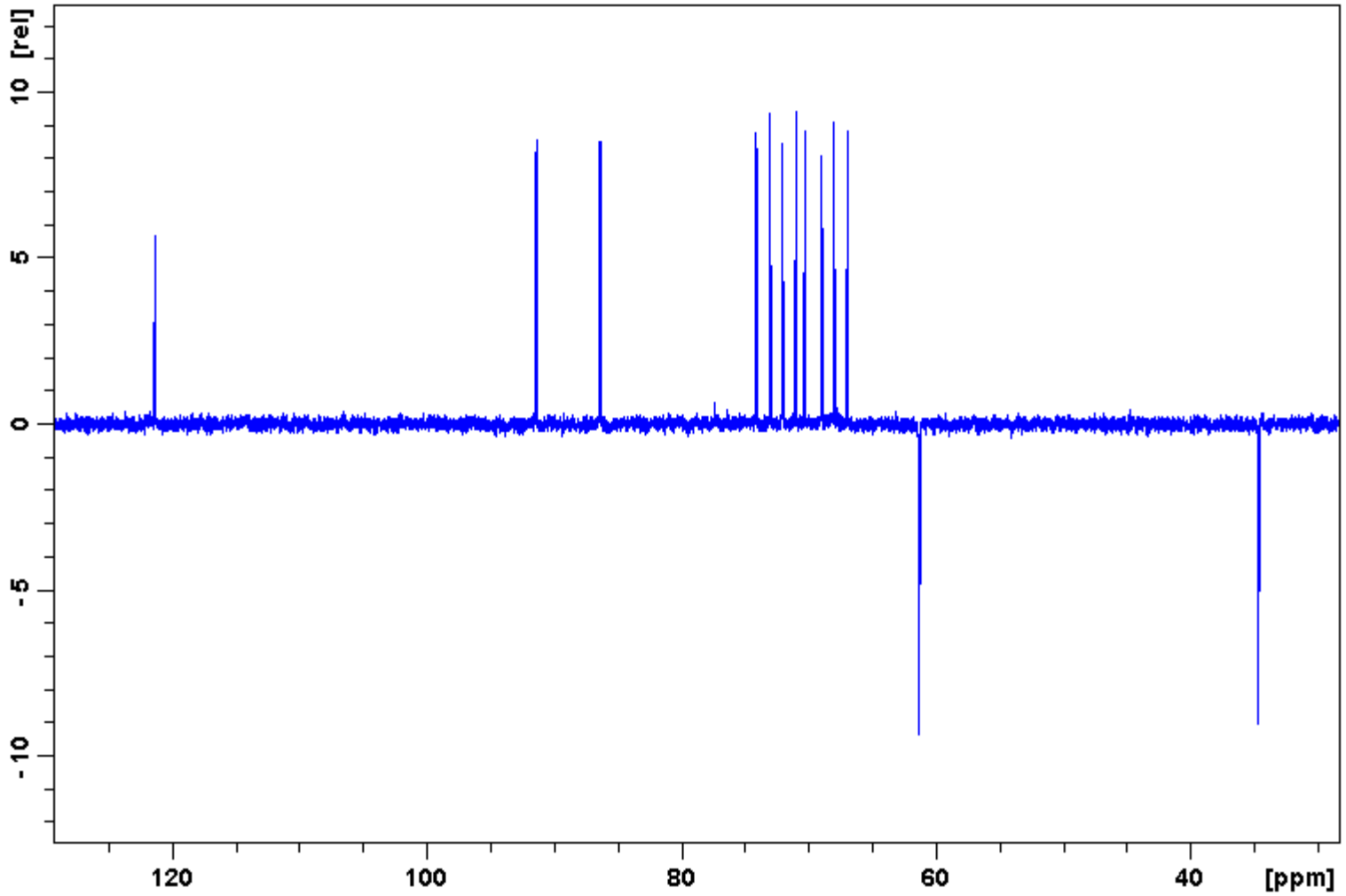

Figure 89: 100 MHz ^{13}C DEPT-135 Spectrum of **15**.

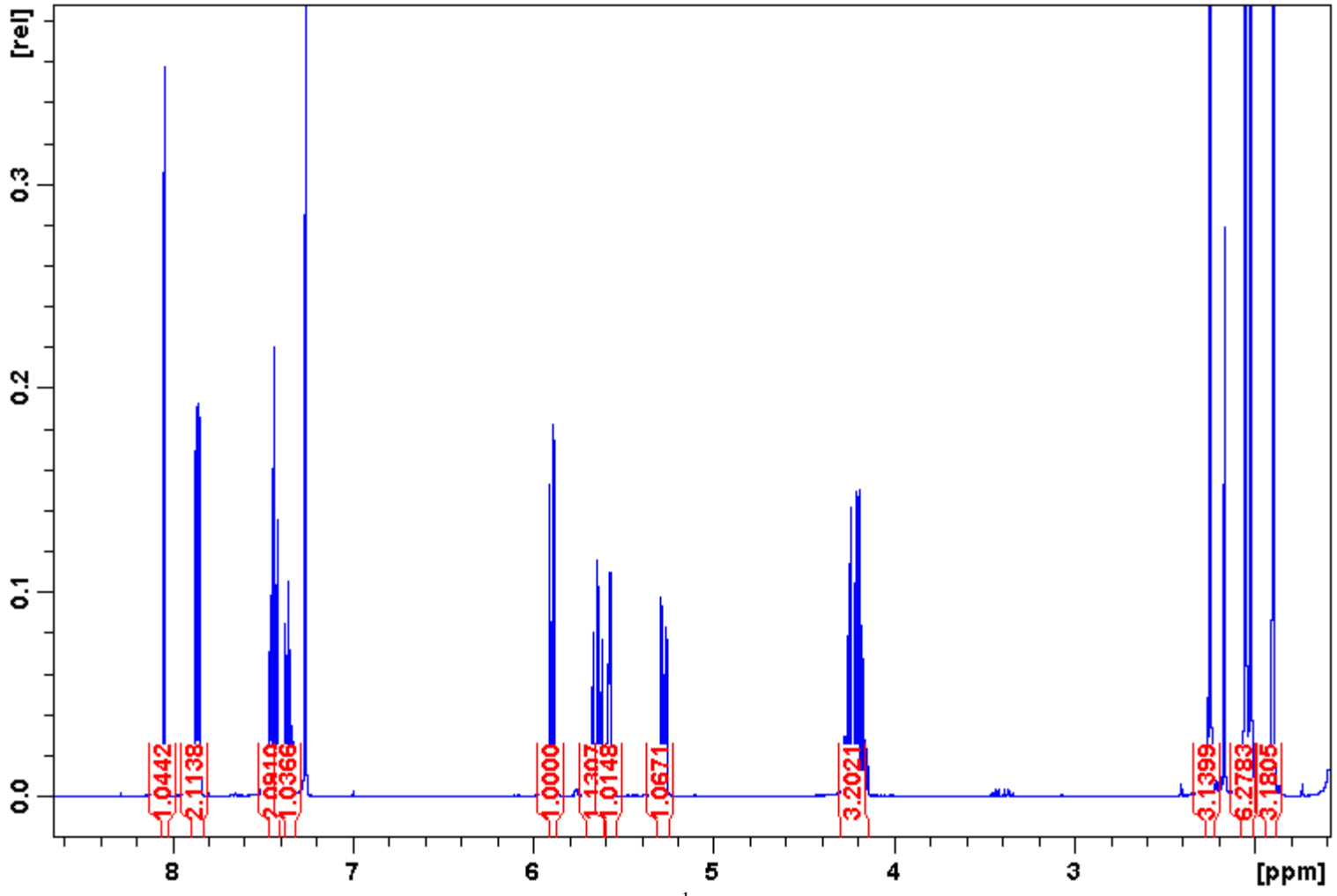

Figure 90: 400 MHz ^{1}H Spectrum of **16**.

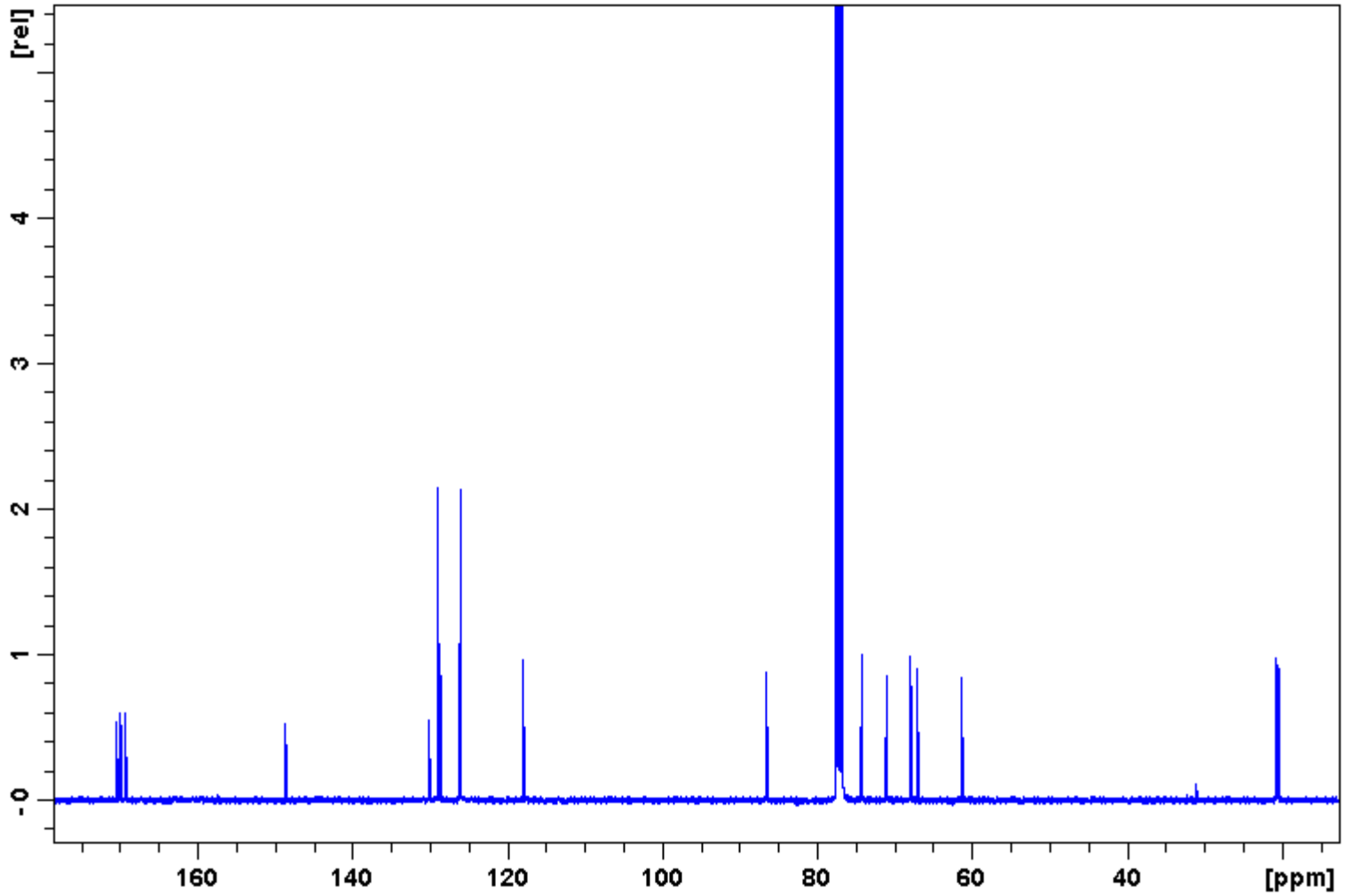

Figure 91: 100 MHz ^{13}C Spectrum of **16**.

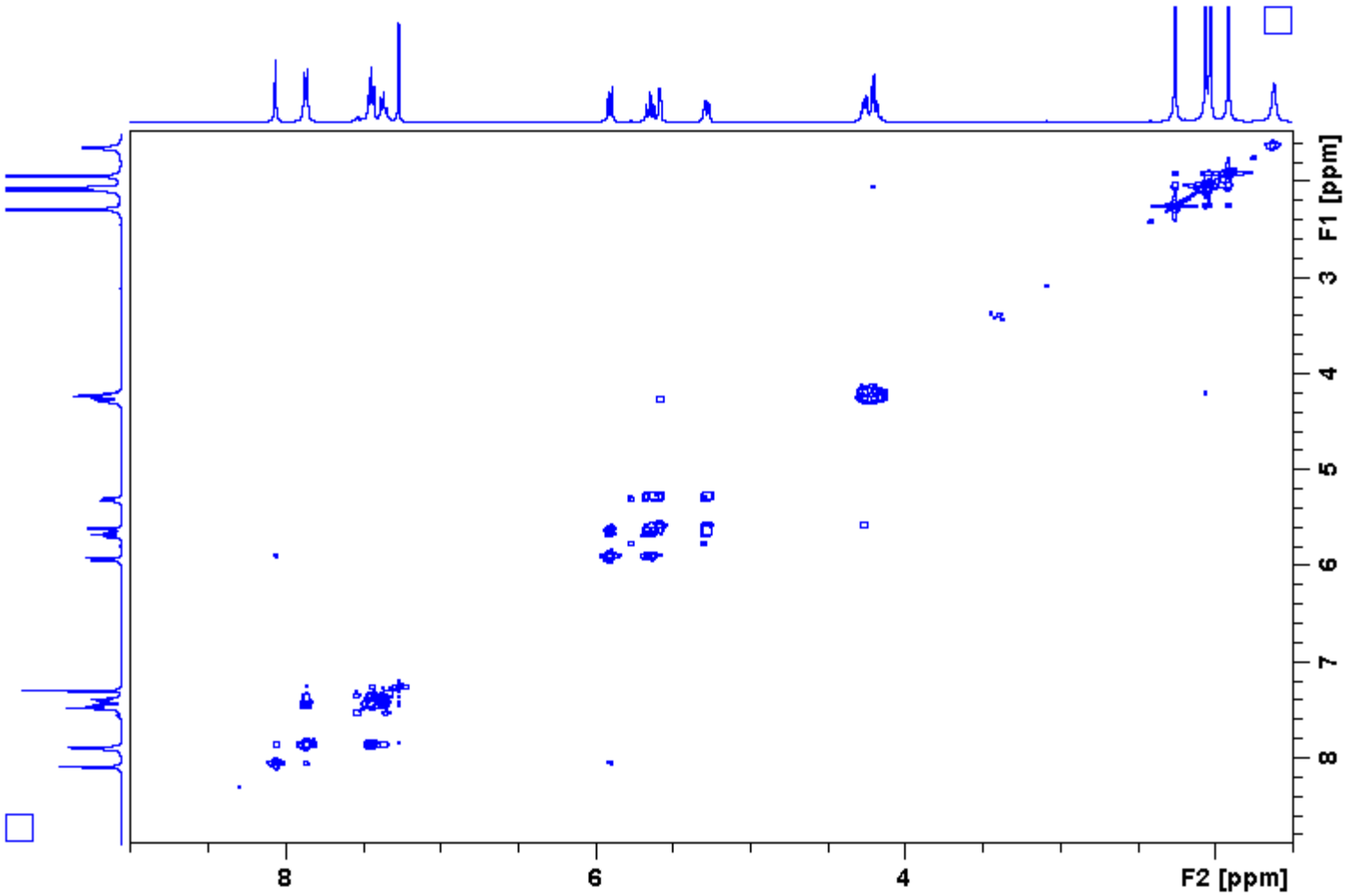

Figure 92: 400 MHz ^{1}H-^{1}H COSY Spectrum of **16**.

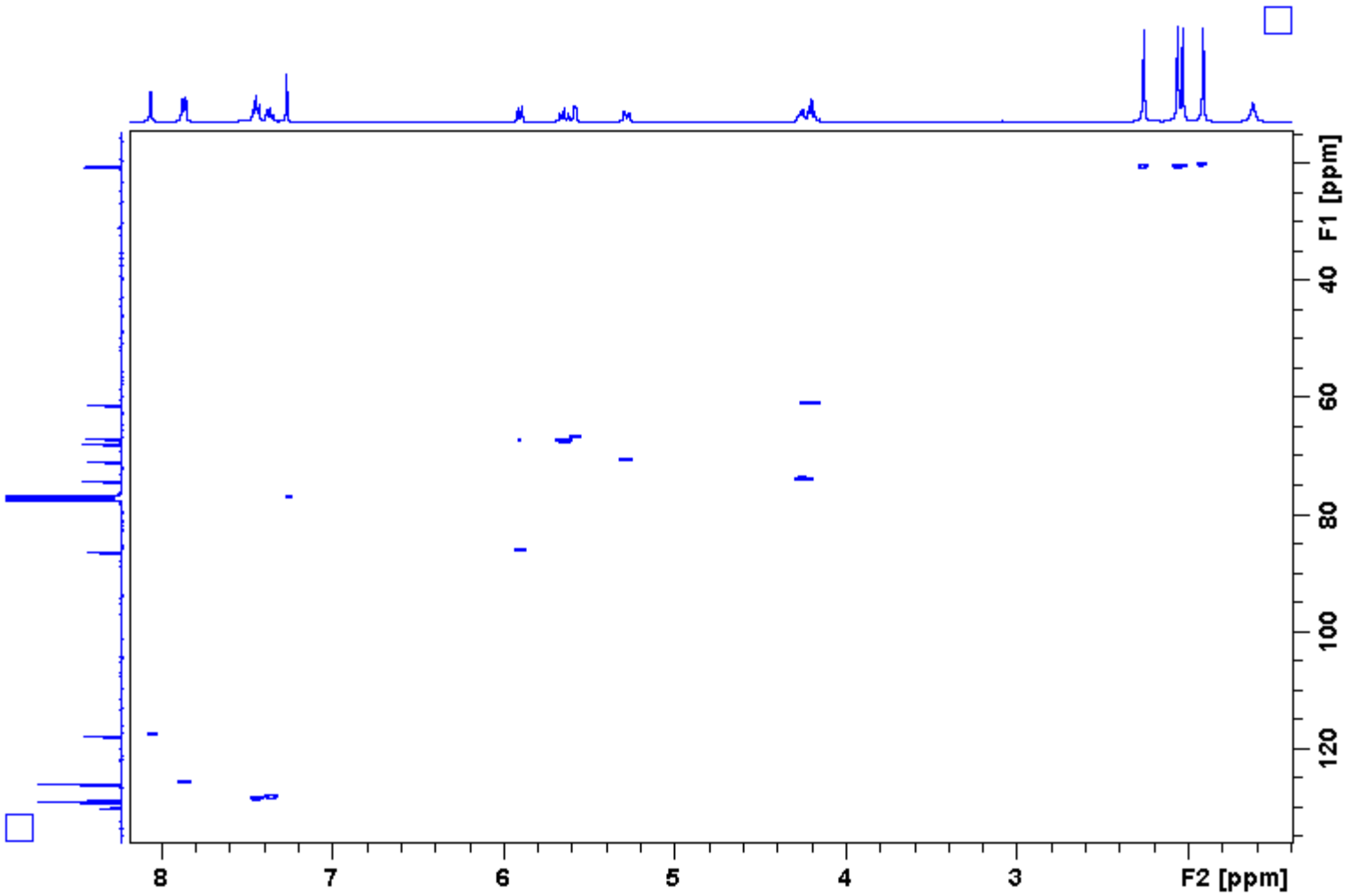

Figure 93: 400 MHz ^{1}H-^{13}C HSQC Spectrum of **16**.

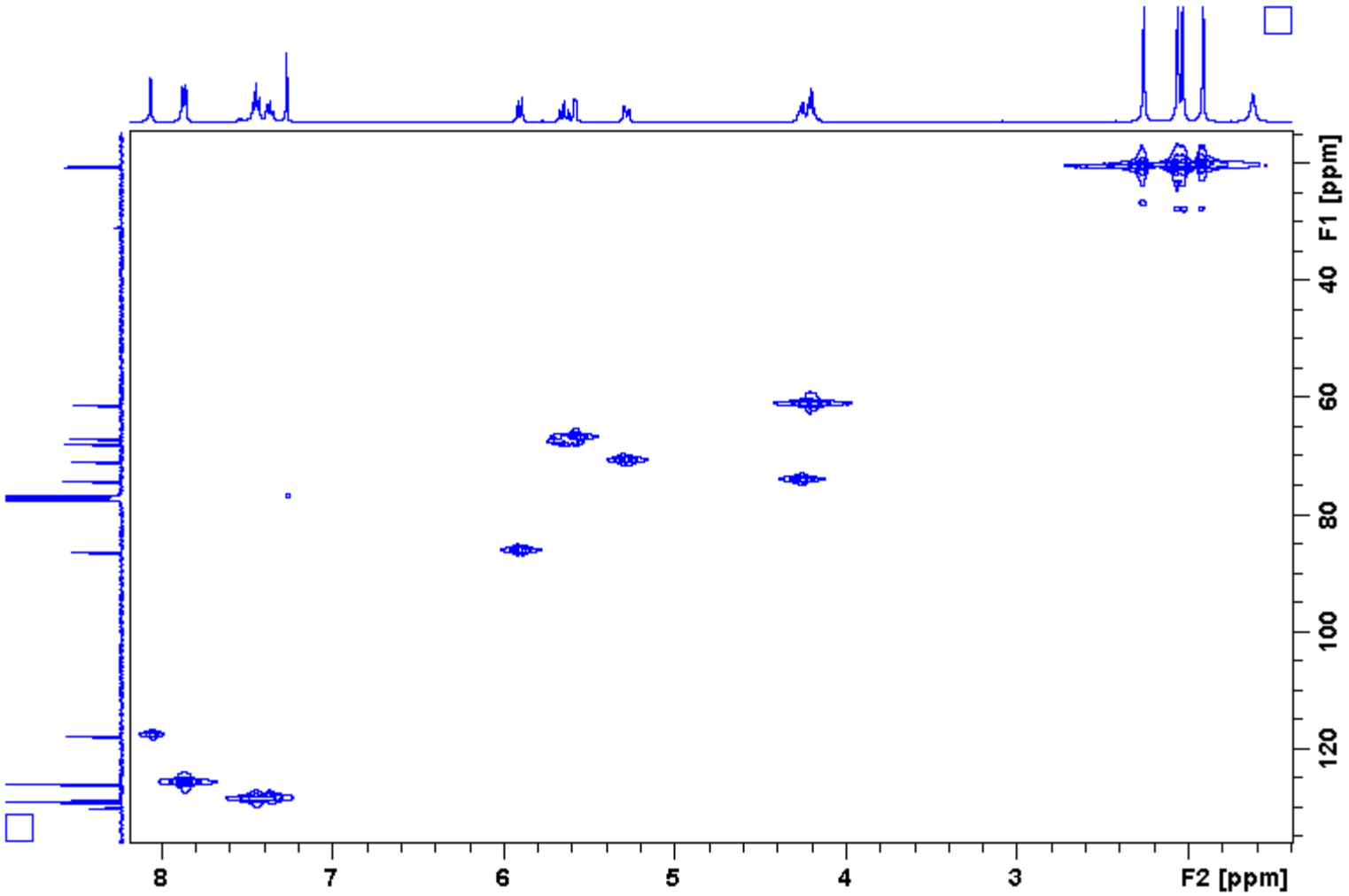

Figure 94: 400 MHz ^{1}H-^{13}C HMQC Spectrum of **16**.

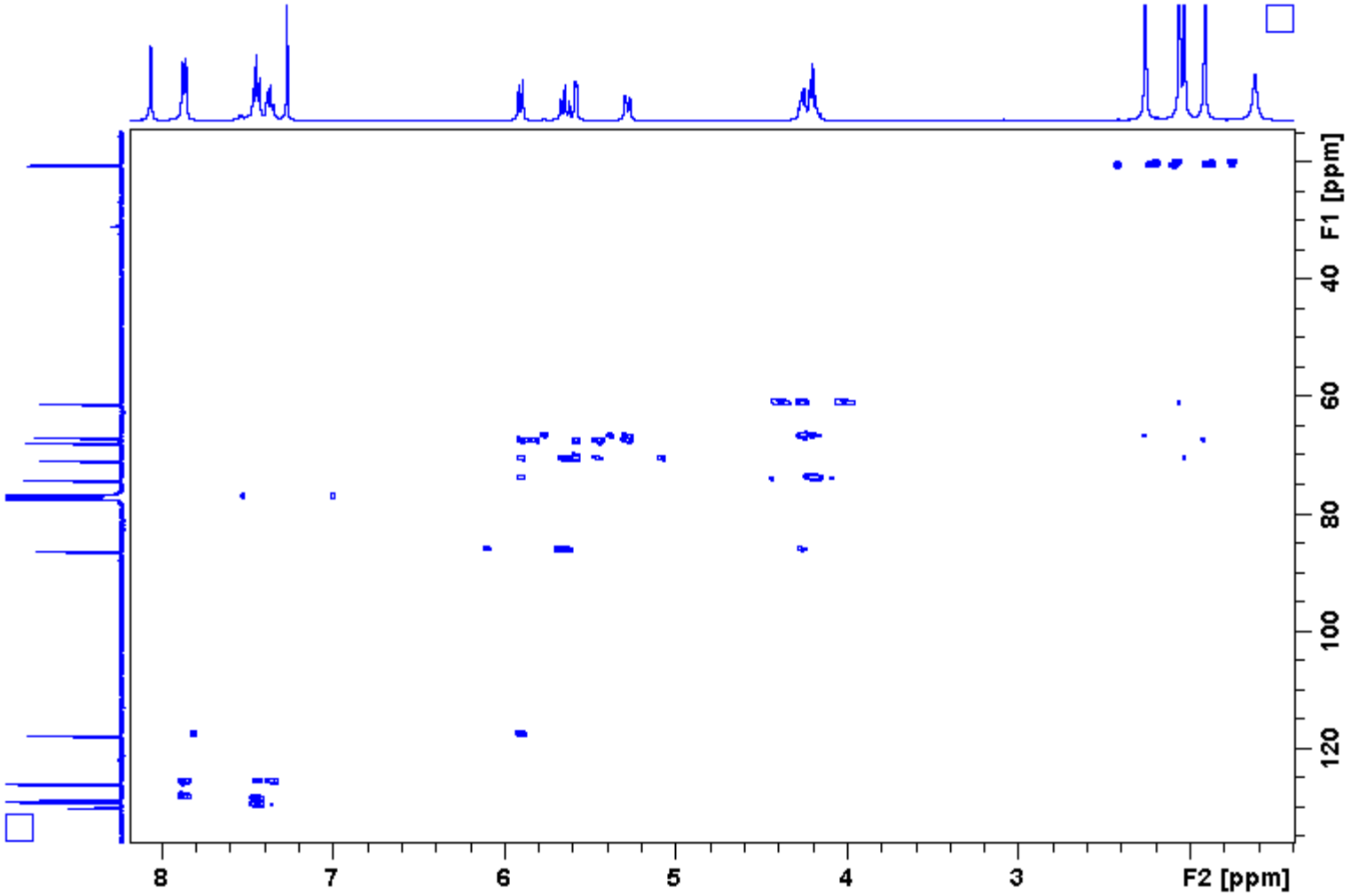

Figure 95: 400 MHz ^{1}H-^{13}C HMBC Spectrum of **16**.

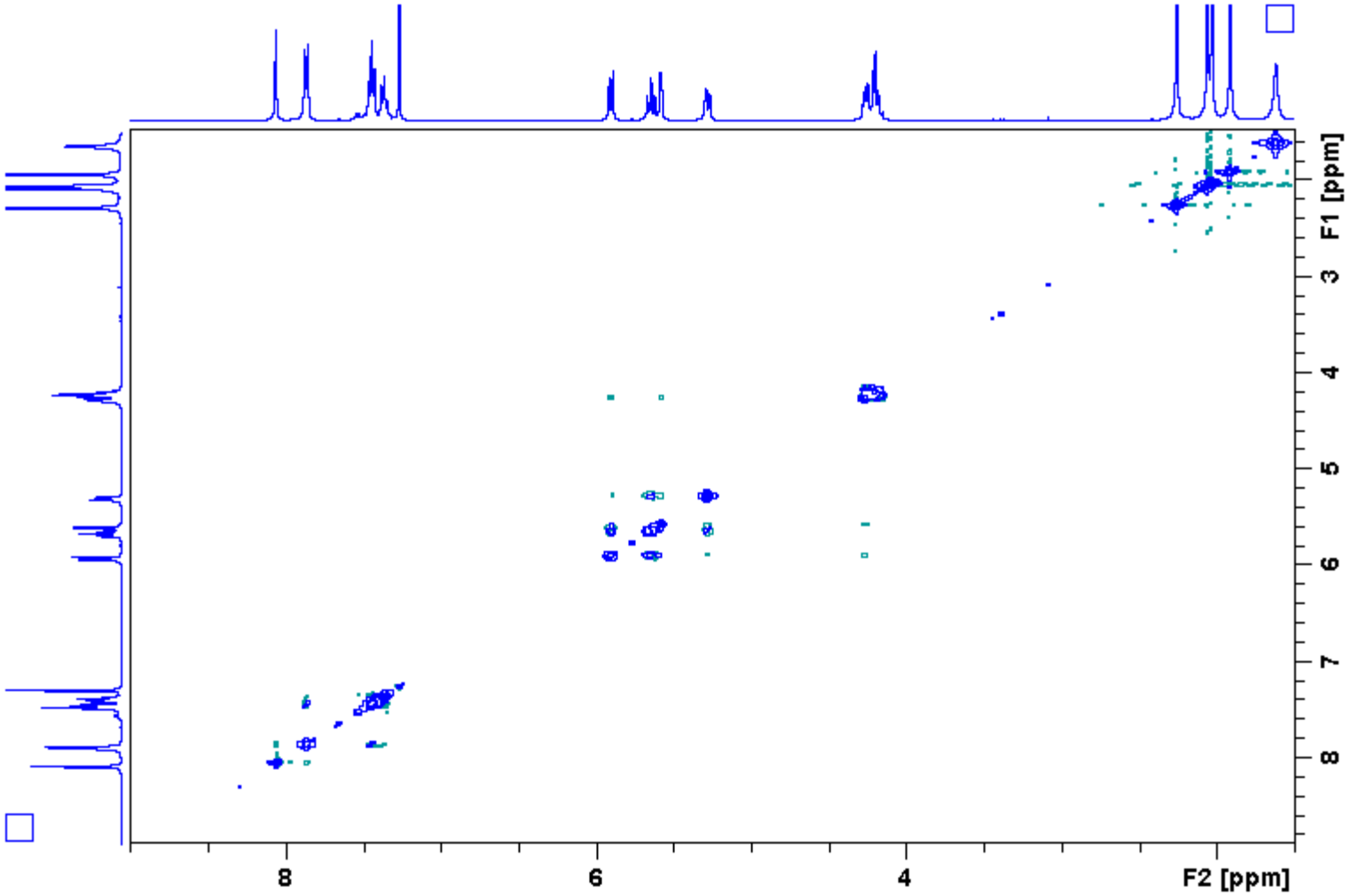

Figure 96: 400 MHz ^{1}H-^{1}H NOESY Spectrum of **16**.

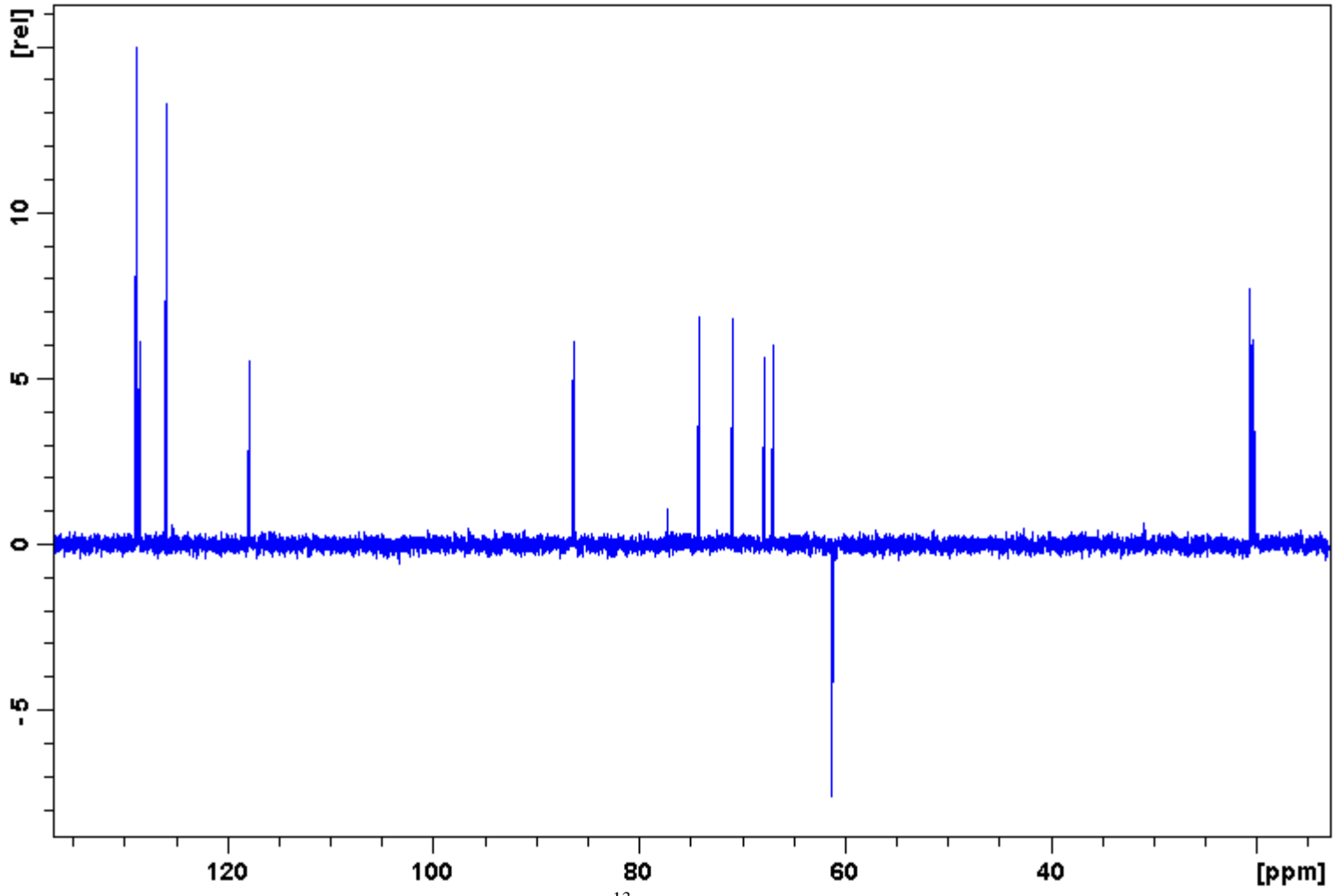

Figure 97: 100 MHz ^{13}C DEPT-135 Spectrum of **16**.

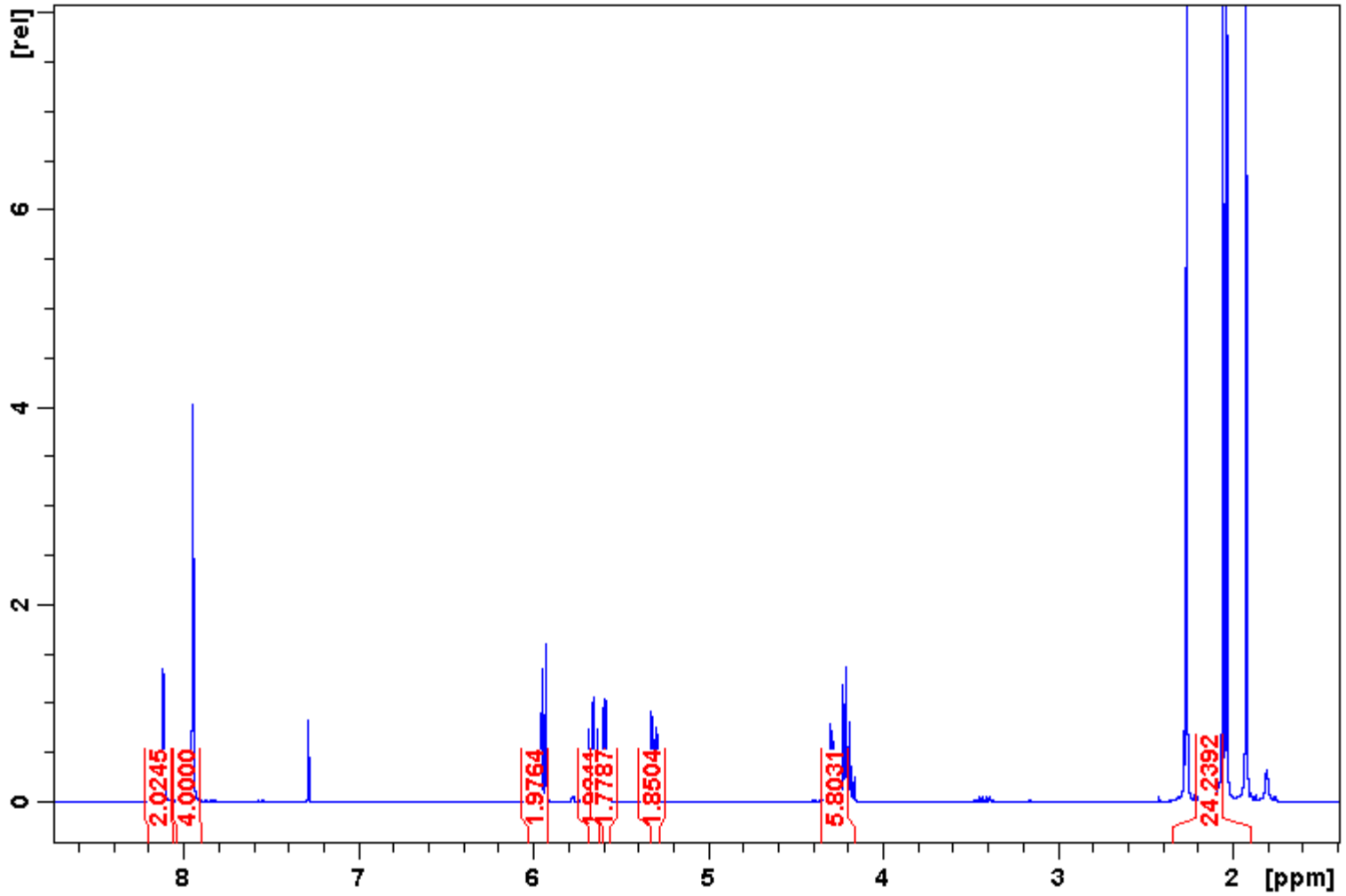

Figure 98: 400 MHz ^{1}H Spectrum of **17**.

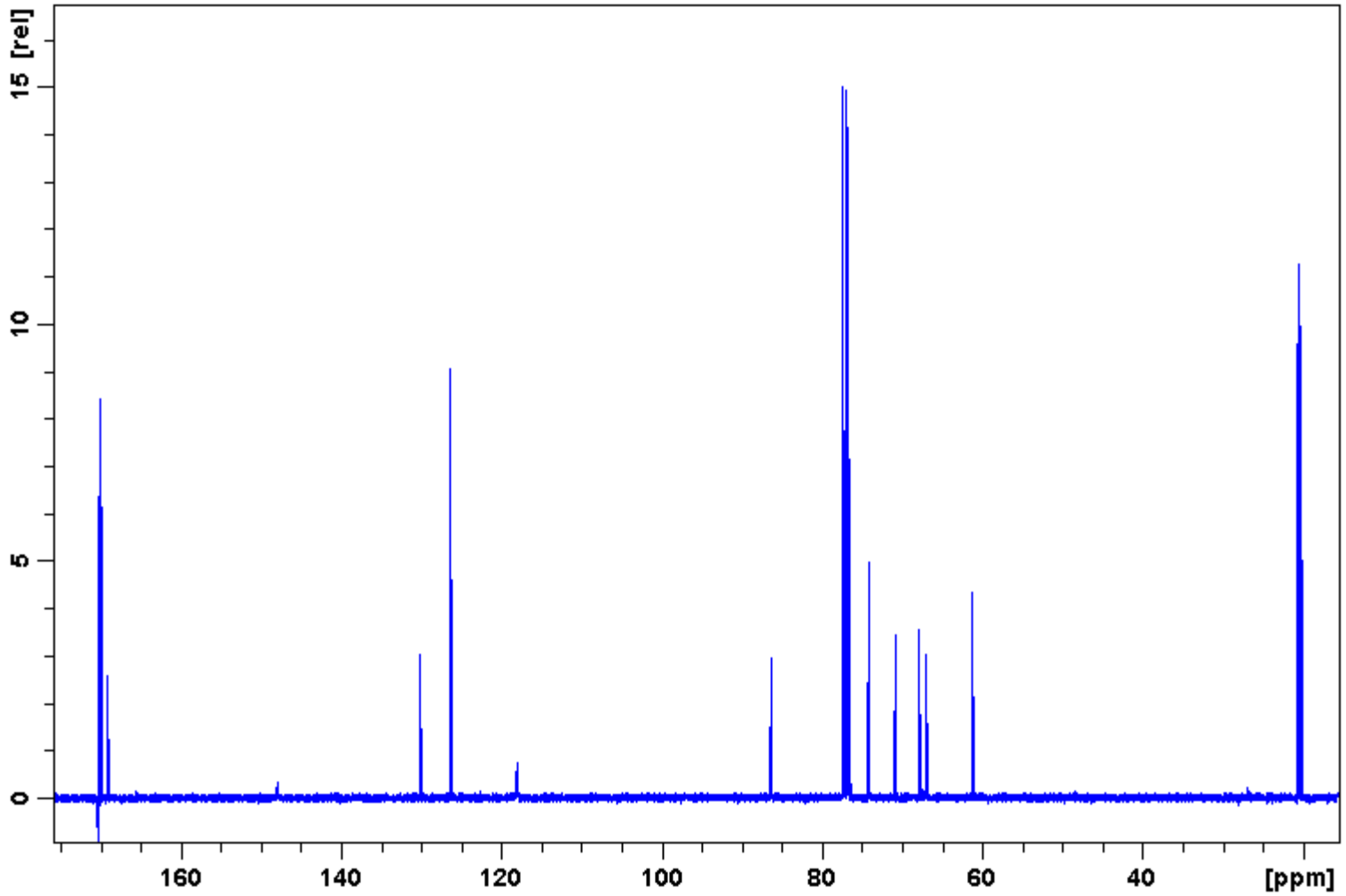

Figure 99: 100 MHz ^{13}C Spectrum of **17**.

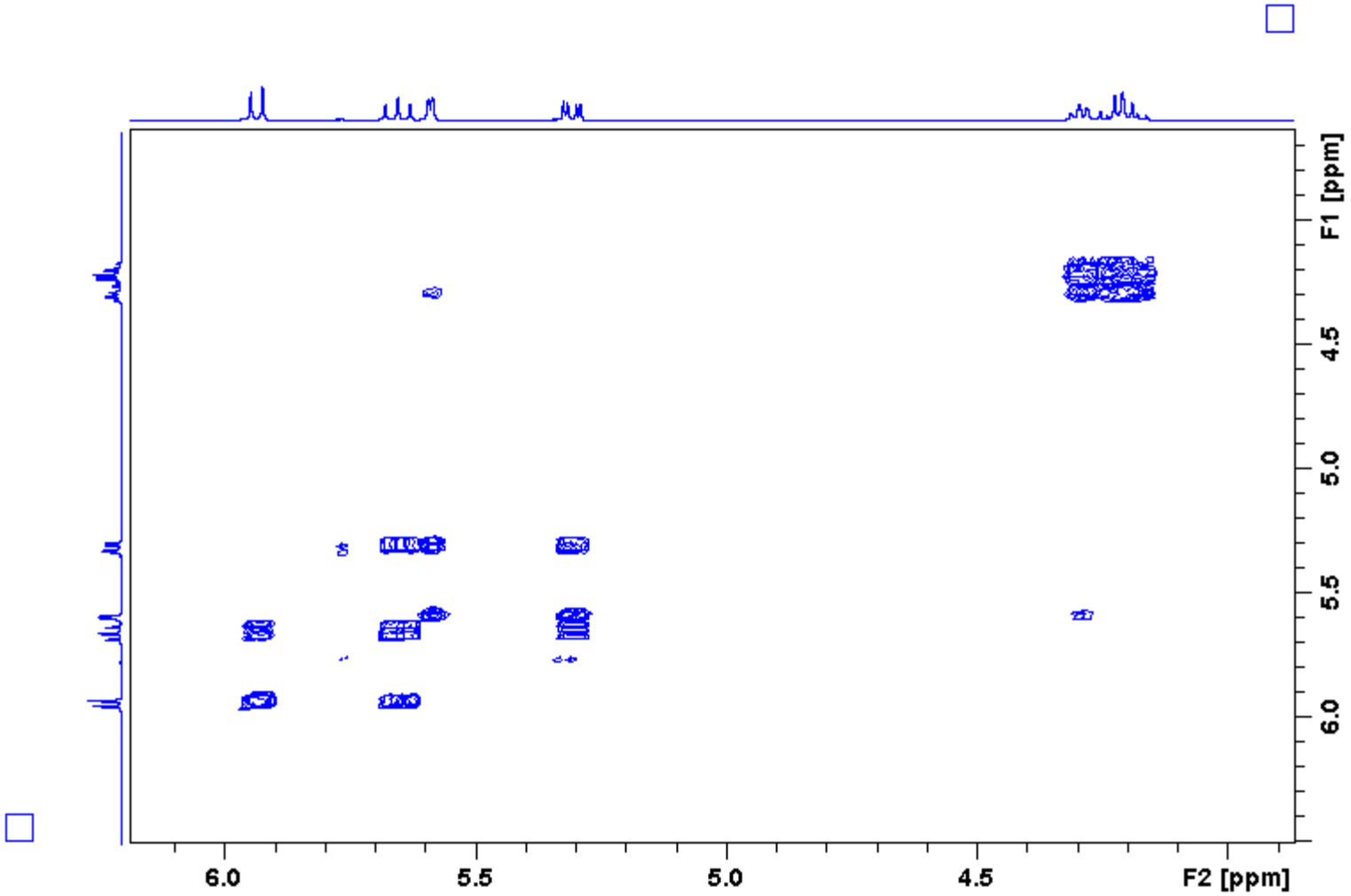

Figure 100: 400 MHz ^{1}H-^{1}H COSY Spectrum of **17**.

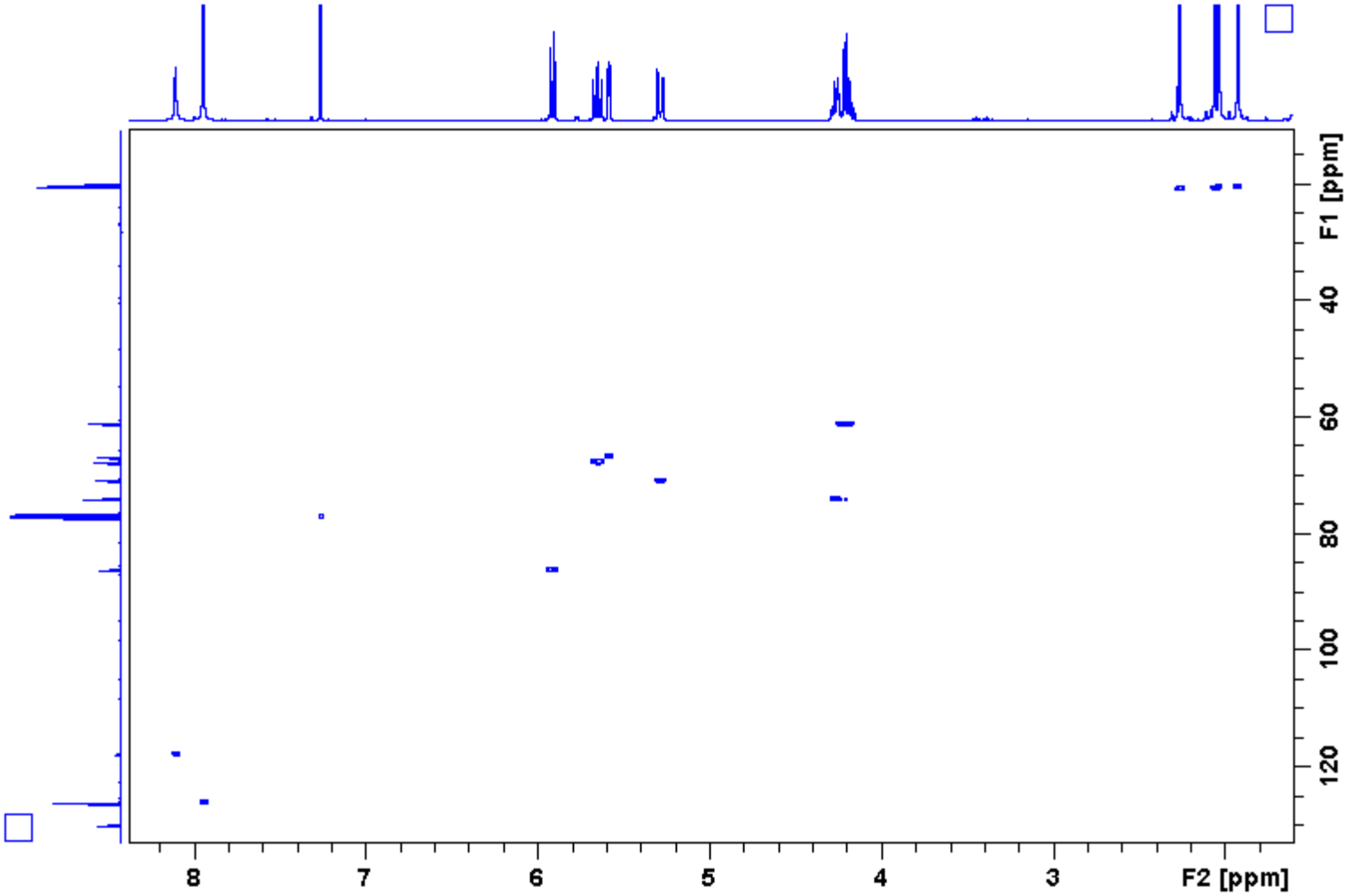

Figure 101: 400 MHz ^{1}H-^{13}C HSQC Spectrum of **17**.

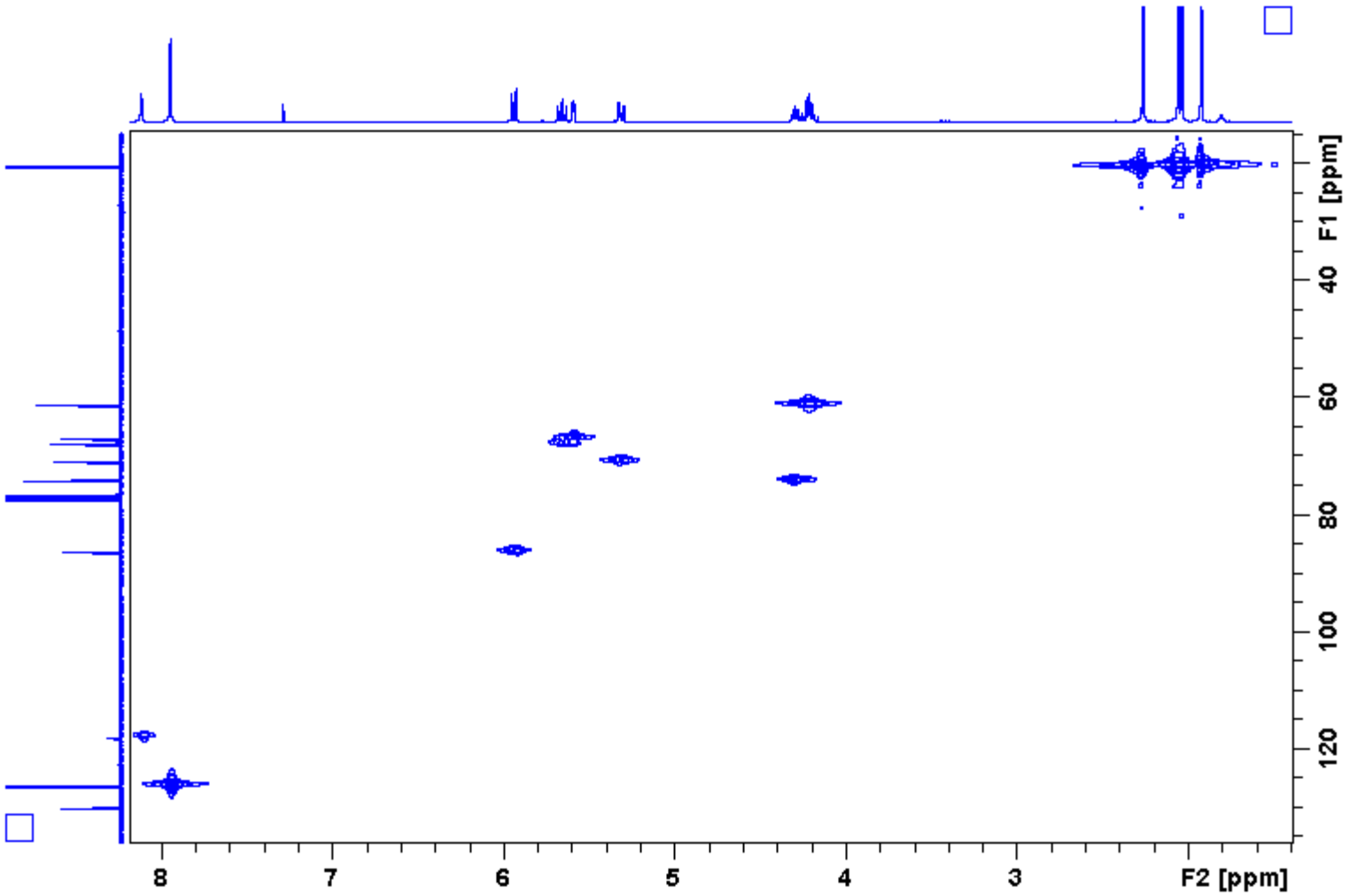

Figure 102: 400 MHz ^{1}H-^{13}C HMQC Spectrum of **17**.

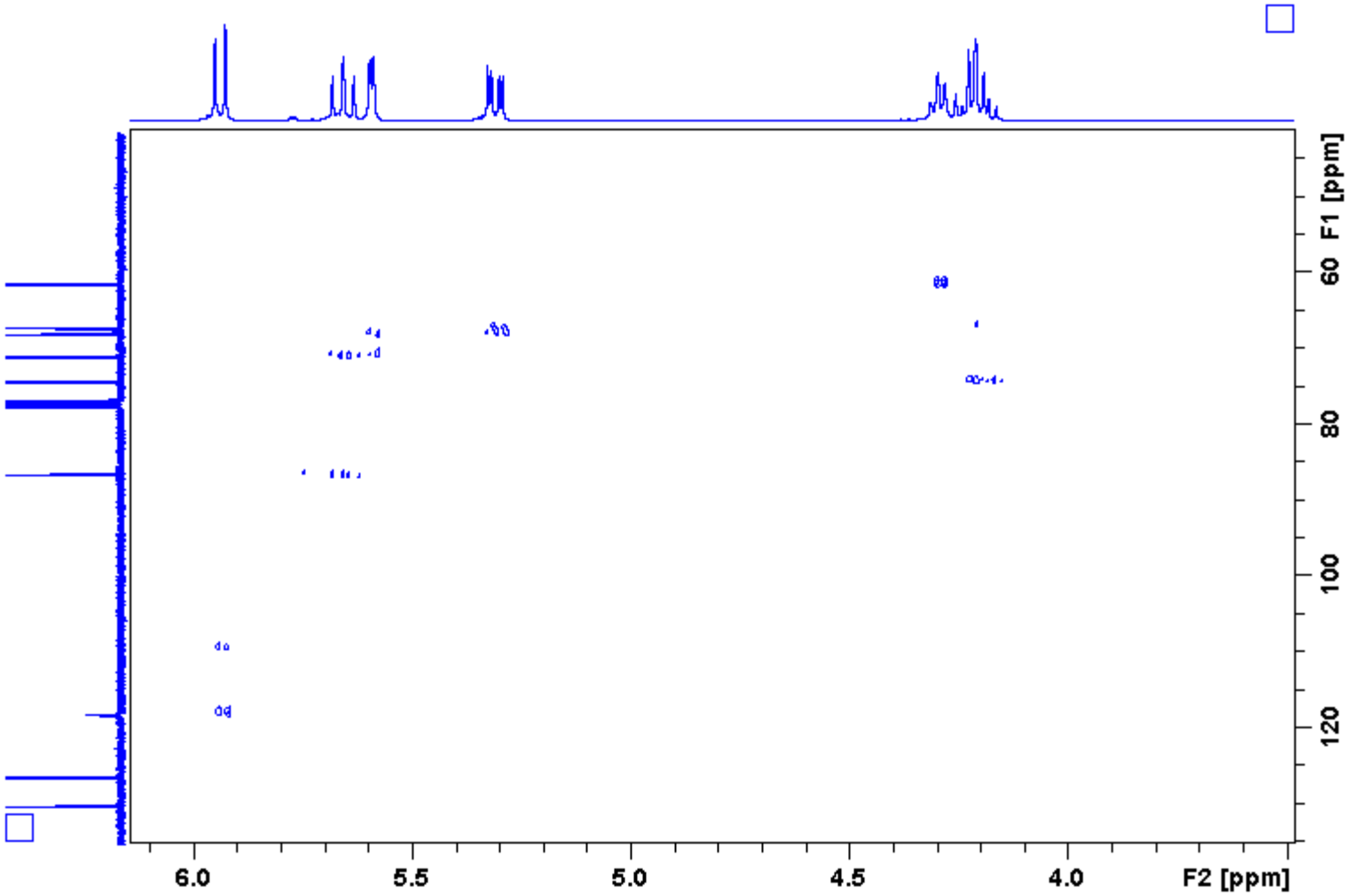

Figure 103: 400 MHz ^{1}H-^{13}C HMBC Spectrum of **17**.

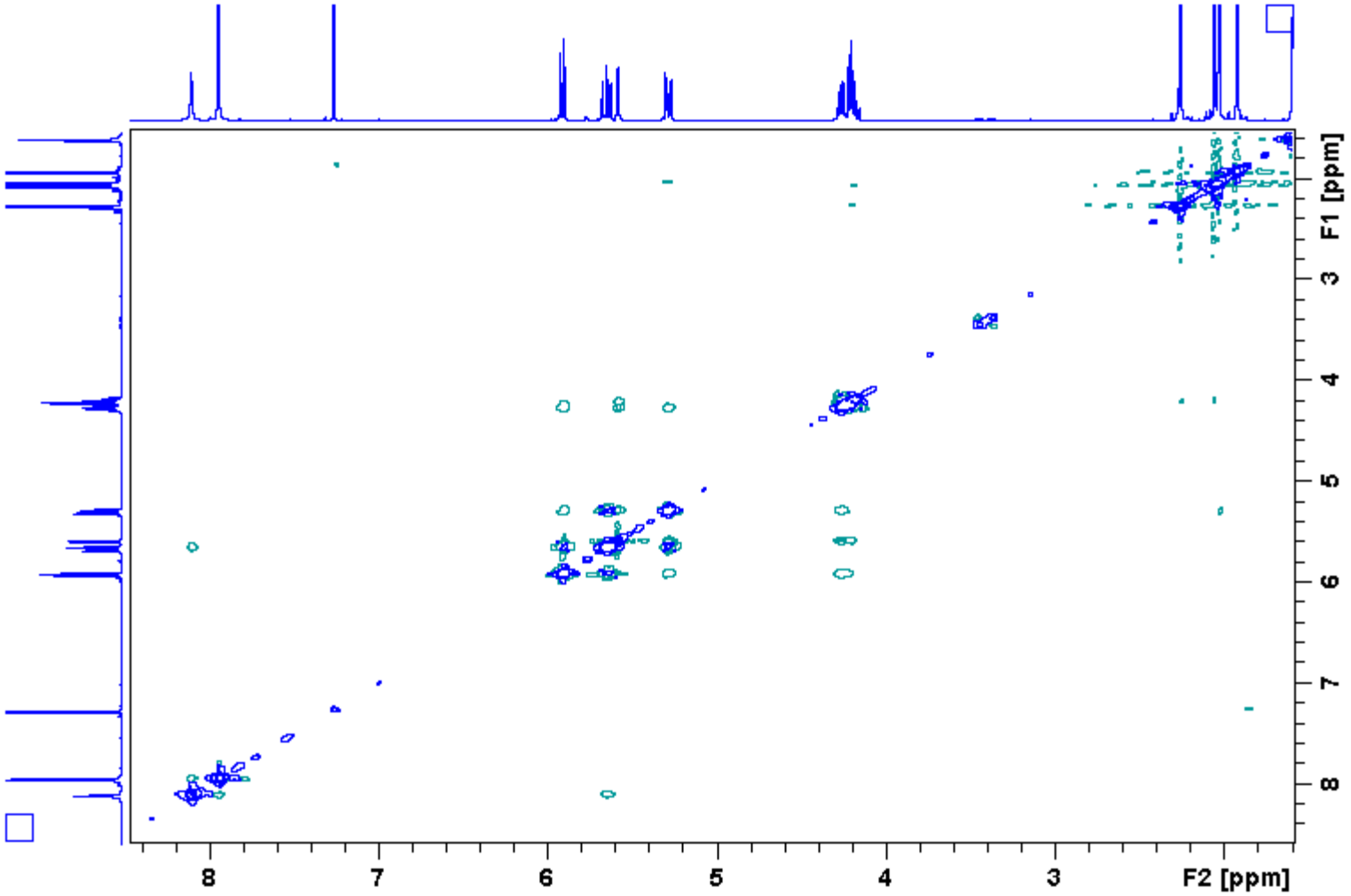

Figure 104: 400 MHz ^{1}H-^{1}H NOESY Spectrum of **17**.

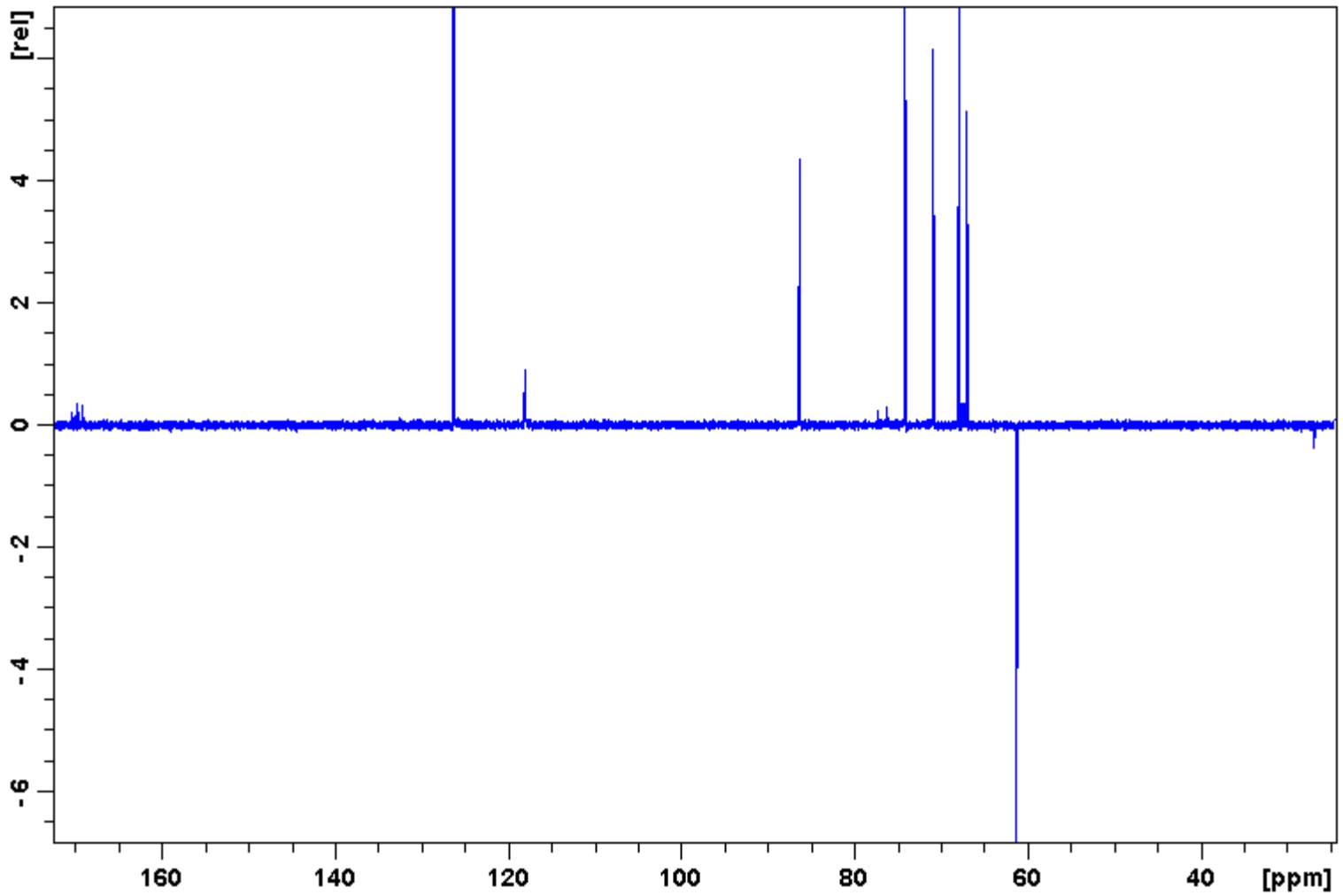

Figure 105: 100 MHz ^{13}C DEPT-135 Spectrum of **17**.

Appendix B

Mass Spectrum List Report

Analysis Info

Analysis Name	BGL-0951.d	Acquisition Date	07/19/08 20:56:31
Method	XQ Default.ms	Operator	Administrator
Sample Name	BGL-1-095	Instrument	Esquire-LC_00135
Comment	BGL-1-095 isp		

Acquisition Parameter

Ion Source Type	ESI	Ion Polarity	Positive	Alternating Ion Polarity	n/a
Mass Range Mode	Std/Normal	Scan Begin	150.00 m/z	Scan End	350.00 m/z
Capillary Exit	101.6 Volt	Skim 1	30.3 Volt	Trap Drive	44.9
Accumulation Time	10948 µs	Averages	10 Spectra	Auto MS/MS	Off

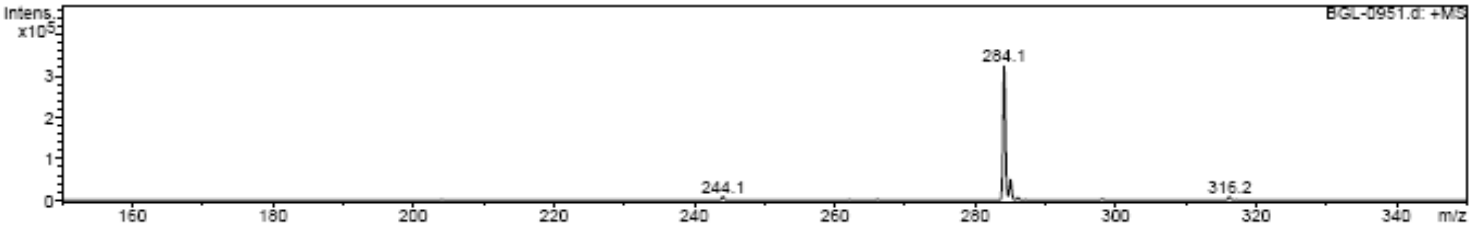

#	m/z	I	FWHM	S/N
1	244.1	9185	0.4	181.6
2	284.1	323205	0.4	6368.9
3	285.0	49068	0.4	969.9
4	286.1	6686	0.4	132.2
5	316.2	8526	0.4	168.5

Figure 106: Mass Spectrum of **3α/β**.

Mass Spectrum List Report

Analysis Info

Analysis Name	BGL-0058.d	Acquisition Date	07/19/08 16:03:23
Method	XQ Default.ms	Operator	Administrator
Sample Name	BGL-1-005	Instrument	Esquire-LC_00135
Comment	BGL-1-005 2Ac isp		

Acquisition Parameter

Ion Source Type	ESI	Ion Polarity	Positive	Alternating Ion Polarity	n/a
Mass Range Mode	Std/Normal	Scan Begin	250.00 m/z	Scan End	500.00 m/z
Capillary Exit	108.7 Volt	Skim 1	35.3 Volt	Trap Drive	48.2
Accumulation Time	5285 µs	Averages	10 Spectra	Auto MS/MS	Off

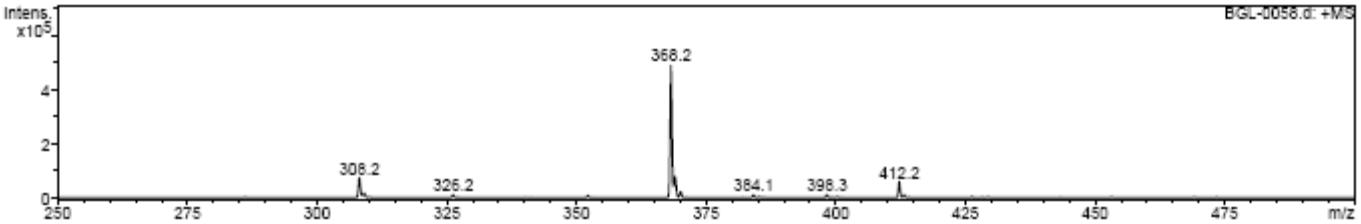

#	m/z	I	FWHM	S/N
1	308.2	73199	0.4	367.3
2	309.1	17412	0.4	87.4
3	326.2	11380	0.4	57.1
4	368.2	490429	0.4	2460.9
5	369.0	77946	0.4	391.1
6	370.1	22603	0.4	113.4
7	384.1	10886	0.4	54.6
8	396.3	10948	0.4	54.9
9	412.2	59106	0.4	296.6
10	413.2	11108	0.4	55.7

Figure 107: Mass Spectrum of **4α/β**.

Mass Spectrum List Report

Analysis Info

Analysis Name	BGL-0510.d	Acquisition Date	07/19/08 21:40:20
Method	XQ Default.ms	Operator	Administrator
Sample Name	BGL-1-051	Instrument	Esquire-LC_00135
Comment	BGL-1-051 Bn-2 & isp		

Acquisition Parameter

Ion Source Type	ESI	Ion Polarity	Positive	Alternating Ion Polarity	n/a
Mass Range Mode	Std/Normal	Scan Begin	300.00 m/z	Scan End	650.00 m/z
Capillary Exit	116.2 Volt	Skim 1	40.4 Volt	Trap Drive	51.9
Accumulation Time	14197 µs	Averages	10 Spectra	Auto MS/MS	Off

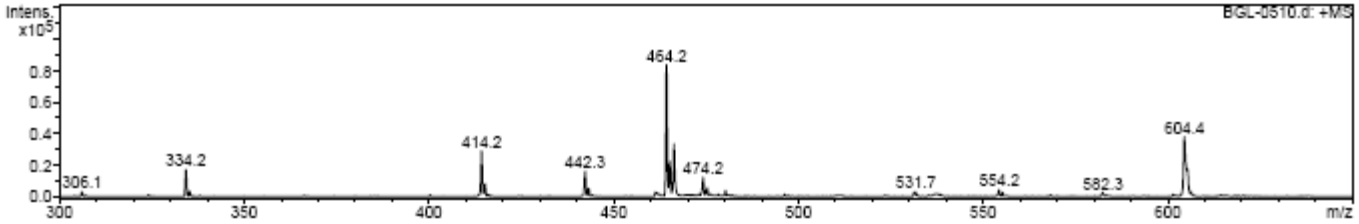

#	m/z	I	FWHM	S/N
1	334.2	16973	0.4	136.4
2	414.2	28970	0.4	232.9
3	415.2	8127	0.4	65.3
4	442.3	15933	0.4	128.1
5	464.2	83766	0.4	673.3
6	465.2	22436	0.4	180.3
7	466.3	33446	0.4	268.8
8	474.2	12172	0.4	97.8
9	604.4	38054	0.4	305.9
10	605.2	17511	0.3	140.8

Bruker Daltonics DataAnalysis 3.0 printed: 07/19/08 21:42:48 Page 1 of 1

Figure 108: Mass Spectrum of **5α/β**.

Mass Spectrum List Report

Analysis Info

Analysis Name	BGL-0692.d	Acquisition Date	07/19/08 18:33:10
Method	XQ Default.ms	Operator	Administrator
Sample Name	BGL-1-069	Instrument	Esquire-LC_00135
Comment	BGL-1-069 Bn-2		

Acquisition Parameter

Ion Source Type	ESI	Ion Polarity	Positive	Alternating Ion Polarity	n/a
Mass Range Mode	Std/Normal	Scan Begin	200.00 m/z	Scan End	600.00 m/z
Capillary Exit	113.1 Volt	Skim 1	38.4 Volt	Trap Drive	50.3
Accumulation Time	9133 µs	Averages	10 Spectra	Auto MS/MS	Off

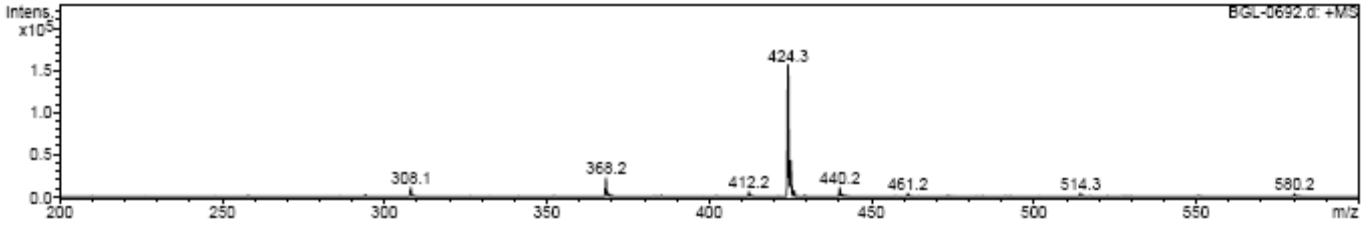

#	m/z	I	FWHM	S/N
1	308.1	10677	0.4	105.7
2	368.2	21945	0.4	217.2
3	369.2	3540	0.4	35.0
4	412.2	6094	0.4	60.3
5	424.3	156442	0.4	1548.3
6	425.1	42631	0.4	421.9
7	426.2	6775	0.4	67.1
8	440.2	10671	0.4	105.6
9	461.2	3996	0.4	39.5
10	514.3	4228	0.4	41.8

Bruker Daltonics DataAnalysis 3.0 printed: 07/19/08 18:36:43 Page 1 of 1

Figure 109: Mass Spectrum of **6α/β**.

Mass Spectrum List Report

Analysis Info

Analysis Name	BGL-0812.d	Acquisition Date	07/19/08 19:39:54
Method	XQ Default.ms	Operator	Administrator
Sample Name	BGL-1-081	Instrument	Esquire-LC_00135
Comment	BGL-1-081 Bn-2 & Ms-2		

Acquisition Parameter

Ion Source Type	ESI	Ion Polarity	Positive	Alternating Ion Polarity	n/a
Mass Range Mode	Std/Normal	Scan Begin	375.00 m/z	Scan End	650.00 m/z
Capillary Exit	124.4 Volt	Skim 1	45.9 Volt	Trap Drive	56.3
Accumulation Time	5216 µs	Averages	10 Spectra	Auto MS/MS	Off

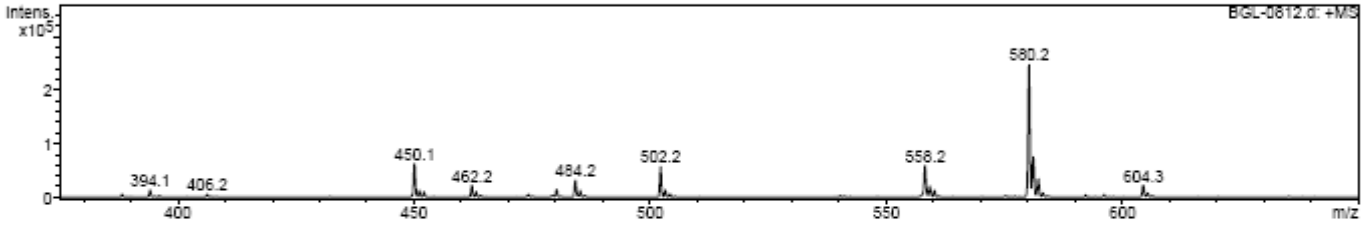

#	m/z	I	FWHM	S/N
1	450.1	63084	0.4	256.8
2	462.2	22438	0.4	91.3
3	484.2	31296	0.4	127.4
4	502.2	56760	0.4	231.0
5	558.2	59552	0.4	242.4
6	559.2	20707	0.4	84.3
7	580.2	247685	0.4	1008.1
8	581.1	75344	0.4	306.7
9	582.2	33941	0.4	138.1
10	604.3	22331	0.4	90.9

Bruker Daltonics DataAnalysis 3.0 printed: 07/19/08 19:41:56 Page 1 of 1

Figure 110: Mass Spectrum of **7α/β**.

Mass Spectrum List Report

Analysis Info

Analysis Name	BGL-1021.d	Acquisition Date	07/19/08 17:25:22
Method	XQ Default.ms	Operator	Administrator
Sample Name	BGL-1-101	Instrument	Esquire-LC_00135
Comment	BGL-1-101 OMe		

Acquisition Parameter

Ion Source Type	ESI	Ion Polarity	Positive	Alternating Ion Polarity	n/a
Mass Range Mode	Std/Normal	Scan Begin	100.00 m/z	Scan End	400.00 m/z
Capillary Exit	99.3 Volt	Skim 1	28.5 Volt	Trap Drive	43.9
Accumulation Time	8711 µs	Averages	10 Spectra	Auto MS/MS	Off

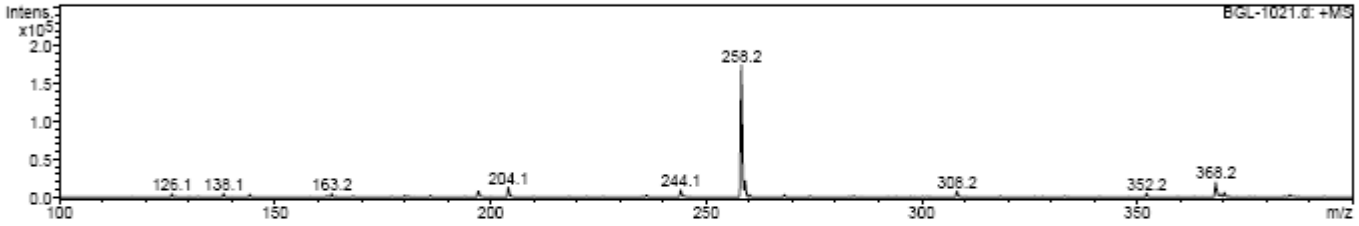

#	m/z	I	FWHM	S/N
1	136.1	4833	0.4	28.6
2	197.2	7889	0.5	46.7
3	204.1	13085	0.4	77.5
4	244.1	9493	0.4	56.2
5	258.2	174361	0.4	1032.5
6	259.1	21847	0.3	129.4
7	308.2	7929	0.4	47.0
8	352.2	5023	0.4	29.7
9	368.2	19721	0.4	116.8
10	370.2	5994	0.4	35.5

Bruker Daltonics DataAnalysis 3.0 printed: 07/19/08 17:25:58 Page 1 of 1

Figure 111: Mass Spectrum of **8α/β**.

Mass Spectrum List Report

Analysis Info

Analysis Name	BGL-1033.d	Acquisition Date	07/19/08 17:58:33
Method	XQ Default.ms	Operator	Administrator
Sample Name	BGL-1-103	Instrument	Esquire-LC_00135
Comment	BGL-1-103 OMe & isp		

Acquisition Parameter

Ion Source Type	ESI	Ion Polarity	Positive	Alternating Ion Polarity	n/a
Mass Range Mode	Std/Normal	Scan Begin	150.00 m/z	Scan End	400.00 m/z
Capillary Exit	102.9 Volt	Skim 1	31.2 Volt	Trap Drive	45.5
Accumulation Time	39218 µs	Averages	10 Spectra	Auto MS/MS	Off

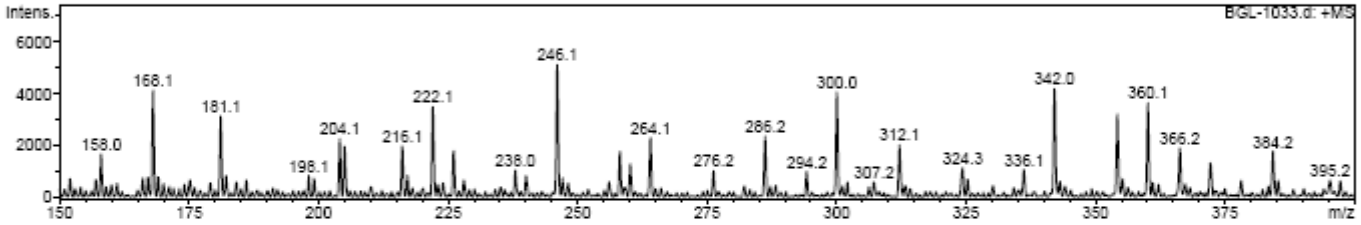

#	m/z	I	FWHM	S/N
1	168.1	4104	0.4	33.9
2	181.1	3112	0.4	25.7
3	222.1	3466	0.4	28.6
4	246.1	5084	0.4	42.0
5	264.1	2268	0.4	18.7
6	286.2	2337	0.4	19.3
7	300.0	4033	0.4	33.3
8	342.0	4161	0.4	34.3
9	354.2	3186	0.4	26.3
10	360.1	3630	0.4	30.0

Bruker Daltonics DataAnalysis 3.0 printed: 07/19/08 18:03:19 Page 1 of 1

Figure 112: Mass Spectrum of **9α/β**.

Mass Spectrum List Report

Analysis Info

Analysis Name	BGL-0993.d	Acquisition Date	07/19/08 16:48:52
Method	XQ Default.ms	Operator	Administrator
Sample Name	BGL-1-099	Instrument	Esquire-LC_00135
Comment	BGL-1-099 2Ac isp		

Acquisition Parameter

Ion Source Type	ESI	Ion Polarity	Positive	Alternating Ion Polarity	n/a
Mass Range Mode	Std/Normal	Scan Begin	100.00 m/z	Scan End	400.00 m/z
Capillary Exit	105.4 Volt	Skim 1	33.0 Volt	Trap Drive	46.6
Accumulation Time	50000 µs	Averages	10 Spectra	Auto MS/MS	Off

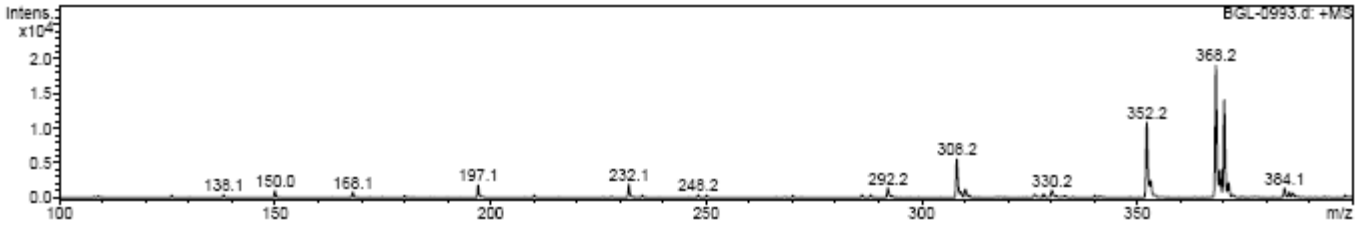

#	m/z	I	FWHM	S/N
1	197.1	1809	0.4	75.6
2	232.1	1953	0.4	81.7
3	292.2	1377	0.4	57.6
4	308.2	5514	0.4	230.5
5	352.2	10865	0.4	454.3
6	353.1	2450	0.4	102.4
7	368.2	19032	0.4	795.7
8	369.2	3954	0.3	165.3
9	370.2	14111	0.4	590.0
10	371.1	2159	0.4	90.3

Bruker Daltonics DataAnalysis 3.0 printed: 07/19/08 17:22:42 Page 1 of 1

Figure 113: Mass Spectrum of **10α/β**.

Mass Spectrum List Report

Analysis Info

Analysis Name	BGL-1111.d	Acquisition Date	07/19/08 19:15:20
Method	XQ Default.ms	Operator	Administrator
Sample Name	BGL-1-111	Instrument	Esquire-LC_00135
Comment	BGL-1-111 Ms-2 & Ac-2		

Acquisition Parameter

Ion Source Type	ESI	Ion Polarity	Positive	Alternating Ion Polarity	n/a
Mass Range Mode	Std/Normal	Scan Begin	300.00 m/z	Scan End	700.00 m/z
Capillary Exit	117.6 Volt	Skim 1	41.4 Volt	Trap Drive	52.6
Accumulation Time	209 µs	Averages	10 Spectra	Auto MS/MS	Off

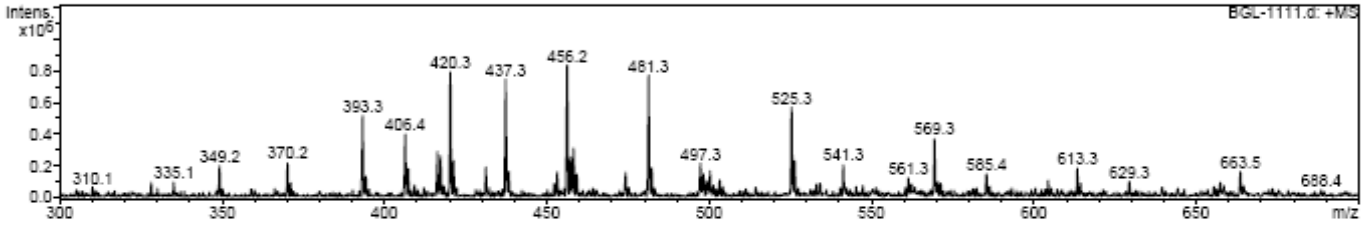

#	m/z	I	FWHM	S/N
1	393.3	515002	0.4	37.6
2	406.4	397588	0.4	29.0
3	416.3	288051	0.4	21.0
4	420.3	793383	0.4	58.0
5	437.3	745779	0.4	54.5
6	456.2	837276	0.4	61.2
7	458.2	309234	0.4	22.6
8	481.3	773107	0.4	56.5
9	525.3	568217	0.4	41.5
10	569.3	369896	0.4	27.0

Bruker Daltonics DataAnalysis 3.0 printed: 07/19/08 19:17:20 Page 1 of 1

Figure 114: Mass Spectrum of **11α/β**.

Mass Spectrum List Report

Analysis Info

Analysis Name	BGL-1090.d	Acquisition Date	07/19/08 22:31:58
Method	XQ Default.ms	Operator	Administrator
Sample Name	BGL-1-109	Instrument	Esquire-LC_00135
Comment	BGL-1-109 fr 8-9		

Acquisition Parameter

Ion Source Type	ESI	Ion Polarity	Positive	Alternating Ion Polarity	n/a
Mass Range Mode	Std/Normal	Scan Begin	300.00 m/z	Scan End	600.00 m/z
Capillary Exit	117.6 Volt	Skim 1	41.4 Volt	Trap Drive	52.6
Accumulation Time	1402 µs	Averages	10 Spectra	Auto MS/MS	Off

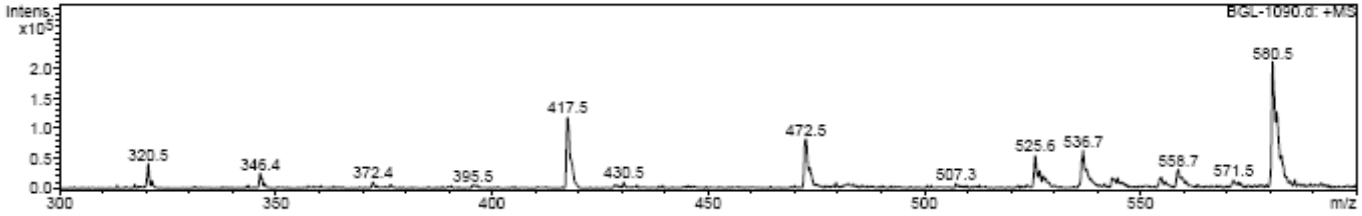

#	m/z	I	FWHM	S/N
1	320.5	40899	0.5	31.6
2	417.5	118317	0.8	91.5
3	472.5	82133	0.7	63.5
4	473.5	34718	0.6	26.9
5	525.6	54421	0.5	42.1
6	536.7	62896	0.6	48.7
7	537.5	31772	0.4	24.6
8	580.5	210719	0.5	163.0
9	581.5	127018	0.5	98.3
10	582.5	54534	0.7	42.2

Figure 115: Mass Spectrum of **13α/β**.

Appendix C

Relaxation Table

14				**15**				**16**				**17**			
peak (ppm)	t1 (s)	t2 (s)	exp. T1	peak (ppm)	t1	t2	exp. t1	peak (ppm)	t1	t2	exp. t1	peak (ppm)	t1	t2	exp. t1
7.971	1.588	0.244	7.94	7.870	1.421	0.204	7.105	8.082	1.703	0.103	8.515	8.128	1.112	0.154	5.56
5.867	0.981	0.135	4.905	6.905	0.587	0.088	2.935	7.895	1.961	1.000	9.805	7.966	0.445	0.075	2.225
5.845	0.984	0.140	4.92	5.832	0.951	0.128	4.755	7.878	1.714	0.109	8.57	5.943	0.840	0.122	4.2
5.786	1.108	0.156	5.54	5.809	0.947	0.135	4.735	7.484	1.719	0.093	8.595	5.920	0.871	0.126	4.355
5.766	1.118	0.159	5.59	5.774	1.099	0.150	5.495	7.466	1.767	0.114	8.835	5.693	1.463	0.221	7.315
5.572	1.135	0.161	5.675	5.754	1.078	0.151	5.39	7.448	1.806	1.000	9.03	5.670	1.467	0.217	7.335
5.332	0.603	0.087	3.015	5.584	1.545	0.194	7.725	7.403	2.113	0.254	10.565	5.645	1.494	0.214	7.47
5.322	1.048	0.160	5.24	5.559	1.024	0.150	5.12	7.385	2.240	0.252	11.2	5.607	0.955	1.000	4.775
5.299	0.647	0.101	3.235	5.322	1.332	0.186	6.66	7.365	2.876	0.425	14.38	5.600	0.958	0.136	4.79
5.274	0.888	0.110	4.44	5.299	1.357	0.192	6.785	5.930	1.151	0.067	5.755	5.319	0.901	0.129	4.505
5.266	0.872	1.000	4.36	5.266	0.939	0.120	4.695	5.908	1.194	0.070	5.97	5.312	0.901	0.128	4.505
5.251	0.613	0.095	3.065	5.261	0.907	0.130	4.535	5.685	1.841	0.117	9.205	5.294	0.879	0.127	4.395
5.241	0.467	0.120	2.335	5.238	0.797	0.175	3.985	5.663	1.852	0.119	9.26	5.286	0.886	0.127	4.43
5.218	0.888	0.150	4.44	5.233	1.054	0.158	5.27	5.637	1.782	0.116	8.91	4.289	0.605	0.093	3.025
5.175	1.526	0.248	7.63	5.211	1.461	0.201	7.305	5.597	1.119	0.068	5.595	4.274	0.531	0.085	2.655
5.155	1.613	0.278	8.065	5.140	1.683	0.245	8.415	5.307	1.026	0.058	5.13	4.238	0.469	0.077	2.345
4.238	0.641	0.106	3.205	5.117	1.686	0.259	8.43	5.286	1.001	1.000	5.005	4.223	0.454	0.076	2.27
4.216	0.745	0.110	3.725	4.582	0.366	0.060	1.83	4.281	0.704	1.000	3.52	4.203	0.437	0.074	2.185
4.203	0.705	0.155	3.525	4.567	0.348	0.061	1.74	4.266	0.661	1.000	3.305	2.294	0.824	0.125	4.12
2.261	0.856	0.137	4.28	4.506	0.331	0.058	1.655	4.231	0.607	1.000	3.035	2.281	0.863	0.144	4.315
2.135	0.897	0.141	4.485	4.241	0.575	0.084	2.875	4.218	0.602	1.000	3.01	2.077	0.984	0.161	4.92
2.072	1.049	0.162	5.245	4.223	0.531	0.084	2.655	4.200	0.586	1.000	2.93	2.051	0.886	0.149	4.43
2.056	0.868	0.135	4.34	4.193	0.476	0.076	2.38	2.274	1.156	0.070	5.78	1.943	0.873	0.138	4.365
2.036	0.871	0.131	4.355	4.170	0.484	0.074	2.42	2.195	5.437	0.945	27.185	1.625	2.169	0.380	10.845
2.029	0.861	0.138	4.305	4.137	0.840	0.119	4.2	2.077	1.286	0.079	6.43				

1.915	0.834	0.138	4.17	4.112	0.872	0.131	4.36	2.049	1.107	0.067	5.535
1.619	5.000	1.362	25	2.246	0.874	0.136	4.37	1.930	1.124	0.067	5.62
				2.142	0.894	0.136	4.47	1.619	0.958	1.000	4.79
				2.114	0.888	1.000	4.44				
				2.072	1.061	0.159	5.305				
				2.056	0.842	0.129	4.21				
				2.029	0.858	1.000	4.29				
				2.024	0.781	0.130	3.905				
				1.905	0.815	0.130	4.075				
				1.637	3.324	0.718	16.62				
				1.271	0.722	0.100	3.61				

Table 3: ^{1}H Relaxation times for **14**, **15**, **16**, **17**.

Relative Experiment times (hr:min:sec) using sample concentration of approximately 100 mg/1 mL

Experiment	**14**	**15**	**16**	**17**
^{1}H (256/512 scans)	21:27	21:27	21:34	42:59
^{13}C CPD (15k/10k scans)	14:38:11	14:38:11	14:37:20	9:44:58
^{1}H t1 relaxation	42:17	33:57	33:57	58:57
^{1}H t2 relaxation	42:17	33:57	33:57	58:57
^{13}C DEPT-135	1:59:20	58:22	58:22	1:56:30
^{1}H-^{1}H COSY	16:42	12:18	1:06:09	1:06:19
^{1}H-^{1}H NOESY	6:28:57	16:42:44	11:54:19	6:52:12
^{1}H-^{13}C HSQC	15:20	1:59:20	56:03	32:22
^{1}H-^{13}C HMQC	4:41:42	14:28	2:20:32	4:03:22
^{1}H-^{13}C HMBC	9:27:43	7:27:43	2:14:34	4:43:15

Table 4: Relative Experiment Times for **14**, **15**, **16**, **17**.